VOL. 23 NO. 1 OCTOBER 1969
PUBLISHED MONTHLY

JOURNAL OF

ELECTROANALYTICAL CHEMISTRY

AND INTERFACIAL ELECTROCHEMISTRY

International Journal devoted to all Aspects of Electroanalytical Chemistry, Double Layer Studies, Electrokinetics, Colloid Stability, and Electrode Kinetics.

E L S E V I E R

GENERAL INFORMATION

Detailed *Suggestions and Instructions to Authors* were published in the June 1969 issue of the journal, *J. Electroanal. Chem.*, 21 (1969) 565–572. A free reprint can be obtained by application to the publisher.

Types of contributions

(a) Original research work not previously published in other periodicals (regular papers).
(b) Reviews on recent developments in various fields.
(c) Short communications.
(d) Preliminary notes.

A Preliminary Note is a brief report of work which has progressed to the stage when it is considered that the science of chemistry would be advanced if the results were made available as soon as possible to others working on the same subject. Preliminary Notes can in general be published within 4–8 weeks of their acceptance by the editor although this implies that proofs cannot be sent to the author(s). The publisher will attend to correction of the proof but it should be remembered that errors in the manuscript will also appear in the published Note. Preliminary Notes, clearly marked as such, must be sent to Dr. R. Parsons (address given below).

Languages: Papers will be published in English, French or German.

Submission of papers

Papers should be sent to one of the following Editors:
Professor J. O'M. Bockris, John Harrison Laboratory of Chemistry,
University of Pennsylvania, Philadelphia 4, Pa. 19104, U.S.A.
Dr. R. H. Ottewill, Department of Chemistry, The University, Bristol 8, England.
Dr. R. Parsons, Department of Chemistry, The University, Bristol 8, England.
Professor C. N. Reilley, Department of Chemistry,
University of North Carolina, Chapel Hill, N.C. 27515, U.S.A.

Authors should preferably submit two copies in double-spaced typing on pages of uniform size. Legends for figures should be typed on a separate page. The figures should be in a form suitable for reproduction, drawn in Indian ink on drawing paper or tracing paper, with lettering etc. in thin pencil. The sheets of drawing or tracing paper should preferably be of the same dimensions as those on which the article is typed. Photographs should be submitted as clear black and white prints on glossy paper. Standard symbols should be used in line drawings, the following are available to the printers:

All references should be given at the end of the paper. They should be numbered and the numbers should appear in the text at the appropriate places.
A summary of 50 to 200 words should be included.

Reprints

Fifty reprints will be supplied free of charge. Additional reprints (minimum 100) can be ordered at quoted prices. They must be ordered on order forms which are sent together with the proofs.

Publication

The *Journal of Electroanalytical Chemistry and Interfacial Electrochemistry* appears monthly. For 1969, each volume has 3 issues and 4 volumes will appear.
Subscription price: Sfr. 316.— (U.S. $ 74.60) per year incl. postage. Additional cost for copies by air mail available on request. For subscribers in the U.S.A. and Canada, 2nd class postage paid at Jamaica, N.Y. For advertising rates apply to the publishers.

Subscriptions should be sent to:

ELSEVIER SEQUOIA S.A., P.O. Box 851, 1001 Lausanne 1, Switzerland

Think of any electrochemical experiment... Chances are the PAR Model 170 can perform it.

Our new Model 170 Electrochemistry System thrives on variety. It offers — for the first time in a single instrument — all the circuitry and control functions necessary to perform virtually every commonly-used electrochemical technique.

For example, it allows you to perform chronopotentiometry or chronoamperometry without requiring any auxiliary equipment. It also contains built-in controls for current reversal at a potential threshold. What's more, the 170's 100 volts of potentiostat compliance, and its 1 amp capability at this voltage (or 5 amps at 20 volts) mean that you can work in the most exotic solvent systems.

The 170 can also perform:

- phase-sensitive ac polarography
- pulse polarography
- dc polarography
- anodic stripping analysis
- cyclic voltammetry
- pH and specific ion measurement
- direct potentiometry
- controlled-potential electrolysis
- controlled-current electrolysis
- chronopotentiometry
- chronoamperometry
- pulse response studies

The Model 170 contains a built-in X-Y plotter for accurate current-voltage curve recording as well as a highly stable coulometric integrator and an accurate time-base generator. The only external equipment occasionally required is an oscilloscope.

The price? With mechanical drop timer and built-in X-Y recorder, $11,500. For more information, write Princeton Applied Research Corporation, Box 565, Princeton, N. J. 08540, or call (609) 924-6835.

For those applications requiring a less complex instrument with capability to perform dc, ac and pulse polarography, inquire about the Model 171 Polarographic Analyzer and Recorder.

PAR **PRINCETON APPLIED RESEARCH CORPORATION**

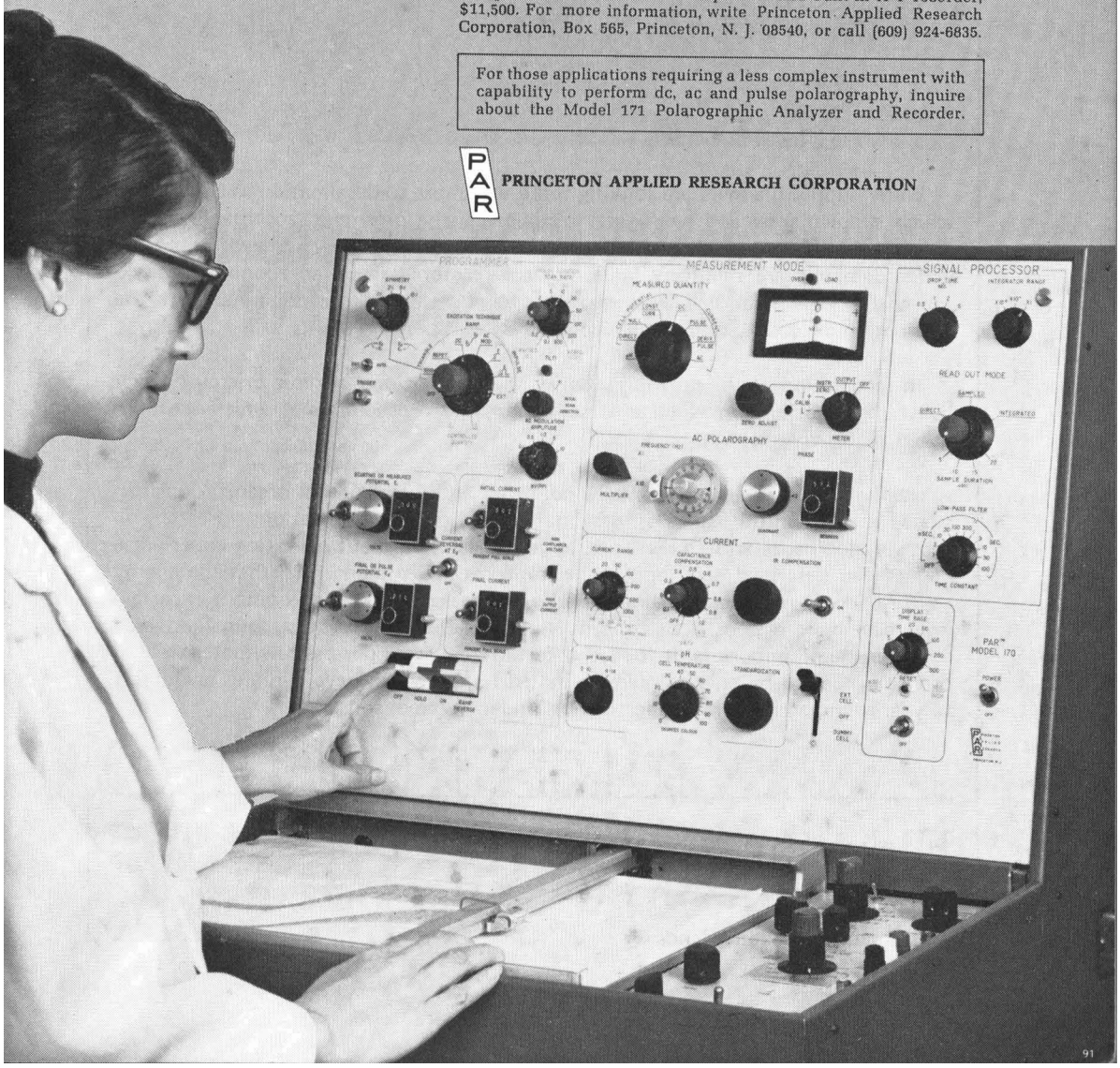

NUCLEAR DESALINATION

Proceedings of a Symposium on Nuclear Desalination held by the International Atomic Energy Agency in Madrid, 18-22 November 1968

Published for the International Atomic Energy Agency, Vienna, Austria

6½ x 9½", xvi + 941 pages, 302 illus., 1969, Dfl. 110.00
SBN 444-40806-1

Water supply planners are looking more and more to desalination as a means by which supplemental and new water supplies can be offered at acceptable cost in those regions where natural water supplies are becoming fully utilized. There the water demands are relatively large, nuclear reactors can be an economic energy source for a desalination plant, especially when desalination is combined with the production of electricity in dual-purpose and multi-purpose plants.

In recognition of the growing interest, the International Atomic Energy Agency held a Symposium on Nuclear Desalination, the proceedings of which are published in this volume.

Nearly 300 participants from 36 countries and international organizations discussed more than 60 papers on desalination and reactor applications, research, recent developments and studies, and large desalination plant operating experience. Papers also described agro-industrial complexes and the potential that the energy centre concept may hold for integrated and large-scale area development in certain underdeveloped regions. This concept is of special interest to those countries which are now major importers of food and fertilizers; which possess raw materials that can be processed by energy-intensive industries; or which have climates favourable to year-round agriculture and fertile but 'under-watered' soils.

Elsevier

P.O. Box 211
Amsterdam - The Netherlands

186 E

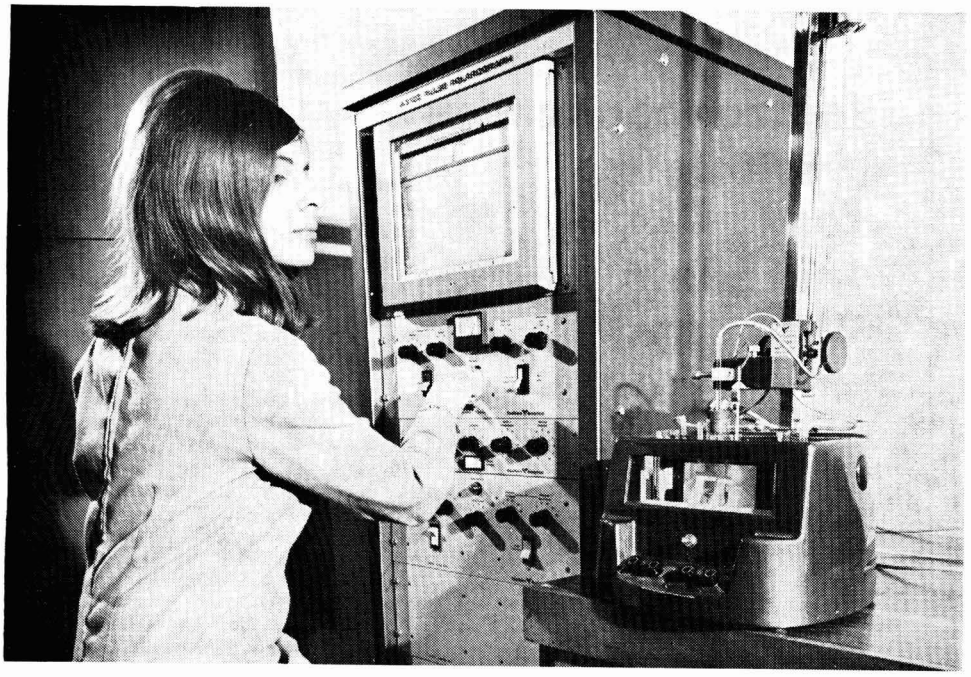

If you need to find 10^{-9}M, without spending 10^{4}£, get a Southern A3100

When it comes to determining minute traces (in even the smallest samples), there's nothing like pulse polarography at anywhere near the price. And the Southern A3100 is the most sophisticated pulse polarograph you can buy. It has higher sensitivity, resolution and selectivity than any other electrochemical instrument in analytical work, and its wide range of variable parameters makes it an invaluable tool in electrode reaction studies or reaction kinetics research.

With all adjustments made for maximum sensitivity, it will determine reversibly-reducible ions down to about 10^{-9}M and by the use of hanging drop techniques this can be extended to 10^{-10} to 10^{-11}M. The sensitivity for irreversible reactions is about 10^{-8}M to $5x10^{-8}$M.

For determining impurities in metals and semiconductors, corrosion products, residual monomers and other organic materials, and for electrokinetic research—the A3100 can solve your analytical problems at a down-to-earth price.

And if $5x10^{-9}$M will do, look at the A1660

Southern also makes an advanced differential cathode-ray polarograph that is useful in a wide range of analytical applications including metallurgical analysis, effluent analysis, and determination of trace metals and essential minerals in food and drugs. Based on original work by Davis and Seaborn, the A1660 features high sensitivity plus exceptional versatility. Ask for the descriptive leaflet. For full details, contact Southern Analytical Limited, Camberley, Surrey. Camberley 3401. Telex: 85210.

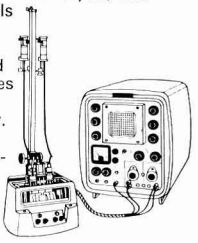

SOUTHERN ANALYTICAL

337

JOURNAL OF ELECTROANALYTICAL CHEMISTRY AND INTERFACIAL ELECTROCHEMISTRY

VOL. 23 (1969)

JOURNAL
of
ELECTROANALYTICAL CHEMISTRY
and
INTERFACIAL ELECTROCHEMISTRY

AN INTERNATIONAL JOURNAL DEVOTED TO ALL ASPECTS OF ELECTROANALYTICAL CHEMISTRY, DOUBLE LAYER STUDIES, ELECTROKINETICS, COLLOID STABILITY AND ELECTRODE KINETICS

VOL. 23 1969

ELSEVIER SEQUOIA S.A.

LAUSANNE

PRINTED IN THE NETHERLANDS

ELECTROANALYTICAL CHEMISTRY AND INTERFACIAL ELECTROCHEMISTRY
Elsevier Sequoia S.A., Lausanne – Printed in The Netherlands

ANODIC STRIPPING PULSE VOLTAMMETRY

GARY D. CHRISTIAN
Department of Chemistry, University of Kentucky, Lexington, Kentucky 40506 (U.S.A.)
(Received August 14th, 1968; in revised form March 31st, 1969)

Anodic or cathodic stripping voltammetry has proved to be a remarkably sensitive tool for the trace determination of metals or anions which can be plated on an electrode and subsequently stripped from the electrode. This technique in essence has been known for many years. Grower[1] and later Francis[2] and Ogarev[3] measured the coulombs required to dissolve a metal and determine the thickness of metal coatings. Zbinden[4], Elema[5] and Zakharevskii[6] determined trace metals by deposition followed by dissolution. Lord *et al.*[7] determined 5×10^{-10} g of silver in 20 μl volume by measuring the coulombs required for dissolution of the deposited silver from a platinum electrode. DeMars and Shain[8] and Kemula and Kublick[9] employed the hanging mercury drop electrode for anodic stripping voltammetry.

Besides linear varying potential stripping voltammetry, current step methods have been used[10]. Barker[11,12] used anodic stripping analysis to increase the sensitivity of square wave polarography. Sturm and Ressel[13] have also described anodic stripping voltammetry in square wave polarography. The principal disadvantage of square wave polarography is the requirement of a high concentration of supporting electrolytes. Underkofler and Shain[14] investigated a.c. polarography at stationary electrodes and applied this to stripping analysis. They achieved an order of magnitude increase in sensitivity over conventional d.c. methods by using a phase selective detector. Eisner and coworkers[15] also obtained an order of magnitude enhancement in sensitivity using a.c. stripping analysis. Roizenblat and Brainina[16] determined traces of metals by a.c. stripping analysis at graphite electrodes. The pre-electrolysis time was a twentieth of that required for d.c. stripping analysis.

A major problem in stripping analysis is the presence of trace impurities in supporting electrolytes which interfere with the determination of very small amounts of material. Pulse polarography[17,18], besides enhancing the sensitivity over square wave polarography, can employ very dilute supporting electrolytes. The present paper reports on the use of this sensitive tool for anodic stripping voltammetry at the hanging mercury drop electrode. Pulse polarography at the hanging mercury drop electrode has been described[19]. Anodic stripping voltammetry of biological samples has been reported in which addition of an supporting electrolyte is not required[20]. Kaplan and Rezakova[21] determined tellurite and selenosulfate by pulse polarography by cathodic stripping analysis at a stationary mercury electrode. They showed that the selenium and tellurium were accumulated on the electrode as a surface film.

EXPERIMENTAL

Reagent-grade chemicals were used throughout. Water used to prepare solu-

tions was deionized on a mixed-bed ion-exchange resin and was then distilled from alkaline permanganate. Hydrochloric acid was distilled before use. A stock 10^{-3} *M* solution of cadmium was prepared and standardized by titrating with EDTA[22]. More dilute solutions ($\geqslant 10^{-6}$ *M*) were prepared by diluting this stock solution prior to use. Solutions to be analyzed (10^{-9}–10^{-6} *M*) were prepared by adding 5 μl of an appropriate solution to 5 ml of electrolyte in the cell. The micropipette was calibrated coulometrically[23] to an accuracy of 0.2%.

Pulse polarographic measurements were made with a Melabs pulse polarographic analyzer, Model CPA-3, which utilizes a three-electrode system. A platinum counter electrode was used with a saturated calomel electrode (SCE) as reference. A pulse of 100 ms duration was applied to the electrode every 2 s. The resulting current was measured for 33 ms starting 50 ms after the application of the pulse.

Currents were recorded on either a Bausch and Lomb VOM-7 recorder or a Sargent Model SRL recorder.

Conventional anodic stripping polarograms were obtained on a Sargent Model FS polarograph using the cell previously described[20].

The hanging mercury drop electrode was prepared as previously described[20]. The mercury drop suspended from the electrode was collected from the same capillary employed before[19] and had an area of 0.0509 cm^2. A fresh drop was suspended for each polarogram. After each series of runs in a given solution, the electrode was re-etched in *aqua regia* and replated to prevent contamination from previous runs.

Solutions were de-aereated with nitrogen (introduced through a Teflon catheter tube) for 10 min prior to electrodeposition and anodic stripping. During the course of the experiment, a nitrogen atmosphere was maintained above the solution. Solutions were thermostatted at 23.0 ± 0.2°C.

Solutions were stirred during electrodeposition with a magnetic stirrer driven by a synchronous rotating motor. Following deposition for a measured time, the stirring was stopped for 10 s and then the potential was scanned in a positive direction to strip the deposited metal anodically from the electrode. A pulse was applied during pre-electrolysis.

After each set of experiments on a given solution, the cell was cleaned by boiling in *aqua regia*.

RESULTS AND DISCUSSION

Differential mode

A residual current polarogram is shown in Fig. 1. The curve goes through a maximum at about -0.5 V *vs.* SCE. The peak at -0.35 V was a lead peak due to an impurity in the electrolyte. A typical anodic stripping peak for 2×10^{-8} *M* cadmium is shown in Fig. 2. A nearly full (0.05 μA) scale deflection peak (*ca.* 0.035 μA) was obtained after only 5 min electrodeposition using one-tenth maximum sensitivity of the polarograph. The large lead peak was due to the impurity in the electrolyte. Using the Sargent Model FS polarograph, a 10^{-7} *M* cadmium solution gave a stripping peak of 0.047 μA after 5 min electrodeposition; this was 47% full scale deflection at maximum sensitivity of the instrument. Normally, an electrolysis time of 30 min would be required to obtain a satisfactory stripping peak of 10^{-8} *M* cadmium. Thus, the pulse polarographic method appears to be about an order of magnitude more

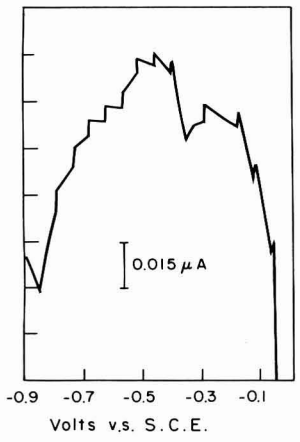

Fig. 1. Differential anodic stripping residual curve for 0.01 *M* HCl. Pre-electrolyzed 60 s, 30 mV pulse, potential scan rate 3.3 mV s^{-1}.

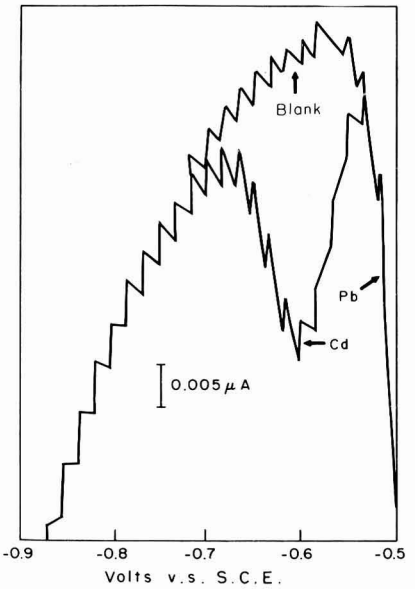

Fig. 2. Differential anodic stripping peak for 2×10^{-8} *M* Cd in 0.01 *M* HCl. Pre-electrolyzed 5 min, 100 mV pulse, potential scan rate 10 mV s^{-1}.

sensitive than the conventional techniques and perhaps more so. A limit of the sensitivity is the slope of the residual curve. Hence, while it is possible to use the maximum sensitivity, this is difficult except in ideal cases. A stripping peak of 0.011 μA above the blank was obtained for 10^{-9} *M* cadmium in 0.01 *M* ammonia–0.005 *M* ammonium sulfate after 30 min pre-electrolysis, which demonstrates the linearity between peak height and electrolysis time and concentration.

Calibration curves were run in 0.01 *M* hydrochloric acid. A linear curve was obtained for $1\text{–}5 \times 10^{-8}$ *M* cadmium (pre-electrolyzed 5 min at −0.9 V *vs.* SCE, +100 mV pulse, potential scan rate 10 mV s^{-1}) and for $1\text{–}6 \times 10^{-6}$ *M* cadmium (pre-electrolyzed 1 min at −0.9 V *vs* SCE, +30 mV pulse, potential scan rate 33.3 mV s^{-1}). The reproducibility is indicated in Table 1 for 10^{-8} *M* cadmium. These data were obtained by drawing a straight line from shoulder to shoulder on the polarogram

TABLE 1

REPRODUCIBILITY OF STRIPPING PEAKS

1×10^{-8} *M* Cd, pre-electrolyzed 5 min, 100 mV pulse, potential scan rate 10 mV s^{-1}.

i peak/μA	*Sensitivity μA full scale*
0.0118	0.05
0.0121	0.015
0.0120	0.05
0.0119	0.05

and measuring from this to the peak. This was satisfactory and more convenient for routine analyses provided a definite peak was obtained and it had been ascertained that impurities in the blank were insignificant.

The effect of potential scan rate on peak height is shown in Table 2. A maximum was reached at about 10 mV s^{-1}. Reproducibility was not good at the two faster scan rates. The peak potential was essentially independent of scan rate. Table 3 summarizes the effect of pulse magnitude on the peak height. The larger the pulse, the greater the peak height. Again, the peak potential did not change significantly.

TABLE 2

EFFECT OF VOLTAGE SCAN RATE ON DIFFERENTIAL STRIPPING PEAK

1×10^{-6} *M* Cd in 0.01 *M* HCl, pre-electrolyzed 60 s, pulse 30 mV

mV s^{-1}	*i peak*/μA	E_{peak}/*V vs. SCE*
100	0.034	−0.52
33.3	0.090	−0.52
10	0.111	−0.54
3.33	0.082	−0.53

TABLE 3

EFFECT OF PULSE MAGNITUDE ON DIFFERENTIAL STRIPPING PEAK

1×10^{-6} *M* Cd in 0.01 *M* HCl, pre-electrolyzed 60 s, potential scan rate 33.3 mV s^{-1}

Pulse/mV	*i peak*/μA	E_{peak}/*V vs. SCE*
10	0.026	−0.50
30	0.090	−0.52
100	0.27	−0.50

TABLE 4

EFFECT OF SUCCESSIVE SCANS ON PEAK HEIGHT FOLLOWING PRE-ELECTROLYSIS

1×10^{-6} *M* Cd in 0.01 *M* NH_3–0.005 *M* $(NH_4)_2SO_4$, pH 9.2, pre-electrolyzed 60 s, 100 mV pulse, potential scan rate 10 mV s^{-1}

No. of scans	*i peak*/μA
1	0.35
2	0.21
3	0.15
4	0.11

When analyzing very dilute solutions using a high polarograph sensitivity, it is sometimes difficult to get the peak on scale. The effect of multiple anodic scans was investigated and is given in Table 4. Polarograms were run from −0.8 to −0.3 V *vs.* SCE and then were re-run immediately. It is evident that the entire amalgam was not stripped in a single scan, and the peak height decreased exponentially with successive scans. A calibration curve of this type could be used to correct the initial scan if the peak was not recorded on this scan.

One of the main advantages of pulse polarography over square wave polarography is that dilute supporting electrolyte solutions can be employed. This is because the duration of the pulse is relatively long (*e.g.*, 100 ms) allowing sufficient time for the charging current to decay to a negligibly small value (*ca.* 50 ms) before measuring the faradaic current. In square wave polarography, supporting electrolyte concentrations of the order of 1 *M* are commonly required because of the shorter pulses applied with the necessity for the charging current to decay rapidly ; the time required for the charging current to decay to a given fraction of its initial value is proportional to the resistance of the cell circuit. With a three-electrode circuit, the *IR* drop in the solution is of small significance. Parry and Osteryoung[24] have used 10^{-3} *M* supporting electrolytes. The problem of electrolyte impurities is particularly severe in anodic stripping voltammetry, and hence pulse polarography offers a distinct advantage. It appears that extremely small concentrations of electrolyte can be employed. A series of stripping peaks was obtained using different concentrations of electrolyte. Peak characteristics are summarized in Table 5. Reasonable peaks were obtained even

TABLE 5

EFFECT OF SUPPORTING ELECTROLYTE CONCENTRATION ON STRIPPING PEAK

3×10^{-6} *M* Cd in KCl, pre-electrolyzed 60 s, 100 mV pulse, potential scan rate 3.33 mV s^{-1}

KCl/M	*i peak/μA*	$E_{peak/V\ vs.\ SCE}$	*½ peak width/mV*
0	0.81	−0.598	138
1×10^{-5}	0.78	−0.597	128
1×10^{-4}	0.81	−0.606	132
1×10^{-3}	0.84	−0.607	130
1×10^{-2}	0.84	−0.605	120

with no supporting electrolyte. The peak potential generally shifted to more negative potentials as the electrolyte concentration was increased up to 10^{-4} *M*. Also, the half-peak width generally became smaller as the electrolyte was increased. The cadmium in the solution with no supporting electrolyte probably served as the electrolyte and smaller concentrations of cadmium may require some electrolyte. The reproducibility was not as good at very low concentrations of electrolytes, and the concentration should be kept at 10^{-3} *M* or more if possible.

Integral mode

A stripping peak and blank in this mode are shown in Fig. 3. A comparison of wave height in the integral mode and peak height in the differential mode was made by pre-electrolyzing a 10^{-6} *M* cadmium solution for 1 min. The wave height in the former mode was 0.66 μA while the peak height in the differential mode was 0.11 μA. This greater sensitivity was opposed by the steepness of the residual curve slope in the integral mode and better sensitivity can be obtained in the differential mode.

Besides a hanging mercury drop electrode, anodic stripping pulse voltammetry should be applicable to other stationary and solid electrodes such as platinum[7,25], graphite[26], carbon paste[27], mercury plated[28,29], composite graphite-mercury[30], and mercury pool[10,31] electrodes. Some of these, especially the mercury plated or deposited electrodes, should give a further increase in sensitivity over the hanging

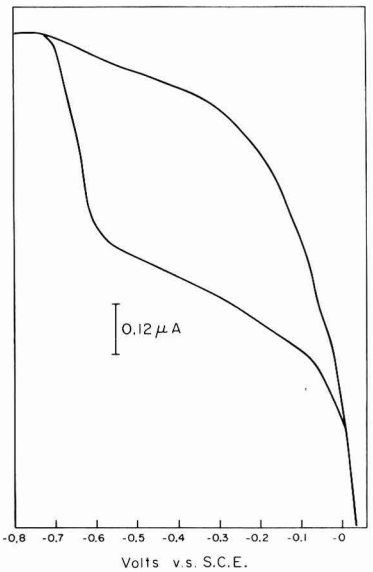

Fig. 3. Integral stripping peak and blank for 1×10^{-6} *M* Cd in 0.01 *M* NH_3–0.005 *M* $(NH_4)_2SO_4$. Pre-electrolyzed 60 s, potential scan rate 3.33 mV s^{-1}.

mercury drop electrode. In addition to anodic stripping methods, cathodic stripping analysis should be applicable to this technique for the determination of anions[32,33]. The sensitivity of stripping methods has been reported to be increased by an order of magnitude by heating the test solution to near boiling during the pre-electrolysis step[34].

SUMMARY

The anodic oxidation of cadmium amalgam at the hanging mercury drop electrode was studied. Sensitivity was increased about an order of magnitude over conventional stripping methods. Effects of pulse magnitude and potential scan rate in the differential mode were investigated. Very dilute supporting electrolytes could be employed, a major advantage in these sensitive stripping methods.

REFERENCES

1 G. G. GROWER, *Proc. Am. Soc. Testing Materials*, 17 (1917) 129.
2 H. T. FRANCIS, *J. Electrochem. Soc.*, 93 (1948) 79.
3 A. OGAREV, *J. Applied Chem. USSR, English Transl.*, 19 (1946) 311.
4 C. ZBINDEN, *Bull. Soc. Chim. Biol.*, 13 (1931) 35.
5 B. ELEMA, *Antonie van Leeuwenhoek, J. Microbiol. Serol. Jubilee Vol. Albert J. Kluyver*, 12 (1947) 243.
6 M. S. ZAKHAREVSKII, *Ref. Zh. Khim.*, 2 (1939) 84.
7 S. S. LORD, JR., R. C. O'NEILL AND L. B. ROGERS, *Anal. Chem.*, 24 (1952) 209.
8 R. D. DEMARS AND I. SHAIN, *Anal. Chem.*, 29 (1957) 1825.
9 W. KEMULA AND Z. KUBLICK, *Anal. Chim. Acta*, 18 (1958) 104.
10 J. T. PORTER AND W. D. COOKE, *J. Am. Chem. Soc.*, 77 (1955) 1481.
11 G. C. BARKER, *At. Energy Res. Estab. G. Brit.*, C/R-1563 (1957).

12 G. C. BARKER, *Anal. Chim. Acta*, 18 (1958) 118.
13 F. V. STURM AND M. RESSEL, *Z. Anal. Chem.*, 186 (1962) 63.
14 W. L. UNDERKOFLER AND I. SHAIN, *Anal. Chem.*, 37 (1965) 218.
15 U. EISNER, C. YARNITZKY, Y. NEMIROWSKY AND M. ARIEL, *Israel J. Chem.*, 4 (1966) 215.
16 E. M. ROIZENBLAT AND KH. Z. BRAININA, *Zavodsk. Lab.*, 32 (1966) 145.
17 G. C. BARKER AND A. W. GARDNER, *At. Energy Res. Estab. G. Brit.*, C/R-2297 (1958).
18 V. I. BODYU, I. V. KOTLOVA AND U. S. LYAPIKOV, *Zavodsk. Lab.*, 28 (1963) 1042.
19 G. D. CHRISTIAN, *J. Electroanal. Chem.*, 22 (1969) 333.
20 C. L. NEWBERRY AND G. D. CHRISTIAN, *J. Electroanal. Chem.*, 9 (1965) 468.
21 B. YA. KAPLAN AND A. S. REZAKOVA, *Zh. Analit. Khim.*, 21 (1966) 1268.
22 H. A. FLASCHKA AND A. J. BARNHARD, JR. in C. L. WILSON AND D. W. WILSON, Eds., *Comprehensive Analytical Chemistry*, Vol. IB, Elsevier Publishing Co., New York, 1960, p. 354.
23 G. D. CHRISTIAN, *Microchem. J.*, 9 (1965) 16.
24 E. P. PARRY AND R. A. OSTERYOUNG, *Anal. Chem.*, 37 (1965) 1634.
25 M. M. NICHOLSON, *Anal. Chem.*, 32 (1960) 1058.
26 S. P. PERONE, *Anal. Chem.*, 35 (1963) 2091.
27 E. S. JACOBS, *Anal. Chem.*, 35 (1963) 2112.
28 S. BRUCKENSTEIN AND T. NAGAI, *Anal. Chem.*, 33 (1961) 1201.
29 K. W. GARDINER AND L. B. ROGERS, *Anal. Chem.*, 25 (1953) 1393.
30 W. R. MATSON, D. K. ROE AND D. E. CARRIT, *Anal. Chem.*, 37 (1965) 1594.
31 J. G. NIKELLY AND W. D. COOKE, *Anal. Chem.*, 29 (1957) 933.
32 I. SHAIN AND S. P. PERONE, *Anal. Chem.*, 33 (1966) 325.
33 R. G. BALL, D. L. MANNING AND O. MENIS, *Anal. Chem.*, 32 (1960) 621.
34 YU. A. KARBAINO AND A. G. STROMBERG, *Sovrem. Metody Khim. Spectral. Anal. Mater.*, (1967) 230.

ELECTROANALYTICAL CHEMISTRY AND INTERFACIAL ELECTROCHEMISTRY
Elsevier Sequoia S.A., Lausanne – Printed in The Netherlands

ON THE IMPEDANCE OF GALVANIC CELLS

XXVI. APPLICATION OF THE COMPLEX PLANE METHOD IN THE CASE OF MIXED CURRENTS

B. G. DEKKER, M. SLUYTERS-REHBACH AND J. H. SLUYTERS
Laboratory of Analytical Chemistry, State University, Utrecht (The Netherlands)
(Received March 22nd, 1969)

INTRODUCTION

The impedance of a galvanic cell has proved to be a very useful datum for the study of faradaic processes and double-layer phenomena at the electrode–solution interface[1,2]. In general, the kinetic parameters and the double-layer capacity can be obtained by analysis of the impedance data according to the complex plane method[2]. Procedures for analysing data have been proposed for a number of cases, limited, however, to electrode processes with one electrode reaction proceeding.

Within the framework of our study on the hydrogen evolution on mercury in concentrated acid solutions[3], the impedance of the mercury electrode in a concentrated HI solution was measured. It was found that this system gives rise to the appearance of a so-called mixed current caused by the simultaneous occurrence of two electrode reactions, *viz.* the Hg/HgI_4^{2-} reaction and the $H^+/H_2(Hg)$ reaction.

The aim of this paper is to investigate the applicability of the complex plane method to cases of mixed currents.

ANALYSIS OF CELL IMPEDANCES IN THE CASE OF TWO SIMULTANEOUSLY PROCEEDING ELECTRODE REACTIONS

We confine our discussion to the simultaneous proceeding of two electrode reactions because the equations for more than two processes are somewhat cumbersome. Moreover, it will appear that the results in that case are trivial or that the complex plane method is not feasible.

Two simple electrode reactions are considered, *i.e.* the exchange of n_i electrons occurs in one charge transfer step, in the absence of coupled chemical reactions and of chemical reactions between the components in the solution.

$$Ox_1 + n_1 e \rightleftarrows Red_1 \quad (1)$$

$$Ox_2 + n_2 e \rightleftarrows Red_2 \quad (2)$$

Both reactions will be characterized by a large number of factors, such as the electrode potential, E, the standard potentials, E°, the specific heterogeneous rate constants, k_{sh}, the transfer coefficients, α, the diffusion coefficients, D, the temperature, and the initial presence of Ox and Red. The complex plane analysis yields the values of the impedance parameters θ_i (transfer resistances) and σ_i (Warburg coefficients) and C_d (double-layer capacity), eventually as a function of E. Once these are known, an

attempt can be made to calculate the values of k_{sh}, α and D from the parameters obtained using the equations derived by Timmer *et al.*[4]

It is known from d.c. polarography that in the case of several simultaneously proceeding oxidation or reduction reactions, the d.c. current at a certain potential is equal to the algebraic sum of the currents for each process. Wagner and Traud[5] showed that the same additivity holds for the superposition of an anodic and a cathodic wave. It is reasonable to assume that this also holds for a.c. currents, which means that two faradaic impedances Z_{F_1} and Z_{F_2} in parallel appear in the equivalent circuit of the cell impedance, given by[1]

$$Z_{F_i} = \theta_i + \sigma_i \omega^{-\frac{1}{2}}(1-j) \tag{3}$$

where ω is the angular a.c. frequency and $j=\sqrt{-1}$, the imaginary unit. The equivalent circuit of the cell impedance is presented in Fig. 1, where R_Ω is the ohmic resistance of the cell and C_d the double-layer capacity. Note that in this modified Randles circuit[1], possible (strong) specific adsorption of reactants has not been considered[6].

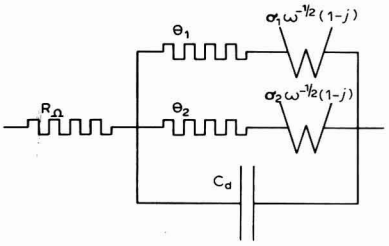

Fig. 1. Equivalent circuit of the impedance of a galvanic cell with two simultaneoulsy proceeding electrode reactions.

The usual procedure in the analysis is the calculation of the real and imaginary components of the admittance of the electrode–solution interface (electrode admittance) after subtraction of R_Ω from the real part of the cell impedance, Z', and combination of the remainder with the imaginary part, Z'':

$$Y'_{el} = \frac{Z' - R_\Omega}{(Z'-R_\Omega)^2 + (Z'')^2} \tag{4a}$$

$$Y''_{el} = \frac{Z''}{(Z'-R_\Omega)^2 + (Z'')^2} \tag{4b}$$

It follows from Fig. 1 and eqn. (3) that

$$Y'_{el} = \frac{1}{\sigma_1 \omega^{-\frac{1}{2}}} \frac{p_1+1}{p_1^2+2p_1+2} + \frac{1}{\sigma_2 \omega^{-\frac{1}{2}}} \frac{p_2+1}{p_2^2+2p_2+2} \tag{5a}$$

$$Y''_{el} = \frac{1}{\sigma_1 \omega^{-\frac{1}{2}}} \frac{1}{p_1^2+2p_1+2} + \frac{1}{\sigma_2 \omega^{-\frac{1}{2}}} \frac{1}{p_2^2+2p_2+2} + \omega C_d \tag{5b}$$

where the irreversibility quotients, p_i, are defined by

$$p_i = p'_i \omega^{\frac{1}{2}} = \frac{\theta_i}{\sigma_i \omega^{-\frac{1}{2}}} \tag{6}$$

These equations are generally valid for reversible as well as irreversible reactions.

It can be seen that the value of C_d need not be known for the evaluation of θ_i and σ_i (eqn. (5a)) which is an outstanding feature of the complex plane method. As a particular advantage of the method, C_d can be determined in the presence of the electrode reactions if θ_i and σ_i are known (see eqn. (5b)). This is especially important for those cases where C_d cannot be measured in the absence of electroactive species[7]. In this paper C_d will be considered as unknown.

Evaluation of θ_i, σ_i and C_d

The frequency-dependence of Y'_{el} at a fixed potential is, in the complex plane analysis, the criterion of the extent to which an electrode reaction is reversible. The reaction behaves reversibly if Y'_{el} increases linearly with $\omega^{\frac{1}{2}}$ within the range covered by the measurements, normally between $\omega_1 = 2 \times 10^3$ and $\omega_2 = 2 \times 10^4 \, s^{-1}$. The reaction may be said to be irreversible if Y'_{el} is independent of $\omega^{\frac{1}{2}}$ in the frequency range mentioned. In the case of one electrode reaction, the values of p', σ and θ can be evaluated from the frequency-dependence of Y'_{el} by a curve-fitting procedure, *cf.* ref. 8. In the following it will be discussed for which values of p'_1 and p'_2 the values of θ_1, θ_2, σ_1 and σ_2 can be determined from the frequency-dependence of the total electrode admittance.

When it is assumed that neither of the electrode reactions has a negligible contribution to the total electrode admittance, it is useful to consider three cases: (A) $p'_1 \approx p'_2$, (B) $p'_1 \neq p'_2$ where $3 \times 10^{-3} < p'_i < 3 \times 10^{-1}$ and (C) $p'_1 \ll p'_2$.

(*A*) $p'_1 \approx p'_2$

(*i*) $3 \times 10^{-3} < p'_i < 3 \times 10^{-1}$

In Fig. 2 values of Y'_{el} for reaction 1 (curve 1) and 2 (curve 2) and of the sum-admittance (curve 3) are represented as a function of $\omega^{\frac{1}{2}}$; the values are calculated numerically, using the data: $\theta_1 = 6$ Ωcm^2, $\sigma_1 = 200$ Ωcm^2 s$^{-\frac{1}{2}}$, $\theta_2 = 15$ Ωcm^2 and $\sigma_2 = 500$ Ωcm^2 s$^{-\frac{1}{2}}$ (*i.e.* $p'_1 = p'_2 = 3 \times 10^{-2}$). From Fig. 2 it appears that Y'_{el} increases non-linearly in the above-mentioned frequency range for all three curves. This means that curve (3) is composed of the admittances of two quasi-reversible electrode reactions. From the frequency-dependence of Y'_{el} the value of p'_1 ($= p'_2$) can be deter-

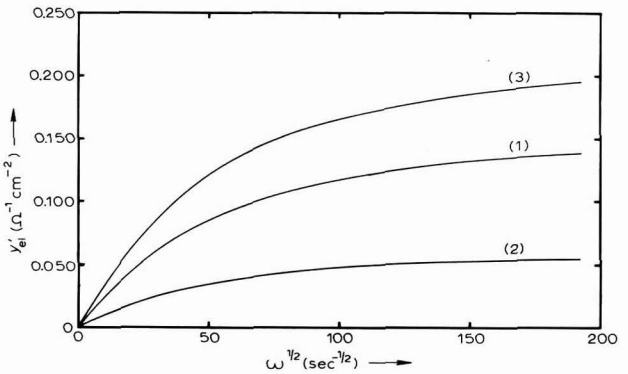

Fig. 2. Plots of Y'_{el} *vs.* $\omega^{\frac{1}{2}}$: (1) $p'_1 = 3 \times 10^{-2}$, $\theta_1 = 6$ Ω cm^2, $\sigma_1 = 200$ Ω cm^2 s$^{-\frac{1}{2}}$; (2) $p'_2 = 3 \times 10^{-2}$, $\theta_2 = 15$ Ω cm^2, $\sigma_2 = 500$ Ω cm^2 s$^{-\frac{1}{2}}$; (3) sum of (1) and (2).

mined in the usual way, *i.e.* by a curve-fitting procedure using eqn. (5a). However, it is not possible to evaluate the separate values of θ_1, σ_1, θ_2 and σ_2. In this case the substitution values are found:

$$\theta_s = \frac{\theta_1\theta_2}{\theta_1+\theta_2} \text{ and } \sigma_s = \frac{\sigma_1\sigma_2}{\sigma_1+\sigma_2}$$

Insertion of the results into eqn. (5b) gives C_d.

(*ii*) $p'_i < 3\times10^{-3}$

In this case both reactions behave reversibly in the frequency range mentioned. From the slope of the Y'_{el} (sum) *vs.* $\omega^{\frac{1}{2}}$ plot (which is a straight line with zero intercept) the value of σ_s can be calculated. It can be derived from eqns. (5) that C_d can be calculated from

$$C_d = \frac{Y''_{el} - Y'_{el}}{\omega} \tag{7}$$

(*iii*) $p'_i > 3\times10^{-1}$

In this case both reactions behave irreversibly in the frequency range mentioned. Y'_{el} (sum) is independent of frequency and equals $1/\theta_s$. The value of C_d can be obtained from eqn. (5b) which becomes:

$$Y''_{el} = \omega C_d \tag{8}$$

Thus, in the particular case where $p'_1 = p'_2$, the sum-admittance behaves as if one electrode reaction is proceeding. When p'_1 is almost equal to p'_2, the same results will be obtained with a relatively small error. If the measurements could be performed at much higher frequencies (*e.g.* in case (i) $\omega^{\frac{1}{2}} \gg 200\ s^{-\frac{1}{2}}$) both reactions behave irreversibly, and at measurements at very low frequencies (*e.g.* in case (i) $\omega^{\frac{1}{2}} < 10\ s^{-\frac{1}{2}}$) both reactions behave reversibly. For these cases the same results would be obtained as have already been discussed above.

(*B*) $p'_1 \neq p'_2$ *where* $3\times10^{-3} < p'_i < 3\times10^{-1}$

It appears from eqns. (5) that the impedance parameters, θ_i and σ_i, and hence the values of C_d, can be evaluated from the frequency dispersion of the sum-admittance by applying a mathematical variation procedure. However, in general this will not be feasible in view of the accuracy of the Y'_{el} values, the limited frequency region of the measurements, and the large number of parameters.

If the measurements could be performed at very high (*e.g.* $\omega^{\frac{1}{2}} \gg 200\ s^{-\frac{1}{2}}$) or very low (*e.g.* $\omega^{\frac{1}{2}} \ll 10\ s^{-\frac{1}{2}}$) frequencies the values of θ_s and σ_s could be obtained, and hence also the values of C_d for both cases.

(*C*) $p'_1 \ll p'_2$

(i) In Fig. 3, numerically calculated values of Y'_{el} for reaction 1 (curve 1) and 2 (curve 2) and values of the sum-admittance (curve 3) are represented as a function of $\omega^{\frac{1}{2}}$; the data used for the calculation are: $\theta_1 = 1.5\ \Omega cm^2$, $\sigma_1 = 500\ \Omega cm^2 s^{-\frac{1}{2}}$ (*i.e.* $p'_1 = 3\times10^{-3}$) and $\theta_2 = 30\ \Omega cm^2$, $\sigma_2 = 100\ \Omega cm^2 s^{-\frac{1}{2}}$ (*i.e.* $p'_2 = 3\times10^{-1}$).

It can be seen in Fig. 3 that in the frequency range normally covered by the measurements, the sum-admittance (curve 3) is composed of the admittances of a reversible (curve 1) and an irreversible electrode reaction (curve 2). In this case, eqn. (5a) reduces to:

$$Y'_{el} = \frac{\omega^{\frac{1}{2}}}{2\sigma_1} + \frac{1}{\theta_2} \tag{9a}$$

The Y'_{el} *vs.* $\omega^{\frac{1}{2}}$ plot is a straight line as in case (Aii) but now it has an intercept $1/\theta_2$. From the slope and the intercept of the plot the values of both σ_1 and θ_2 are readily obtained. Since eqn. (5b) reduces to

$$Y''_{el} = \frac{\omega^{\frac{1}{2}}}{2\sigma_1} + \omega C_d \tag{9b}$$

the values of C_d can be calculated by insertion into this equation of the σ_1 values found.

Figure 3 illustrates once more that both the values of p'_i and the frequency range in which the measurements are performed are important for the possibility of evaluating the impedance parameters from the Y'_{el} *vs.* $\omega^{\frac{1}{2}}$ plot. Two other combinations have to be considered:

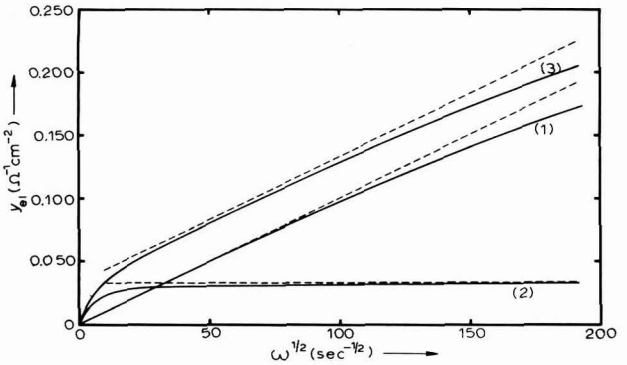

Fig. 3. Plots of Y'_{el} *vs.* $\omega^{\frac{1}{2}}$: (1) $p'_1 = 3 \times 10^{-3}$, $\theta_1 = 1.5\ \Omega\ cm^2$, $\sigma_1 = 500\ \Omega\ cm^2\ s^{-\frac{1}{2}}$; (2) $p'_2 = 3 \times 10^{-1}$, $\theta_2 = 30\ \Omega\ cm^2$, $\sigma_2 = 100\ \Omega\ cm^2\ s^{-\frac{1}{2}}$; (3) sum of (1) and (2). The broken lines show the divergence from straight lines.

(ii) The sum-admittance is composed of the admittances of a reversible and a quasi-reversible electrode reaction (*e.g.* this is the case in the example discussed above (Fig. 3) in the frequency range between $\omega_1^{\frac{1}{2}} \approx 0$ and $\omega_2^{\frac{1}{2}} = 30\ s^{-\frac{1}{2}}$). By substitution of $p'_1 = 0$ (reversible case) into eqn. (5a) one obtains:

$$\frac{Y'_{el}}{\omega^{\frac{1}{2}}} = \frac{1}{2\sigma_1} + \frac{1}{\sigma_2} \frac{p'_2 \omega^{\frac{1}{2}} + 1}{(p'_2 \omega^{\frac{1}{2}} + 1)^2 + 1} \tag{10}$$

It appears from eqn. (10) that it is possible to evaluate the unknown parameters, σ_1, θ_1 and σ_2, by means of a variation method. The accuracy of the results will be largely dependent on the accuracy of the Y'_{el} values and of the width of the frequency range used. The value of C_d can be calculated by insertion of the results into eqn. (5b).

(iii) The sum-admittance is composed of the admittances of a quasi-reversible and an irreversible electrode reaction (*e.g.* this is the case in the example discussed above (Fig. 3) at $\omega^{\frac{1}{2}} > 100$). By substitution of $p'_2 = \infty$ (irreversible case) into eqn. (5a) one obtains:

$$Y'_{el} = \frac{\omega^{\frac{1}{2}}}{\sigma_1} \frac{p'_1 \omega^{\frac{1}{2}} + 1}{(p'_1 \omega^{\frac{1}{2}} + 1)^2 + 1} + \frac{1}{\theta_2} \tag{11}$$

Also, in this case it is possible to evaluate the unknown parameters by means of a variation method. The accuracy is of the same order as discussed above (case ii). The value of C_d can be calculated by insertion of the results into eqn. (5b).

Application to the mercury electrode in concentrated HI

As an example we give the results of an analysis of the impedance of the DME in 57% HI. Experimental details will be described in a subsequent paper.

Figure 4 shows the d.c. current–voltage curve of the cell.

As mercury dissolves in very concentrated hydriodic acid with the evolution of hydrogen gas[9] it is likely that the current–voltage curve of Fig. 4 is composed of the current–voltage curves of two simultaneously proceeding electrode reactions, *viz.*

$$Hg + 4\,I^- \rightleftarrows HgI_4^{2-} + 2e \quad \text{(I)} \qquad \text{and} \qquad 2H^+ + 2e \rightleftarrows H_2 \quad \text{(II)}$$

The measured current–voltage curve is a so-called mixed current curve and is equal to the algebraic sum of the current–voltage curve for each process[5].

The impedance of the cell was measured as a function of potential (at 10 potentials in the potential range -530 to -630 mV) and as a function of frequency (420–2000 Hz). The potential region of the impedance measurements is indicated by two arrows in Fig. 4. The ohmic resistance R_Ω of the cell was found by measurements of Z' at some higher frequencies (up to 10 kHz) and extrapolation of Z' to infinite frequency. The value of Y'_{el} was calculated (eqn. (4a)) and plotted against $\omega^{\frac{1}{2}}$ for each potential. Straight lines were obtained at all potentials: between -530 and -590 mV, Y'_{el} increases linearly with $\omega^{\frac{1}{2}}$, and at potentials more negative than -590 mV, Y'_{el} is independent of $\omega^{\frac{1}{2}}$.

Measurements on the Hg/Hg_2^{2+} electrode reaction (*e.g.* in $HClO_4$ solutions[10]

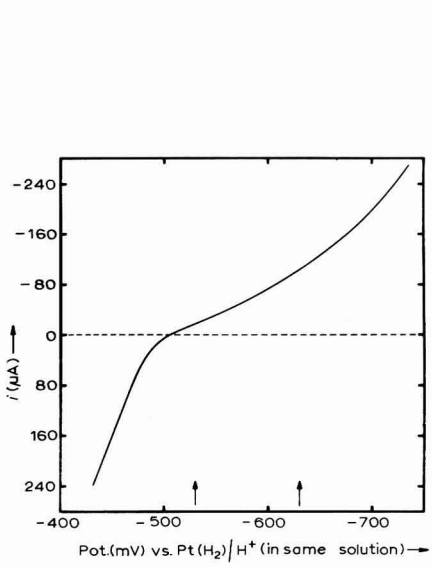

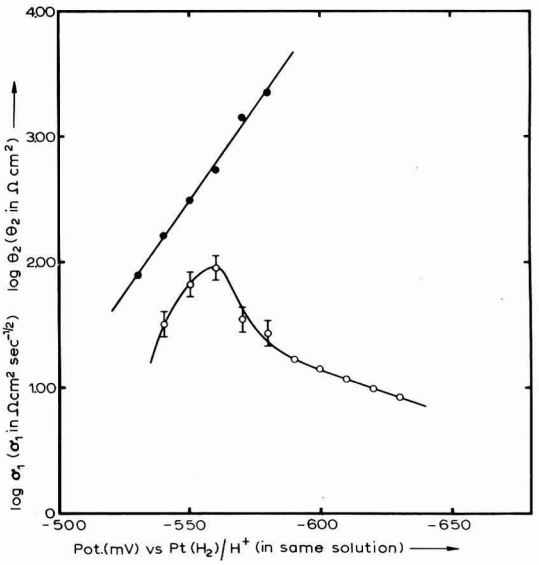

Fig. 4. D.c. current–voltage curve of the DME in 57% HI at 15°C. The vertical arrows indicate the potential region of the impedance measurements.

Fig. 5. Plot of the logarithmic value of the Warburg coefficient σ_1(●) and the activation polarization resistance θ_2(○) as a function of potential for the mercury electrode in 57% HI at 15°C.

and in HCl solutions[11]) have always shown that the reaction is reversible. It is therefore reasonable to assume that reaction (I) is reversible. The H^+/H_2(Hg) electrode reaction (reaction (II)) is known to be irreversible (see *e.g.* Vetter[12]).

Making allowance for the above, the experimental results have been analysed with eqn. (9a). The value of σ_1 (reaction (I)) was calculated from the slope of the Y'_{el} *vs.* $\omega^{\frac{1}{2}}$ plot and the value of θ_2 (reaction (II)) was calculated from the intercept. The results are presented in Fig. 5 in which log σ_1 and log θ_2 are plotted against the potential, E.

The log σ_1 *vs.* E plot is a straight line which is in accord with theory[4]. The slope of the line $-29.45\ V^{-1}$ agrees reasonably well with the theoretical slope, corresponding to $n=2$.

It is not possible to calculate the value of the diffusion coefficient $D_{HgI_4^{2-}}$, since the formal potential is unknown.

It can be seen in Fig. 5 that the log θ_2 *vs.* E curve is linear in the potential region -590 to -630 mV which is in agreement with theory[4] and previous measurements on the H^+/H_2(Hg) electrode reaction[3]. The equation of the line was calculated: log $\theta_2 = 5.40 + 7.10\ \eta$ (for the H^+/H_2(Hg) electrode reaction the potential E is equal to the overpotential η). The value of the cathodic transfer coefficient β was calculated from the slope of the line, and the value of the exchange current density, i_0, was obtained from the intercept: $\beta = 0.40$[5] and log $i_0 = -6.6$[2].

The shape of the log θ_2 *vs.* E plot in the potential region -540 to -590 mV is of interest (note that this is the potential range in which reaction (I) proceeds measurably): going from cathodic to anodic potentials the value of log θ_2 increases more steeply than the linear part at $E < -590$ mV. When a straight line is fitted through this part of the curve, a value $\beta = 1.3 \pm 0.3$ is calculated for the transfer coefficient. From a recent study by Krishtalik[13] concerning the hydrogen overpotential on mercury in acidified KI solutions, it is known that $\beta = 1$ in the case of a barrierless

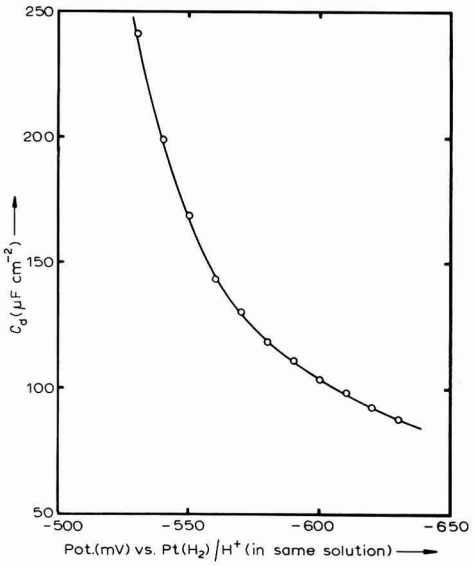

Fig. 6. Capacity–potential curve for mercury in 57% HI at 15°C.

discharge. Since also the shape of the log θ_2 *vs.* E plot between -560 and -630 mV is qualitatively similar to the plots that can be calculated from the experiments of Krishtalik, it is likely that in the potential region -560 to -590 mV barrierless discharge occurs.

It is not clear, however, why log θ_2 decreases at potentials larger than -560 mV. The values of C_d for the potential region between -530 and -590 mV were calculated from eqn. (9b), while for the potential region -590 to -630 mV eqn. (8) was used for the calculation. The results are presented in Fig. 6. No frequency-dependence of the calculated C_d-values was found which means that the equivalent circuit of the electrode impedance used for the determination of σ_1, θ_2 and C_d is able to describe the experiments.

CONCLUSION

In general, the complex plane method of analysing impedance data can also be applied to cases of two simultaneously proceeding electrode reactions. However, the accuracy of the results depends strongly on the values of the irreversibility quotients of both reactions and on the frequency range in which the measurements are performed.

ACKNOWLEDGEMENT

This investigation was supported in part by the Netherlands Foundation for Chemical Research (SON) with financial aid from the Netherlands Organization for the Advancement of Pure Research (Z.W.O.).

SUMMARY

The applicability of the complex plane method for the evaluation of the impedance parameters in the case of two simultaneously proceeding electrode reactions is discussed. It is shown that the possibility of the evaluation depends strongly on the values of the irreversibility quotients of both reactions and on the frequency range in which the measurements are performed. The theory is applied to impedance measurements with the dropping mercury electrode in azeotropic HI, in which case a mixed current appears.

REFERENCES

1 J. E. B. RANDLES, *Discussions Faraday Soc.*, 1 (1947) 11.
2 M. SLUYTERS-REHBACH, D. J. KOOIJMAN AND J. H. SLUYTERS, in G. J. HILLS (Ed.), *Polarography* (1964), MacMillan, London, p. 135.
3 B. G. DEKKER, M. SLUYTERS-REHBACH AND J. H. SLUYTERS, *J. Electroanal. Chem.*, 21 (1969) 137.
4 B. TIMMER M. SLUYTERS-REHBACH AND J. H. SLUYTERS, *J. Electroanal. Chem.*, 14 (1967) 169.
5 C. WAGNER AND W. TRAUD, *Z. Elektrochem.*, 44 (1938) 391.
6 M. SLUYTERS-REHBACH, B. TIMMER AND J. H. SLUYTERS, *J. Electroanal. Chem.*, 15 (1967) 151.
7 M. SLUYTERS-REHBACH AND J. H. SLUYTERS, *Rec. Trav. Chim.*, 83 (1964) 217, 581.
8 M. SLUYTERS-REHBACH AND J. H. SLUYTERS, *Electrochim. Acta*, 11 (1966) 73.
9 P. PASCAL, *Nouveau Traité de Chimie Minérale, Tome 5 (zinc–cadmium–mercure)*, Masson, Paris, 1962, p. 586.
10 M. SLUYTERS-REHBACH AND J. H. SLUYTERS, *Rec. Trav. Chim.*, 83 (1964) 967.
11 R. D. ARMSTRONG, M. FLEISCHMANN AND R. M. THIRSK, *Trans. Faraday Soc.*, 61 (1965) 2238.
12 K. J. VETTER, *Elektrochemische Kinetik*, Springer-Verlag, Berlin, 1961, pp. 410–497.
13 L. I. KRISHTALIK, *Electrochim. Acta*, 13 (1968) 1045.

ELECTROANALYTICAL CHEMISTRY AND INTERFACIAL ELECTROCHEMISTRY
Elsevier Sequoia S.A., Lausanne – Printed in The Netherlands

ON THE IMPEDANCE OF GALVANIC CELLS

XXVII. THE TEMPERATURE-DEPENDENCE OF THE KINETIC PARAMETERS OF THE HYDROGEN ELECTRODE REACTION ON MERCURY IN CONCENTRATED HI

B. G. DEKKER, M. SLUYTERS-REHBACH AND J. H. SLUYTERS
Laboratory of Analytical Chemistry, State University, Croesestraat 77-A, Utrecht (The Netherlands)
(Received March 22nd, 1969)

INTRODUCTION

In a previous paper[1] we presented a study concerning the temperature-dependence of the kinetic parameters of the hydrogen evolution reaction on Hg in 1 *M* HCl, 7.5 *M* HCl and 5.2 *M* $HClO_4$. In the case of 1 *M* HCl and 5.2 *M* $HClO_4$, the transfer coefficient β was found to be independent of temperature; in the case of 7.5 *M* HCl β was found to increase linearly with temperature. From the temperature-dependences of the exchange current densities i_0 the values of the apparent heats of activation ΔH were calculated: for 1 *M* HCl and 5.2 *M* $HClO_4$, $\Delta H \approx 20$ kcal mol^{-1} and for 7.5 *M* HCl, $\Delta H = 11.1$ kcal mol^{-1}. An explanation for these results was sought by considering that the experimentally determined β and i_0 values are influenced by specific adsorption of anions, which is potential-dependent. This would cause i_0 to be potential-dependent also and consequently β would contain a contribution from $\partial \ln i_0/\partial E$[1,2].

From this it appeared worthwhile to study the temperature-dependence of β and i_0 for a solution with strong specific anion adsorption such as iodide solutions[3]. In this paper, the results obtained in 57% HI solution (≈ 7.6 *M*) are described and discussed.

EXPERIMENTAL

The impedance of a dropping mercury electrode placed in the azeotropic mixture of hydriodic acid and water (the solution contains 57% HI) was measured.

The measuring cell was similar to that described previously[1]: in the hope of improving the purity of the solution the main compartment of the cell was made of quartz. Three electrodes were placed in the cell: a mechanically controlled dropping mercury electrode, a mercury pool counter electrode and a platinized hydrogen reference electrode. The whole system was saturated with hydrogen gas, which was purified by passage through a column filled with BTS-Katalysator (BASF) at a temperature of 50°C, and then equilibrated with a solution of the same composition and temperature as in the measuring cell. The mercury used for the electrodes was doubly-distilled.

The azeotropic hydriodic acid solution was obtained by distillation of a concentrated HI solution in a purified nitrogen atmosphere. The receiver flask was

made of quartz. A small amount of hypophosphorous acid was added to the solution in the distillation vessel in order to keep this solution and the distillate free from iodine[4]. The distillation and all other manipulations with hydriodic acid were performed with exclusion of light.

All glassware was cleaned with dichromic acid and steamed out for a few hours. Immediately before use it was rinsed with doubly-distilled water and dried.

The impedance measurements were performed with the a.c. bridge as described elsewhere[5]. The potential range investigated was taken as wide as possible: on the cathodic side it is limited by the rapid evolution of hydrogen bubbles which disturbs regular dropping of the mercury, and on the anodic side by the very high capacity values which cannot be determined accurately with the a.c. bridge.

The temperature was controlled to within $\pm 0.1^\circ$C.

RESULTS

The components Z' and Z'' of the cell impedance were measured at fixed potentials as a function of frequency (420–2000 Hz). The ohmic resistance R_Ω of the cell was found by extrapolation of Z' to infinite frequency. From these data the components Y'_{el} and Y''_{el} of the electrode admittance were calculated as described earlier[1].

The measurements were performed at temperatures $+25^\circ$, $+15^\circ$, $+5^\circ$, -5°, -15°, -25° and -35°C. In a previous paper[6] it has been shown that in 57% HI at $+15^\circ$C, the potential region where the hydrogen reaction is measurable, partly coincides with the potential region where mercury dissolves to HgI_4^{2-}. This appeared to be the case also at $+25^\circ$ and $+5^\circ$C. In this potential region (-540 to -590 mV) Y'_{el} is a linear function of the square root of the frequency $\omega^{\frac{1}{2}}$, from which it can be deduced[6] that one of the reactions, Hg/HgI_4^{2-}, is reversible and the other $H^+/H_2(Hg)$ irreversible. The Warburg coefficient σ_1 of the former reaction, the transfer resistance θ_2 of the latter, and the double-layer capacity C_d have been obtained according to the equations:

$$Y'_{el} = \frac{\omega^{\frac{1}{2}}}{2\sigma_1} + \frac{1}{\theta_2} \quad (1a) \qquad Y''_{el} = \frac{\omega^{\frac{1}{2}}}{2\sigma_1} + \omega C_d \quad (1b)$$

At potentials more negative than -590 mV, the θ_2 values were obtained directly as $\theta_2 = 1/Y'_{el}$ since the contribution of the Hg/HgI_4^{2-} reaction is here negligible. The results are presented in Figs. 1 and 2.

At potentials more negative than -590 mV, the $\log \theta_2$ *vs.* E plots are linear, which is in accordance with the theory for a completely charge transfer controlled electrode reaction[7].

From the slopes and the intercepts, the values of the cathodic transfer coefficients β and the exchange current densities i_0 of the hydrogen evolution reaction were calculated. The results are given in Figs. 3 and 4.

An important conclusion from Fig. 3 is that the transfer coefficient decreases with temperature. The temperature coefficient of β was calculated from the slope of the line $\partial\beta/\partial T = -1.4 \times 10^{-3}$ degree^{-1}.

The apparent heat of activation at the reversible potential, ΔH, was calculated from the slope of the $\log i_0$ *vs.* $1/T$ plot (Fig. 4): $\Delta H = 21.6 \pm 1.8$ kcal mol^{-1}. This

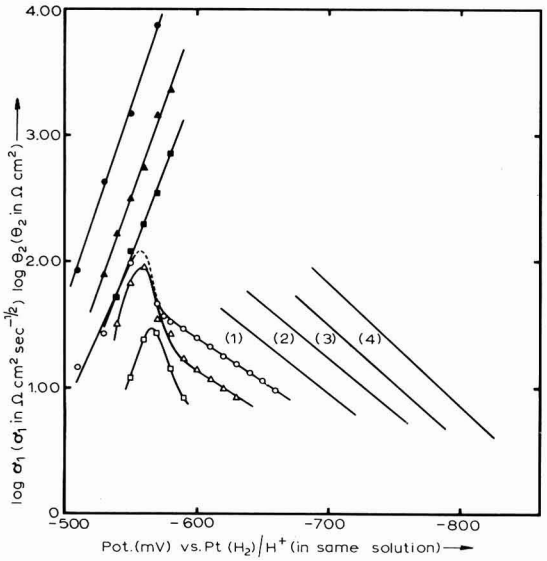

Fig. 1. Plots of the logarithmic values of the Warburg coefficients σ_1 (dark spots) and the activation polarization resistances θ_2 (light spots) as a function of potential for a mercury electrode in 57% HI at several temps.: (■, □) +25°; (▲, △) +15°; (●, ○) +5°C; and exptl. log θ_2 lines for: (1) −5°; (2) −15°; (3) −25°; (4) −35°C.

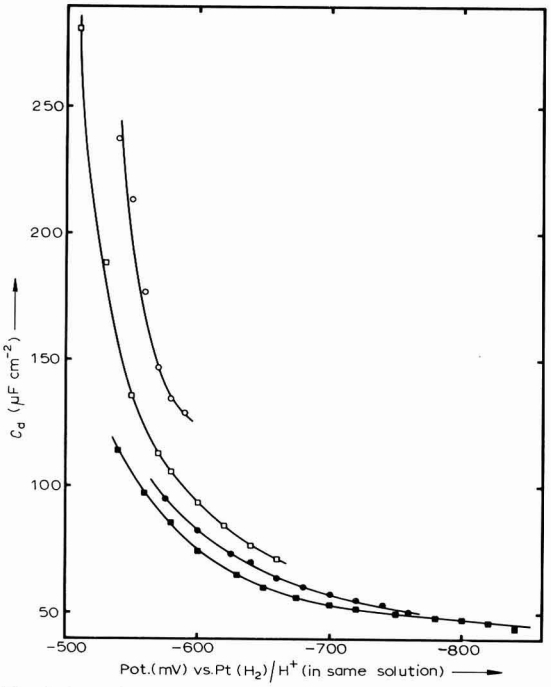

Fig. 2. Capacity–potential curves for mercury in 57% HI at several temps.: (○) +25°; (□) +5°; (●) −15°; (■) −35°C.

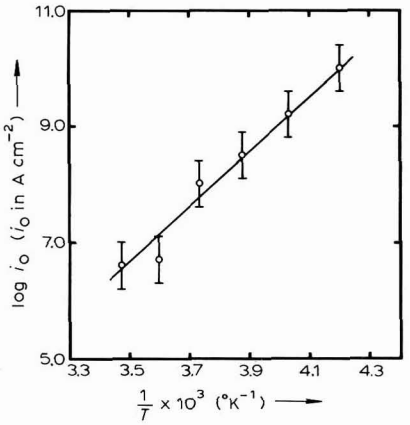

Fig. 3. Dependence of β on temp. for Hg in 57% HI.

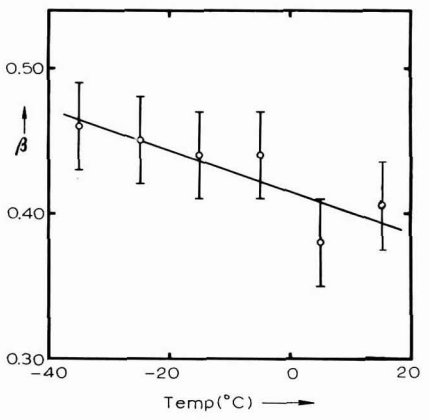

Fig. 4. Dependence of i_0 on temp. for Hg in 57% HI.

value is in agreement with the values of about 20 kcal mol^{-1} which are normally found for the hydrogen evolution reaction on mercury[8].

DISCUSSION

(A) The most notable result of the measurements is that the transfer coefficient, β, decreases with temperature (Fig. 3) in the temperature and potential range investigated. To the authors' knowledge such a phenomenon has not been reported before. Previously[1] we reported on the results of measurements on the H^+/H_2(Hg) reaction in 7.5 M HCl, in which case an increase of β with temperature was found. The explanation was sought by considering that the experimentally determined value of β is not a "real" transfer coefficient but contains a contribution from the potential-dependence of i_0. In that case the observed "apparent transfer coefficient" β_{app} is equal to:

$$\beta_{app} = \beta - \frac{RT}{nF}\left(\frac{\partial \ln i_0}{\partial E}\right)_T = \beta - g \qquad (2)$$

where β is considered as a fundamental constant (independent of E and T).

The potential-dependence of i_0 can be caused by the Frumkin effect, but it is also very probable that the accelerating effect of the specifically adsorbed iodide ions q'_- is responsible. That this effect (which has been demonstrated for other electrode reactions on mercury[9]) exists also for the hydrogen electrode, may be inferred from the variation of log i_0 with the nature and concentration of the anion, *e.g.* at 15°C we have found for log i_0 -13.3 in 5.2 M $HClO_4$, -13.1 in 1 M HCl, -9.9 in 7.5 M HCl, and in the present paper, -6.6 in 7.6 M HI. The amount of specific adsorption from the concentrated solutions is not known, but, in view of what is known from double-layer measurements at lower concentrations[10,11], it is reasonable to expect that it increases in the same direction.

Continuing the argument in this way, the temperature-dependence of β_{app} could be due to that of g, represented by

$$g = \frac{RT}{nF}\left(\frac{\partial \ln i_0}{\partial q'_-}\right)_{E,T}\left(\frac{\partial q'_-}{\partial E}\right)_T \qquad (3)$$

From our experiments it would appear that, with increasing temperature, g decreases for 7.5 M HCl and increases for 7.6 M HI. Recently, Minc and Andrzejczak[12] investigated the adsorption of NCS^- on mercury for concentrations up to 6 M and at two temperatures. From their experiments it can be seen that the temperature coefficient of $(\partial q'_-/\partial E)_T$ can be either positive or negative, depending on the concentration and the temperature. In this connection it will be interesting to determine q'_- as a function of potential and temperature for concentrated Cl^- and I^- solutions. With such data the influence of the first derivative in (3) could also be investigated, using the model recently introduced by Parsons[13], which relates $(\partial \ln i_0/\partial q'_-)_{E,T}$ to the second virial coefficient $B_{1,1}$ in the adsorption isotherm.

If, on the other hand, the temperature-dependence of β_{app} must be traced to that of the "real" β in eqn. (2), it is worthwhile to note that in 7.6 M HI a decrease of β with temperature is found together with an increase in the double-layer capacity, whereas in 7.5 M HCl the increase in β with temperature coincides with a decrease in the double-layer capacitance. If changes in the capacitance in these concentrated solutions may be interpreted as changes in the double-layer thickness, this would mean that both in HCl and HI there is a simultaneous increase in β and the double-layer thickness. This is in contradiction with what could be expected from a theory proposed by Parsons and Bockris[14].

(B) In Fig. 1 a kind of hump appears in the log θ_2 *vs.* E curves in the potential region where the hydrogen evolution reaction coincides with the mercury dissolution reaction. There is no doubt that the equivalent circuit of the impedance used for the evaluation of the impedance parameters σ_1, θ_2 and C_d is correct. Two arguments for the correctness of the analysis can be given.

(i) The log σ_1 *vs.* E plots are straight lines, which is in accordance with the theory for a completely diffusion-controlled electrode reaction[7]. From the slopes of the lines, the number of electrons involved in the electrode reactions can be calculated. For all temperatures (*i.e.* $+5°$, $+15°$ and $+25°$C) $n=1.7$, which is in reasonable agreement with the theoretical value $n=2$.

(ii) No frequency dispersion in the calculated C_d-values was observed. Moreover, the general shape of the C_d *vs.* E curves is similar to those obtained for I^- solutions by other workers[3,15].

Going from -590 mV to less negative potentials, the initial increase in the slope of the log θ_2 *vs.* E curves could be interpreted as a change in the apparent transfer coefficient. The inaccuracy of the log θ_2 values and the small potential range of the measurements prevented any significant temperature-dependence being observed: for all temperatures investigated, the slopes of the right-hand side of the humps correspond to $\beta_{app}=1.3\pm0.3$.

Recently, Krishtalik[16] presented a study of the hydrogen reduction on mercury in various supporting electrolytes, especially with a view to the so-called "barrierless discharge" theory. In the case of barrierless discharge, the transfer coefficient is theoretically equal to unity. According to Krishtalik, the phenomenon was observed at very low current densities in a potential region somewhat more positive than the potential region of our measurements. It is likely, therefore, that our result $\beta=1.3\pm0.3$

indicates the occurrence of barrierless discharge. It is not possible to calculate the heat of activation ΔH from our experiments owing to the inaccuracy of the log θ_2 *vs.* E lines.

The phenomenon that log θ_2 decreases on the anodic side of the hump is of special interest. This could mean that some irreversible oxidation reaction takes over the role of the irreversible hydrogen evolution reaction. In such a case, the θ_2 value obtained must be considered as a substitution value: $\theta_2 = \theta_H \theta_3 / \theta_H + \theta_3$, θ_H being the transfer resistance of the $H^+/H_2(Hg)$ reaction, and θ_3 that of the other reaction. However, this explanation is unlikely since it is not clear which reaction can take over the role of the hydrogen reduction reaction. Another explanation can be sought in considering that the presence of HgI_4^{2-} species diminishes the heat of activation of the hydrogen evolution reaction. The model for such a catalysing effect is not yet understood and this will have to be investigated further.

ACKNOWLEDGEMENT

The investigations were supported in part by the Netherlands Foundation for Chemical Research (SON) with financial aid from the Netherlands Organisation for the Advancement of Pure Research (ZWO).

SUMMARY

The impedance of a dropping mercury electrode in 57% HI (≈ 7.6 M) was measured at temperatures between $-35°$ and $+25°C$. In a certain potential and temperature region, two reactions were found to be proceeding simultaneously: the reversible Hg/HgI_4^{2-} reaction and the irreversible $H^+/H_2(Hg)$ reaction. Analysis of the impedance data gave information about the impedance parameters of both electrode reactions, and about the double-layer capacity. The temperature-dependences of the transfer coefficient and the exchange current density of the $H^+/H_2(Hg)$ reaction are reported. The transfer coefficient decreases with temperature. The apparent heat of activation is 21.6 kcal mol^{-1}.

REFERENCES

1 B. G. DEKKER, M. SLUYTERS-REHBACH AND J. H. SLUYTERS, *J. Electroanal. Chem.*, 21 (1969) 137.
2 M. SLUYTERS-REHBACH, B. TIMMER AND J. H. SLUYTERS, *Z. Physik. Chem. N.F.*, 52 (1967) 89.
3 D. C. GRAHAME, *J. Am. Chem. Soc.*, 80 (1958) 4201.
4 W. CONARD FERNELIUS, *Inorganic Synthesis*, McGraw-Hill, New York, 2 (1946) 210.
5 M. SLUYTERS-REHBACH AND J. H. SLUYTERS, *Rec. Trav. Chim.*, 82 (1963) 535.
6 B. G. DEKKER, M. SLUYTERS-REHBACH AND J. H. SLUYTERS, *J. Electroanal. Chem.*, 23 (1969) 9.
7 B. TIMMER, M. SLUYTERS-REHBACH AND J. H. SLUYTERS, *J. Electroanal. Chem.*, 14 (1967) 169.
8 B. E. CONWAY, *Electrochemical data*, Elsevier Publishing Co., Amsterdam-Houston-London-New York, 1952, p. 337.
9 M. SLUYTERS-REHBACH, J. S. M. C. BREUKEL AND J. H. SLUYTERS, *J. Electroanal. Chem.*, 19 (1968) 85.
10 R. PAYNE, *J. Phys. Chem.*, 70 (1966) 204.
11 P. DELAHAY, *Double Layer and Electrode Kinetics*, Wiley (Interscience), New York, 1965, p. 61.
12 S. MINC AND J. ANDRZEJCZAK, *J. Electroanal. Chem.*, 17 (1968) 101.
13 R. PARSONS, *J. Electroanal. Chem.*, 21 (1969) 35.
14 R. PARSONS AND J. O'M. BOCKRIS, *Trans. Faraday Soc.*, 47 (1951) 914.
15 E. DUTKIEWICZ AND R. PARSONS, *J. Electroanal. Chem.*, 11 (1966) 100.
16 L. I. KRISHTALIK, *Electrochim. Acta*, 13 (1968) 1045.

ELECTROANALYTICAL CHEMISTRY AND INTERFACIAL ELECTROCHEMISTRY
Elsevier Sequoia S.A., Lausanne – Printed in The Netherlands

THE RESISTANCE AND INTRINSIC TIME CONSTANT OF GLASS ELECTRODES

ANDERS WIKBY AND GILLIS JOHANSSON
Department of Analytical Chemistry, University of Umeå, 901 87 Umeå (Sweden)
(Received March 21st, 1969)

As part of a programme to study the properties of glass electrodes we have reinvestigated the resistances measured with direct current and with alternating current. Such measurements should provide information about the solid state side of the glass–solution interface. We hoped originally that changes in solution would affect the resistance, at least to some small extent. This was not the case, but instead a quite unexpected energy barrier appeared in the surface.

Earlier measurements of the resistance provided a check on the usefulness of the glass composition[1]. Too high resistances resulted in slow response or current leaks in the electrometer connections. Both d.c.[2] and a.c.[3] were used and it was observed that a.c. measurements gave a much lower value. The high d.c.-value was attributed to a back e.m.f., but it was nevertheless concluded that the relevant quantity for a glass electrode was the d.c.-value. These experiments are reviewed in Dole's classical monograph[4]. The existence of an internal e.m.f. was later rejected. Since the d.c. resistance obeys Ohm's law Eckfeldt and Perley[5] collected evidence to dismiss the polarization theory. They showed that much of the discrepancy between the a.c. and d.c. measurements could be explained by treating the glass as a dielectric. Distèche and Dubuisson[6] used a pulse technique to obtain an equivalent circuit for the glass electrode. The values obtained were quite different from those obtained by measurements with d.c. and the differences could not be explained by the authors. The present work shows that they used an over-simplified equivalent circuit and that the contributions from cable and electrometer capacitances may be in error. Impedance measurements seemed to provide very little information about the electrode properties and therefore few investigations were made between the thirties and the present time.

During recent years glass electrodes selective to cations other than hydrogen have been investigated in several reports. Eisenman[7] has edited a monograph on the subject. He and his co-workers[8] have determined the current–voltage relations of some membranes in this respect. Buck[9,10] and Buck and Krull[11] have recently measured the d.c. and a.c. resistances of glass electrodes with modern equipment. By using the Cole–Cole plot they were able to distinguish a surface impedance on their porous electrodes. They did not observe it on other electrodes, probably owing to the high total resistances of these.

The electrical properties of glasses not specifically designed for electrode purposes have been studied extensively and reviewed in several monographs, *e.g.* by Morey[12]. Some Russian investigations have been briefly reported in the papers

of a conference[13]. More recent work has been critically reviewed by Owen[14] and in the following report his work is relevant to much of the discussion.

EXPERIMENTAL

In order to obtain the detailed information and accuracy which is necessary for a separation of different processes, a pulse technique was developed. A pulse technique enables the whole time course to be observed in a continuous record whereas bridge measurements with sinusoidal currents require a number of points collected at different frequencies. In addition bridge measurements are difficult to make at very low frequencies. The resolution of a time course should, therefore, be higher than for a comparable bridge method since seven frequency decades are covered in a single pulse. At first we tried applying a constant voltage pulse over the electrode and a standard resistor (the cable capacitance being neutralized as described below), and measuring the voltage developed over the latter. It was found that the value of the standard resistor appeared in parallel to the equivalent circuit of the electrode thus complicating the calculation. In order to obtain simpler relations, the pulse was applied directly over the electrode. It was then found to be advantageous to employ constant current rather than constant voltage mainly because the stability of the circuit towards self-oscillations became higher.

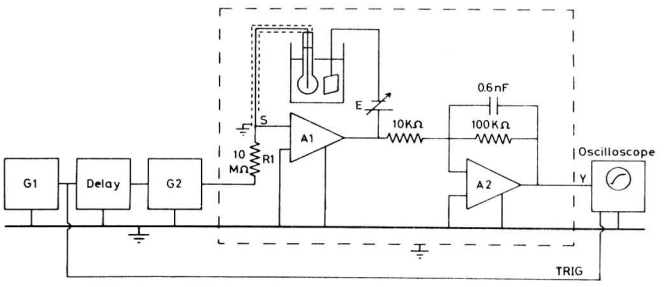

Fig. 1. Circuit diagram for impedance measurements of glass electrodes. (G1, G2) pulse generators; (A1) operational amplifier type 301; (A2) type 111 (Analog Devices).

The final circuit is shown in Fig. 1. An HP instrument function generator, G 1, provided triggering pulses to the oscilloscope and a delayed output triggered another pulse generator, G 2, providing a square wave pulse output. The pulse length could be set on this generator and the repetition frequency set by G 1. The interval between pulses was always much longer than the pulse duration. The output impedance of G 2 was very much lower than R_1. The current through R_1 was 500 pA in all the experiments except when Ohm's law was being tested. The point S is at virtual ground because the operational amplifier A 1 (Analog Devices type 301) sends a current through the electrode chain in the same direction as the current through R_1, and when the amplification of A 1 is sufficiently high these currents are precisely equal. The d.c. voltage of the electrode chain was counterbalanced by a battery-operated, low impedance voltage E. The output of amplifier A 1 was thus equal to the voltage required to force the same current through the glass electrode as that which flowed through R_1. The inner reference of the glass electrode

was connected to point S and since S was at virtual ground the capacitance between the inner conductor and the earthed shield will not be charged. The outer reference electrode chain was connected to the output of the amplifier *via* the low impedance of *E*. Owing to the low output resistance of the amplifier, the hum and noise picked up by this reference electrode was small. The output from A 1 was amplified ten times in a second step employing the operational amplifier A 2 (Analog Devices, 111). In order to limit high frequency noise, the rise time of this stage was reduced by a capacitor. The amplifiers were shielded in a box and this box and the cell with the electrode chain were shielded in a large earthed metal cage as shown by the dotted line. The output from A 2 was connected to the y-axis of a Tektronix 564 storage oscilloscope. The horizontal amplifier, type 3A7, was a differential comparator with a built-in compensation voltage which could be set with a resolution of 1 : 10000. Time resolution was obtained by a delayed sweep, type 3B3. A recorder in parallel with the oscilloscope, eventually backed off with a potentiometer, was used for recording the slow part of the time course. A careful calibration was made so that the readings on the oscilloscope and recorder were compatible. When slow processes were studied the pulse generators were replaced by a manually operated switch.

Corresponding values of the voltage and the time were recorded. Readings were taken over the range 100 μs to several minutes. The voltage at time t is subtracted from the value at "infinite time", *i.e.*, when a steady state is observed on the recorder, and the difference plotted against t on semilogarithmic paper. This procedure follows that of Isaacs and Leach[15]. A single time constant will give a straight line. If several time constants are obtained these can be resolved by evaluating the slowest and subtracting its corresponding straight line from the earlier part of the graph. This procedure can be repeated until all time constants are resolved, provided the measurements are made with sufficient care and precision.

The electrode chain consisted of an inner and an outer Ag/AgCl electrode. Only fresh electrodes with a voltage difference smaller than 0.1 mV were used. Commercial reference electrodes could not be used owing to drift. The cell was kept at constant temperature by circulating water from a thermostat provided with refrigerator and thyristor regulation. The temperature was set to within 0.1°C, but the temperature stability was several times better. Thermal insulation of the thermostat and water hose was provided.

RESULTS

Time constants

A typical plot of the voltage–time curve for the glass electrode, Ingold LOT-102, at 22.2°C, is shown in Fig. 2. This electrode had been hydrated in phosphate buffer at pH 7.0 for three days. The measurements were made in the phosphate buffer with added 0.05 *M* KCl. A logarithmic plot of the voltage differences against time is shown in Fig. 3. The method used to obtain a second time constant is also shown. These Figures display the behaviour in the range from one to tens of seconds, that in the milliseconds range only showing up as a step in the early parts of the curves.

Resolution of these early parts requires an expansion such as is shown in Fig. 4, where the upper curve corresponds to the initial portion of the upper curve in Fig. 3. The middle curve, τ_2, is a plot of the residue obtained when the contributions of the

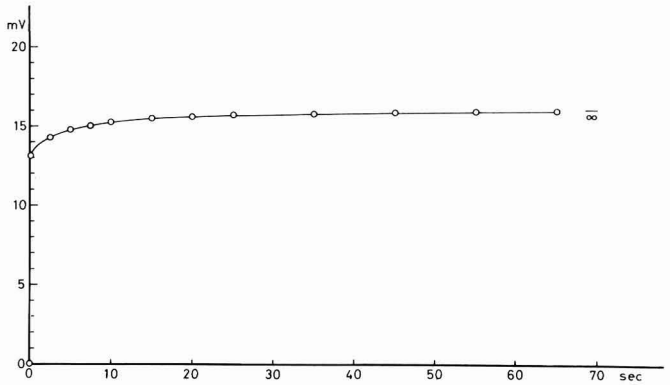

Fig. 2. Voltage developed over the electrode Ingold LOT-102 at 22.2°C plotted *vs.* time. The current was 500 pA.

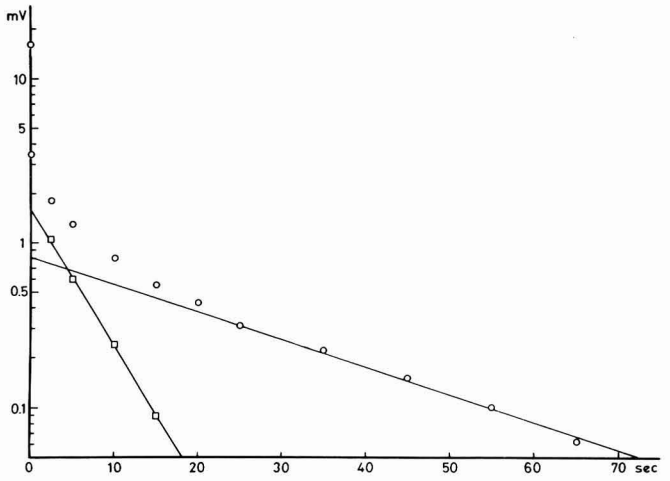

Fig. 3. (○) Logarithm of voltage difference from the value at infinite time of Fig. 2 plotted *vs.* time; the line drawn is τ_4. (□) Difference between points ○ and line τ_4. The line through points □ is τ_3.

slower time constants are subtracted from the curve. The lowest curve, τ_1, is obtained when the contribution τ_2 is also subtracted. There are additional time constants between τ_2 and τ_3 but they cannot be resolved using this procedure. Their equivalent resistances, however, can be obtained as a difference using the total d.c. resistance.

The temperature variation of the time constants has been measured between 15° and 46°C. A plot of the logarithms of the time constants against $1/T$ is shown in Fig. 5. The contributions from τ_3 and τ_4 become too small to be evaluated at the higher temperatures. Within the temperature range covered all the time constants gave linear plots.

The slopes of the lines in Fig. 5 have the dimensions of activation energy. It can be seen that the slopes of those corresponding to slow processes are equal but differ from those corresponding to the two fast ones. The latter in turn have equal slopes.

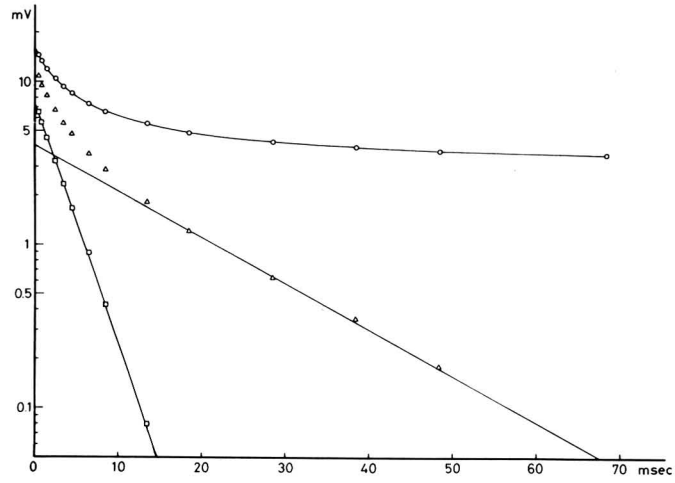

Fig. 4. Time expansion of Fig. 3. (○) Unresolved curve; (△) difference between curve ○ and straight lines drawn in Fig. 3 (about a third time constant see text); the line drawn through points △ is τ_2; (□) difference between the points △ and line τ_2; the line through points □ is τ_1.

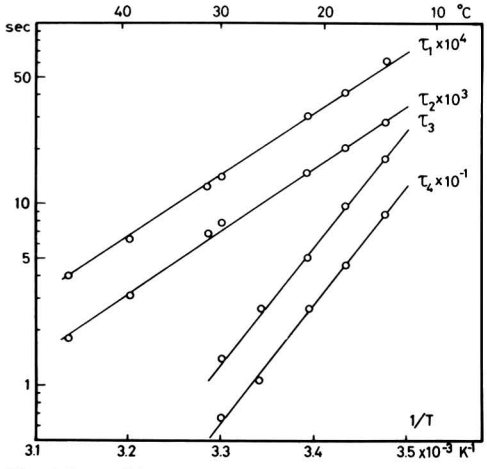

Fig. 5. Logarithm of time constants plotted *vs.* reciprocal absolute temp.

Resistances

The d.c. resistance is considered as a measure of the conduction process in glass. The logarithm of the resistance is usually plotted agains $1/T$ to determine the activation energy. The d.c. resistance, R_{tot}, can be found from the voltage at "infinite time" and is plotted against $1/T$ in Fig. 6. This plot is usually represented by

$$\log R_{tot} = \log A + \frac{\Delta H}{RT} \tag{1}$$

according to Owen[14]. The relation is called the Rasch–Hinrichsen equation. ΔH is the activation energy for the current transport, R the gas constant and T the absolute

temperature. A is a constant; its significance will be discussed later. Deviations from linearity were found in the present study.

Each time constant can be represented by an equivalent circuit consisting of a resistor in parallel with a capacitor (see Fig. 7). The values of the resistors can be found from the intercepts at zero time in Figs. 3 and 4. The resistances R_1–R_4 are plotted in the same way as the d.c. resistance, R_{tot}, in Fig. 6. It is seen that the activation energies of the resistances of the slow processes are equal and different from those of the fast processes. The resistance R_4 was found to be less reproducible than the others, partly owing to difficulties in evaluation and partly to sensitivity to treatments of the electrode, especially the previous thermal history. This point was not investigated systematically as the influence on the other results was small.

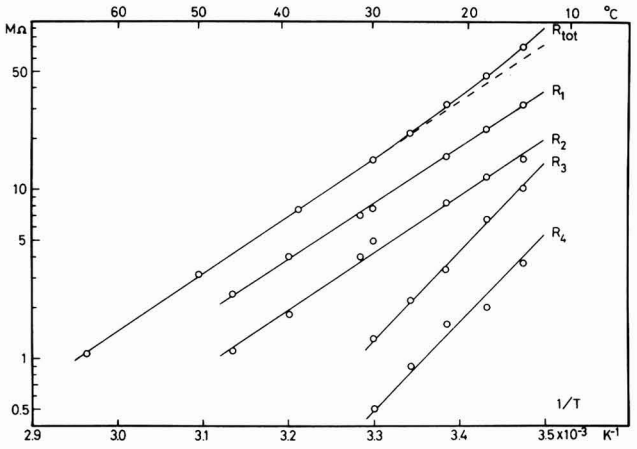

Fig. 6. Logarithm of resistances plotted *vs.* reciprocal absolute temp.

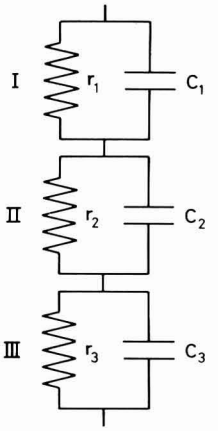

Fig. 7. Equivalent circuit used for test of the method. Values of r and C are given in Table 1.

Equivalent circuit and measuring system

The resolution of different time constants and different resistances from a complicated record might be questioned. Uncertainties in the measuring system might affect the overall result in an indefinite way. Equivalent circuits according to Fig. 7, with values of the resistors and capacitors close to those calculated were therefore made. Comparison of the measured values with those calculated from the components is shown in Table 1. The components were checked in a bridge and the stray capacitance of the equivalent circuit box was taken into account. The tests show that the results should be very reliable and that a resolution can be made quite accurately.

Another equivalent circuit was connected in series with two reference electrodes immersed in the same solution. No effect attributable to the reference electrodes could be seen: they behaved as a short circuit.

According to the Nernst equation, changes in the external solution cause variations in the e.m.f. of the glass electrode. Alteration of the pH of the external solution produced no detectable changes in the time constants or in the resistances. This agrees with the findings of Buck and Krull[11].

These measurements show that the accuracy of the measuring system is better than the reproducibility of the glass electrodes and that all time-dependences originate in the glass electrodes.

Hydration of the glass electrode

Electrodes that had never been immersed in water were obtained directly from Dr. Ingold. During storage they were kept in a desiccator but they were not dried further by heating. As is well known in glass technology[16] the glass contains moisture which is firmly bound. Removal of this moisture would have changed the electrodes. The non-hydrated electrodes are thus in equilibrium with a certain amount of water vapor, the actual vapor pressure of which causes some differences at the start of the hydration process. This was not investigated further.

TABLE 1

TEST OF THE MEASURING SYSTEM AND THE GRAPHIC EVALUATION

		$r/M\Omega$	C/nF	$r \cdot C/s$		$Error/\%$
				Calcd.	*Meas.*	
Test A	I	9.98	0.221	0.00221	0.00221	0.0
	II	30.96	994.6	30.79	30.70	0.3
	III	—	—	—	—	—
Test B	I	10.05	0.102	0.00103	0.00102	1.0
	II	30.73	0.201	0.00618	0.00613	0.8
	III	—	—	—	—	—
Test C	I	10.00	0.219	0.00219	0.00222	1.4
	II	10.06	1100.9	11.08	10.90	1.6
	III	31.02	994.1	30.84	31.01	0.5

The variation of the d.c. resistance for the Ingold electrode is plotted against the square root of the time (see curve A in Fig. 8). Initially this function is linear but large deviations are evident for higher values of t. Rana and Douglas[17] found a similar function when they measured the rate of leaching of ions from the surface. The rate of the hydration process is dependent on temperature, the leaching solution, electrode pretreatment, and possibly other parameters. Measurements of the whole time process during hydration were also made and the results are shown in Fig. 9. From this Figure it can be seen directly that the faster region remains unchanged and that the resistance changes accompanying hydration occur only in the slower region, *i.e.* R_3 and R_4 change. A detailed analysis with resolution of the different parts shows that R_1 and R_2 vary by less than 2% but that the variations in R_3 and R_4 are approximately 500%. The time constants τ_3 and τ_4 are initially very large but decrease during hydration.

These experiments suggest that the faster processes involving R_1, R_2, τ_1, and τ_2 should be independent of hydration, *i.e.* they originate in the interior of the glass. The slower processes involving R_3, R_4, τ_3, τ_4, on the other hand, should be assigned to the surface.

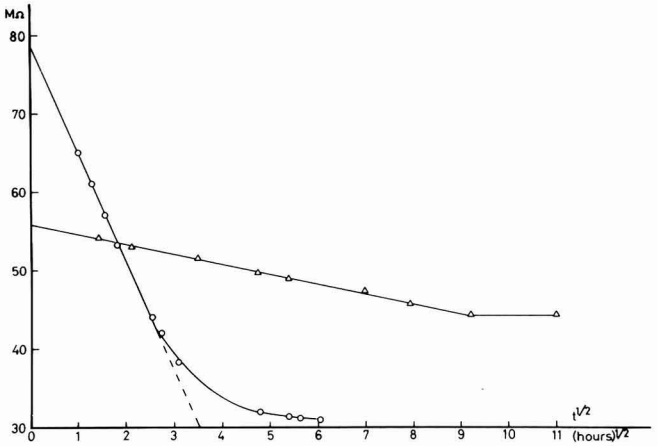

Fig. 8. Total d.c. resistance plotted *vs.* square root of time of hydration. (○) curve A (Ingold LOT-102); (△) curve B (Metrohm EA 107 T).

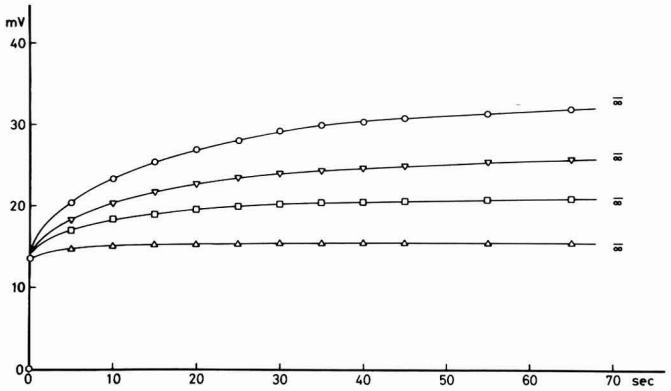

Fig. 9. Voltage developed over electrode LOT-102 at 22.2°C plotted *vs.* time. After hydration during: (○) 0.82; (▽) 3.33; (□) 7.75; (△) 36.50 h. All measurements were made with a current step of 500 pA.

Thickness

Three electrodes of the same glass, Ingold LOT-102, were hydrated and compared in order to obtain further proof that the fast processes originate in the glass body and the slow processes in the surface. The thickness was measured with an inverted microscope provided with a micrometer dial coupled to the moving objective. The microscope was focused on the outer glass surface and the dial was read to 0.001 mm. It was then focused on the inner surface through the glass and the dial was read again. The difference in these readings times the refractive index gives the thickness. Owing to pits, scratches and irregularities, the thickness measurements are considered uncertain to ± 0.005 mm. Measurements were made on the bottom and along a circular path around the electrode bulb. Mean values are presented in Table 2. The refractive index was determined for a broken electrode in a polarizing microscope using liquids of known refractive index. The resistance and time constant

were determined as described earlier. The electrode (Normal II) had been stored in non-aqueous solvent before hydration and showed a higher surface resistance. The Table also shows the quotients Q_1 (=Normal I/Thin) and Q_2 (=Normal II/Thin). The quotient for resistances R_1 and R_2 equals that of the thicknesses measured around the circumference. The agreement is not so good when the thicknesses measured at the bottom are considered, but as the thickness around the circumference represents a larger total surface, it is certainly the more significant figure. The overall resistance R_{tot} is not proportional to the thickness and the ratio changes with temperature. The contribution to R_{tot} from the surface, R_s, diminishes as the temperature increases so that the ratio approaches 4.2 (at 45°C, not included in the Table). The ratio of the time constants is unity at all temperatures. This proves conclusively that R_1, R_2, τ_1 and τ_2 originate in the glass body and that the quantities, R_3, R_4, τ_3 and τ_4, must be properties of the surface layers.

TABLE 2

VARIATION OF RESISTANCES AND TIME CONSTANTS WITH THICKNESS OF THE ELECTRODE

	Electrode			*Quotient*	
	Thin	*Normal I*	*Normal II*	Q_1	Q_2
	μm	μm	μm		
Thickness, bottom	65	215	222	3.3	3.4
Thickness, side	89	383	367	4.3	4.1
	MΩ	*MΩ*	*MΩ*		
R_1 15.2°	7.1	29.5	28.2	4.2	4.0
21.7°	3.9	16.5	16.8	4.2	4.3
R_2 15.2°	3.6	15.3	15.5	4.3	4.3
21.7°	2.0	8.4	8.1	4.2	4.2
R_{tot} 15.2°	36.0	66.0	71.0	1.8	2.0
21.7°	15.5	33.0	36.0	2.1	2.3
	ms	*ms*	*ms*		
τ_1 15.2°	5.79	5.60	5.79	0.97	1.00
21.7°	3.13	3.03	3.09	0.97	0.99
τ_2 15.2°	23.8	26.7	23.6	1.12	0.99
21.7°	14.7	14.7	14.9	1.00	1.01

Measurements on EA 107 T

The Ingold electrode had been selected because of its low total resistance which made more accurate measurements possible. Measurements on a glass electrode of different composition should give further information. Exploratory measurements on electrodes with d.c. resistance of the order 500 MΩ showed that the main part of this originates in the glass body. The surface processes thus become very uncertain. The accuracy of the measuring apparatus also becomes lower in the high resistance range because of noise and hum. The electrode finally selected was a Metrohm EA 107 T, a low temperature electrode. The composition was unknown. This was

first placed in a non-aqueous solvent, 2-propanol, to permit measurements to be made before the onset of hydration, which occurred upon its subsequent immersion in water. The hydration process is shown in Fig. 8, curve B. It is slower than normal, about five times, because it had previously been stored in isopropanol. The rate of hydration is considerably slower than that of the Ingold LOT-102 electrode so that the desired information should be obtainable.

The measurements resulted in the same general picture as above and four time constants were again obtained. The slow time constants were affected by hydration but not the fast ones. Measurements in the temperature range 10°–35°C have been made and the results are summarized in Table 3. The activation energies of the glass body processes are of the same size but they are different for those of the surface.

TABLE 3

SUMMARY OF DATA FOR THE METROHM AND INGOLD ELECTRODES

Quantity	*Unit*	*Value at 24.6°C*	*ΔH*/kcal mol⁻¹*	
		Metrohm EA 107 T	*Metrohm EA 107 T*	*Ingold LOT 102*
τ_1	ms	3.6	15.5	15.4
τ_2	ms	16.1	16.1	15.4
τ_3	s	2.8	19.6	29.4
τ_4	s	18.0	21.5	29.7
R_1	MΩ	6.3	15.7	15.1
R_2	MΩ	12.4	16.6	15.3
R_3	MΩ	3.5	19.8	23.8
R_4	MΩ	2.7	27.4	23.8
R_g	MΩ	19.0	16.3	15.2
R_s	MΩ	6.4	24.7**	24.2
R_{tot}	MΩ	25.4	18.8**	17.8**

* Estimated uncertainty, ±0.4 units.
** Plot of log R against $1/T$ non-linear.

Although the Ingold electrodes contained time constants which could not be resolved the Metrohm electrode contained just four time constants so that all could be resolved.

The total resistances are approximately the same but the partition of the resistances differs greatly. It is also apparent that the activation energies of the glass body processes are very similar while they differ for the surfaces.

DISCUSSION

Several processes have been resolved in our measurements and two can be assigned to the surface and two to the glass body as shown above. Although the different properties of the surface and the glass body have been recognized earlier, no measurements have been performed, as far as we know, that quantitatively separate the surface and glass body contributions to the total conductance. The surface properties have generally been measured under different conditions and the theory is not well developed[18]. Buck and Krull[11] have observed a contribution from the surface to the conductivity on porous electrodes, but not on so-called ideal electrodes.

The electron beam experiments done by Muray[19] and the film depositions done by Snow and Deal[20] can also give important information about glass surfaces.

Resistance of the glass body

The processes occurring in the glass body will be discussed initially. They are characterized by the time constants τ_1 and τ_2, associated with the resistances R_1 and R_2.

The probability p that an ion in an energy well will jump to a neighbouring well may be written.

$$p = \frac{kT}{h} \exp(-\Delta G/NkT) = \frac{kT}{h} \exp(\Delta S/Nk) \times \exp(-\Delta U/NkT) \quad (2)$$

where N is Avogadro's number, k Boltzmann's constant, h Planck's constant, T the absolute temperature, ΔG Gibb's free energy, ΔS the entropy of activation, and ΔU the activation energy or the height of the energy barrier between the two wells. The depth of the well is dependent on binding and elastic forces[21]. The pre-exponential factor is a vibrational frequency which according to Eyring's rate equation is given by kT/h.

If λ is the distance between the wells, e the ionic charge and E an applied electric field, the probability of a jump occurring in the direction of the field will increase to:

$$p_+ = \tfrac{1}{2} \frac{kT}{h} \exp(\Delta S/Nk) \times \exp - [(\Delta U/NkT) - (E\,e\lambda/2kT)] \quad (3)$$

The probability of a jump in the opposite direction will then be:

$$p_- = \tfrac{1}{2} \frac{kT}{h} \exp(\Delta S/Nk) \times \exp - [(\Delta U/NkT) + (E\,e\lambda/2kT)] \quad (4)$$

The current density, i, is given by

$$i = ne\lambda(p_+ - p_-) = \frac{kT}{h} ne\lambda \times \exp(\Delta S/Nk) \times \exp(-\Delta U/NkT) \sinh \frac{eE\lambda}{2kT} \quad (5)$$

where n is the number of identical wells/cm^3. If the field is so small that $\frac{1}{2}\, eE\lambda \ll kT$, the hyperbolic function can be expanded and since the resistivity, R_9, is E/i it follows that

$$R_9 = \frac{2h}{e^2\lambda^2 n} \exp(-\Delta S/R) \times \exp(\Delta U/RT) \quad (6)$$

In the literature this resistivity is usually called the d.c. resistivity and eqn. (6) is a more complete version of eqn. (1) which has been used in the evaluation of our measurements. With alternating current the capacitance of the sample must be taken into account as well as losses arising from processes other than conduction. Stevels[18,22] differentiates between four contributing mechanisms: (1) the conduction; (2) ionic relaxation; (3) deformation and (4) vibration. Factors (3) and (4), which occur at high frequencies, do not affect our measurements and will not be discussed further. Contributions (1) and (2) are fundamentally the same but this has not always been understood. That they are different aspects of the same physical process will be evident

when an ion is considered which in d.c. migrates in one direction (conduction). In an a.c. field it will oscillate and this will be equivalent to the rotation of a dipole. The a.c. measurements are evaluated through use of the Debye equation in the same way as dielectric measurements are and the differences in the equations as well as the names and significance of the evaluated parameters might have contributed to the confusion. The resistance times the capacitance has dimensions of time and is called the relaxation time, τ. These relations have been discussed by Owen[14]. Taylor[23-25] has found that the activation energy is the same for the resistance measured with d.c. methods as for the relaxation time measured by a.c. methods. Taylor also finds a broad distribution of relaxation times, *i.e.* they do not follow the simple Debye equation. The activation energy, however, was the same for the whole spectrum of relaxation times because the form of the loss curves was independent of temperature. The cause of the distribution was therefore ascribed to a variation in the entropy of activation. This was criticized by Owen[14], on the grounds that a constant activation energy and a varying entropy are unlikely and have not been observed elsewhere.

Our expressions can be converted to the usual dielectric formulae by substituting the time function e^{-kt} for the usual $e^{j\omega t}$ [26,27]. The information contained in the results is fundamentally the same. Such a transformation has not been made as it would be more difficult to separate the resulting peak-shaped curves than to separate the straight lines resulting from our procedure. It is in fact so difficult to separate loss curves visually, that this form of presentation may support the assumption of a continuous distribution of relaxation times even in cases where a few discrete processes are dominant. In the glasses we have studied, the behaviour can be expressed by two main exponentials and for the Ingold electrode a third small contribution. It is also evident that the expression for each resistance is of the type given by eqn. (6). The curves in Fig. 6 show that the activation energies are equal. The differences between the processes causing different time constants must therefore occur in the pre-exponential terms.

If the jump probabilities are such that n ions are available to jump either the distance λ_1 and λ_2, etc., the resistivity of the glass body, R_g, can be expressed by a series

$$R_g = \frac{2h}{e^2\lambda_1^2 n}\exp(-\Delta S/R)\times\exp(\Delta U/RT) + \frac{2h}{e^2\lambda_2^2 n}\exp(-\Delta S/R)\exp(\Delta U/RT)+\ldots \tag{7}$$

This explanation can account for our experimental results. The activation energies for the different jumps are identical because it is the same process that accounts for all the time constants. As far as we know this explanation is not contradicted by other experiments given in the literature.

Charles[28] has studied the dielectric properties of phase-separated leachable borosilicate glasses and deduced that even Pyrex is phase-separated. This conclusion is drawn from the similarity of the frequency-dependence of Pyrex to that of a visibly phase-separated glass. As a distribution of relaxation times seems to be quite general this argument can be questioned. It is well known that the activation energy varies with glass composition and it should therefore be different in the two phases. It seems unlikely that eqn. (7) can be explained by phase-separation as it is found that the activation energies are equal. The Ingold electrode shows three time constants, and an aluminium–glass electrode, to be described in a future paper, has

shown four time constants, which make such an explanation very unlikely.

Charles[29] and Muray[30] have supposed that the conductive species are defects, *e.g.* a doubly-occupied mobile state $\equiv Si-O^- Na_2^{2+}$. To form the defect from the stable-bound state $\equiv Si-O^- Na^+$, an energy ΔW will be required. The sodium ion will have to pass over an energy barrier, ΔU, to move to another oxygen in the lattice, *i.e.* the activation energy of defect movement is ΔU. This model is plausible but other models are also possible. Haven and Verkerk[31] discuss two conduction processes, namely by indirect interstitial and by vacancy mechanisms. The concentration of defects was of the order one-hundredth–one-thousandth of the sodium concentration. Their experiments could not differentiate between the mechanisms. Since they should have different activation energies it is unlikely that our results are due to more than one type of process. If the defect concentration follows a Bolzmann distribution law, as supposed by Muray, the temperature dependence will be:

$$n = n_0 \exp(-\Delta W/RT) \exp(\Delta S_D/R) \tag{8}$$

ΔS_D is the entropy change of dissociation. The entropy change of defect movement must be zero because all conductive species must be supposed to be in an equilibrium. In analogy to simple gas reactions or ion collisions in solution, $\Delta S_{movem.} = 0$. The size of ΔS_D is difficult to estimate but Charles[32] found that the pre-exponential term was sensitive to pressure variations. In order to make at least a tentative estimate of the jump distance, ΔS_D will be set to zero at atmospheric pressure.

Following Mott and Gurney[33], Charles and Muray obtained an equation for the conductivity in which ΔH in eqn. (1) had been separated into ΔW and ΔU. Equation (7) should then be rewritten as:

$$R_g = \sum_i \frac{2h}{e^2 \lambda_i^2 n_0} \exp[(\Delta W + \Delta U)/RT] \tag{9}$$

where n_0 represents the possible number of defects. The activation energy measured experimentally will, according to this model, be the sum of two terms. They cannot be separated directly, but at very low termperatures the rate of defect formation may be slow. Such frozen-in defects have been observed[34]. The present measurements have been restricted to the temperature range where defect equilibrium can be assumed, but we have observed changes in slope just below the temperature regions reported in this paper.

The lithium content of the Ingold electrode was found to be 6.86% by weight by flame emission analysis, the density was 2.53 g cm^{-3}. This gives $n_0 = 1.51 \times 10^{22}$ atoms lithium/cm^3 and, if n_0 is set equal to the lithium concentration, eqn. (9) gives $\lambda_1 = 2.3$ Å, $\lambda_2 = 3.1$ Å, and $\lambda_3 = 5.9$ Å, the latter being uncertain because its contribution to the total glass resistance was small. Had the total glass resistance been used, a λ-value of 1.8 Å would have resulted. These values were independent of temperature. A random-network model for glass will give almost a continuous range of distances. The interesting feature of the present findings is that a few well defined values dominate. Even if the glass is irregular over longer distances a definite order must exist on the molecular level for the conducting species. For comparison it can be mentioned that the distance between two oxygen bound to the same silicon is 2.8 Å and the minimum distance between two oxygen on two neighbouring silicon is 3.2 Å. The

distance between the interstices in two neighbouring hexagons in cristobalite is 5.6 Å. The jump distances have been discussed in detail by Owen[14]. The values discussed by him are either unreasonably large or small and very temperature-dependent. The present experiments seem to provide a much better base for estimates than was available previously.

The resistivity of glasses has been plotted as a function of composition[35-37] as discussed by Stevels[18] and Owen[14]. The logarithm of the resistivity gives linear segments with kinks at a composition that usually corresponds to the replacement of a bridging oxygen, ≡Si–O–Si≡, with a non-bridging, ≡Si–O^-Na^+, in the lattice. Sometimes a similar picture is obtained for the activation energy. It is very likely that changes in composition will affect ΔW but that ΔU will remain effectively constant since the fundamental process should be the same.

The electrodes used are rapidly chilled during manufacture and it is known[38] that the resistance may be up to five times lower in a chilled than in an annealed glass. During the annealing procedure smaller aggregates equilibrate to form larger molecules or polymers. The number of non-bridging oxygen will then decrease, *i.e.* n becomes smaller. At still lower temperature the equilibrium will freeze and the number of non-bridging oxygen be independent of temperature. The electrode function would not be affected by annealing unless the electrode had been hydrated[39].

The resistance of the glass surface

The surface resistance has been neglected in most reports as pointed out by Muray[30]. However, he himself uses information from surface phenomena to explain volume conductivity. The term surface resistance obviously covers several conduction mechanisms, a fact which has sometimes been overlooked. A classification is difficult at present but electrolytic conduction in the outer, leached, hydrated part can be separated from other effects. The electrolytic conductance has been measured by Kuznetsov[40]. The conclusion that the conductance is electrolytic was founded on the temperature-dependence.

The surface resistance observed in the present measurements is almost of the same magnitude as the resistance of the glass body (Fig. 6), although the thickness of the surface layers must be very small in comparison. Measurements on non-hydrated electrodes gave values of the surface resistance which were about ten times higher than for the hydrated surface. The measurements were made in non-aqueous solvents or with mercury contacts. The reproducibility was lower than reported in Fig. 6, especially for the mercury contacts. To gain further information, the resistances were measured with currents from 500 pA–10 nA and it was found that Ohm's law was obeyed by both the surface resistance, R_s, and the glass body resistance, R_g. Changes in the composition of the aqueous solution did not affect the surface resistance.

A number of aspects must be taken into account in order to locate and explain this surface resistance. During hydration water is taken up by the glass, and alkali ions subsequently move out and become replaced by hydrogen ions in the silica lattice. The distribution of ions at different depths has been determined by Boksay *et al.*[41]. The alkali concentration is very low close to the surface and increases exponentially to the value characteristic of the glass body. This gel layer has a thickness of 10–100 nm. As the composition is changing it is inadequate to calculate a resistivity in this

region. The surface resistance measured by platinum wires along the surface and making contact with it will give a resistance which is much less than that of a glass body as discussed by Holland[16]. This will be true whether the sodium ions are leached away or remain when water is absorbed from a humid atmosphere. Such electrodes can be electrolytically polarized when ions move from one electrode to another. The reactions are similar to those in an aqueous solution. Prolonged electrolysis will of course make the polarization resistance very high[42]. The outer part of the gel layer thus cannot be responsible for the resistances measured by us (Fig. 6), since the magnitudes and the activation energies differ greatly. The present study shows an activation energy of 23.8 kcal mol^{-1} compared to about 2 kcal mol^{-1} found by Kuznetsov[40]. The latter figure is of the same magnitude as for ions in aqueous solution. Further supporting evidence is given by Eisenman and co-workers[8,7], who found that 1-μm thick completely hydrated glass had a resistance of at most 16,500 Ω, measured through the plate from one solution to another. It varied with the potassium concentration of the solutions.

Electrolysis with direct current through the glass body can result in a decrease of current carriers in some layers resulting in a sharp increase of the resistance. Such a depletion can occur at a blocking metal electrode attached to the glass. The same effect can also be observed when current is transferred through the glass *via* a solution, if renewal of current carriers is impossible or too slow. As a result of such phenomena space charges may develop and cause the resistance to increase with time and current. The influence of depletion or concentration polarization due to the passage of current should be very small in our case because we have used a current of only 150 pA cm^{-2}. If all the alkali ions move, the front will advance at a rate of 0.1 nm sec^{-1} for 1μA cm^{-2}. All the ions cannot be moved away through a distance sufficiently large to explain the resistance observed for a pulse. The possibility of defect removal alone can also be dismissed since Ohm's law is obeyed. Had this been responsible, the time constant would have been reduced when the current was increased, provided the rate of defect formation was constant. The high reproducibility of the resistance at a given temperature from pulse to pulse makes a depletion mechanism unlikely. If the current was allowed to flow for one hour or more the resistance began to increase slightly. This experiment was carried out with a sodium-selective electrode. Proctor and Sutton[43,44] have investigated the space charge which results from prolonged electrolysis. At 383°C and 180 V cm^{-1} it required more than one hour before the space charge was fully developed. Probes inserted in the 0.05-cm thick specimen showed that the space charge was located at the surface, more especially at the anode.

Until now several mechanisms have been dismissed but no alternative proposition has been given. The present data do not permit such an explanation to be put forward. Further investigations are necessary. An explanation might be found in the propositions outlined by Muray[30]. The current in the glass is carried by doubly occupied alkali ion defects, and in the solution by different ions, not necessarily univalent alkali ions. There must be some layer in the glass where there is a change from conduction by one species to conduction by the other. The change-over mechanism may have a higher activation energy than either of these conduction processes. Such a layer must be located somewhere between the non-hydrated glass body and the outer gel layer where the conduction is electrolytic.

In the literature there is further information relevant to the conduction mecha-

nism in the surface. We hope to be able to continue the discussion in a paper in the near future when the results from present investigations become available.

Time constants

The glass membrane is in contact with a conducting medium on each side. When a current is passed, the geometric capacitor represented by the glass membrane will be charged and this charging will result in a time constant. Other capacitors, *e.g.* in the leads, have been neutralized in our measuring circuit. When an equivalent circuit is assumed it must be remembered that it may not be unique. Other circuits may fully explain the time constants. The model circuit (Fig. 7), only serves to check the accuracy of the apparatus and need not represent an actual physical model.

The information contained in the time constants is the same as the information in a set of relaxation times, the two quantities being identical.

The activation energies of the time constants τ_1 and τ_2 are equal to those of R_1 and R_2, the equivalent capacitor is therefore independent of temperature. Taylor[23-25] similarly found that the activation energy of the distributed relaxation time is the same as that of the d.c. resistance. He also showed that the form of the distribution is independent of temperature which is equivalent to our result that each process has the same activation energy. It can be concluded that the time constants arise solely from the ionic migration represented by resistances R_1 and R_2.

The time constants τ_3 and τ_4 originating in the surface behave quite differently. The activation energies are higher than those of R_3 and R_4. The equivalent capacitance must therefore change according to an exponential function of the inverse absolute temperature. The time constants contain information in addition to that given by R_3 and R_4. Further discussions on this point will be postponed to a future paper on surface properties.

Application of the assumed model

The model used in this paper follows from a derivation of a single resistivity which was later deduced to be a series combination of resistivities, eqn. (7). As time constants are measured primarily it would have been more satisfactory to derive an equation for the time course. It proved to be very difficult to do such a derivation from a model, mainly because the fundamentals are vague. It can be mentioned that the experimental material can be fitted to an equation of the form:

$$\text{voltage change} = K \times \exp(-K'' t^{\alpha}) \tag{10}$$

One such equation fits to the glass body and another to the surface; α was 0.5 for the Ingold glass but was found to vary with composition. The time-dependence of stress in glass as well as other phenomena have been expressed in the form of eqn. (10). As there is at present no theoretical foundation for this equation, we think that our approach is more satisfactory. By taking diffusion into account it might be possible to obtain functions which in some ranges of the parameters can be approximated by eqn. (10).

ACKNOWLEDGEMENT

The authors wish to thank Dr. Ingold, Zürich, for gifts of specially made electrodes, Dr. O. Ginstrup for advice concerning the constant current generator, Mr. G.

Paavola for doing the measurements on equivalent circuits and Dr. M. Sharp for reading the manuscript.

This work was supported by grants from the Swedish Natural Science Research Council.

SUMMARY

The resistance as well as the time constant of a glass membrane can be separated into one part originating in the glass body and one part in the surface. The surface glass time constant decreases rapidly with temperature, at room temperature it is of the size tens of seconds, while the glass time constant is in the millisecond range. By subdividing the parts further the results could be used for calculating jump distances of the conductive lithium ions. The size of the surface resistance was dependent on the hydration and is presumably caused by an energy barrier. A very accurate pulse technique was developed for the measurements.

REFERENCES

1 W. S. HUGHES, *J. Chem. Soc.*, (1928) 491.
2 D. A. MACINNES AND M. DOLE, *J. Am. Chem. Soc.*, 52 (1930) 29.
3 D. A. MACINNES AND D. BELCHER, *J. Am. Chem. Soc.*, 53 (1931) 3315.
4 M. DOLE, *The Glass Electrode*, John Wiley and Sons Inc., New York, 1941.
5 E. L. ECKFELDT AND G. A. PERLEY, *J. Electrochem. Soc.*, 98 (1951) 37.
6 A. DISTÈCHE AND M. DUBUISSON, *Rev. Sci. Instr.*, 25 (1954) 869.
7 G. EISENMAN, *Glass Electrodes for Hydrogen and Other Cations*, Marcel Dekker, New York, 1967.
8 G. EISENMAN, J. P. SANDBLOM AND J. L. WALKER, JR., *Science*, 155 (1967) 965.
9 R. P. BUCK, *J. Electroanal. Chem.*, 18 (1968) 363.
10 R. P. BUCK, *Anal. Chem.*, 40 (1968) 1432; 40 (1968) 1439.
11 R. P. BUCK AND I. KRULL, *J. Electroanal. Chem.*, 18 (1968) 387.
12 G. W. MOREY, *The Properties of Glass*, ACS Monograph Series, Reinhold Publishing Corp., New York, 1954.
13 O. V. MAZURIN, *Electrical Properties and Structure of Glass*, Vol. 4, Consultants Bureau, New York, 1965.
14 A. E. OWEN, in J. E. BURKE, (Ed)., *Progress in Ceramic Science*, Vol. 3, Pergamon Press, London, 1963, p. 77.
15 H. S. ISAACS AND J. S. L. LEACH, *J. Electrochem. Soc.*, 110 (1963) 680.
16 L. HOLLAND, *The Properties of Glass Surfaces*, Chapman & Hall, London, 1966.
17 M. A. RANA AND R. W. DOUGLAS, *Phys. Chem. Glasses*, 2 (1961) 179.
18 J. M. STEVELS, *Handbuch der Physik*, 20 (1957) 350, Springer Verlag, Berlin.
19 J. J. MURAY, *J. Appl. Phys.*, 33 (1962) 1525.
20 E. H. SNOW AND B. E. DEAL, *J. Electrochem. Soc.*, 113 (1966) 263.
21 O. L. ANDERSON AND D. A. STUART, *J. Am. Ceram. Soc.*, 37 (1954) 573.
22 J. M. STEVELS, *Philips Tech. Rev.*, 13 (1952) 360.
23 H. E. TAYLOR, *Trans. Faraday Soc.*, 52 (1956) 873.
24 H. E. TAYLOR, *J. Soc. Glass Technol.*, 41 (1957) 350 T.
25 H. E. TAYLOR, *J. Soc. Glass Technol.*, 43 (1959) 124 T.
26 W. KAUZMANN, *Rev. Mod. Phys.*, 14 (1942) 12.
27 C. P. SMYTH, *Dielectric Behaviour and Structure*, McGraw-Hill, New York, 1955.
28 R. J. CHARLES, *J. Am. Ceram. Soc.*, 47 (1964) 559.
29 R. J. CHARLES, *J. Appl. Phys.*, 32 (1961) 1115.
30 J. J. MURAY, *J. Appl. Phys.*, 33 (1962) 1517.
31 Y. HAVEN AND B. VERKERK, *Phys. Chem. Glasses*, 6 (1965) 38.
32 R. J. CHARLES, *J. Am. Ceram. Soc.*, 45 (1962) 105.

33 N. F. MOTT AND R. W. GURNEY, *Electronic Processes in Ionic Crystals*, Clarendon Press, Oxford, England, 2nd ed., 1948.
34 C. HIRAYAMA AND D. BERG, *Bull. Am. Ceram. Soc.*, 40 (1961) 551.
35 E. SEDDON, E. J. TIPPETT AND W. E. S. TURNER, *J. Soc. Glass Technol.*, 16 (1932) 450.
36 A. YA. KUZNETSOV AND I. G. MELJNIKOVA, *Zh. Fiz. Khim.*, 24 (1950) 1204.
37 C. L. BABCOCK, *J. Am. Ceram. Soc.*, 17 (1934) 329.
38 J. O. ISARD, *J. Electroanal. Chem.*, 18 (1968) 56.
39 D. HUBBARD AND G. F. RYNDERS, *J. Res. Nat. Bur. Std.*, 40 (1948) 105.
40 A. YA. KUZNETSOV, *Zh. Fiz. Khim.*, 27 (1953) 657, as cited by (16).
41 Z. BOKSAY, G. BOUQUET AND S. DOBOS, *Phys. Chem. Glasses*, 8 (1967) 140.
42 E. C. SALTHOUSE AND D. S. MCILHAGGER, *Proc. Inst. Elec. Engrs. London*, 110 (1963) 983.
43 T. M. PROCTOR AND P. M. SUTTON, *J. Chem. Phys.*, 30 (1959) 212.
44 T. M. PROCTOR AND P. M. SUTTON, *J. Am. Ceram. Soc.*, 43 (1960) 173.

ELECTROANALYTICAL CHEMISTRY AND INTERFACIAL ELECTROCHEMISTRY
Elsevier Sequoia S.A., Lausanne – Printed in The Netherlands

ADSORPTION OF LEAD(II) CHLORIDE BY CHRONOAMPEROMETRIC MEASUREMENTS

MAURIZIO CASELLI AND PAOLO PAPOFF
Istituto di Chimica Analytica dell'Universita' di Bari, (Italy)
(Received December 12th, 1968; in revised form, April 24th, 1969)

The absorption mechanism of a charged reactant on an electrode surface is of interest, particularly when the reactant is able to bind one or more supporting electrolyte anions, and gives different charged complexes.

If the electron transfer and the complex equilibrium rearrangements are not rate-determining steps, the amount of adsorbed reactant at equilibrium may depend on the distribution of the reactant among the different complexes in the solution and on the electrode potential, at constant free surface and temperature. During the approach to equilibrium, the exchange rate for any equilibrium type may be hindered by steric effects or catalyzed by the presence of other adsorbed particles.

In the present paper results are reported for the adsorption of lead(II) as function of KCl, KNO_3, NaCl and $NaClO_4$ concentrations. This system was chosen since it has relatively high electron transfer and equilibria rearrangement rates, and also because lead adsorption appeared to be weak[1,2]. This last fact was of interest from the point of view of checking whether the experimental method used was able to give consistent and accurate information.

The technique employed was chronoamperometry with linear scanning of the potentials, which, as Wopschall and Shain[3] have calculated the theoretical equations in the case of adsorption both of reactant and product, promises quick qualitative information and accurate quantitative data about the adsorption of the system under investigation.

While this work was in progress, Timmer *et al.*[4] published a paper on the same subject. Since these authors used an impedance method, a comparison between the experimental data obtained with the different techniques appeared to us very useful. In fact, it was found that the data obtained by chronoamperometry were as accurate as those from the impedance method which is, however, more sophisticated and time-consuming in the elaboration of the data. Once this was established, by using a greater variation and concentration of supporting electrolyte, our interpretation of the data (which are not in agreement with that of Timmer *et al.*) appears to be the more likely.

EXPERIMENTAL

All chemicals (A.R. grade) were purified by recrystallization followed by heating at a temperature below the melting or decomposition point.

Solutions were prepared with water distilled twice from $KMnO_4$. Mercury

was treated with diluted HNO_3, heated to 400°C with air bubbling through, and distilled in a vacuum still. A $PbCl_2$ stock solution was prepared and diluted to the required concentration before each experiment. The reference electrode was an SCE. The test electrode was a hanging mercury drop electrode, the surface of which was renewed before each scanning of potential. A delay of 30 s after the renewal assured the attainment of adsorption equilibrium (scanning after varying intervals gives identical results).

Owing to the relatively high concentrations of salts in the solutions, a three-electrode system with automatic correction of ohmic drop was used[5]. This correction was effective except at the highest scanning rates where the resistance between electrode surface and the Luggin capillary tip of the third electrode produced detectable lowering of the peak current. In this case, correct values of i_p were obtained by using the equation of Nicholson[6] or De Vries[7].

In order to calculate the value of Γ_{Pb} as a function of the Cl^- concentration, the starting potential should be properly chosen to verify that the charge value on the metal (before the scanning of the potential) is always the same[8] regardless of the Cl^- concentration in the bulk. In the present case we have found that in the range -100 to -300 mV *vs.* SCE, the lead adsorption found is practically independent of the starting potential, *i.e.* of the corresponding variation of the charge on the metal (see Fig. 1, referred to measurements in 1 *M* KCl solutions).

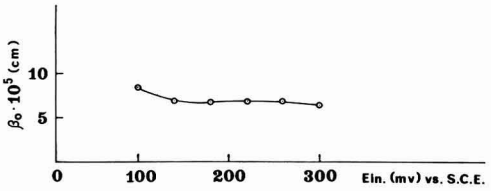

Fig. 1. Effect of the starting potential on the measured values of β_0.

A value of Γ_{Pb} independent of the potential in the region of the half-wave potential was assumed also by Timmer *et al.*[4] and confirmed by us in another section of this paper in a further analysis of their data. A starting potential of -240 mV was therefore generally used in our measurements.

TREATMENT OF THE DATA

The shape of the current *vs.* potential curves and the increase of the cathodic to anodic peak current ratio $(i_p)_c/(i_p)_a$ (Fig. 2), obtained by increasing the scanning rate, suggest[3] that any adsorption of the product may be neglected, the reactant being the only particle adsorbed.

In the treatment of the data, the values of i_p were used in most cases. In some experiments the integrated current *vs.* potential curves were calculated. In the former case, eqn. (49) of Wopschall and Shain[3] was used:

$$\frac{[\psi(\mathrm{at})_p]}{0.446} = i(t)/nFAC_O^*\sqrt{D_O a}\cdot 0.446 = 0.851 + 0.2954\,P_O \qquad (1)$$

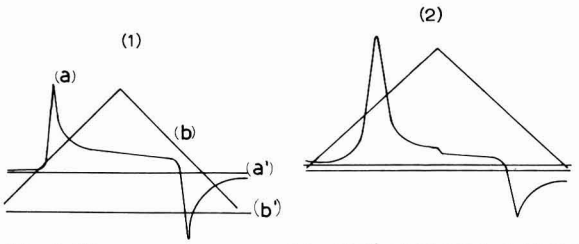

Fig. 2. Chronoamperograms of 5×10^{-4} M Pb(II) in 1 M KCl. Potential scanning rate v: (1) 0.105; (2) 98 Vs^{-1}. (a) Current curve; (b) potential curve; (a'), (b') corresponding starting levels.

where A is the area of the electrode,
C_O^* is the initial bulk concentration of substance O,
D_O is the diffusion coefficient of O,
$a = nFv/RT$,
$P_O = 4\Gamma_O^s\sqrt{a}/K_O\sqrt{\pi D_O}$
v = the rate of the potential sweep,
K_O = the adsorption constant defined by $K_O = \Gamma_O^s C/\Gamma_O$.

For values of P_O greater than 2, the current function ψ(at) can be expressed as the ratio of the peak current function in the presence of adsorption to that in the absence of adsorption

$$\frac{(i_p/v^{\frac{1}{2}}C_O^*)_{ads}}{(i_p/v^{\frac{1}{2}}C_O^*)_{v\to 0}} = R$$

and R is found to be a linear function of P_O within $\pm 3\%$, according to

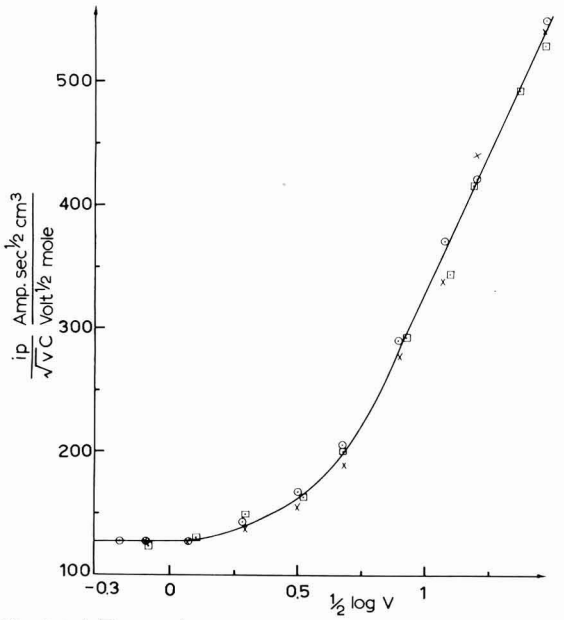

Fig. 3. $i_p/\sqrt{v} \times C$ *vs.* $\frac{1}{2}\log v$ in 1 M KCl for three concns. of Pb(II): (×) 1×10^{-4}; (⊙) 5×10^{-4}; (⊡) 7×10^{-4} M.

$$R = 0.851 + 0.2954P_O \qquad P_O > 2 \tag{2}$$

For $P_O < 2$, R calculated as the peak current ratio is higher than the ψ(at) value.

In order to linearize the function R also at relatively low scanning rates (low P_O), eqn. (2) was modified according to:

$$\frac{R_{exp}}{f(R)} = 0.851 + 0.2954P_O \tag{3}$$

where $f(R)$ is the ratio $R_{theor}/([\psi(at)]_p)_{theor}$.

In Fig. 3 $i_p/v^{\frac{1}{2}}c$ is plotted *vs.* $\frac{1}{2}\log v$. Regardless of the Pb(II) concentration used (10^{-4}–7×10^{-4} M), the experimental points lie on the same curve, which is in agreement with a linear isotherm. Consequently all other measurements were done using a Pb(II) concentration of 5×10^{-4} M.

The curves $R/f(R)$ *vs.* $\sqrt{v}$ are plotted in Fig. 4 for some KCl concentrations. In Table 1 the values of $\beta_0 = \Gamma^s_O/K_O$, calculated from these curves according to (3), are shown for each supporting electrolyte composition and temperature.

Some measurements were also made by integrating the oscillopolarograms between the initial potential E_i and the final potential E_f. In this case, the measured quantity of charge q_{tot} is related[9] to the quantity of charge q_{ads} due to the concentration of adsorbed reactant, by

$$q_{tot} = \frac{Kc}{v^{\frac{1}{2}}} + q_{ads} + q_{dl}$$

where K is a constant dependent on E_i and E_f, c the concentration of the reactant (mol cm^{-3}) in the bulk of the solution and q_{dl} the change in charge density of the double layer on going from E_i to E_f. From the plot q_{tot} *vs.* $v^{-\frac{1}{2}}$ the intercept of the

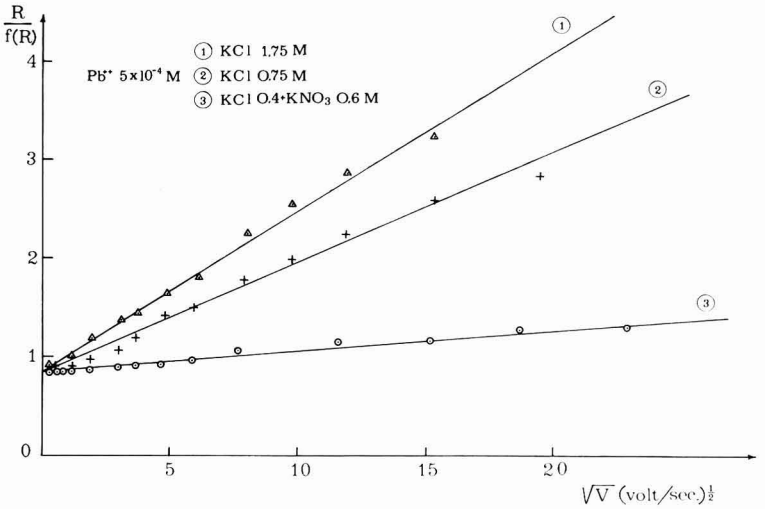

Fig. 4. $R/f(R)$ (see eqn. 3) *vs.* $v^{\frac{1}{2}}$; 5×10^{-4} M Pb(II). (1) 1.75 M KCl; (2) 0.75 M KCl; (3) 0.4 M KCl + 0.6 M KNO_3.

TABLE 1

$T/°C$	*Supporting electrolyte*	$C/mol\ l^{-1}$	E_{in}	$\beta_{0_{exp}} \times 10^5$	$\beta_0 \times 10^5$ *calcd. according to eqn.* (13) (*equil.* 4) $K_{PbCl_3^-} = 1.5 \times 10^6$ $mol^{-1}\ cm^3$	$\Delta\% \frac{(\beta_{0_{calc}} - \beta_{0_{exp}})}{\beta_{0_{exp}}}$ %	$\beta_0 \times 10^5$ *calcd. according to eqn.* (14) (*equil.* 5) $\frac{K_{PbCl_4^{2-}}}{\Gamma^s_{PbCl_4^{2-}}} = 830\ cm^{-1}$	$\Delta\% \frac{(\beta_{0_{calc}} - \beta_{0_{exp}})}{\beta_{0_{exp}}}$ %
25	KCl	0.5	240	2.68	2.88	+ 7.30	2.50	− 6.40
25	KCl	0.75	240	5.51	4.87	−11.50	4.68	−15.10
25	KCl	1	240	7.26 (8.6)*	6.25	−13.90	6.39	−11.97
25	KCl	1	100	8.55				
25	KCl	1	140	7.05				
25	KCl	1	180	6.84				
25	KCl	1	220	6.87				
25	KCl	1	260	6.87				
25	KCl	1	300	6.58				
35	KCl	1	240	3.68 (3.9)*				
45	KCl	1	240	2.06				
25	KCl	1.5	240	7.47	7.91	+ 5.86	8.26	+10.56
25	KCl	1.75	240	7.80	7.68	− 1.50	8.17	+ 4.74
25	KCl	2	240	6.94 (6.2)*	6.88	− 9.23	7.12	+ 2.62
25	$KCl + KNO_3$	0.4 + 0.6	240	1.16	1.01	−12.80	8.18	−29.47
25	$KCl + KNO_3$	0.5 + 0.5	240	1.37	1.77	+28.90	1.48	+ 8.43
25	$KCl + KNO_3$	0.5 + 0.5	180	1.80				
25	$KCl + KNO_3$	0.5 + 0.5	300	1.21				
25	$KCl + KNO_3$	0.75 + 0.25	240	4.25	4.02	− 5.30	3.76	−12.22
25	$KCl + KNO_3$	1 + 1	240	3.22	3.77	+17.08	3.45	+ 5.28
25	NaCl	0.75	240	3.45		$\Delta_m = 11.34$		$\Delta_m = 10.68$
25	NaCl	1	240	5.15				
25	$NaCl + NaClO_4$	0.75 + 0.25	240	3.35				
25	$NaCl + NaClO_4$	1 + 1	240	5.15				
25	LiCl	1	240	5.76				
25	CsCl	1	240	13.9				

* By integrating *i vs. t* curves

curve at $v^{-\frac{1}{2}}=0$ gives the value of $q_{ads}+q_{dl}$. The method is not very accurate since in our case q_{ads} is of the same order of magnitude as q_{dl}, which may differ from the corresponding value obtained in the absence of specific adsorption of the reactant. Nevertheless, the few data obtained for 1 *M* KCl are in fair agreement with the other data (see Table 1). In Fig. 5 the values of q are plotted *vs.* $v^{-\frac{1}{2}}$ for three concentrations of lead(II) in 1 *M* KCl.

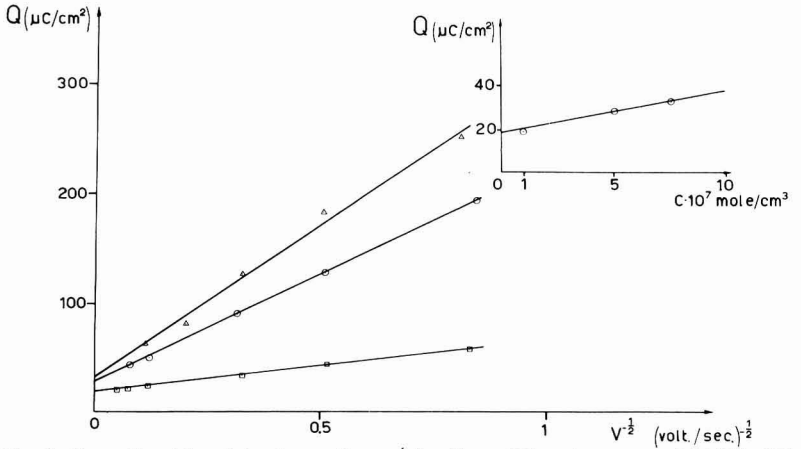

Fig. 5. Capacitive+faradaic charge Q *vs.* $v^{\frac{1}{2}}$ for three different concns. of Pb(II): (□) 1×10^{-4} *M*; (⊙) 5×10^{-4} *M*; (△) 7.5×10^{-4} *M*. Supporting electrolyte 1 *M* KCl; E_i, 250 mV SCE; E_f, 550 mV. In the upper part of the Figure Q at $v=0$ is plotted *vs.* lead concn. The intercept of this curve gives the double-layer charge density change (19 μC cm^{-2}).

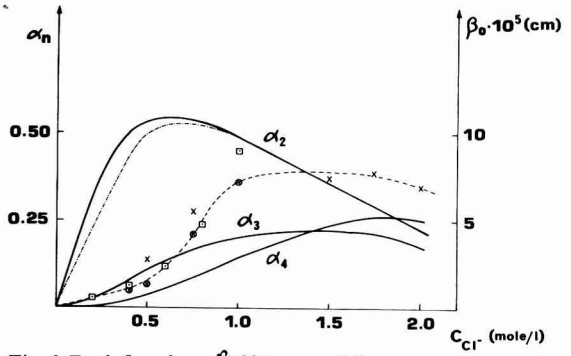

Fig. 6. Expl. β_0 values *vs.* Cl^- concn. Measurements at $\mu=1$: x moles $Cl^-+(1-x)$ moles NO_3^-; (⊡) ref. 4; (⊗) this paper. At μ variable: (×) this paper. (–·–·–) α_2 values in presence of NO_3^- at $\mu=1$.

In Fig. 6 all our values in KCl and KCl+KNO_3 are reported, together with the data of Timmer *et al.* It can be seen that the same curve arbitrarily drawn through the experimental points represents both series of data except for the 1 *M* KCl point where the Timmer value seems to be about 20% too high. This agreement excludes the the suggestion that in our experimental conditions we are dealing with an average concentration of Γ_{Cl^-} in the range of potential explored during the scanning, since Timmer *et al.* worked at a fixed potential instead of a scanning potential.

SUPPORTING ELECTROLYTE EFFECT

The ability of the supporting electrolyte to form complexes with the metal ion, which may preferentially be adsorbed on the electrode surface, and its own competition to occupy free electrode surface, are determining factors in the mechanism of metal ion adsorption both from the kinetic and equilibrium points of view.

In our case, two different mechanisms may explain all the experimental data with about the same extent of reality: the adsorption of $PbCl_3^-$ *via* the adsorbed Cl^- according to:

$$PbCl_{3\,sol}^- + Cl_{ads}^- \rightarrow PbCl_{4\,ads}^{2-} \tag{4}$$

or the adsorption of $PbCl_4^{2-}$ again to give $PbCl_{4\,ads}^{2-}$ according to:

$$PbCl_{4\,sol}^{2-} \rightarrow PbCl_{4\,ads}^{2-} \tag{5}$$

Adsorption of $PbCl_3^-$

Assuming that lead is adsorbed only as a complex (we assume for the sake of simplicity that this complex is $PbCl_3^-$) *via* adsorbed Cl^- according to (4), for the free surface sites, S:

$$S = \Gamma^s_{Cl^-} - \Gamma_{Cl^-} - f\Gamma_{NO_3^-} - f'\Gamma_{PbCl_4^-} \tag{6}$$

where f and f' are conversion factors in order to relate all the concentrations of adsorbed particles to $\Gamma^s_{Cl^-}$ and are respectively equal to $\Gamma^s_{Cl^-}/\Gamma^s_{NO_3^-}$ and $\Gamma^s_{Cl^-}/\Gamma^s_{PbCl_4^{2-}}$. In eqn. (6), the adsorption of Cl^- and NO_3^- has been considered in conjunction with the lead complex adsorption. For each equilibrium:

$$K_{Cl^-} = \frac{S[Cl^-]}{\Gamma_{Cl^-}}\ ;\quad K_{NO_3^-} = \frac{S[NO_3^-]}{f\Gamma_{NO_3^-}}\ ;\quad K'_{PbCl_4^{2-}} = \frac{\Gamma_{PbCl_4^{2-}}}{[PbCl_3^-]\Gamma_{Cl^-}} \tag{7}$$

From the first two eqns. (7),

$$\Gamma_{NO_3^-} = \Gamma_{Cl^-}\frac{K_{Cl^-}}{fK_{NO_3^-}}\frac{[NO_3^-]}{[Cl^-]}$$

Putting the $\Gamma_{NO_3^-}$ value expressed in this way in eqn. (6):

$$S = \Gamma^s_{Cl^-} - \Gamma_{Cl^-} - \frac{K_{Cl^-}}{K_{NO_3^-}}\frac{[NO_3^-]}{[Cl^-]}\cdot\Gamma_{Cl^-} - f'\Gamma_{PbCl_4^{2-}} \tag{8}$$

From this and the first eqn. (7):

$$\Gamma_{Cl^-} = \frac{(\Gamma^s_{Cl^-} - f'\Gamma_{PbCl_4^{2-}})\cdot[Cl^-]}{K_{Cl^-}\left(1 + \frac{[NO_3^-]}{K_{NO_3^-}} + \frac{[Cl^-]}{K_{Cl^-}}\right)} \tag{9}$$

which in absence of NO_3^- and $PbCl_3^-$ assumes the usual form:

$$\Gamma_{Cl^-} = \frac{\Gamma^s_{Cl^-}\cdot[Cl^-]}{K_{Cl^-} + [Cl^-]} \tag{10}$$

From (4) and (9), for $\Gamma_{PbCl_4^{2-}}$

$$\Gamma_{PbCl_4^{2-}} = \frac{K'_{PbCl_4^{2-}}\,\alpha_3 C_{Pb}(\Gamma^s_{Cl^-} - f'\Gamma_{PbCl_4^{2-}})[Cl^-]}{K_{Cl^-}\left(1 + \dfrac{[NO_3^-]}{K_{NO_3^-}} + \dfrac{[Cl^-]}{K_{Cl^-}}\right)} \tag{11}$$

where $\alpha_3 C_{Pb} = [PbCl_3^-]$, depending on the concentration of Cl^-.

In the general case for the equilibrium:

$$(PbCl_m)^{(m-2)-} + n\,Cl^-_{ads} \rightleftarrows (PbCl_{m+n})^{(m+n-2)-}_{ads}$$

one has

$$\Gamma_{PbCl_{m+n}} = \frac{K'_{PbCl_{m+n}}(\Gamma^s_{Cl^-} - f''\Gamma_{PbCl_{m+n}})^n \alpha_m C_{Pb}[Cl^-]^n}{K_{Cl^-}\left(1 + \dfrac{[NO_3^-]}{K_{NO_3^-}} + \dfrac{[Cl^-]}{K_{Cl^-}}\right)^n} \tag{12}$$

Assuming as a first approximation $f'' = 1$, from (12)

$$F_n = \frac{\Gamma_{PbCl_{m+n}} K_{Cl^-}\left(1 + \dfrac{[NO_3^-]}{K_{NO_3^-}} + \dfrac{[Cl^-]}{K_{Cl^-}}\right)^n}{\alpha_m C_{Pb}(\Gamma^s_{Cl^-} - \Gamma_{PbCl_{m+n}})^n} = K'_{PbCl_{m+n}} \cdot [Cl^-]^n \tag{13}$$

It is evident that the plot of F_n *vs.* $[Cl^-]^n$ will give a straight line only if the correct equilibrium has been considered. The experimental result gives a linear relation only in the case of equilibrium (4). In all the other equilibria considered, the slope F_n *vs.* $[Cl^-]^n$ was not a straight line, or the line did not intersect the axes at the origin.

The values of K_{Cl^-} and $K_{NO_3^-}$ used in the calculation of F, were calculated using the data of Grahame and Parsons[10] and of Payne[11] for the specifically adsorbed charge in Cl^- and NO_3^- solutions. The isotherms reported in Fig. 7 were obtained from the corresponding data for q_{ads} and $q_{electrode}$, calculated for the starting potential at various concentrations of anion. In the case of Cl^-, a Langmuir isotherm with $\Gamma^s_{Cl^-} = 4.04 \times 10^{-10}$ mol cm^{-2} and $K_{Cl^-} = 0.62 \times 10^{-3}$ mol cm^{-3} fitted the experimental isotherm fairly well in the range of concentrations used.

In the case of NO_3^-, the corresponding values were 2.62×10^{-10} and 0.48×10^{-3}. As shown in Fig. 7, a Frumkin-type isotherm would better represent the function although, in the range of concentration that we used, the Langmuir isotherm may be considered sufficiently good. No correction has been made for ClO_4^- on account of the low adsorption of this electrolyte.

The α_m values in pure KCl solutions were calculated from literature data[12] which are essentially the same as in ref. 4 except for the use in our calculation of a $K_6 = 2.87$. This constant takes into account both the presence of a $PbCl_6^{4-}$ complex at the highest concentrations of Cl^- and the effect of ionic strength variation in respect to $\mu = 1$. In fact for $[Cl^-] \lesssim 1$ the corrections on α_m due to these effects are practically zero. In solutions containing NO_3^-, the equilibrium of $PbNO_3^-$ formation was considered and a $K_{PbNO_3} = 2.04$ at $\mu = 1$ [13] and 3 at $\mu = 2$ [14] was used in the α_m calculation.

By using the experimental β_0 and the calculated α_m, and K_{Cl^-} and $K_{NO_3^-}$ data in eqn. (13), a straight line was obtained in the case of equilibrium (4). From the slope of this curve a value of $K_{PbCl_3^-} = 1.5 \times 10^6$ cm^3 mol^{-1} was calculated.

In Table 1 the β_0 values calculated using eqn. (13) are reported together with the percentage deviation.

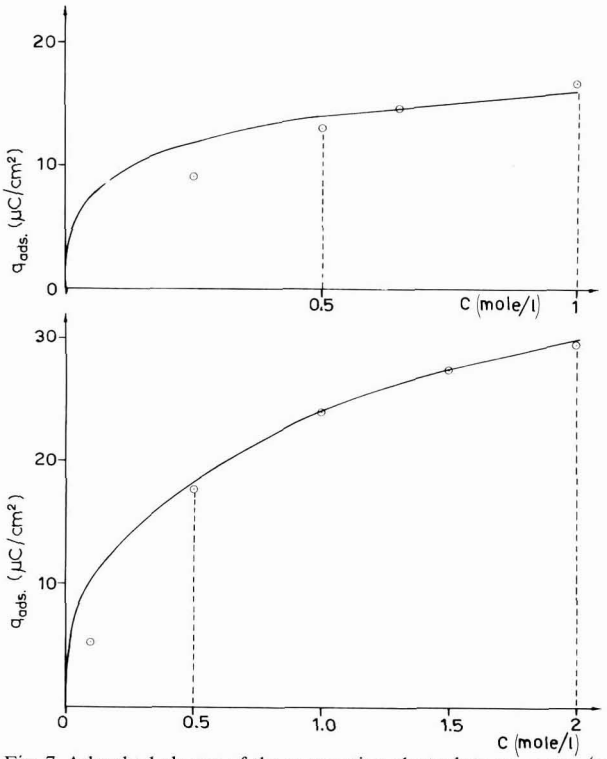

Fig. 7. Adsorbed charge of the supporting electrolyte *vs.* concn. (continuous curve). Upper curve KNO_3; lower curve KCl; $E = 240$ mV SCE. The points represent the calcd. values according to a Langmuir isotherm.

The agreement between experimental and calculated values is good and could be considered as a measure of the confidence in mechanism (4) if the same degree of accordance between experimental and calculated β_0 had not also been found when equilibrium (5) was considered.

In addition, the reason why the particle in the liquid phase in equilibrium with the adsorbed $PbCl_4^{2-}$ should be $PbCl_3^-$, even when the concentration of this complex is very small compared to the others, is not clear. It would be interesting in this sense to know (by use, for instance, of relaxation methods) if it is possible to determine the charge of the particle undergoing reduction in Cl^- solutions of lead(II), and to verify that also in the electron transfer $PbCl_3^-$ must be considered the most effective among the complexes in the formation of the adsorbed particle, reducible on the mercury surface.

Adsorption of $PbCl_4^{2-}$

If equilibrium (5) is considered, the corresponding adsorption equilibrium constant, referred to the free surface sites will be, according to the first two eqns. (7):

$$K_{PbCl_4^{2-}} = \frac{S[PbCl_4^{2-}]}{f'' \Gamma_{PbCl_4^{2-}}} \tag{7a}$$

and eqn. (6) will contain the term, $f'' \Gamma_{PbCl_4^{2-}}$, instead of $f' \Gamma_{PbCl_3^-}$.

From (6) and (7a):

$$S = \frac{K_{PbCl_4^{2-}} f'' \Gamma_{PbCl_4^{2-}}}{PbCl_4^{2-}} = \Gamma^s_{Cl^-} - \Gamma_{Cl^-} - f\Gamma_{NO_3^-} - f''\Gamma_{PbCl_4^{2-}}$$

$$= \Gamma^s_{Cl^-} - \frac{K_{PbCl_4^{2-}} f'' \Gamma_{PbCl_4^{2-}}}{[PbCl_4^{2-}]}\left(\frac{[Cl^-]}{K_{Cl^-}} + \frac{[NO_3^-]}{K_{NO_3^-}}\right) - f''\Gamma_{PbCl_4^{2-}}$$

remembering that $f'' = \Gamma^s_{Cl}/\Gamma^s_{PbCl_4^{2-}}$ and $[PbCl_4^{2-}] = \alpha_4 C_{Pb}$

$$\frac{\alpha_4 C_{Pb}}{\Gamma_{PbCl_4^{2-}}} = \frac{1}{\Gamma^s_{PbCl_4^{2-}}} K_{PbCl_4^{2-}} + \alpha_4 C_{Pb} + \frac{K_{PbCl_4^{2-}}}{K_{Cl^-}}[Cl^-] + \frac{K_{PbCl_4^{2-}}}{K_{NO_3^-}}[NO_3^-]$$

$$= \frac{K_{PbCl_4^{2-}}}{\Gamma^s_{PbCl_4^{2-}}}\left\{1 + \frac{1}{K_{Cl^-}}([Cl^-] + 1.29[NO_3^-]) + \frac{\alpha_4 C_{Pb}}{K_{PbCl_4^{2-}}}\right\} \qquad (14)$$

where 1.29 is the ratio $K_{Cl^-}/K_{NO_3^-}$.

Since $\alpha_4 C_{Pb}/K_{PbCl_4^{2-}}$ is probably negligible compared with the other terms, from the experimental values of Γ_{Pb}/C_{Pb} and the values of α_4, it follows that the intercept of the curve $\alpha_4 C_{Pb}/\Gamma_{PbCl_4^{2-}}$ *vs.* $[Cl^-] + 1.29[NO_3^-]$ is equal to $K_{PbCl_4^{2-}}/\Gamma^s_{PbCl_4^{2-}}$ and the slope $= K_{PbCl_4^{2-}}/\Gamma^s_{PbCl_4^{2-}} \cdot K_{Cl^-}$. Using a value of 830 cm^{-1} for the ratio $K_{PbCl_4^{2-}}/\Gamma^s_{PbCl_4^{2-}}$, the minimum deviation was found between the experimental data of β_O and the corresponding data calculated according to (14).

In Table 1 the calculated β_O and the percentage deviation are reported for each condition of supporting electrolyte. As has been noted previously, the order of agreement between experimental and calculated data is practically the same whether equilibrium (4) or (5) is considered. Consequently, we have no strong evidence at present to prefer one of the equilibria to the other although equilibrium (5) where the same particle, $PbCl_4^{2-}$, is concerned in the two phases, seems to us the more likely. Certainly all other equilibria are to be disregarded. At the same time, the possibility that the lead complex might be adsorbed on the electrode regardless of the adsorption equilibria of Cl^- and NO_3^- on the electrode must be disregarded, as being inconsistent with experimental data.

According to this assumption, for a particular value of m, the ratio β_O/α_m should generally be constant. However, for each value of m between 1 and 4, this

TABLE 2

$C/(mol\ l^{-1})$		$\beta_0 \times 10^5$	$\beta_0/\alpha_2 \times 10^5$	$\beta_0/\alpha_3 \times 10^5$	$\beta_0/\alpha_4 \times 10^5$
Cl^-	NO_3^-				
0.40	+0.60	1.16	2.6	16.4	58.9
0.50		2.68	5.1	25.5	72.4
0.50	+0.50	1.37	2.80	13.8	39.0
0.75		5.51	10.2	33.4	64.8
1.00		7.26	14.2	35.8	50.4
1.00	+1.00	3.22	6.97	17.2	24.4
1.50		7.47	18.0	30.1	28.4
1.75		7.8	21.7	30.3	24.0
2.00		6.94	31.8	39.3	27.8

ratio is subject to very large variations. This can be seen also from Fig. 6 where the shape of the β_O function *vs.* Cl^- is quite different from the shape of the α_m functions.

SUPPORTING ELECTROLYTE CATION EFFECT

This effect was not fully investigated. It is apparent from Table 1 that at the same starting potential and the same Cl^- concentration there is a change in β_O of about -21%, -29%, $+91\%$ when K^+ is substituted by Li^+, Na^+, Cs^+ respectively. These variations are too large to be ascribed to experimental errors and may be explained by assuming that the type of cation affects the adsorption equilibrium of halide or leads complex ions also at a potential as positive as -240 mV *vs.* SCE, or contributes to the formation of ion-pairs to a different degree.

As far as we know, there is no experimental evidence that this is a general effect for many other systems.

EFFECT OF TEMPERATURE

Considering equilibrium (5), the ratio $K_{PbCl_4^{2-}}/\Gamma^s_{PbCl_4^{2-}} = 830\,cm^{-1}$ gives a value of $K_{PbCl_4^{2-}} = 8.3 \times 10^{-8}$ mol cm^{-3} if $\Gamma^s_{PbCl_4^{2-}}$ is estimated to be about $\frac{1}{4}\Gamma^s_{Cl^-}$. From the variation of β_O with temperature in the range 25°–45°C, $\Delta H_{ads} = 12$ kcal mol^{-1}. These data give $\Delta S_{ads} = 7.9$ cal $deg^{-1}\,mol^{-1}$ at 25°C. It must be emphasized that these values of ΔH and ΔS are overall values since the variation of β_O with temperature includes the unknown temperature effect on K_{Cl^-} and $K_{NO_3^-}$ (eqn. (14)).

POTENTIALITY OF CHRONOAMPEROMETRY IN THE STUDY OF ADSORPTION EQUILIBRIUM ON AN ELECTRODE SURFACE

The sensitivity of this method (I) and its reproducibility seem to be good compared with the other two methods of principal importance: impedance (II)[4] and double pulse (III)[15].

The limiting value of Γ^s/K detectable with an internal consistence of ± 2–4%, seems to be 1×10^{-5} cm; the reproducibility of Γ, after repeated sets of experiments is of the same order. I and III do not give information to whether there is a potential effect on K_{ads} within the range of starting and final potential, but give rapid quantitative information on the adsorption equilibria. II is much more time-consuming but allows the dependence of K_{ads} on the $E_i \div E_{fin}$ potential range to be verified to some extent.

In fact, in impedance measurements[4]:

$$C_{If} = \left(\frac{\partial q^*}{\partial E}\right)_\psi - nF\frac{\sigma_R}{\sigma}\left(\frac{\partial \Gamma^*}{\partial E}\right)_\psi$$

where

$$q^* = q + nF\Gamma_O;\ \Gamma^* = \Gamma_O + \Gamma_R;\ \frac{\sigma_R}{\sigma} = [1+\exp(-\varphi_m)]^{-1}$$

$$\varphi_m = \frac{nF}{RT}(E - E_{\frac{1}{2}});\ \psi = C_O\sqrt{D_O} + C_R\sqrt{D_R}$$

C_{lf} is the low frequency capacity derived from the impedance[4].

If $\Gamma_R = 0$ and $(\partial q/\partial E)_\psi$ is assumed to be equal to C_d,

$$C_{lf} - C_d = \frac{nF}{(1+\exp \varphi_m)} \frac{\partial \Gamma_O}{\partial E}$$

In the case of a linear isotherm $\Gamma_O = K_O C_O$ with K_O independent of the potential and $C_O = C_O^* \exp \varphi_m/(1+\exp \varphi_m)$

$$C_{lf} - C_d = \frac{n^2F^2}{RT} \frac{K_O C_O^* \exp \varphi_m}{(1+\exp \varphi_m)^3}$$

The plot $C_{lf} - C_d$ *vs.* $\exp \varphi_m/(1+\exp \varphi_m)^3$ is therefore a straight line with a slope proportional to Γ_O^*. If K depends on the potential[15,16] according to $K_O = K_O^\circ \exp(-\tau\varphi_m)$,

$$C_{lf} - C_d = \frac{n^2F^2}{RT} \frac{K_O^\circ C_O^* \exp[\varphi_m(1-\tau)]}{(1+\exp \varphi_m)^3} - \frac{n^2F^2}{RT} \frac{K_O^\circ C_O^* \tau \exp[\varphi_m(1-\tau)]}{(1+\exp \varphi_m)^2}$$

and the plot $C_{lf} - C_d$ *vs.* $\exp \varphi_m/(1+\exp \varphi_m)^3$ will present the shape of the Fig. 8

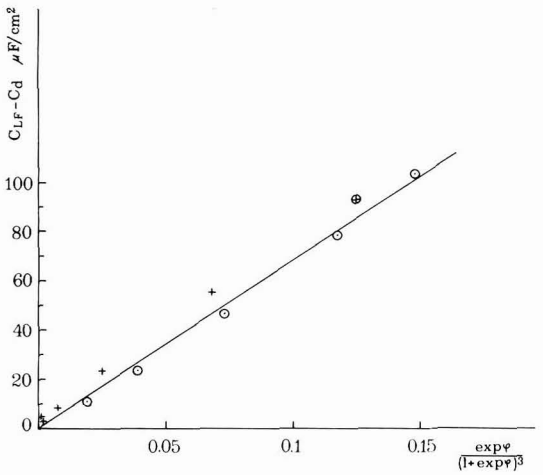

Fig. 8. Theoretical relation between $C_{lf} - C_d$ (function of impedance *vs.* $\exp \psi_m/(\exp \psi_m + 1)^3$. (⊙) referred to potentials cathodic to $E_{\frac{1}{2}}$; (+) to anodic potentials. The unbroken line is calculated for $\Gamma_O = 45 \times 10^{-12}$ mol cm² and K independent of the potential; the points for a value of $K = K^\circ \exp.(-0.0514\ \varphi_m)$.

where the straight line was calculated using $\Gamma_O^* = 45 \times 10^{-12}$ mol cm^{-2} and $\tau = 0$. The points are calculated using $\tau = -0.0514$ which corresponds to a reduction by one half of the K_O value for a potential variation of 175 mV of more cathodic values. Thus the Timmer diagram is of similar shape although it is slightly distorted from linearity.

ACKNOWLEDGEMENT

This work has been partly supported by the C.N.R., Rome.

SUMMARY

Chronoamperometry with linear potential scanning has been used to measure the adsorption of lead (II) on a mercury electrode surface as a function of the concentration of chloride, nitrate and perchlorate in the lead solution. It has been found that the experimental β_O values cannot be interpreted only as a function of the distribution of lead(II) among the different complexes with Cl^- and NO_3^- ions. If the competitive adsorption of these ions is considered, two different mechanisms may explain all the experimental data: the adsorption of the particle $PbCl_3^-$ *via* one adsorbed Cl^- according to: $PbCl_3^- + Cl_{ads}^- \rightleftarrows PbCl_{4\,ads}^{2-}$, or the adsorption of $PbCl_4^{2-}$ according to: $PbCl_4^{2-} \rightleftarrows PbCl_{4\,ads}^{2-}$. The second mechanism seems to be more likely. In the latter case, assuming for $\Gamma^s_{PbCl_4^{2-}}$ a value for $\frac{1}{4}\Gamma^s_{Cl^-} = 10^{-10}$ mol cm^{-2}, an equilibrium constant for a Langmuir linear isotherm of 8.3×10^{-8} mol cm^{-3} was obtained. From the dependence of $K_{PbCl_4^{2-}}$ on the temperature, values of $\Delta H = 12$ kcal mol^{-1} and $\Delta S = 7.9$ cal deg^{-1} mol^{-1} were calculated.

Chronoamperometry presents the same order of precision, accuracy and sensitivity as the other methods and is a good technique for gaining rapid information about the adsorption mechanism of any system that is able ro react on the electrode surface.

REFERENCES

1 G. C. BARKER in E. YEAGER (Ed.), *Transactions of the 1966 Symposium on Electrode Processes*, J. Wiley and Sons, New York, 1961, p. 359.
2 R. W. MURRAY AND D. J. GROSS, *Anal. Chem.*, 38 (1966) 392.
3 R. H. WOPSCHALL AND I. SHAIN, *Anal. Chem.*, 39 (1967) 1514.
4 B. TIMMER, M. SLUYTERS-REHBACH AND J. H. SLUYTERS, *J. Electroanal. Chem.*, 18 (1968) 93.
5 G. DAVOLIO, W. GUERZONI AND P. PAPOFF, *Electrochim. Acta*, 5 (1961) 231.
6 R. S. NICHOLSON, *Anal. Chem.*, 37 (1965) 667.
7 W. T. DE VRIES AND E. VAN DALEN, *J. Electroanal. Chem.*, 10 (1965) 183.
8 R. PARSONS, *J. Electroanal. Chem.*, 7 (1964) 136.
9 R. A. OSTERYOUNG, G. LAUER AND F. C. ANSON, *J. Electrochem. Soc.*, 110 (1963) 926.
10 D. C. GRAHAME AND R. PARSONS, *J. Am. Chem. Soc.*, 83 (1961) 1291.
11 R. PAYNE in E. YEAGER (Ed.), *Transactions of the 1966 Symposium on Electrode Processes*, J. Wiley and Sons, New York, 1967, p. 34.
12 P. PAPOFF, *Suomen Kemistilehti*, 29B (1956) 97. See also L. G. SILLÉN AND A. E. MARTELL, *Stability Constants, Spec. Publ. 17, Chem. Soc. London*, 1964.
13 A. I. BIGGS, H. N. PARTON AND R. A. ROBINSON, *J. Am. Chem. Soc.*, 77 (1955) 5844.
14 H. M. HERSHENSON, M. E. SMITH AND D. N. HUME, *J. Am. Chem. Soc.*, 75 (1953) 507.
15 J. H. CHRISTIE, R. A. OSTERYOUNG AND F. C. ANSON, *J. Electroanal. Chem.*, 13 (1967) 236.
16 R. PARSONS, *J. Electroanal. Chem.*, 5 (1963) 397.

ELECTROANALYTICAL CHEMISTRY AND INTERFACIAL ELECTROCHEMISTRY
Elsevier Sequoia S.A., Lausanne – Printed in The Netherlands

POLAROGRAPHISCHER NACHWEIS DER CARBONYL–SCHWEFEL-WECHSELWIRKUNG IN THIACYCLANONEN

R. HERZSCHUH UND R. BORSDORF
Sektion Chemie der Karl-Marx-Universität, Leipzig (D.D.R.)

(Eingegangen den 28. Mai 1968; revisioniert den 22. April 1969)

Während spektroskopische Untersuchungen über eine Carbonyl–Schwefel-Wechselwirkung in Ketosulfiden bereits vorliegen[1], ist über den polarographischen Nachweis dieser Wechselwirkung nur wenig berichtet worden. Wir haben eine Reihe von Thiacyclanonen (I)–(VIII), die wir teilweise aus anderen Gründen synthetisiert haben[2], sowohl spektroskopisch als auch polarographisch daraufhin untersucht.

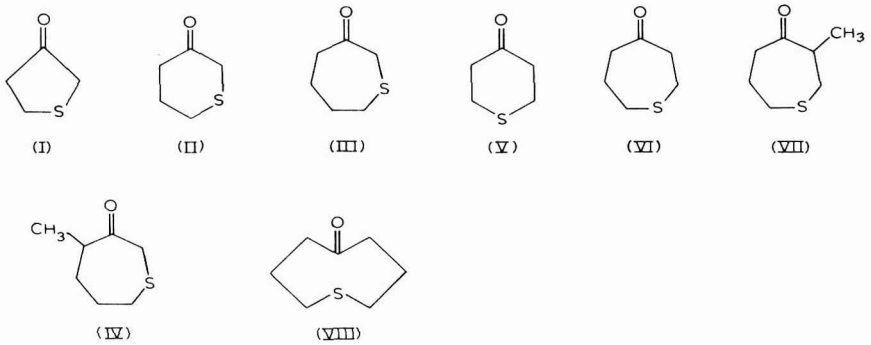

Für die Thiacyclanone (I)–(VIII), in denen die Carbonylgruppe und die Thioäthergruppierung durch eine, zwei bzw. im Thiocanon-5 (VIII) durch drei CH_2-Gruppen voneinander getrennt sind, sollte man—falls keine Wechselwirkung zwischen diesen Gruppen auftritt—ein u.v.-Spektrum erwarten, das sich additiv aus der Absorption dieser beiden Chromophore zusammensetzt. In Abb. 1 ist einmal das u.v.-

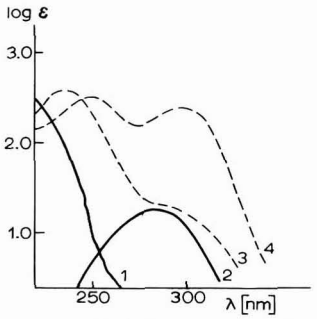

Abb. 1. UV-Spektren in Alkohol von: (1) Diäthylsulfid, (2) Cycloheptanon, (3) Thiepanon-4, (4) Thiepanon-3.

Spektrum des Cycloheptanons, zum anderen das des Diäthylsulfids aufgezeichnet. Es ist ersichtlich, dass weder die als Beispiele angeführten u.v.-Spektren des Thiepanons-3 (III) noch des Thiepanons-4 (VI) dieser Additivität entsprechen. Das gleiche gilt für die Spektren der weiteren in Tabelle 1 verzeichneten Thiacyclanone. Besonders

TABELLE 1

U.V.-ABSORPTIONEN DER THIACYCLANONE

Substanz	λ_{max}/nm	$lg\,\varepsilon$	λ_{max}/nm	$lg\,\varepsilon$
(I)	289	2.06	252	2.37
	298	2.08		
	308	2.04	233	2.32
(II)	307	2.34	250	2.37
(III)	298	2.34	249	2.54
(IV)	301	2.28	252	2.56
(V)				
(VI)	289	1.39	234	2.56
(VII)	295	1.47	237	2.68

gross sind die bathochromen und hyperchromen Veränderungen im u.v.-Spektrum der Thiacyclanone-3, die im nahen u.v. 2 Absorptionsbanden bei etwa 300 nm und mit etwas grösserer Intensität bei 250 nm aufweisen. In den Thiacyclanonen-4 treten dagegen wesentlich geringere Unterschiede von dem zu erwarteten Additivitätsspektrum auf. Eine Bande geringer Intensität um 300 nm ist zweifellos dem $n\rightarrow\pi^*$ Übergang der Carbonylgruppe zuzuschreiben. Der Ursprung der intensiveren Absorption um 230 nm ist unklar. Das u.v.-Spektrum von (VIII) wurde bereits ausführlich diskutiert[3].

Während zuerst angenommen wurde, dass nur der in der Sulfoniumform vorliegende Schwefel auf Grund seines polaren Feldeffektes die polarographische Aktivität der Carbonylgruppe beeinflusst[4], konnte Zuman und Mitarbeiter die erleichterte polarographische Reduktion der Carbonylgruppe im 3-Thianaphthenon nachweisen[5,6].

Untersuchungen von Lund[7] ergaben, dass die Reduktion von arylsubstituierten 3-Thiaketonen unter Lösung der Kohlenstoff–Schwefel-Bindung erfolgen kann.

Wir konnten feststellen, dass sich die Carbonyl–Schwefel-Wechselwirkung in den Thiacyclanonen ebenfalls auf die polarographische Reduktion auswirkt, und untersuchten sie in Abhängigkeit von der Stellung des Schwefelatoms zur Carbonylgruppe und von der Ringgrösse der Thiacyclanone.

Gegenüber der Carbonylgruppe der Cyclanone, die an der Quecksilbertropfelektrode bei sehr negativen Potentialen unter Beteiligung von 2 Elektronen zur Hydroxylgruppe reduziert wird[8], führt der Einbau eines Schwefelatoms in den Cyclanonring zu einer Verschiebung der Halbstufenpotentiale nach positiveren Werten. In Abb. 2 sind die Strom/Spannungskurven einiger Thiacyclanone aufgeführt. Tabelle 2 enthält die von uns vermessenen Halbstufenpotentiale der Verbindungen (I)–(VIII).

Es zeigt sich, dass die Thiacyclanone-4 schwerer als die Thiacyclanone-3 reduziert werden. (VIII) weist von allen untersuchten Thiacyclanonen das negativste

TABELLE 2

HALBSTUFENPOTENTIALE EINIGER THIACYCLANONE UND CYCLANONE

Substanz	$E_{\frac{1}{2}}(SCE)/V$	*Substanz*	$E^*_{\frac{1}{2}}(NCE)/V$
(I)	−1.81	Cyclopentanon	−2.46
(II)	−1.76	Cyclohexanon	−2.40
(III)	−1.82	Cycloheptanon	−2.48
(IV)	−1.88	Cyclooctanon	−2.43
(V)	−1.96		
(VI)	−2.00		
(VII)	−2.14		
(VIII)	−2.15		

* Gemessen in 90% Alkohol[5].

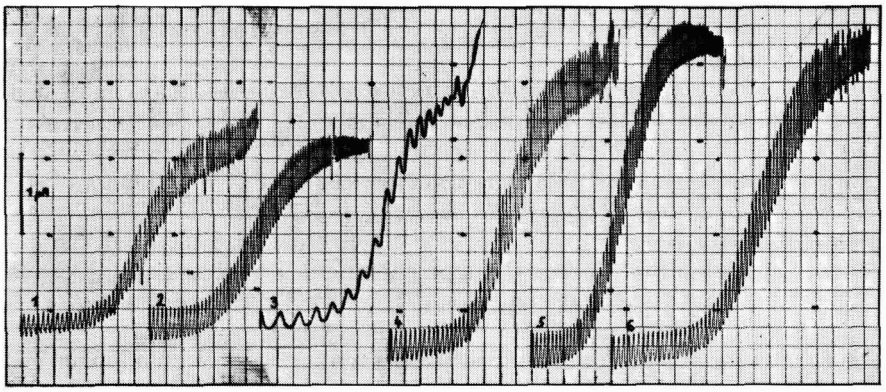

Abb. 2. Polarographische Reduktion der Thiacyclanone in einer alkoholischwässrigen Lösung (Alkohol:Wasser/75:25). Leitelektrolyt: 0.1 *M* $N(C_2H_5)_4ClO_4$. Depolarisatorkonzentration: (1–3) 1×10^{-3} *M*; (4–6) 1.5×10^{-3} *M*; 50 mV/Absz. (1) Thianon-3 (II), Kurvenbeginn −1.5 V; (2) Thianon-4 (V) ab −1.7 V; (3) Thiocanon-5 (VIII) ab −1.9 V (die Registrierung erfolgte mit erhöhter Geschwindigkeit); (4) Thiepanon-3 (III) ab −1.5 V; (5) Thiepanon-4 (VI) ab −1.8 V; (6) 4-Methylthiepanon-3 (IV) ab −1.5 V.

Halbstufenpotential auf, wobei aber auch hier gegenüber Cyclooctanon eine Veränderung nach positiven Werten hin erfolgt. Offensichtlich hängt die Veränderung der Halbstufenpotentiale von der Zahl der zwischen Carbonylgruppe und Schwefel befindlichen Methylgruppen ab, wobei berücksichtigt werden muss, dass sich in (VIII) aus konformativen Gründen Carbonylgruppe und Schwefel sehr nahe kommen[3] und somit auch eine direkte Wechselwirkung unabhängig von der dazwischenliegenden C-Kette in Betracht gezogen werden muss.

Auch die Ringgrösse ist auf die Lage der Halbstufenpotentiale von Einfluss. Ebenso wie bei den Cyclanonen und einigen ihrer Derivate[9] wird bei den Thiacyclanonen-3 die Reduktion in der Reihenfolge 6-Ring < 5-Ring und < 7-Ring erschwert. Ganz analog besitzt (V) gegenüber (VI) das positivere Halbstufenpotential.

Die positivierende Wirkung des Schwefels auf die polarographische Reduktion der Carbonylgruppe zeigt sich auch im Vergleich der Halbstufenpotentiale der

Piperidino-Mannichbasen des Cyclohexanons und des Thianons-4. Letztere Verbindung wird bei einem um *ca.* 0.2 V positiveren Potential reduziert. Auch die Piperidineliminierung zum entsprechenden Methylenketon verläuft bei der Mannichbase des Thianons-4 wesentlich schneller als bei der des Cyclohexanons[10].

EXPERIMENTELLER TEIL

Die polarographischen Untersuchungen wurden in einer auf 20°C thermostatierten Messzelle mit getrennter Bezugselektrode (gesättigte Kalomelelektrode) durchgeführt. Die Registrierung erfolgte mit dem ungarischen Polarographen Typ OH 102 unter Anwendung der Drei-Elektrodenschaltung. Es wurde in 75%iger alkoholisch-wässriger Lösung mit einer 0.1 *M* Konzentration von Tetraäthylammoniumperchlorat als Leitsalz gearbeitet.

In dem untersuchten Konzentrationsbereich (10^{-3}–10^{-4} *M*) ist die Stufenhöhe der Konzentration proportional. Der diffusionsbedingte Charakter des Grenzstromes kommt in seiner linearen Abhängigkeit von der Wurzel der Höhe des Quecksilberniveaus zum Ausdruck.

Durch mikrocoulometrische Bestimmung wurde festgestellt, dass unter den beschriebenen Bedingungen die Reduktionsstufe einem 2-elektronigen Übergang entspricht.

Die Untersuchungen der polarographischen Reduktion von Thianon-3 (II) und Thianon-4 (V) in Britton–Robinson-Puffer bei verschiedenen pH-Werten ergab, dass nur (II) im sauren Bereich (pH = 3–6) eine ein-elektronige Stufe zeigt, die der Reduktion der protonisierten Carbonylgruppe entspricht. Bei höheren pH-Werten (pH = 8–12) wird sowohl von (II) als auch von (V) eine zwei-elektronige nahezu pH-unabhängige Reduktionsstufe gefunden.

Die Ergebnisse der potentialkontrollierten Reduktion der Verbindungen (II) und (V) an einer grossflächigen Quecksilberelektrode untermauern die Ergebnisse. Darüber soll in einer späteren Mitteilung ausführlicher berichtet werden.

Die u.v.-Spektren wurden in Methanol mit dem Universal-Spektrophotometer USP 2 von G. Geppert vermessen.

Herrn Prof. Dr. M. Mühlstädt danken wir für die Unterstützung, die er dieser Arbeit zuteil werden liess.

ZUSAMMENFASSUNG

Die polarographische Reduktion der Carbonylgruppe in Thiacyclanonen ist auf Grund einer Carbonyl–Schwefel-Wechselwirkung gegenüber Cyclanonen beträchtlicht erleichtert. Es kann eine deutliche Abhängigkeit der Halbstufenpotentiale von der gegenseitigen Stellung der Carbonyl- und Thioäthergruppierung festgestellt werden. Thiacyclanone-3 werden leichter als Thiacyclanone-4 und diese leichter als Thiacyclanone-5 reduziert. Die Lage der Halbstufenpotentiale wird weiter durch die Ringgrösse beeinflusst.

SUMMARY

Polarographic reduction of the carbonyl group in thiacyclanone is consider-

ably easier than in cyclanone as a result of a carbonyl–sulphur interaction. A marked dependence of the half-wave potential on the relative position of the carbonyl and thio-ether groupings was established. Thiacyclanone-3 was reduced more easily than thiacyclanone-4 and this more easily than thi cyclanone-5. The position of the half-wave potential was further affected by the size of the ring.

LITERATUR

1 H. H. JAFFÉ UND M. ORCHIN, *Theory and Applications of Ultraviolet Spectroscopy*, J. Wiley and Sons, New York–London, 1964, S. 466.
2 R. BORSDORF, H. KASPER UND H.-D. REPP, *Angew. Chem.*, 79 (1967) 683.
3 N. J. LEONHARD, T. W. MILLIGAN UND T. L. BROWN, *J. Am. Chem. Soc.*, 82 (1960) 4075.
4 P. ZUMAN, *Talanta*, 12 (1965) 1337.
5 N. KUCHARCZYK, M. ADAMOVSKY, V. HORAK UND P. ZUMAN, *J. Electroanal. Chem.*, 10 (1965) 503.
6 *Anmerkung*: Inzwischen ist eine weitere Arbeit von Zuman und Mitarbeiter erschienen, in der die polarographische Reduktion der CO-Gruppe in Ketonen des Typs Ph–CO–CH_2–CHPh–S–R beschrieben wird.
J. ŠESTAKOVA UND P. ZUMAN, *Collection Czech. Chem. Commun.*, 33 (1968) 3227.
7 H. LUND, *Acta Chem. Scand.*, 14 (1960) 1927.
8 P. KABASAKALIAN UND J. MCGLOTTEN, *Anal. Chem.*, 31 (1959) 1091.
9 M. MÜHLSTÄDT UND R. HERZSCHUH, *J. Prakt. Chem.*, 20 (1963) 20; 28 (1965) 216.
10 M. MÜHLSTÄDT, R. BRODDACK UND R. HERZSCHUH, unveröffentlicht.

ELECTROANALYTICAL CHEMISTRY AND INTERFACIAL ELECTROCHEMISTRY
Elsevier Sequoia S.A., Lausanne – Printed in The Netherlands

EFFECTS OF THE ELECTRICAL DOUBLE LAYER AND THIOUREA ADSORPTION ON THE POLAROGRAPHIC CATALYTIC CURRENTS OF THE NICKEL(II)–THIOUREA COMPLEX

YA. I. TUR'YAN AND O. E. RUVINSKII
Institute of Technology, Yaroslavl (U.S.S.R.)

(Received January 7th, 1969)

INTRODUCTION

In contrast to an earlier report[1] in which the formation of one pre-wave of $Ni(H_2O)_6^{2+}$ (Ni^{2+}) in an aqueous solution of thiourea (Tu) was briefly mentioned, we found[2] two catalytic pre-waves of Ni^{2+} in the presence of thiourea (Fig. 1). The limiting current of the first catalytic pre-wave ($E_{\frac{1}{2}} = -0.58 \pm 0.02$ V *vs.* SCE) was assumed to be determined by the kinetics of formation of the mono-thiourea complex, $[Ni(H_2O)_5Tu]^{2+}$, from the Ni^{2+} ions and thiourea adsorbed at the electrode (surface wave[3]). Similiar processes proceeding in the adsorption layer with the participation of other metal complexes have been described elsewhere[4–10]*. The second (total) catalytic pre-wave in the region of the limiting current is determined by the kinetics of two parallel processes: the formation of the $[Ni(H_2O)_5Tu]^{2+}$ complex in the adsorption layer and the formation of an analogous complex in the bulk reaction layer.

The reduction of the adsorbed $[Ni(H_2O)_5Tu]^{2+}_{ads}$ complex corresponds to

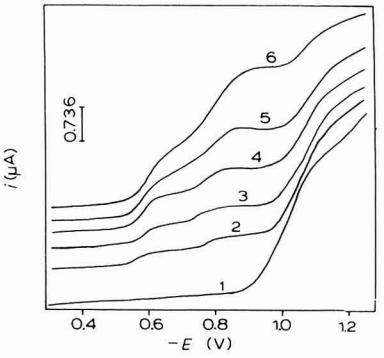

Fig. 1. Pre-waves of Ni^{2+} (1×10^{-3} *M*) in the presence of thiourea: (1) 0; (2) 5.0×10^{-3}; (3) 1.0×10^{-2}; (4) 1.9×10^{-2}; (5) 6.5×10^{-2}; (6) 0.1 *M*; supporting electrolyte, 3.0 *M* $NaNO_3$; initial potential −0.2 V.

* In contrast to the report in ref. 9, Kolthoff *et al.*[11] did not take into account the effect of adsorption on the kinetic current (pre-wave) of the cobalt(II)–cysteine complex.

the first wave. The reduction of both $[Ni(H_2O)_5Tu]^{2+}_{ads}$ and the analogous complex from the bulk of solution corresponds to the second (total) wave. The concentration of the $[Ni(H_2O)_5Tu]^{2+}$ complex in the bulk of the aqueous solution is negligibly small[12,13].

In the present paper, quantitative aspects of the effects of electrical double-layer structure and of thiourea adsorbed on the dropping mercury electrode on the limiting currents of the catalytic pre-waves of the Ni^{2+} ions, are discussed.

EXPERIMENTAL

Analytical-grade $NaClO_4$ and $NaNO_3$ were used to prepare supporting electrolytes. Chemically pure $Ni(NO_3)_2$ was used. Polarographic solutions contained small amounts of $HClO_4$ or HNO_3 (to pH 6.0–6.5) to prevent hydrolysis of Ni^{2+} [14]. Analytical-grade thiourea was twice-recrystallized to remove thiocyanate ions (less than 0.01% according to i.r.-spectra) since, in the presence of thiocyanate, Ni^{2+} gives pre-waves about at the same potentials[15].

All potential values are given *versus* the saturated calomel electrode (SCE) which was used as a reference electrode. Average currents were corrected for the residual current at given potentials. The parameters of the capillary are: $m^{\frac{2}{3}}t_1^{\frac{1}{6}} = 1.93$ $mg^{\frac{2}{3}}s^{-\frac{1}{2}}$ at $E = -1.4$ V, $t_1 = 3.7$ s at $E = -0.7$ V, $t_1 = 3.5$ s at $E = -0.9$ V. The current–voltage curves were recorded with a LP-60 polarograph (Czechoslovakia). The experiments were performed at $25^\circ \pm 0.2^\circ$C. Oxygen was removed by purging with purified nitrogen.

RESULTS AND DISCUSSION

It follows from ref. 2, that the following approximate kinetic equation[3] corresponds to the first surface pre-wave (the limiting current is at the potentials of -0.62–0.65 V close to the point of zero charge, p.z.c., of mercury surface in the presence of thiourea[16–18]):

$$Z_{i_k} = \frac{\bar{i}_k}{\bar{i}_d - \bar{i}_k} = \frac{nF\bar{q}}{\bar{x}} \cdot k_a \Gamma_{Tu} \qquad (1)$$

where $\bar{i}_k$ is the average limiting catalytic current of the first pre-wave, $\bar{i}_d^q$ the average limiting diffusion current of Ni^{2+}, Γ_{Tu} the concentration of adsorbed thiourea (mol cm^{-2}), $\bar{x}$ the Ilkovič constant and k_a the rate constant of the formation of the mono-thiourea complex of Ni^{2+} in the adsorption layer (l mol^{-1} s^{-1}).

$$\frac{\bar{x}}{nF\bar{q}} = 1.23 \times 10^{-3} \left(\frac{D_{Ni^{2+}}}{t_1}\right)^{\frac{1}{2}},$$

where $D_{Ni^{2+}}$ is the diffusion coefficient of Ni^{2+} ($cm^2 s^{-1}$) and t_1 is the drop time (s).

The quantitative aspect of the effect of thiourea adsorption was discussed using the data for thiourea adsorption taken from the recent report[19] (0.1 *M* KNO_3, p.z.c.) providing the adsorption equilibrium established rather rapidly. It should be noted that a comparison of thiourea adsorption for NaF, KNO_3 and $NaNO_3$ solutions of different concentrations showed that the adsorption data under suitable thiourea bulk concentrations (C_{Tu}) and potential, were similar[16,19–21]. This made

it possible for us to compare the catalytic currents ($\bar{i}_k$) obtained in 0.5 *M* $NaClO_4$ and 0.5 *M* $NaNO_3$ (Fig. 2) with the value of Γ_{Tu} obtained in 0.1 *M* KNO_3. The value of $\bar{i}_{d_{Ni^{2+}}}$ (Fig. 2) was obtained in 0.2 *M* $NaClO_4$ ($NaNO_3$) since at greater concentrations of the supporting electrolyte, $\bar{i}_{d_{Ni^{2+}}}$ was distorted by the kinetic retardation[22,23].

It can be seen from Fig. 3 that the equation (1) holds true over the entire range of C_{Tu} (the slope of plots log Z_{i_k}–log Γ_{Tu} is close to unity), which confirms the following mechanism for the first catalytic pre-wave: the formation of the mono-thiourea complex of nickel from Ni^{2+} ions and the thiourea adsorbed.

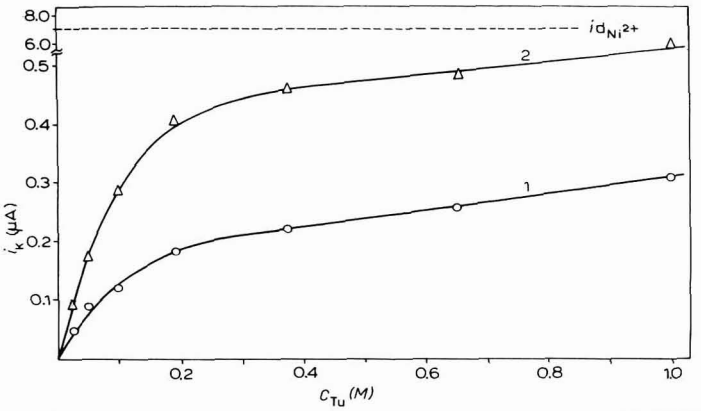

Fig. 2. The limiting currents of the first catalytic pre-wave, 1×10^{-3} *M* $Ni(NO_3)_2$. Supporting electrolytes: (1) 0.5 *M* $NaClO_4$; (2) 0.5 *M* $NaNO_3$.

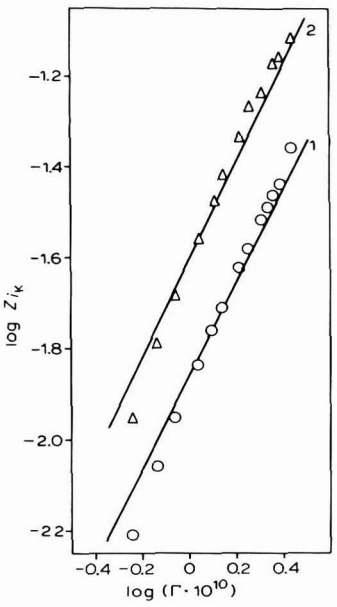

Fig. 3. Relationship between log Z_{i_k} and log Γ_{Tu} (in mol cm^{-2}) (eqn. (1)). (1) 0.5 *M* $NaClO_4$; (2) 0.5 $NaNO_3$.

$$[Ni(H_2O)_6]_r^{2+} \xrightarrow[\text{diff.}]{} [Ni(H_2O)_6]_s^{2+} + Tu_{ads} \xrightarrow{k_a} [Ni(H_2O)_5Tu]_{ads}^{2+} \rightarrow$$
$$\xrightarrow{2e} Ni(Hg) + Tu_{ads}$$

Species in the bulk of solution and at the electrode surface are denoted by the symbols "r" and "s", respectively.

From Fig. 3, and based on eqn. (1), the rate constants of complex formation in the adsorption layer, $k_a = 2.2 \times 10^2$ l mol^{-1} s^{-1} ($NaClO_4$) and 3.8×10^2 l mol^{-1} s^{-1} ($NaNO_3$), were found. For the calculation, the value of $D_{Ni^{2+}} = 6 \times 10^{-6}$ cm^2 s^{-1} obtained by a non-polarographic method[24], was used. A similar value for $D_{Ni^{2+}}$ was obtained from the polarographic data.

With decreasing concentration of the supporting electrolyte ($\leqslant 0.2$ *M*) the limiting current of the total pre-wave ($\Sigma\bar{i}_k$) increased sharply and only one catalytic pre-wave (Figs. 4 and 5) could be observed on the polarogram.

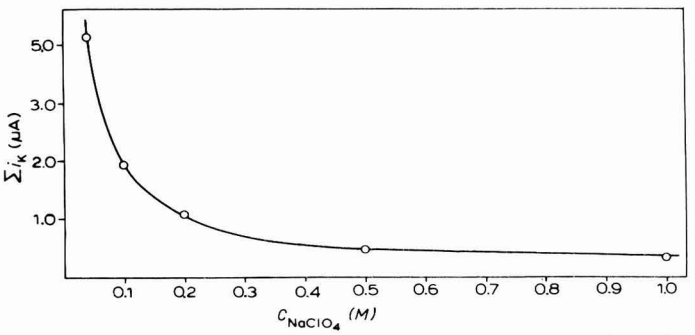

Fig. 4. Relationship between $\Sigma\bar{i}_k$ and the concn. of supporting electrolyte. $C_{Ni^{2+}} = 1 \times 10^{-3}$ *M*, $C_{Tu} = 4 \times 10^{-3}$ *M*.

Since the limiting current, $\Sigma\bar{i}_k$, was believed to be determined by two parallel processes of complex formation (surface and bulk processes) and the current is at potentials of -0.85 to -0.87 V as distinguished from the p.z.c., it is necessary to consider the effect[25] of a double-layer on the kinetics. This problem was studied theoretically elsewhere[26,27]. Taking into consideration the bulk process[28], we find:

$$Z_{\Sigma i_k} = \frac{\Sigma\bar{i}_k}{\bar{i}_d - \Sigma\bar{i}_k} = \frac{nF\bar{q}}{\bar{x}} k_a \Gamma_{Tu} \exp\left(-\psi_1 \frac{2F}{RT}\right) + \frac{10^{-3} nF\bar{q}}{\bar{x}} \mu k_r C_{Tu} \qquad (2)$$

where k_r is the rate constant of the formation of complex $[Ni(H_2O)_5Tu]^{2+}$ in the bulk of solution and μ is the thickness of reaction layer:

$$\mu = \left(\frac{D_{NiTu^{2+}}}{k_r K_1}\right)^{\frac{1}{2}}$$

where K_1 is the instability constant of $[Ni(H_2O)_5Tu]^{2+}$; ψ_1 is the potential on the outer Helmholtz plane (V).

If the associative mechanism[29,30] is assumed to be true for the formation of the nickel–thiourea complex as well as for other nickel complexes[31], then k_r may be assumed to be equal to 10^3–10^4 l mol^{-1} s^{-1}. As in this case the value of K_1 is apprecia-

bly greater than unity and k_a is equal to $(2–4) \times 10^2$ l mol^{-1} s^{-1}, the second term in eqn. (2) may be neglected if the ionic strengths are low. Hence, at low ionic strengths we have:

$$Z_{\Sigma i_k} = \frac{rF\bar{q}}{\bar{x}} \times k_a \Gamma_{Tu} \exp\left(-\psi_1 \frac{2F}{RT}\right) \quad (3)$$

This equation is in a good agreement with the experimental data at ionic strengths $\leqslant 0.2$ (Fig. 6). The straight line in Fig. 6 has the theoretical slope of 34 V^{-1}. When plotting this relationship, the values of the ψ_1-potentials calculated according to the Gouy–Chapman theory for NaF solutions[32] corrected for the shift of p.z.c. due to

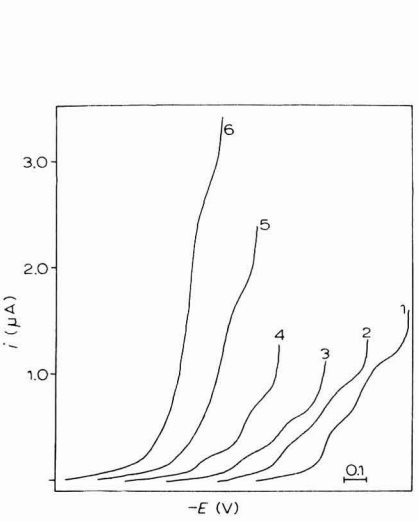

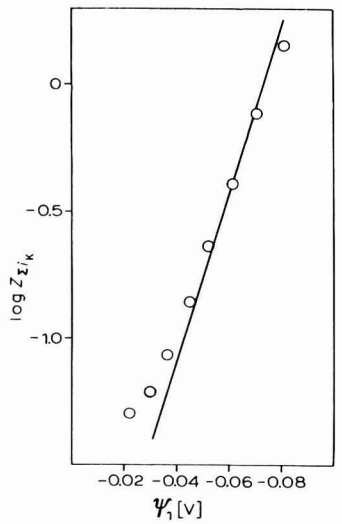

Fig. 5. Pre-waves of Ni^{2+} (1×10^{-3} *M*) in the presence of 4.9×10^{-3} *M* thiourea. Supporting electrolyte $NaClO_4$: (1) 5.0; (2) 3.0; (3) 1.0; (4) 0.5; (5) 0.2; (6) 0.1 *M*.

Fig. 6. Relationship between log $Z_{\Sigma i_k}$ and the ψ_1-potential (eqn (3)). $C_{Ni^{2+}} = 1 \times 10^{-3}$ *M*, $C_{Tu} = 4 \times 10^{-3}$ *M*. Supporting electrolyte $NaClO_4$.

the thiourea adsorption were used. The insignificant effect produced by thiourea adsorbed on the diffusive double-layer structure[33] and negligibly small ClO_4^- (or NO_3^-) adsorption at the potential of -0.85 V were also taken into account. The investigation of pre-waves in NaF solution would fail to interpret simply the resulting data because of complex formation[34] between Ni^{2+} and F^-.

The deviation of experimental points from the theoretical plot at concentrations of the supporting electrolyte above 0.2 *M* (Fig. 6) may be explained both as the influence of the second term in eqn. (2) and by possible violation of Gouy–Chapman theory.

The extrapolation of the straight line in Fig. 6 to $\psi_1 = 0$ gave the average value of k_a of 2.4×10^2 l mol^{-1} s^{-1} (eqn. (3), $\Gamma_{Tu} = 2.5 \times 10^{-11}$ mol cm^{-2} at -0.85 V[19]), *i.e.*, the value which is close to that obtained from the first pre-wave in the vicinity of the p.z.c. Identical results were obtained using the Koutecký method[35] which was also

used by Mark and McCoy[8] for catalytic currents with participation of *o*-phenylenediamine.

As the concentration of supporting electrolyte increases (above 1.0 *M*) the first and the second (total) pre-waves also increase. This is not connected with a salting-out effect[21], but is rather accounted for by increase in the rate constant as a result of changing the activity coefficients and by the influence of possible association processes of Ni^{2+} ions with the anions of the supporting electrolyte[36] in the surface layer.

The greater catalytic current of the first pre-wave (and, hence, of k_a) in nitrate media in comparison with perchlorate may be explained by the fact that these anions have different effects on the kinetics of complex formation with the thiourea adsorbed, rather than by a change in the ψ_1-potential owing to NO_3^- [37,38] and ClO_4^- [39,40] specific adsorption, taking into consideration the desorbing action of thiourea on these anions[17,19].

ACKNOWLEDGEMENT

The authors wish to thank Dr. N. B. Grigoryev for valuable consultations and Mrs. V. Ya. Golkova for kind assistance.

SUMMARY

Effects of the electrical double-layer and the adsorption of thiourea on the catalytic pre-waves of nickel(II) caused by the formation and subsequent reduction of nickel(II)–mono-thiourea complex have been investigated. It has been shown that the kinetic equation is in good agreement with the experimental data over the entire range of thiourea concentrations, providing the thiourea adsorbed is taken into consideration. The quantitative estimation of the influence of the ψ_1-potential on kinetics is possible for 1-1 electrolyte concentrations of $\leqslant 0.2$ *M*. The rate constant of the interaction between $Ni(H_2O)_6$ ion and thiourea adsorbed at a mercury surface, $k_a = (2\text{–}4) \times 10^2$ l mol^{-1} s^{-1} ($\psi_1 = 0$), was found.

REFERENCES

1 R. D. De Mars, *J. Electrochem. Soc.*, 108 (1961) 779.
2 Ya. I. Tur'yan and O. E. Ruvinskii, *Elektrokhimiya*, 4 (1968) 1446.
3 S. G. Mairanovskii, *Catalytic and Kinetic waves in Polarography*, Nauka, Moscow, 1966, p. 164.
4 H. B. Mark, *J. Electroanal. Chem.*, 7 (1964) 276.
5 A. I. Engel, J. Lawson and D. A. Aikens, *Anal. Chem.*, 37 (1965) 203.
6 I. Kůta, *Z. Anal. Chem.*, 216 (1966) 242.
7 H. Sohr and Kh. Lohs, *J. Electroanal. Chem.*, 13 (1967) 114.
8 H. B. Mark and L. R. McCoy, *Rev. Polarog. Kyoto*, 14 (1967) 122.
9 S. G. Mairanovskii and E. F. Mairanovskaya, *Reports on the Electrochemistry of Organic Compounds*, Nauka, Moscow, 1968, p. 33.
10 H. B. Mark, L. R. McCoy, E. Kirova-Eisner and H. C. MacDonald, *J. Phys. Chem.*, 72 (1968) 1083.
11 I. M. Kolthoff, P. Mader and S. E. Khalafalla, *J. Electroanal. Chem.*, 18 (1968) 315.
12 K. Swanithan and H. Irving, *J. Inorg. Nucl. Chem.*, 28 (1968) 171.
13 V. M. Shulman, S. V. Larionov, T. V. Kramareva and E. I. Arykova, *Zh. Neorgan. Chim.*, 11 (1966) 1076.

14 K. A. BURKOV, L. S. LILIČ AND L. G. SILLEN, *Acta Chem. Scand.*, 19 (1965) 14.
15 YA. I. TUR'YAN AND G. F. SEROVA, *Zh. Fiz. Khim.*, 31 (1957) 1976.
16 F. W. SCHAPINK, M. OUDEMAN, K. W. LEU AND I. N. HELLE, *Trans. Faraday Soc.*, 56 (1960) 415.
17 A. M. MOROZOV, N. B. GROGORYEV AND J. A. BAGOTSKAYA, *Elektrokhimiya*, 3 (1967) 585.
18 N. B. GRIGORYEV AND V. S. KRYLOV, *Elektrokhimiya*, 4 (1968) 763.
19 R. PARSONS AND P. C. SYMONS, *Trans. Faraday Soc.*, 64 (1968) 1077.
20 B. CASE AND F. C. ANSON, *J. Phys. Chem.*, 71 (1967) 402.
21 N. B. GRIGORYEV AND B. B. DAMASKIN, *Reports on the Electrochemistry of Organic Compounds*, Nauka, Moscow, 1968, p. 66.
22 J. DANDOY AND L. GIERST, *J. Electroanal. Chem.*, 2 (1961) 1176.
23 N. S. HUSH AND I. W. SCARROTT, *J. Electroanal. Chem.*, 7 (1964) 26.
24 R. H. SANBORN AND E. F. ORLEMANN, *J. Am. Chem. Soc.*, 77 (1955) 3726.
25 A. N. FRUMKIN, V. S. BAGOTSKII, Z. A. IOFA AND B. N. KABANOV, *Kinetics of Electrode Processes*, MGU, Moscow, 1952, p. 175.
26 L. GIERST AND H. HURWITZ, *Z. Elektrochem.*, 64 (1960) 36.
27 H. HURWITZ, *Z. Elektrochem.*, 65 (1961) 178.
28 J. HEYROVSKY AND I. KŮTA, *The Fundamental of Polarography*, Czech. Acad. Sci., Praha, 1962, p. 316.
29 M. EIGEN, *Z. Elektrochem.*, 64 (1960) 115.
30 M. EIGEN AND K. TAMM, *Z. Elektrochem.*, 66 (1962) 107.
31 R. H. HOLYER, C. D. HUBBARD, S. F. A. KETTLE AND R. G. WILKINS, *Inorg. Chem.*, 4 (1965) 929.
32 C. D. RUSSELL, *J. Electroanal. Chem.*, 6 (1963) 486.
33 R. PARSONS, *The Main Problems of Modern Theoretical Electrochemistry*, Mir, Moscow, 1965, p. 282.
34 S. AHRLAND AND K. ROSENYREN, *Acta Chem. Scand.*, 10 (1956) 727.
35 I. KOUTECKÝ, *Collection Czech. Chem. Commun.*, 18 (1953) 597.
36 L. GIERST, L. VANDERBERGEN, E. NICOLAS AND A. TRABONI, *J. Electrochem. Soc.*, 113 (1966) 1025.
37 R. PAYNE, *J. Phys. Chem.*, 69 (1965) 4113.
38 B. B. DAMASKIN, V. F. IVANOV, N. I. MELECHOVA AND L. F. MAYOROVA, *Elektrokhimiya*, 4 (1968) 1342.
39 R. PAYNE, *J. Phys. Chem.*, 70 (1966) 204.
40 B. B. DAMASKIN, A. N. FRUMKIN, V. F. IVANOV, N. I. MELECHOVA AND V. F. CHONINA, *Elektrokhimiya*, 4 (1968) 1336.

ELECTROANALYTICAL CHEMISTRY AND INTERFACIAL ELECTROCHEMISTRY
Elsevier Sequoia S.A., Lausanne – Printed in The Netherlands

EFFECT OF THE ELECTRICAL DOUBLE LAYER AND PYRIDINE ADSORPTION ON THE CATALYTIC POLAROGRAPHIC CURRENT OF NICKEL(II)–PYRIDINE COMPLEXES

YA. I. TUR'YAN AND O. N. MALYAVINSKAYA
Institute of Technology, Yaroslavl (USSR)
(Received January 7th, 1969)

INTRODUCTION

As was noted in previous work[1], the $Ni(H_2O)_6^{2+}$ (Ni^{2+}) kinetic polarographic pre-wave occurs in the presence of pyridine (Py). This, in the authors' opinion[1], is due to a chemical formation reaction on the electrode, and reduction of the Ni(II)–pyridine complex*. Such an explanation of the nature of the pre-wave has been confirmed[2–8]. The polarographic kinetic pre-waves of reduction of some other metallic complexes have been explained similarly[9–32]. However, it has not been made clear whether the chemical reaction of formation of the Ni(II)–pyridine complex takes place in the bulk of solution or with the participation of pyridine adsorbed on mercury. Some data[6,8] suggest that the process occurs in the bulk of solution. However, the investigation of the effect of the addition of alcohol has challenged the conclusion reached earlier[6] about the completely bulk nature of the Ni(II)–pyridine complex formation reaction. The above conclusion has become more doubtful after the publication of showing the involvement of adsorbed *o*-phenylenediamine[18,25,30], cysteine[23] and thiourea[31] in the chemical reaction of formation of Ni^{2+} complexes on the electrode (appearance of the catalytic pre-wave).

This work investigates further the nature of the electrode reaction of the formation and reduction of the DME of the Ni^{2+}–pyridine complex.

EXPERIMENTAL

The pre-wave of Ni^{2+} (5×10^{-5} *M* $Ni(NO_3)_2$, reagent-grade), was investigated in the presence of excess pyridine (5×10^{-5}–5×10^{-3} *M*), which made it possible to obtain a sufficiently distinct separation of the pre-wave from the nickel reduction wave (the measurement of the pre-wave height is shown in Fig. 1). Pyridine purified by distillation was 99.9% pure. The salts of alkali metals (C.P.) having anions least capable of complexation and association with Ni^{2+} ($NaClO_4$, $NaNO_3$, KNO_3, $LiNO_3$, $CsNO_3$) served as supporting electrolytes. The solutions investigated were adjusted to $pH \leqslant 6.5$ by the addition of $HClO_4$ or HNO_3 to avoid hydrolysis[34] of Ni^{2+}. The pH was controlled by a glass electrode placed in the polarographic cell. Oxygen was removed by purging with purified nitrogen which passed through a vessel

* Since pyridine is regenerated during the complex reduction on the electrode, this pre-wave should more reasonably be referred to as a catalytic wave[2,3].

containing the solution under investigation before entering the polarographic cell. Special experiments confirmed that pyridine was not blown off from the polarographic solution.The polarographic cell was thermostatted. Experiments for which the temperature is not indicated, were made at 25°C. All solutions were prepared with twice-distilled water. The polarograms were obtained by means of a LP-60 recording polarograph (Czechoslovakia). The average currents corrected for residual current

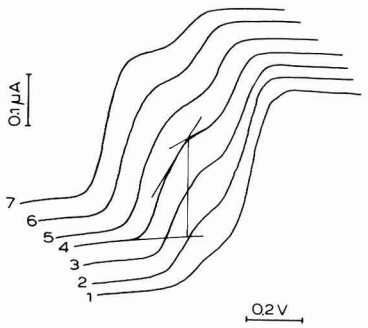

Fig. 1. Pre-waves of Ni^{2+} (5×10^{-5} *M*) in the presence of pyridine: (1) 1.0×10^{-4}; (2) 2.0×10^{-4}; (3) 4.0×10^{-4}; (4) 6.0×10^{-4}; (5) 8.6×10^{-4}; (6) 1.1×10^{-3} (7) 1.6×10^{-3} *M*; supporting electrolyte, 0.05 *M* $NaNO_3$; pH, 6.5; initial potential, −0.5 V.

were measured. The capillary characteristics were: $m = 2.17$ mg s^{-1}, $t_1 = 3.75$ s at −0.90 V *versus* the normal calomel electrode, which was used as reference electrode. A pre-wave limiting current was measured at the same potential. The calomel electrode was separated from the polarographic solution by an electrolyte bridge filled with the solution investigated. Since the currents studied were very small (5×10^{-5} *M* Ni^{2+}) the correction for the cell resistance was not made.

RESULTS AND DISCUSSION

It can be seen from Figs. 2 and 3 (index: o denotes total concentration, index: r denotes equilibrium concentration) that the limiting current of the pre-wave (i_k) at $C^o_{Ni^{2+}}$ = const. and pH = const., increased with increase in pyridine concentration, whereas at $C^o_{Ni^{2+}}$ = const., pH = const. and C^o_{Py} = const., it increased with decrease of the supporting electrolyte concentration (C) at $C < 1.0$ *M*, and especially at $C < 0.2$ *M*. The limiting diffusion current i_d (Fig. 2) corresponding to the second (total) wave was obtained at $C \leqslant 0.2$ *M*, in order to eliminate the kinetic retardation[35-38]. It was taken into consideration that the diffusion coefficient (D) of Ni^{2+} at $C = 0.1$–3.0 *M* varied slightly[39]. Some increase of i_k with increase of the supporting electrolyte concentration was noticed at $C > 0.5$ *M* and $C^o_{Ni^{2+}}$ = const., pH = const. and C^o_{Py} = const. (Figs. 2 and 3). The decrease in pH led to a reduction of i_k, whereas at pH < 4.0 (Fig. 4) the pre-wave disappeared completely. The nature of the cation greatly affected the magnitude of i_k at low concentrations of supporting electrolyte ($C \leqslant 0.5$ *M*) (Fig. 3). The value of i_k increased in the direction: $Cs^+ < Na^+ < Li^+$. This effect was markedly lower in more concentrated solutions. The nature of the anions investigated (ClO_4^-, NO_3^-) had only a slight effect on i_k. The temperature coefficient of i_k was large (5%/degree; 0.02 *M* $NaNO_3$), thus confirming the kinetic nature of the pre-wave.

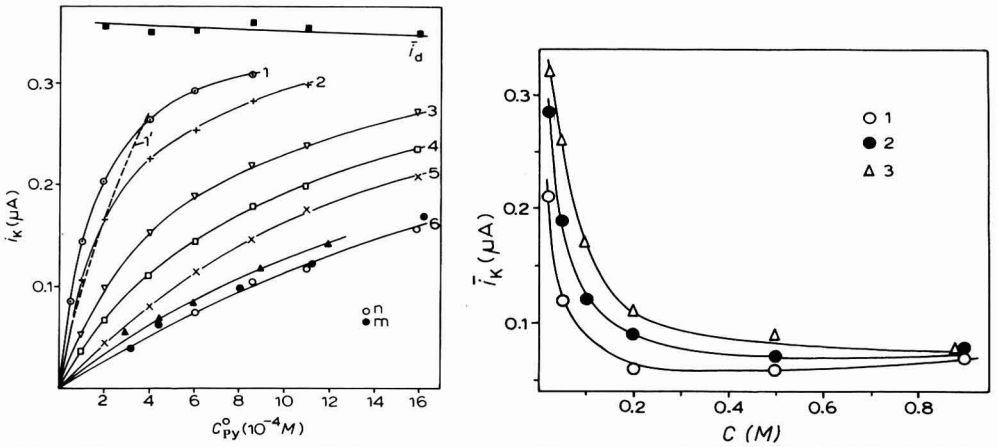

Fig. 2. Dependence of pre-wave limiting current on pyridine concn. in $NaNO_3$ soln.: (1) 0.02; (2) 0.03; (3) 0.05; (4) 0.07; (5) 0.1; (6) 1.0 (points-m); (7) 4.0 M. $C^o_{Ni^{2+}} = 5 \times 10^{-5}$ M. pH = 6.5. Curve (1') $\bar{i}_k$–C^r_{Py} (pH) in 0.02 M $NaNO_3$ at $C^o_{Py} = 4.0 \times 10^{-4}$ M. Points-n on curve (6) represent $\bar{i}_k$–C^r_{Py} (pH) in 1.0 M $NaNO_3$; $C^o_{Py} = 4.9 \times 10^{-3}$ M.

Fig. 3. Dependence of pre-wave limiting current on concn. of supporting electrolyte: (1) $CsNO_3$; (2) $NaNO_3$; (3) $LiNO_3$. $C^o_{Ni^{2+}} = 5 \times 10^{-5}$ M; $C^o_{Py} = 6 \times 10^{-4}$ M; pH = 6.5.

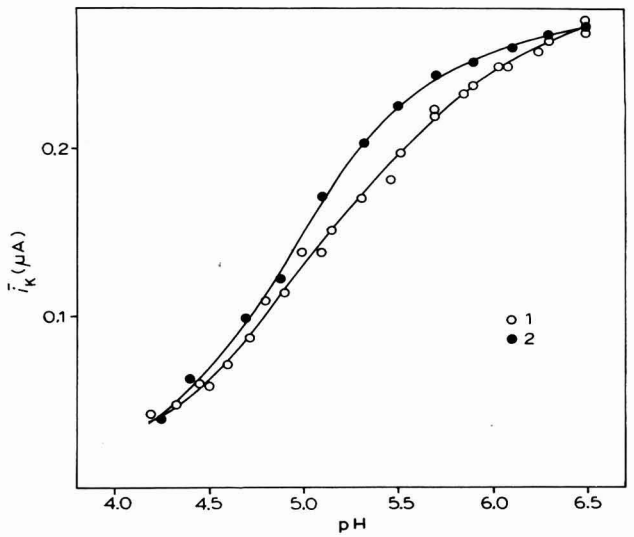

Fig. 4. Dependence of pre-wave limiting current on pH. $C^o_{Ni^{2+}} = 5 \times 10^{-5}$ M; $NaNO_3$: (1) 0.02; (2) 1.0 M; C^o_{Py}: (1) 4.0×10^{-4}; (2) 4.9×10^{-3} M.

The instability constant of the $[Ni(H_2O)_5Py^{2+}]^{2+}$ ($[NiPy]^{2+}$) complex

$$K'_1 = \frac{C^r_{Ni^{2+}} \cdot C^r_{Py}}{C^r_{NiPy^{2+}}} \tag{1}$$

and the dissociation constant of the pyridinium-ion $[PyH^+]$

$$K_a = \frac{C^r_{Py} \cdot C^r_{H^+}}{C^r_{PyH^+}} \tag{2}$$

in the solutions investigated were determined by a potentiometric titration according to the procedure[40] that takes into account the equilibrium concentration of $[NiPy]^{2+}$ and $[PyH]^{+}$ (see Table 1). This was necessary because the data available[40-52] do not correspond to the concentration and nature of the supporting electrolytes investigated by us and, in addition, these data (particularly those for K'_1) are contradictory. Our results (Table 1) are close to the data given elsewhere[40,44,45,48,49] at a

TABLE 1

INSTABILITY CONSTANTS (K'_1) OF $[NiPy]^{2+}$ COMPLEX AND DISSOCIATION CONSTANTS (K_a) OF PYRIDINIUM ION, PyH^{+}, *vs.* CONCENTRATION AND SALT NATURE AT 25°C
K'_1 and K_a both in mol l^{-1}

C/mol l^{-1}	$CsNO_3$		$NaNO_3$		$LiNO_3$	
	$K'_1 \times 10^3$	$K_a \times 10^6$	$K'_1 \times 10^3$	$K_a \times 10^6$	$K'_1 \times 10^3$	$K_a \times 10^6$
0.02	10.9	5.9	10.9	5.9	10.9	5.9
0.03			10.8	5.9		
0.05			10.7	5.6		
0.07			10.5	5.5		
0.1	10.2	5.3	10.3	5.4	10.4	5.4
0.2			9.9	5.0		
1.0	7.2	3.5	8.2	3.9	8.9	4.5

corresponding ionic strength. The re-evaluation of K'_1 for other temperatures was carried out using $\Delta H = -3.0$ kcal[48,53]. As the temperature influence on i_k was investigated at pH 6.5 when the concentration of protonated pyridine was low, the temperature correction for K_a was not used. Since the magnitudes of the instability constants of the pyridine complexes of Ni^{2+} have a coordinating number more than unity[43,46,47,51,52], the concentration of these complexes in the solution investigated by us ($C^{o}_{Py} < 5 \times 10^{-3}$ M) may be neglected.

The results of the dependence of i_k on C^{r}_{Py} at $C^{o}_{Ni^{2+}} = \text{const.}$ and pH = const. and pH 6.5 expressed as a $\{\log [i_k/(i_d - i_k)]\}$ *vs.* $\{\log C^{r}_{Py}\}$ plot are given by a straight line with a slope close to unity. This indicates a predominance of kinetic retardation at the $[NiPy]^{2+}$ complex formation stage[4,6]. It should be stressed however that to account for the substantial effect of both concentration and nature (cation) of the supporting electrolyte on the i_k-value and, hence, the rate of complex formation, the electrode process scheme must be represented as follows:

$$\begin{array}{ccccccc} \{Ni^{2+}\} & \xrightarrow[\text{diff.}]{} & \{Ni^{2+}\}_S & \xrightarrow[k_1]{Py_{ads.}} & \{NiPy^{2+}\}_{ads.} & \xrightarrow{2e} & Ni(Hg) + Py_{ads.} \\ \Big\| \{Py\} & & \Big\| \{Py\} & & & & \\ \{NiPy^{2+}\} & \xrightarrow[\text{diff.}]{} & \{NiPy^{2+}\}_S & \xrightarrow[k_2]{Py_{ads.}} & \{NiPy_2^{2+}\}_{ads.} & \xrightarrow{2e} & Ni(Hg) + Py_{ads.} \end{array} \qquad (3)$$

involving chemical reactions with the participation of pyridine adsorbed on mercury.

Index S in scheme (3) denotes species near an electrode surface, whereas the absence of the index corresponds to those in the bulk of the solution.

It should be noted that the presence of two parallel processes of reduction (scheme 3) is seen from a bend of the polarogram of the pre-wave (Fig. 1). Kemula *et al.*[5] succeeded in observing a more distinct splitting of the pre-wave. They assumed it to be a result of the separated reduction of $[NiPy]^{2+}$ and $[NiPy_2]^{2+}$.

If we take into account the surface nature of the catalytic pre-wave investigated, and, hence, the essential effect of an electrical double layer and pyridine adsorption on a limiting catalytic current, then, based on refs. 54–58, we have the following equations for scheme (3).

$$i_k = 2F\bar{q}k_1 C^{S}_{Ni^{2+}} \cdot \Gamma_{Py} + 2F\bar{q}k_2 C^{S}_{NiPy^{2+}} \cdot \Gamma_{Py} , \tag{4}$$

$$i_k = (\bar{x}_{Ni^{2+}} \cdot C^{r}_{Ni^{2+}} + \bar{x}_{NiPy^{2+}} \cdot C^{r}_{NiPy^{2+}}) - (\bar{x}_{Ni^{2+}} \cdot C^{S'}_{Ni^{2+}} + \bar{x}_{NiPy^{2+}} \cdot C^{S'}_{NiPy^{2+}}) , \tag{5}$$

$$i_d = \bar{x}_{Ni^{2+}} \cdot C^{r}_{Ni^{2+}} + \bar{x}_{NiPy^{2+}} \cdot C^{r}_{NiPy^{2+}} , \tag{6}$$

$$K'_1 = \frac{C^{S'}_{Ni^{2+}} \cdot C^{S'}_{Py}}{C^{S'}_{NiPy^{2+}}} , \tag{7}$$

$$C^{S}_{Ni^{2+}} \cong C^{S'}_{Ni^{2+}} \exp\left(-\psi_1 \frac{2F}{RT}\right) , \tag{8}$$

$$C^{S}_{NiPy^{2+}} \cong C^{S'}_{NiPy^{2+}} \exp\left(-\psi_1 \frac{2F}{RT}\right) . \tag{9}$$

Index : S is concentration (mol l^{-1}) directly at an electrode surface ; index : S′ shows concentration (mol l^{-1}) at the boundary between the diffuse part of an electrical double layer and a diffusion layer ; k_1 and k_2 are rate constants (l $mol^{-1}\,s^{-1}$) of the heterogenous reactions of complexation, of $[NiPy]^{2+}$ and $[NiPy_2]^{2+}$, respectively, $\bar{q}$ is the average surface of the mercury drop (cm^2), Γ_{Py} the surface concentration of an adsorbed pyridine (mol cm^{-2}), $\bar{x}$ the Ilkovič constant and ψ_1 the potential at the external surface of the Helmholtz region.

Based on eqns. (4)–(9) and considering

$$C^{S'}_{Py} \cong C^{r}_{Py} , \tag{10}$$

as the complex $[NiPy]^{2+}$ has a relatively low stability (Table 1) and, in addition, $C^{o}_{Py} \geqslant C^{o}_{Ni^{2+}}$, we have :

$$\frac{i_k\left(\frac{\bar{x}_{Ni^{2+}}}{\bar{x}_{NiPy^{2+}}} \cdot K'_1 + C^{r}_{Py}\right)}{i_d - i_k} = \frac{2F\bar{q}}{\bar{x}_{NiPy^{2+}}} (k_1 K'_1 + k_2 C^{r}_{Py}) \Gamma_{Py} \cdot \exp\left(-\psi_1 \frac{2F}{RT}\right) \tag{11}$$

It follows from the data given by Barradas *et al.*[59], who studied pyridine adsorption on mercury in the low pyridine concentration range (up to $1 \cdot 10^{-3}$ *M*), that the Henry adsorption isotherm is obeyed for the solution with $C^{o}_{Py} \leqslant 5 \cdot 10^{-3}$ *M* (−0.90 V) studied by us, this being given by eqn. (12) :

$$\Gamma_{Py} = 10^{-3} K_{Py} \cdot C^{r}_{Py} \tag{12}$$

K_{Py} (cm) is the constant at a given temperature, concentration and nature of the supporting electrolyte. If a rapid establishment of adsorption equilibrium on a

mercury drop surface at the drop time used[25] is assumed, then from (11) and (12) using $\bar{x}$ and q[60] we have:

$$y = \frac{i_k \left\{ K_1' \left(\frac{D_{Ni^{2+}}}{D_{NiPy^{2+}}} \right)^{\frac{1}{2}} + C_{Py}^r \right\}}{(i_d - i_k) C_{Py}^r} = a + bC_{Py}^r \tag{13}$$

$$a = 0.81\, k_1 K_{Py} K_1' \left(\frac{t_1}{D_{NiPy^{2+}}} \right)^{\frac{1}{2}} \cdot \exp\left(-\psi_1 \frac{2F}{RT} \right) \tag{14}$$

$$b = 0.81\, k_2 K_{Py} \left(\frac{t_1}{D_{NiPy^{2+}}} \right)^{\frac{1}{2}} \cdot \exp\left(-\psi_1 \frac{2F}{RT} \right), \tag{15}$$

a and b are constants for a given concentration and nature of the supporting electrolyte. Therefore, the dependency y–C_{Py}^r should be linear under these conditions.

TABLE 2

VALUES OF a AND b (EQN. (13)) *vs.* CONCENTRATION OF $NaNO_3$(C)

C/mol l^{-1}	a	$b \times 10^{-3}$
0.02	97.2	38
0.03	50.5	17
0.05	21.1	9.6
0.07	13.3	5.8
0.1	8.7	3.4
0.2	6.0	2.3
1.0	4.2	1.0

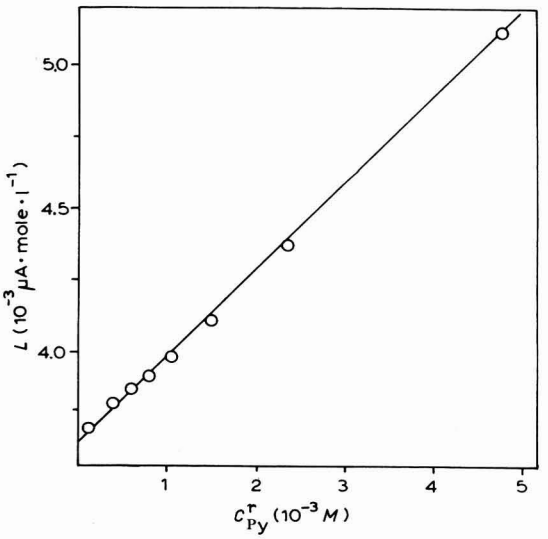

Fig. 5. Dependence of L (eqn. (16)) on pyridine equilibrium concn. $C_{Ni^{2+}}^o = 5 \times 10^{-5}$ M; pH = 6.5; 0.1 M $NaNO_3$; $C_{Py}^o = 1.0 \times 10^{-4}$–$5.0 \times 10^{-3}$ M.

It should be noted that Mark and McCoy[25] used the Koutecký equation[61] for describing a simpler heterogenous catalytic chemical reaction. This equation does not differ practically from an approximate solution based on the same principles as given above.

For determining $D_{NiPy^{2+}}$ from (1) and (6) we have

$$L = i_d(K'_1 + C^r_{Py}) = \bar{x}_{Ni^{2+}} \cdot C^o_{Ni^{2+}} K'_1 + \bar{x}_{NiPy^{2+}} \cdot C^o_{Ni^{2+}} \cdot C^r_{Py} \quad (16)$$

The graphical solution of eqn. (16) (Fig. 5) gives $\bar{x}_{Ni^{2+}}/\bar{x}_{NiPy^{2+}} = 1.15$, and taking $D_{Ni^{2+}} = 6.0 \times 10^{-6}$ cm^2 s^{-1} (0.1 *M* $NaClO_4$)[39], we have $D_{NiPy^{2+}} = 4.5 \times 10^{-6}$ cm^2 s^{-1}.

Equation (13) is in a good agreement with experimental data: for a given supporting electrolyte concentration the dependency y–C^r_{Py} (Fig. 6) is linear. The y

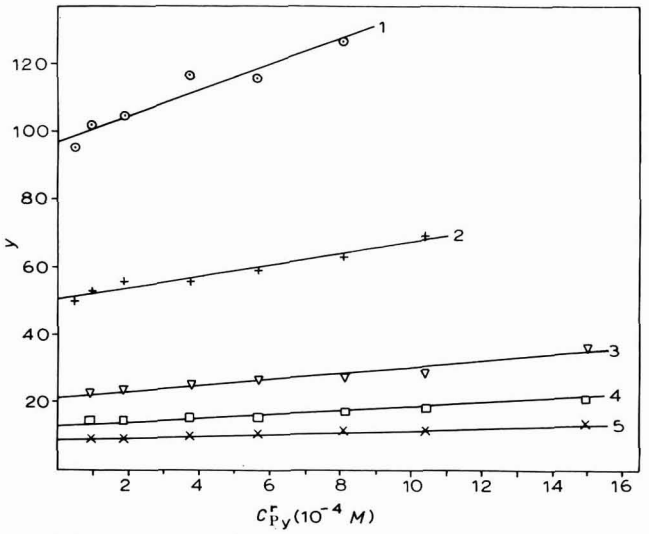

Fig. 6. Dependence of y (eqn. (13)) on pyridine equilibrium concn. in $NaNO_3$ soln.: (1) 0.02; (2) 0.03; (3) 0.05; (4) 0.07; (5) 0.1 *M*. $C^o_{Ni^{2+}} = 5 \times 10^{-5}$ *M*; pH = 6.5.

values obtained within a range $i_k = (0.1\text{–}0.9) \cdot i_d$ were taken for a more exact determination of a and b by the least-square root method.

The dependence of a and b on the supporting electrolyte concentration ($NaNO_3$) is expressed by eqns. (14) and (15) only at $C \leqslant 0.05$ *M* (Fig. 7) if the ψ_1 values of Russell[62] are used. These values were determined from Gouy–Chapman theory for NaF solutions*. The effect of pyridine adsorption on the ψ_1-potential at $C^o_{Py} \leqslant 5 \times 10^{-3}$ *M* may be neglected[59].

The deviation of the experimental points with a theoretical slope 33.9 V^{-1} at $C > 0.05$ *M* (Fig. 7) may be explained as follows: (1) a supposed violation of the Gouy–Chapman theory; (2) an acceleration of complexation under the effect of a supposed association of Ni^{2+} and $[NiPy]^{2+}$ with supporting electrolyte anion in a

* We have not carried out the catalytic pre-wave investigation in NaF solution as a complex formation effect[63] occurs between Ni^{2+} and F^-.

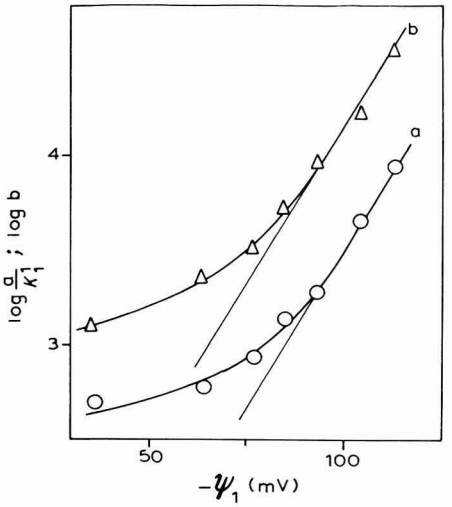

Fig. 7. Dependence of log a/K'_1 (eqn. (14)) and log b (eqn. (15)) on potential of Helmholtz region. $C^{o}_{Ni^{2+}} = 5 \times 10^{-5}$ M; pH = 6.5.

pre-electrode layer; (3) an acceleration of complexation due to a salting-out effect (pyridine activity coefficient increases with increase of the supporting electrolyte concentration[50] and, consequently, K_{Py} also increases which has already been mentioned in connection with the Ni^{2+}–*o*-phenylendiamine system[25]; (4) the acceleration of complexation due to displacement of the ψ_1-potential towards the negative side when the supporting electrolyte concentration increases as a result of specific anion adsorption arising in the presence of pyridine (observation of Conway *et al.*[64] for KCl solutions). It is difficult to prefer any of the latter three factors since each of them should lead to an increase of the reaction rate of complex formation, which has been experimentally observed: the catalytic current decrease with increase of the supporting electrolyte concentration is initially hindered, but then increased at $C > 0.5$ M (Figs. 2, 3 and 7). One should take into consideration that the observation of Conway *et al.*[64] of specific adsorption of Cl^--anions under the effect of pyridine is characteristic for more concentrated pyridine solutions.

The catalytic current increases, depending on the cation nature of the supporting electrolyte, in the direction: $Cs^+ < Na^+ < Li^+$ (Fig. 3). This can be explained by a corresponding change of ψ_1-potential (eqns. (14) and (15)) due to the specific cation adsorption[65]. Under these conditions, the change of complex stability constants in the solution (Table 1) could not essentially affect the kinetics of the electrode process. It should be noted that although a similar explanation (ψ_1-effect) has been given[3] as to the effect of the nature of the anion, yet in the latter case the effects of association and complexation with Ni^{2+} may be superimposed. At the same time, as the authors noted[20], a cation effect ($Na^+ < Li^+$) on the catalytic pre-wave in the system, Ni^{2+}–*o*-phenylendiamine[20] was determined by variation of ψ_1-potential.

The i_k–pH curves (Fig. 4) at $C^{o}_{Ni^{2+}} = \text{const.}$ and $C^{o}_{Py} = \text{const.}$, the character of which was first determined by Mark and Reilley[3], may be explained by eqn. (13) when the supporting electrolyte concentration is high enough (1.0 M) and the ψ_1-

potential value becomes small. In this case, the i_k–C^r_{Py} curve (C^o_{Py} = const.) obtained from the i_k–pH dependency by eqn. (2) (Fig. 2, curve 6; points-m correspond to C^r_{Py} on abscissa) practically coincided with the i_k–C^o_{Py} curve at pH 6.5 (Fig. 2, curve 6; n-points; pH 6.5 and, consequently, $C^o_{Py} = C^r_{Py}$). The i_k–C^r_{Py} curve (pH) lies markedly lower than the i_k–C^o_{Py} curve at low concentrations of the supporting electrolyte (0.02 M) if the pH is decreased (pH < 6.0) (Fig. 2, dotted curve 1′ and curve 1). This may be explained by a pronounced increase of concentration of hydroxonium ions in the pre-electrode layer under these conditions (ψ_1-effect) which results in a stronger influence of a sufficiently rapid raction[66] in the pre-electrode layer:

$$[NiPy]^{2+}_{ads}([NiPy_2]^{2+}_{ads}) + H_3O^+ \rightarrow Ni^{2+} + [PyH]^+ + H_2O \qquad (17)$$

thus bringing about the drop of catalytic current.

The rate constants of heterogeneous chemical reactions in the absence of the electrical field effect were calculated from eqns. (14) and (15) and Fig. 7 by extrapolation of straight lines having the theoretical slope 33.9 V^{-1}, to $\psi_1 = 0$; these are $k_1 = 4.0 \times 10^2$ l mol^{-1} s^{-1} and $k_2 = 1.8 \times 10^3$ l mol^{-1} s^{-1}. The value of $K_{Py} = 5.65 \times 10^{-6}$ cm (1 M KCl; −0.90 V *vs.* NCE) obtained from the data of Barradas *et al.*[59]* and corrected in accordance with the pyridine activity coefficient in the solution 1 M KCl $f_{Py} = 1.34$[50] was used in these calculations. As we were interested in the value of K_{Py} in the indifferent electrolyte solution ($NaNO_3$) with concentration $C < 0.1$ M ($C^o_{Py} \leqslant 5 \times 10^{-3}$ M) for which $f_{Py} = 1.0$[50], the corrected value was $K_{Py} = 4.21 \times 10^{-6}$ cm.

It is interesting to note that the correlation of rate constants obtained for heterogenous reactions of complexation k_1 and k_2 is characteristic for some bulk reactions[13,68] of complex formation involving Ni^{2+} ion. However, a closer correlation in the k_1 and k_2 values has been found for bipyridine[53].

An experimental activation energy of heterogenous reaction of complex formation $[NiPy]^{2+}$ was determined by us from the log $y' - 1/T$ dependency (5–35°C) (eqns. (13)–(15)) where

$$y' = \frac{y}{K'_1}\left(\frac{D_{NiPy^{2+}}}{t_1}\right)^{\frac{1}{2}} \qquad (18)$$

The second term in eqn. (13) can be neglected as a very low concentration of pyridine ($C^o_{Py} = 5 \times 10^{-5}$ M) was used in these experiments. Also, since the supporting electrolyte solution concentration was 0.02 M and $\psi_1 > RT/F$ then if the Gouy–Chapman theory is applicable, we may accept the following with sufficient accuracy[69]

$$\psi_1 \cong \frac{2RT}{F} \ln (\text{const.}) + \frac{RT}{F} \ln T - \frac{2RT}{F} \ln (-\varphi_a) + \frac{RT}{F} \ln C \qquad (19)$$

The constant term does not depend on temperature. It follows from eqns. (13), (14), (18) and (19) that the variation of y' with temperature is mainly accounted for by the variation of k_1 and K_{Py} with temperature, *i.e.* the expression log $y' - 1/T$ must be a straight line within a narrow temperature range. This has been observed experimentally (Fig. 8). The experimental activation energy was determined as $E_{exp} = 13.8$ kcal mol^{-1}. The E_{exp} value is higher than that of $E = 12$ kcal mol^{-1} [53] for a corresponding

* Comparison[67] of pyridine-on-mercury adsorption data obtained by various techniques confirms the conclusion that the K_{Py} values[59] used are sufficiently reliable.

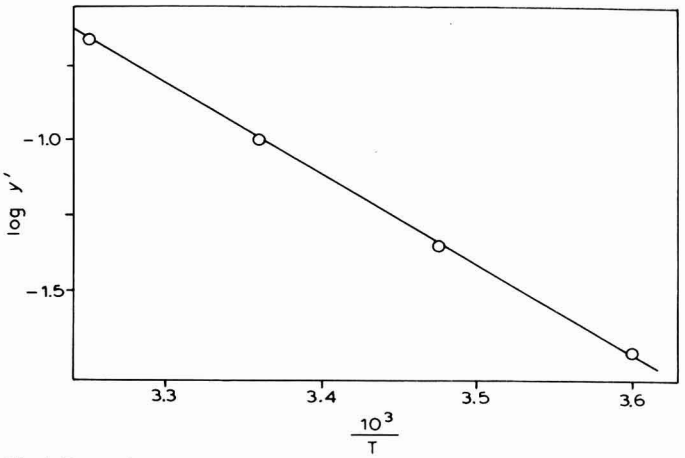

Fig. 8. Dependence of log y' (eqn. (18)) on temp. 0.02 M $NaNO_3$; $C^o_{Ni^{2+}} = 5.0 \times 10^{-5}$ M; $C^o_{Py} = 5.0 \times 10^{-5}$ M; pH = 6.5.

bulk reaction. E_{k_1} will have a still higher value for a heterogenous reaction as $E_{exp} = E_{k_1} - \bar{Q}_{Py}$ ($\bar{Q}_{Py}$ is the heat of pyridine adsorption) and $\bar{Q}_{Py}$ is a positive value.

In general, the results obtained allow us to conclude that the suggestion of Mark *et al.*[18,30] that the adsorbed organic amine participating in a chemical reaction is responsible for the production of the catalytic nickel pre-wave, can also be extended to pyridine*. One should take into account, however, the existence of two parallel reactions of mono- and dipyridine nickel complex formation on the electrode. The absence of an electrical effect upon the instability constant of the pyridine–cobalt complex determined by the change of catalytic current of the pyridine–nickel complex in the presence of cobalt ions[8] is not in contradiction to a surface nature of the catalytic pre-wave, because the adsorbed pyridine concentration was determined from the condition of process equilibria in the solution bulk.

ACKNOWLEDGEMENT

We wish to thank Mrs. G. S. Dokolina and Mr. Yu. M. Kozin for their kind assistance in our work.

SUMMARY

The effect of the electrical double layer (concentration and nature of supporting electrolyte), pH, temperature and adsorption of pyridine on the Ni^{2+} catalytic polarographic pre-wave in the presence of pyridine has been studied.

Two concurrent reactions are shown to proceed on the electrode forming complexes $[NiPy]^{2+}_{ads}$ (from Ni^{2+} and Py_{ads}), and $[NiPy_2]^{2+}_{ads}$ (from $[NiPy]^{2+}$ and Py_{ads}), which are reduced at close potentials. Both complexes are formed in reactions with mercury-adsorbed pyridine, in accordance with the concept by Mark and co-

* The probability of participation of adsorbed pyridine in the above reaction was indicated by Mairanovskii as early as 1961 (private communication).

workers of the character of organic amine involvement in similar processes. The kinetic equation, checked by employing the ψ_1-potential on the basis of Gouy–Chapman theory, is valid at the supporting electrolyte concentrations $C \leqslant 0.05$. When $C > 0.05$, the calculated catalytic currents are lower than the experimental catalytical currents. The effect of the solution pH is in accordance with the kinetic equation only at large C-values ($C = 1.0$ M). The retardation of the catalytic process is observed at $C = 0.02$ M and low pH-values (< 6.0). The causes of discrepancy between the experimental and theoretical data are discussed. The effect of the nature of the cation on the catalytic current ($Cs^+ < Na^+ < Li^+$) is in a qualitative agreement with changes of ψ_1-potential. Rate constants were established for heterogeneous chemical reactions of formation of $[NiPy]^{2+}_{ads}$ and $[NiPy_2]^{2+}_{ads}$ in the absence of electrical field effects.

REFERENCES

1 YA. I. TUR'YAN AND G. F. SEROVA, *Zh. Fiz. Khim.*, 31 (1957) 1976.
2 H. B. MARK AND C. N. REILLEY, *J. Electroanal. Chem.*, 4 (1962) 189.
3 H. B. MARK AND C. N. REILLEY, *Anal. Chem.*, 35 (1963) 195.
4 YA. I. TUR'YAN, *Dokl. Akad. Nauk SSSR*, 146 (1962) 848.
5 W. KEMULA, Z. JEFTIC AND Z. GALUS, *J. Electroanal. Chem.*, 10 (1965) 387.
6 YA. I. TUR'YAN AND O. N. MALYAVINSKAYA, *Elektrokhimiya*, 2 (1966) 1185.
7 YA. I. TUR'YAN AND O. N. MALYAVINSKAYA, *Elektrokhimiya*, 3 (1967) 773.
8 YA. I. TUR'YAN AND O. E. RUVINSKII, *Elektrokhimiya*, 4 (1968) 221; *Dokl. Akad. Nauk SSSR*, 179 (1968) 148.
9 N. TANAKA AND R. TAMAMUSHI, *Sb. Mezinarod. Polarog. Sjezdu Praze*, 1st Congres, 1951, Prirodovedcke vydavatelstvi, Prague, 1 (1951) 486.
10 V. KALOUS, *Chem. Listy*, 50 (1956) 213.
11 YA. I. TUR'YAN, *Zh. Fiz. Khim.*, 31 (1957) 2423.
12 S. TRIBALAT AND D. DELAFOSSE, *Anal. Chim. Acta*, 19 (1958) 74.
13 YA. I. TUR'YAN AND G. F. SEROVA, *Dokl. Akad. Nauk SSSR*, 125 (1959) 595; *Zh. Fiz. Khim.*, 34 (1960) 1009.
14 S. TRIBALAT, *J. Electroanal. Chem.*, 1 (1960) 443.
15 A. A. VLCEK AND J. KŮTA, *Nature*, 185 (1960) 95.
16 R. D. DEMARS, *J. Electrochem. Soc.*, 108 (1961) 779.
17 G. M. HABASHY, *J. Chem. U.A.R.*, 4 (1961) 169; *J. Electroanal. Chem.*, 8 (1964) 237.
18 H. B. MARK, *J. Electroanal. Chem.*, 7 (1964) 276; 8 (1964) 253.
19 H. B. MARK, *Anal. Chem.*, 36 (1964) 940.
20 L. R. MCCOY AND H. B. MARK, *Anal. Chem.*, 37 (1965) 591.
21 A. J. ENGEL, J. LAWSON AND D. A. AIKENS, *Anal. Chem.*, 37 (1965) 203.
22 M. ZIELINSKI AND J. KŮTA, *Abhandl. Deut. Akad. Wiss. Berlin, Elektrochem. Meth. Prinz. Molekular-Biologie, Symposium Jena, May, 1965*, Akademie Verlag, Berlin, 1966, p. 433.
23 J. KŮTA, *Z. Anal. Chem.*, 216 (1966) 242.
24 Z. GALUS AND Z. JEFTIC, *J. Electroanal. Chem.*, 14 (1967) 415.
25 H. B. MARK AND L. R. MCCOY, *Rev. Polarog. Kyoto*, 14 (1967) 122.
26 H. SOHR AND KH. LOHS, *J. Electroanal. Chem.*, 13 (1967) 114.
27 S. G. MAIRANOVSKII AND E. F. MAIRANOVSKAYA, *Novosti Elektrokhimii Organicheskikh Soedinenii*, Nauka, Moscow, 1968, p. 33.
28 I. M. KOLTHOFF, P. MADER AND S. E. KHALAFALLA, *J. Electroanal. Chem.*, 18 (1968) 315.
29 H. B. MARK, *Rev. Polarog. Kyoto*, 15 (1968) 2.
30 H. B. MARK, L. R. MCCOY, E. KIROVA-EISNER AND H. C. MACDONALD, *J. Phys. Chem.*, 72 (1968) 1083.
31 YA. I. TUR'YAN AND O. E. RUVINSKII, *Elektrokhimiya*, 4 (1968) 1446.
32 YA. I. TUR'YAN AND O. N. MALYAVINSKAYA, *Elektrokhimiya*, 5 (1969) 103.
33 YA. I. TUR'YAN AND E. V. SAKSIN, *Elektrokhimiya*, in press.
34 K. A. BURKOV, L. S. LILIC AND L. G. SILLÉN, *Acta Chem. Scand.*, 19 (1965) 14.

35 A. A. VLCEK, *Chem. Listy*, 50 (1956) 828.
36 J. DONDOY AND L. GIERST, *J. Electroanal. Chem.*, 2 (1961) 116.
37 N. S. HUSH AND J. W. SCARROT, *J. Electroanal. Chem.*, 7 (1964) 26.
38 E. VERDIER AND F. ROUELLE, *J. Chim. Phys.*, 62 (1965) 297.
39 R. H. SANBORN AND E. F. ORLEMANN, *J. Am. Chem. Soc.*, 77 (1955) 3726.
40 E. G. TIMOFEEVA, A. A. KNIASEVA AND S. I. KALINICHENKO, *Tr. Mosk. Khim. Tekhnol. Inst.*, 54 (1967) 102.
41 H. T. S. BRITTON AND W. G. WILLIAMS, *J. Chem. Soc.*, (1936) 96.
42 R. J. BRUCHLMANN AND F. H. VERHOEK, *J. Am. Chem. Soc.*, 70 (1948) 1401.
43 J. BJERRUM, *Chem. Rev.*, 46 (1950) 381.
44 H. C. BROWN AND J. R. MIHM, *J. Am. Chem. Soc.*, 77 (1955) 1723.
45 R. K. MURMANN AND F. BASOLO, *J. Am. Chem. Soc.*, 77 (1955), 3484.
46 A. V. ABLOV AND L. V. NASAROVA, *Zh. Neorgan. Khim.*, 2 (1957) 53.
47 YA. I. TUR'YAN AND G. F. SEROVA, *Zh. Fiz. Khim.*, 31 (1957) 2200.
48 G. ATKINSON AND J. E. BAUMAN, *Inorg. Chem.*, 2 (1963) 64.
49 M. K. POLIEVKTOV AND S. G. MAIRANOVSKII, *Isv. Akad. Nauk SSSR, Ser. Khim.*, N 3 (1965) 413.
50 N. P. KOMAR AND NGUEN TIN ZUNG, *Zh. Fiz. Khim.*, 40 (1966) 1077.
51 YA. D. FRIDMAN, M. G. LEVINA AND R. J. SOROCHAN, *Zh. Neorgan. Khim.*, 11 (1966) 1641.
52 M. S. SUN AND D. G. BREWER, *Can. J. Chem.*, 45 (1967) 2729.
53 R. H. HOLYER, C. D. HUBBARD, S. F. A. KETTLE AND R. G. WILKINS, *Inorg. Chem.*, 4 (1965) 929.
54 A. N. FRUMKIN, *Z. Phys. Chem.*, (A) 164 (1933) 21.
55 L. GIERST AND H. Z. HURWITZ, *Z. Elektrochem.*, 64 (1960) 36.
56 H. Z. HURWITZ, *Z. Elektrochem.*, 65 (1961) 178.
57 S. G. MAIRANOVSKII, *Kataliticheskie i Kineticheskie Volni v Polarographii*, Nauka, Moscow, 1966, p. 162.
58 YA. I. TUR'YAN, Sbornik "*Elektrokhimicheskie Processi s Uchastiem Organicheskikh Leschestv*", Nauka, Moscow, in press.
59 R. G. BARRADAS, P. G. HAMILTON AND B. E. CONWAY, *Collection Czech. Chem. Commun.*, 32 (1967) 1790.
60 J. HEYROVSKÝ AND J. KŮTA, *Osnovi Polarography*, Mir, Moscow, 1965, p. 53.
61 J. KOUTECKÝ, *Collection Czech. Chem. Commun.*, 18 (1953) 597.
62 C. D. RUSSELL, *J. Electroanal. Chem.*, 6 (1963) 486.
63 S. AHRLAND AND K. ROSENYRN, *Acta Chem. Scand.*, 10 (1956) 727.
64 B. E. CONWAY, R. G. BARRADAS, P. G. HAMILTON AND J. M. PARRY, *J. Electroanal. Chem.*, 10 (1965) 485.
65 A. N. FRUMKIN, B. B. DAMASKIN AND H. V. NIKOLAEVA-FEDOROVICH, *Dokl. Akad. Nauk SSSR*, 115 (1957) 751.
66 G. A. MELSON AND R. G. WILKINS, *J. Chem. Soc.*, (1962) 4208.
67 B. B. DAMASKIN, A. A. SURVILA, S. YA. VASINA AND A. J. FEDOROVA, *Elektrokhimiya*, 3 (1967) 825.
68 G. G. HAMMES AND J. STEIFIELD, *J. Am. Chem. Soc.*, 84 (1962) 4639.
69 A. N. FRUMKIN, V. S. BAGOTSKII, Z. A. JOFA AND B. N. KABANOV, *Kinetika Elektrodnikh Protsessov*, Moscow, Gos. Universitet, 1952, p. 16.

ELECTROANALYTICAL CHEMISTRY AND INTERFACIAL ELECTROCHEMISTRY
Elsevier Sequoia S.A., Lausanne – Printed in The Netherlands

CONTRIBUTION A L'ETUDE DU DOSAGE DE SUBMICROTRACES DE FER PAR POLAROGRAPHIE INVERSE SUR GOUTTE DE MERCURE PENDANTE

I. ÉTAT DU FER SUR L'ÉLECTRODE ET MÉCANISME D'OXYDATION ÉLECTROCHIMIQUE

W. HAERDI, J. BUFFLE ET D. MONNIER
Institut de Chimie Analytique de l'Université, 1211, Genève 4 (Suisse)
(Reçu le 29 mars 1969)

Le fer joue le rôle d'oligo-élément dans bon nombre de processus biologiques et le problème du dosage de très petites quantités de cet élément prend passablement d'importance. Dans cette optique, nous avons abordé l'étude de son dosage par polarographie inverse en utilisant les conditions suivantes: une électrode indicatrice à goutte de mercure pendante, une électrode de référence Ag/AgCl, la possibilité de contrôler le pH de la solution au moyen d'une électrode de verre, un barbotage d'azote purifié pour éliminer l'oxygène, du KSCN 2 *M* comme électrolyte, du Fe(II) (sous forme de sel de Mohr) comme dépolarisant et un pH voisin de la neutralité.

Une étude préliminaire de l'influence de différents facteurs sur le pic de dissolution du fer[1] nous avait fait remarquer la remarquable étroitesse de ce pic. Au cours de cette première partie, nous avons recherché les causes de cette étroitesse en particulier par l'étude de l'état et du mécanisme d'oxydation électrochimique du fer déposé sur l'électrode.

Nous ne rapportons ici que les résultats les plus importants, cette étude étant décrite plus en détails en ref. 2.

TABLE DES SYMBOLES

$b_{\frac{1}{2}}$	largeur du pic obtenu en polarographie inverse pour $i = i_m/2$
C_O	concentration de la forme oxydée d'un couple ox–red
D_O	coefficient de diffusion de la forme oxydée d'un couple ox–red
D_R	coefficient de diffusion de la forme réduite d'un couple ox–red
E	potentiel de l'électrode indicatrice
E_i	potentiel initial de balayage anodique
E_0	potentiel normal du couple Fe^0/Fe^{2+}
E'_0	potentiel normal du couple Fe^{2+}/Fe^{3+}
E_{red}	potentiel imposé pour la préélectrolyse
F	constante de Faraday = 96500 C
i	courant mesuré au temps t et au potentiel E
i_m	courant maximum du pic de dissolution
K_e	constante de dissociation de l'eau = 10^{-14}
k_0	constante de vitesse d'une réaction électrochimique pour $E = E_0$

l épaisseur du film de mercure dans lequel le métal est dissous
n nombre d'électrons global utilisé pour l'oxydation de Fe^0 en Fe^{2+}
n' nombre d'électrons global utilisé pour l'oxydation de Fe^{2+} en Fe^{3+}
n'' nombre d'électrons global utilisé pour la réduction de Fe^{2+} en Fe^0
n_β nombre d'électrons échangés au cours de l'étape lente de la réaction électrochimique principale
p épaisseur de la couche de réaction chimique
PS produit de solubilité de $Fe(OH)_3$
Q_{red} quantité d'électricité utilisée pour la préélectrolyse
R constante des gaz parfaits ($=8.314$ J $^\circ K^{-1}$ mol^{-1})
S surface de l'électrode
T température
t temps
v vitesse de balayage
β coefficient de transfert électronique pour l'oxydation du Fe^0
(X) concentration de l'élément X en solution.

I. ÉTAT DU FER SUR L'ÉLECTRODE

Des équations mathématiques ont été établies pour calculer théoriquement les pics de dissolution d'un métal dissous soit dans la totalité d'une goutte de mercure[3], soit dans un film de mercure très mince[4]. La comparaison de ces courbes avec le pic de dissolution du fer que nous obtenons (ref. 1, Fig. 1 et 7) nous a permis de constater que ce dernier se rapproche beaucoup plus des pics obtenus sur films de mercure.

Dans notre cas, l'existence d'un film analogue est vraisemblable, étant donnée la très faible solubilité du fer dans le mercure. Celle-ci est de l'ordre de 10^{-60} %[5], mais cette valeur est très controversée car la plupart des auteurs estiment qu'il n'existe pas de véritable amalgame de fer mais seulement une dispersion plus ou moins fine de ce métal dans le mercure[6-8]. Or il est certain que sous cette forme la diffusion du fer dans l'électrode devrait être très ralentie et le pic de dissolution correspondant passablement étalé. L'étroitesse des pics que nous obtenons ne s'accorde pas du tout avec cette constatation. C'est pourquoi il est tout à fait vraisemblable de penser que le fer existe à l'état de dépôt à l'extérieur de l'électrode.

I.1 *Influence de la vitesse de balayage*

Nous avons essayé d'étayer cette hypothèse en utilisant la théorie de de Vries[9] qui relie l'influence de la vitesse de balayage au courant maximum du pic, i_m, dans les cas où le métal amalgamé diffuse dans des films de mercure d'épaisseurs variables. En reprenant cette théorie et en traçant les courbes $\log i_m = f(\log v)$, nous obtenons le graphique représenté à la Fig. 1.

Quelle que soit l'épaisseur du film de diffusion du métal, l, ces courbes tendent vers des droites de pente 1.0 si v tend vers 0 mV s^{-1}, et de pente 0.5 si v tend vers l'infini. La vitesse v_i correspondant à l'intersection de ces deux droites, pour une même épaisseur l, est caractéristique de cette dernière, et on peut tracer la courbe $l = f(v_i)$.

Dans le cas du fer, la mesure de v_i conduit à une valeur de l de 10 μ c'est-à-dire une valeur très petite par rapport au rayon de la goutte qui est de 260 μ.

Notons cependant que la théorie de de Vries a été établie dans le cas de systèmes

ox–red rapides et réversibles, et d'une électrode plane. Ces conditions ne sont pas respectées dans notre cas, mais nous avons montré[2] que l'approximation que nous faisons en considérant notre électrode comme plane conduit à une erreur de $+1.5\%$ sur la hauteur du pic de dissolution, c'est-à-dire une erreur faible par rapport à l'erreur pratique que l'on effectue lors de la détermination de la hauteur du pic. D'autre part, on a montré[10] qu'un pic est d'autant plus bas et étalé que le système ox–red correspondant est moins réversible. En d'autres termes, pour une même épaisseur de film de mercure, la vitesse v_i est d'autant plus faible que le système est plus irréversible. La valeur de 10 μ que nous trouvons pour le fer est donc une valeur maximum, ce qui confirme l'hypothèse d'un dépôt de fer sur l'électrode.

I.2. *Preuve de l'existence d'un dépôt de fer*

Pour mieux prouver l'existence de ce dépôt de fer, nous avons eu recours à du ^{59}Fe radioactif, émetteur de rayons γ.

La Fig. 2 montre l'influence du potentiel de préélectrolyse sur le pic de dissolution (courbe 1) et sur la quantité de fer se trouvant à l'intérieur de la goutte, cette quantité étant représentée par l'activité totale de la goutte (courbe 2). On voit que,

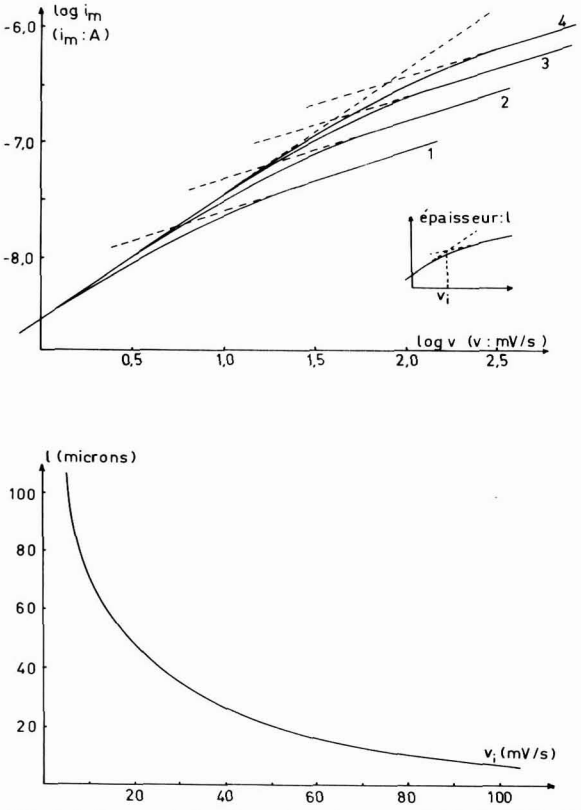

Fig. 1. Influence de la vitesse de balayage v sur le courant maximum du pic de dissolution. l: (1) 100 μ; (2) 50 μ; (3) 25 μ; (4) 4 μ. Constantes utilisées pour les calculs: $n=2$; $D_O=0.72\times10^{-5}$ cm^2 s^{-1}; $E_i-E_0=$ 134 mV; $T=25°C$; $D_R=1.8\times10^{-5}$ cm^2 s^{-1}; $C_O=10^{-9}$ mol ml^{-1}; $S=0.78$ mm^2.

jusque vers -1.35 V, le pic de dissolution observé en polarographie inverse est dû entièrement à l'oxydation de Fe^0 déposé à la surface de la goutte. Ce n'est que pour des potentiels plus négatifs que le métal pénètre dans l'électrode. Notons que cette valeur de -1.35 V dépend passablement de la composition du milieu, puisque dans KSCN 2 M elle est de -1.55 V[1]. La courbe 3 a été obtenue en mesurant l'activité de la goutte de mercure après les deux étapes, de préélectrolyse d'une part, et de dissolution d'autre part, ces étapes étant effectuées dans des conditions identiques à celles utilisées pour l'obtention de la courbe 1. On voit que, une fois que le fer a pénétré dans le mercure, il n'est pas possible d'en dissoudre plus de 15% environ par un simple balayage anodique. Ce résultat confirme l'hypothèse selon laquelle le fer se trouve sous forme de dispersion dans le mercure, la taille des grains empêchant toute diffusion suffisamment rapide pour permettre l'apparition d'un pic de dissolution.

II. ÉTUDE DU MÉCANISME D'OXYDATION ÉLECTROCHIMIQUE DU Fe^0

II.1. *Cas de l'oxydation électrochimique de dépôts métalliques*

La théorie de de Vries[9] relie également la vitesse de balayage à la largeur $b_{\frac{1}{2}}$ du pic de dissolution, pour des films de mercure d'épaisseur variable. En représentant la fonction $b_{\frac{1}{2}} = f(\log v)$ nous obtenons la courbe 1 de la Fig. 3. L'allure de cette courbe ne varie pas avec l. Elle ne fait que subir un déplacement vers la droite lorsque l diminue. Mais, dans tous les cas, lorsque v tend vers 0 mV s^{-1}, $b_{\frac{1}{2}}$ tend vers une valeur minimum de 38.3 mV.

Or, la courbe 4 montre que dans le cas du Fe^0, cette valeur est beaucoup plus faible et se situe à environ 15 mV. Ce résultat ne s'explique pas par le fait que le fer est à l'état de dépôt. En effet, les théories élaborées pour les dissolutions de dépôts monomoléculaires (courbe 2) ou plurimoléculaires (courbe 3) prouvent que la largeur

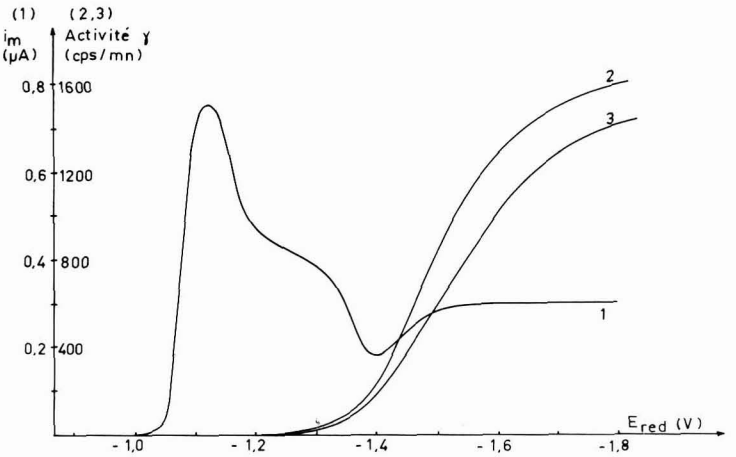

Fig. 2. Influence du potentiel de préélectrolyse sur: (1) la hauteur du pic de dissolution; (2) la quantité de fer pénétrant dans la goutte durant la préélectrolyse; (3) la quantité de fer restant dans la goutte après la dissolution. Conditions opératoires: électrolyte: KSCN 2 M; T: 20°C; réducteur: NH_2OH 2.4×10^{-2} M; vitesse de balayage: 16.6 mV s^{-1}; (Fe^{3+}): 3.6×10^{-6} M; préélectrolyse: 5 min; pH: 4; surface d'électrode: 0.86 mm^2; tampon: CH_3COOH 5×10^{-3} $M + CH_3COO^-$ 10^{-3} M.

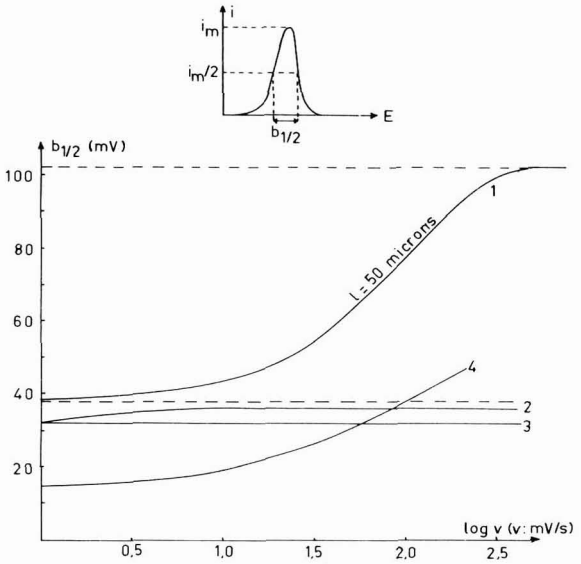

Fig. 3. Influence de la vitesse de balayage sur la largeur du pic de dissolution d'un métal: dissous dans un film mince de mercure (courbe 1[9]), à l'état de dépôt monomoléculaire (courbe 2[11]), à l'état de dépôt pluri-moléculaire (courbe 3[12]), du fer (courbe 4). Conditions opératoires: Courbes 1, 2 et 3: calculs théoriques. Courbe 4: électrolyte: KSCN 2 M; T: 20°C; (Fe^{2+}): 3.6×10^{-6} M; surface d'électrode: 0.86 mm^2; pH: 7.0; dissolution sans agitation.

minimum des pics de dissolution faisant intervenir un échange de 2 électrons est toujours supérieure à 32 mV.

D'autre part, on peut montrer théoriquement[13] que la superposition d'une réaction chimique sur une réaction électrochimique ne peut conduire qu'à un étalement du pic correspondant et ne permet donc pas d'expliquer l'étroitesse du pic du fer.

II.2. *Cas du fer*

Nous avons cherché à savoir si la superposition d'une réaction électrochimique secondaire ne pourrait pas être à l'origine de cette étroitesse. Dans nos conditions, la seule réaction électrochimique secondaire possible consiste en l'oxydation du Fe^{2+} produit à l'électrode, en Fe^{3+}, lequel peut immédiatement précipiter sous forme d'hydroxyde. Nous avons donc établi les expressions mathématiques des pics d'oxydation du fer en considérant comme conditions initiales:

– d'une part que l'unique réaction électrochimique est l'oxydation, considérée comme totalement irréversible:

$$Fe^0 \rightarrow Fe^{2+} + 2e^- \qquad (1)$$

– et d'autre part que cette même réaction principale est suivie de la réaction secondaire suivante:

$$Fe^{2+} \rightleftarrows Fe^{3+} + e^- \qquad (2)$$

considérée comme instantanée. Le Fe^{3+} ainsi produit est lui-même précipité instantanément à l'état de $Fe(OH)_3$:

$$Fe^{3+} + 3\ OH^- \rightleftarrows Fe(OH)_3 \tag{3}$$

Pour l'établissement des équations, nous avons considéré que ni le Fe^0 ni le Fe^{3+} n'étaient influencés par des phénomènes de diffusion, le premier étant à l'état de dépôt à l'extérieur de l'électrode, et le second précipitant dès sa formation. Sur la base de ces conditions, les calculs, décrits en ref. 2, nous ont permis d'obtenir les équations suivantes:
sans réaction secondaire:

$$i(t) = \frac{n}{n''} Q_{red} k_0 \exp\left[-\frac{k_0 e^{(\phi(E_i - E_0))}(e^{\phi vt} - 1)}{\phi v}\right] e^{(\phi(E_i - E_0 + vt))} \tag{4}$$

avec réaction secondaire:

$$i(t) = \frac{(n+n')}{n''} Q_{red} k_0 \exp\left[-\frac{k_0 e^{(\phi(E_i - E_0))}(e^{\phi vt} - 1)}{\phi v}\right] e^{(\phi(E_i - E_0 + vt))} - \frac{(n'F)^2 SpPS(H^+)^3 v}{RTK_e^3} \times \exp\left\{-\frac{n'F}{RT}(E_i - E_0' + vt)\right\} \tag{5}$$

Avec: $\phi = \dfrac{\beta n_\beta F}{RT}$ et $E = E_i + vt$

Symboles: voir table des symboles

Le second membre de l'éqn. (5) contient un terme supplémentaire par rapport à l'éqn. (4). Les calculs montrent que, dans nos conditions, ce terme est négligeable par rapport au premier. Le seul effet de la réaction électrochimique secondaire est donc d'augmenter le courant d'oxydation du pic d'un rapport constant qui provient de la différence du nombre global d'électrons échangés dans les deux cas. Mais cette réaction ne modifie en rien la largeur du pic de dissolution comme on peut le voir par la comparaison des courbes correspondantes (Fig. 4).

L'étroitesse du pic d'oxydation du fer ne s'expliquant pas par la superposition d'une réaction chimique ou électrochimique secondaire, deux hypothèses peuvent être envisagées:
– soit l'existence d'un phénomène purement physique dont nous n'avons pas tenu compte lors de l'établissement de nos équations;
– soit le fait que le nombre d'électrons n_β échangé lors de l'étape lente de la réaction d'oxydation est supérieur à 2. En effet, en l'absence de phénomènes physiques secondaires, la Fig. 5, établie à partir de l'éqn. (4), montre que le seul facteur physique susceptible de modifier la largeur du pic de dissolution est le produit βn_β, et que celui-ci doit atteindre la valeur de 4 environ, pour que la largeur du pic soit de 15 mV. β étant toujours compris entre 0 et 1, ce résultat signifie que n_β doit atteindre la valeur minimum de 4.

Dans ces conditions, il faudrait alors admettre que la réaction d'oxydation du fer s'écrit, non pas comme nous l'avons représenté à l'éqn. (1), mais de la manière suivante:

$$Fe_m^0 \rightarrow mFe^{2+} + 2me^- \tag{6}$$

laissant ainsi supposer que le Fe^0 se trouve à la surface de l'électrode non pas sous forme de dépôt amorphe, mais plutôt à l'état de microcristaux. Notons toutefois

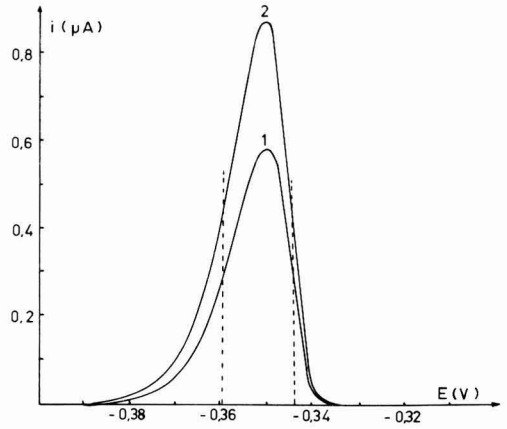

Fig. 4. Courbes de dissolution calculées selon les éqns. (4) (courbe 1) et (5) (courbe 2). Constantes utilisées pour les calculs: $n=2$; $E_0'=-0.77$ V; $\beta n_\beta=4.0$; $S=8.6\times10^{-3}$ cm^2; $n'=1$; $E_i=-0.4$ V; $T=293$ °K; $k_0=10^{-6}$ cm^2 s^{-1}; $n''=2$; $v=10$ mV s^{-1}; $p=10^{-6}$ cm; $Q_{red}=1.7\times10^{-6}$ C; $E_0=-0.44$ V; $PS=10^{-36}$; pH = 8.0.

qu'une telle interprétation nécessite de poser certaines réserves, la quantité de Fe^0 déposé durant une préélectrolyse représentant l'équivalent d'une couche monomoléculaire.

CONCLUSION

En résumé, il apparaît donc que, au cours de la polarographie inverse du Fe(II), la phase de préélectrolyse conduit à une "amalgamation" irréversible du fer métallique si le potentiel imposé est trop négatif. Par contre, si ce n'est pas le cas, le fer reste sous forme de dépôt à la surface de l'électrode. L'application de la phase de dissolution à ce dépôt conduit à l'obtention d'un pic dont la remarquable étroitesse est due non pas à une réaction chimique ou électrochimique superposée à la réaction d'oxydation principale, mais beaucoup plus probablement à l'état physique du fer sur l'électrode.

RÉSUMÉ

On a étudié l'état du fer déposé sur une électrode de mercure à potentiel constant par influence de la vitesse de balayage sur le pic de dissolution obtenu en polarographie inverse et au moyen de traceurs radioactifs.

Si le potentiel de préélectrolyse n'est pas trop négatif (> -1.55 V par rapport à Ag/AgCl, dans KSCN 2 *M*), le fer reste à l'état de dépôt à l'extérieur de l'électrode. Dans le cas contraire, le fer pénètre dans le mercure mais ne peut plus être réoxydé par balayage anodique.

La remarquable étroitesse du pic de dissolution du fer est attribuée à son état physique sur l'électrode, ce métal y étant peut-être déposé à l'état de microcristaux.

SUMMARY

The state of iron deposited at constant potential, on HMDE, was studied by

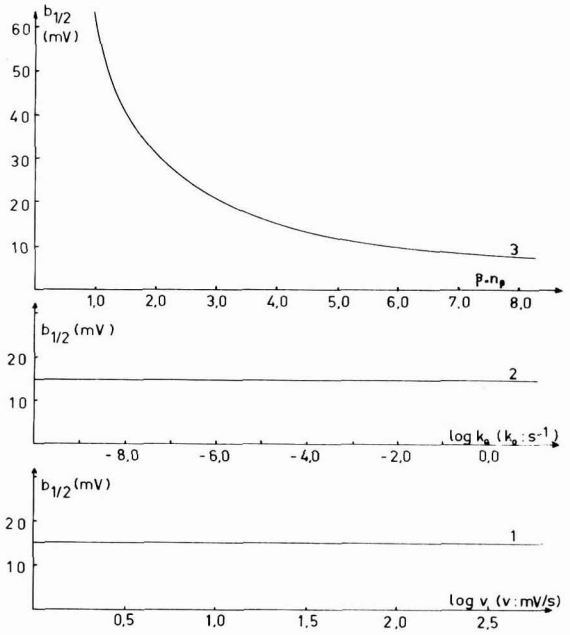

Fig. 5. Influence de la vitesse de balayage (1), de la constante de vitesse de réaction (2), et du produit βn_β (3) sur la largeur $b_{\frac{1}{2}}$ du pic de dissolution calculé par l'éqn. (4). Constantes utilisées pour les calculs: voir Fig. 4.

means of the influence of stripping rate on the dissolution peak obtained by anodic stripping polarography, and also by means of radioactive tracers.

If reduction potential is not too negative (> -1.55 V *vs.* Ag/AgCl, in KSCN $2M$), iron stays on the electrode surface. In the opposite case, iron penetrates into the electrode, but it can no more be reoxidized by anodic stripping.

The great sharpness of dissolution peak of iron is attributed to the physical state of the deposit. This metal is perhaps deposited like microcrystals.

BIBLIOGRAPHIE

1 J. BUFFLE, D. MONNIER ET W. HAERDI, *Chimia (Aarau)*, 21 (1967) 578.
2 J. BUFFLE, Thèse de doctorat, Genève, 1968.
3 W. REINMUTH, *J. Am. Chem. Soc.*, 79 (1957) 6358.
4 D. K. ROE ET E. A. TONI, *Anal. Chem.*, 37 (1965) 1503.
5 L. MARSCHALL ET L. F. EPSTEIN, *J. Am. Chem. Soc.*, 72 (1950) 3514.
6 G. JANGG ET F. I. NORTON, *Metall*, 16 (1962) 14.
7 G. JANGG, E. FITZER, O. ADLHART ET H. HOLM, *Z. Metallk.*, 49 (1958) 557.
8 F. LIHL, *Z. Metallk.*, 44 (1953) 160.
9 a.W. T. DE VRIES ET E. VAN DALEN, *J. Electroanal. Chem.*, 8 (1964) 366; b W. T. DE VRIES, *J. Electroanal. Chem.*, 9 (1965) 448.
10 J. HEYROVSKY ET J. KUTA, *Principles of Polarography*, Academic Press, New York, 1966, p. 220.
11 M. M. NICHOLSON, *J. Am. Chem. Soc.*, 79 (1957) 6358.
12 I. BERZINS ET P. DELAHAY, *J. Am. Chem. Soc.*, 75 (1953) 555.
13 R. S. NICHOLSON ET I. SHAIN, *Anal. Chem.*, 36 (1964) 706.

ELECTROANALYTICAL CHEMISTRY AND INTERFACIAL ELECTROCHEMISTRY
Elsevier Sequoia S.A., Lausanne – Printed in The Netherlands

CONTRIBUTION A L'ETUDE DU DOSAGE DE SUBMICROTRACES DE FER PAR POLAROGRAPHIE INVERSE SUR GOUTTE DE MERCURE PENDANTE

II. ÉTUDE DES RÉACTIONS SECONDAIRES

J. BUFFLE, W. HAERDI ET D. MONNIER
Institut de Chimie Analytique de l'Université, 1211, Genève 4 (Suisse)

(Reçu le 29 mars, 1969)

Dans un précédent article[1] nous avions déjà montré l'influence de différents facteurs sur le pic de dissolution du fer. L'influence tout à fait inhabituelle de ces facteurs nous ont montré l'existence de réactions secondaires superposées aux réactions électrochimiques de réduction et d'oxydation. La mise au point d'une méthode de dosage reproductible nécessitant la connaissance et le contrôle de ces réactions secondaires, nous avons cherché à les déterminer.

Dans une première partie[2] nous avions étudié les causes de l'étroitesse du pic de dissolution du fer. La présente étude, effectuée dans les mêmes conditions, a comporté deux parties fondamentales:

– l'étude des réactions d'oxydation chimique du dépot de Fe^0;

– l'étude des phénomènes de protection du dépôt de fer par adsorption de composés non électroactifs.

Nous ne rapportons ici que les résultats les plus importants, cette étude étant décrite plus en détails en ref. 3.

TABLE DES SYMBOLES

E	potentiel de l'électrode indicatrice
E_{red}	potentiel imposé durant la préélectrolyse
h	hauteur de la colonne de mercure en polarographie classique
i	courant mesuré au temps t et au potentiel E
i_m	courant maximum du pic de dissolution
PS	produit de solubilité de $Fe(OH)_3$
T	température
t'	temps écoulé depuis le début de la formation de la goutte en polarographie classique
t_{red}	durée de préélectrolyse
α	facteur exprimant le degré de complexation de Fe(III)
β_n^L	constante cumulative de stabilité du complexe du Fe(III) avec le ligand, L: $\beta_n^L = \frac{(FeL_n)}{(Fe)\cdot(L)^n}$
(X)	concentration de l'élément X en solution.

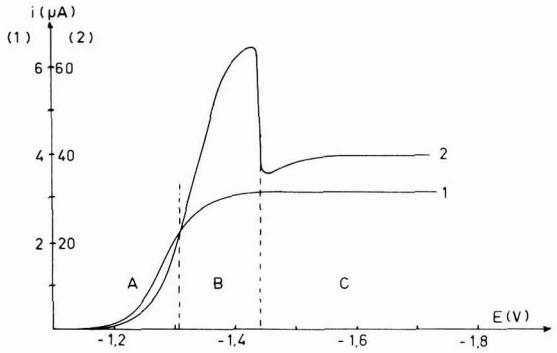

Fig. 1. Courbe de réduction du Fe^{2+} en polarographie classique à gouttes tombantes. (Fe^{2+}): (1) 8×10^{-4}; (2) 1.1×10^{-2} *M*. Conditions opératoires: électrolyte: Na_2SO_4 0.1 *M*; hauteur de Hg: 40.5 cm; pH: 6.0; temps de goutte: 10 s; *T*: 20°C; vitesse de balayage: 1 mV s^{-1}.

I. OXYDATION CHIMIQUE DU FER METALLIQUE DÉPOSÉ SUR L'ÉLECTRODE

I.1. *Polarographie classique du Fe(II)*

Si le temps de goutte est suffisamment long, la polarographie classique du Fe(II) permet d'obtenir les courbes 1 ou 2 (Fig. 1) selon que la concentration du Fe(II) en solution est inférieure ou supérieure à 5×10^{-4} *M*. L'étude de l'influence des facteurs physiques (*T*, *h*) sur cette courbe montre que dans les secteurs A et B la réduction de Fe(II) est précédée par une réaction chimique que nous avons admis comme étant celle proposée par Ivanov et Iofa[4]:

$$Fe(H_2O)_n^{2+} + H_2O \rightleftarrows Fe(OH)(H_2O)_n^{+} + H^{+} \quad (1)$$

$$Fe(OH)(H_2O)_n^{+} + 2e^{-} \rightarrow Fe^{0} + nH_2O + OH^{-} \quad (2)$$

En outre en B l'influence de T montre que si (Fe^{2+}) est suffisamment grand, la réduction de cet ion est influencée par un phénomène d'adsorption. Ce phénomène ne se faisant plus sentir en C, et la limite entre les secteurs B et C ayant lieu à un potentiel qui correspond à celui pour lequel Fe^0 pénètre à l'intérieur du mercure (voir ref. 2: I.2) nous avons pensé que le phénomène d'adsorption portait sur le Fe^0

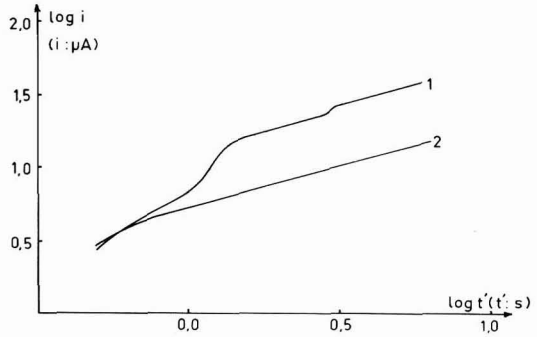

Fig. 2. Courbes log $(i) = f(\log t')$ aux potentiels: (1) -1.375; (2) -1.45 V; Conditions opératoires: (Fe^{2+}): 3.8×10^{-3} *M*; électrolyte: Na_2SO_4 0.1 *M*; pH: 5.2; hauteur de Hg; 40.5 cm; *T*: 20°C.

déposé sur l'électrode et que le maximum polarographique lui était lié.

L'étude du courant instantanné sur une goutte tombante dans le cas ou la concentration du fer est supérieure à 5×10^{-4} *M* confirme cette idée. En effet, d'après la loi d'Ilkovič:

$$i = Kt'^{\frac{1}{6}} \tag{3}$$

K = constante de proportionnalité.

Dans les cas normaux, la courbe représentant $\log i = f(\log t')$ est donc une droite. On voit (Fig. 2) que cette relation est suivie si le potentiel imposé à la goutte vaut -1.45 V, c'est à dire lorsque le Fe^0 pénètre à l'intérieur de l'électrode. Par contre au potentiel de -1.375 V, pour lequel le Fe^0 reste en surface, le courant présente de brusques augmentations indiquant un apport rapide de Fe(II) à l'électrode, laissant ainsi supposer que le Fe^0 déposé peut être facilement réoxydé par les oxydants chimiques de la solution.

L'étude que nous avons faite concernant l'influence des oxydants de la solution (H^+, O_2, Fe^{3+}) sur le maximum polarographique a confirmé cette hypothèse et nous permet de penser que, lorsque l'électrode est portée à un potentiel compris dans le domaine B, le Fe^0 entre dans le cycle suivant:

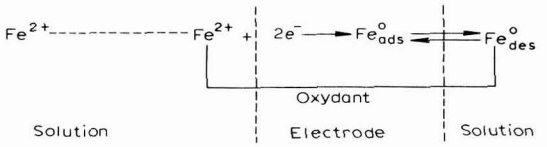

En milieu suffisamment acide (pH < 5) et en solution pure, l'oxydant dont la concentration est la plus élevé est H^+ et ceci explique pourquoi Ivanov et Iofa[4] observent une réduction simultanée de H^+ et de Fe^{2+} au pH < 4.5.

1.2. *Étude de l'oxydation chimique du Fe^0 par polarographie inverse*

Nous avons étudié l'influence de la concentration de l'oxygène dissous sur

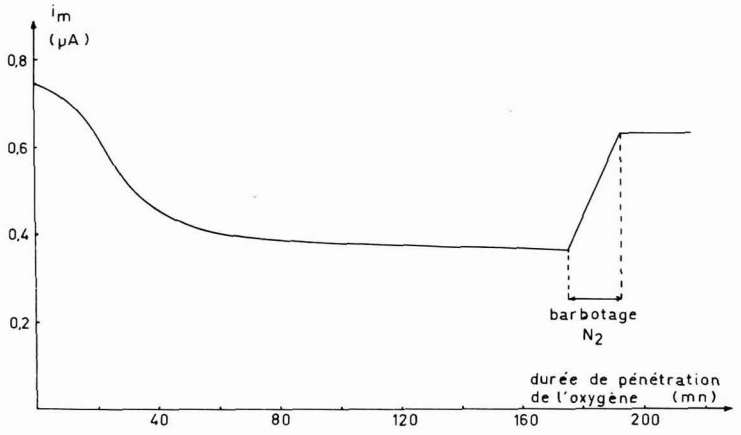

Fig. 3. Influence de l'oxygène dissous sur la hauteur du pic de dissolution du Fe^0. Conditions opératoires: (Fe^{2+}): 1.8×10^{-6} *M*; préélectrolyse: 3 min à -1.5 V; électrolyte: KSCN 2 *M*; *T*: 40°C; pH: 6.5.

le courant maximum du pic de dissolution en polarographie inverse (Fig. 3).

Pour cela, nous avons laissé pénétrer l'oxygène très lentement dans une solution préalablement désoxygénée, et nous avons enregistré le pic de dissolution après des durées de pénétration de l'oxygène variables. On peut constater une forte diminution de i_m en fonction du temps. Remarquons qu'une élimination de l'oxygène après l'expérience permet de retrouver un pic de hauteur presqu'identique à la hauteur initiale, ce qui signifie que l'oxydation a bien porté principalement sur le Fe^0 de l'électrode, et peu sur le Fe(II) de la solution. Remarquons également que, au bout de 3 h, la quantité d'O_2 dissous dans la solution n'était pas encore dosable par polarographie classique. Sa concentration était donc inférieure à 10^{-5} M.

Nous avons également étudié l'influence d'impuretés métalliques de concentrations variables, sur le pic de dissolution du Fe^0. Or nous avons pu constater que tous les éléments (Cu^{2+}, Pb^{2+}, Tl^+) plus nobles que le fer conduisent à une diminution du pic de dissolution, même à de très faibles concentrations, et ceci dans une mesure d'autant plus élevée que l'impureté métallique est plus oxydante. Au contraire, les éléments moins nobles que le fer (Mn, Zn) produisent une augmentation du pic de dissolution lorsque leur concentration est passablement plus élevée que celle de Fe^{2+}, ce qui peut s'expliquer par une sorte de protection anodique.

I.3. *Influence de l'oxydation chimique sur la courbe $i_m = f(E_{red})$*

Nous avons vu (ref. 2, Fig. 2; ref. 3, Fig. 6) que la courbe $i_m = f(E_{red})$ a l'allure présentée sur la Fig. 4, courbe 3, et nous avons vu également que E_{min} et E_{max} dépendent considérablement de la nature de l'électrolyte (ref. 2: I.2).

E_{min} est le potentiel de début de réduction du Fe^{2+} en Fe^0. D'autre part, nous avons vu que la brusque diminution de i_m lorsque E est voisin de E_{max} s'explique par une pénètration du fer dans le mercure.

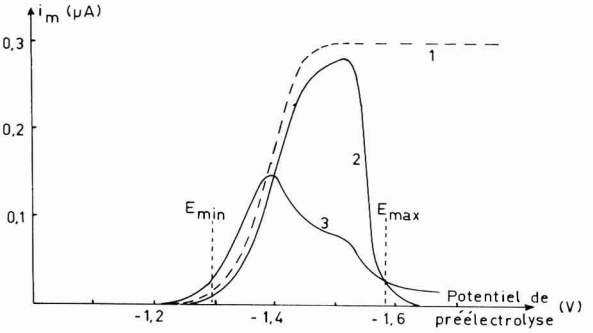

Fig. 4. Influence de l'oxydation chimique sur les courbes $i_m = f(E_{red})$: (1) courbe de réduction de Fe(II) schématique en polarographie classique; (2) barbotage d'N_2: 3 h, $v = 25$ mV s^{-1}; (3) barbotage d'N_2: 20 min, $v = 2.5$ mV s^{-1}. Conditions opératoires: électrolyte: KSCN 2 M; (Fe^{2+}): 7.3×10^{-6} M; T: 20°C; pH: 7.5; préélectrolyse; 2 min; surface d'électrode: 0.86 mm^2.

La dépression située entre E_{min} et E_{max}, quant à elle, peut s'expliquer par le phénomène d'oxydation que nous avons vu ci dessus. En effet, lorsque E devient suffisamment négatif, la réduction de H^+ au voisinage de l'électrode élève le pH, facilitant ainsi l'oxydation du Fe^0 en Fe^{2+} puis en Fe^{3+} ce dernier étant éliminé par précipitation. La Fig. 4, courbe 2 que nous avons obtenue en effectuant une très forte

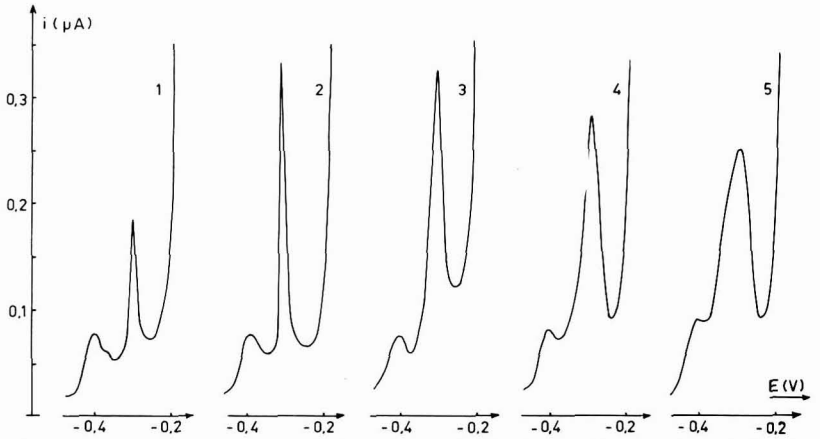

Fig. 5. Influence de $Al(OH)_3$ sur l'allure du pic de dissolution. Concns. de Al(III): (1) 0; (2) 3.7×10^{-6}; (3) 7.4×10^{-6}; (4) 1.8×10^{-5}; (5) 3.7×10^{-5} *M*. Conditions opératoires: électrolyte: KSCN 2 *M*; (Fe^{2+}): 3.6×10^{-6} *M*; préélectrolyse: 5 min à -1.5 V; vitesse de balayage: 20 mV s^{-1}; pH: 7.0; surface de l'électrode: 0.86 mm^2; *T*: 20°C.

désoxygènation de la solution et en utilisant une vitesse de balayage rapide, c'est à dire dans des conditions où l'oxydation du Fe^0 est difficile, semble confirmer cette idée.

II. PROTECTION DU DÉPÔT DE Fe^0 PAR ADSORPTION

On voit sur la Fig. 3 qu'à partir d'une certaine durée de pénètration de l'oxygène la hauteur du pic reste constante. Le Fe^0 s'oxydant en Fe(II) qui peut être facilement transformé en Fe(III) en présence d'oxygène, l'idée d'une protection du dépôt de Fe^0 par $Fe(OH)_3$ vient immédiatement à l'esprit.

II.1. *Protection par $Al(OH)_3$*

Nous avons confirmé cette idée en ajoutant dans une solution faiblement

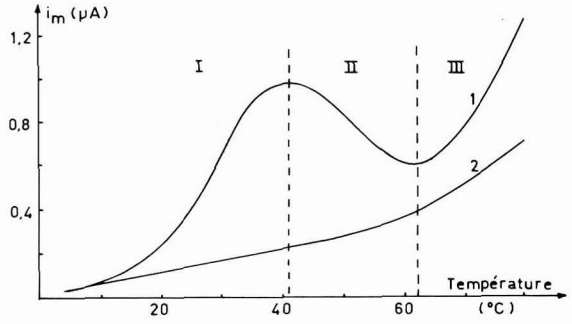

Fig. 6. Influence de la temp. sur le courant de dissolution du Fe^0(1) et du Zn^0(2). Conditions opératoires: électrolyte: KSCN 2 *M*; (Fe^{2+}) 1.8×10^{-6} *M*; préélectrolyse: 3 min à -1.5 V; vitesse de balayage: 20 mV s^{-1}; pH: 6.2; surface de l'électrode: 0.86 mm^2; (Zn^{2+}): 10^{-6} *M*.

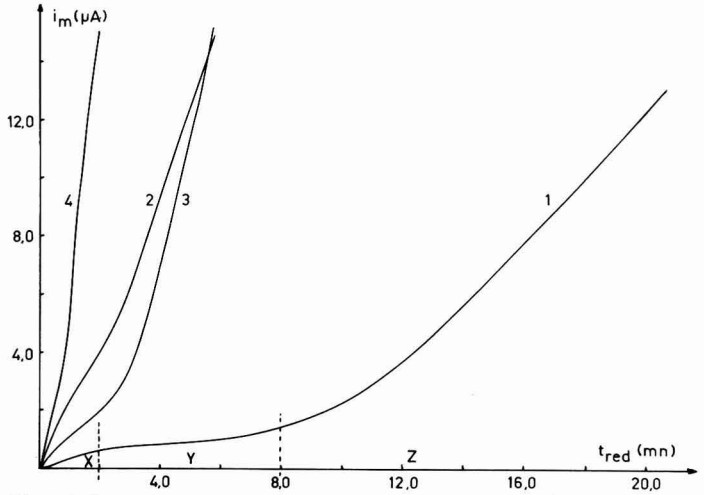

Fig. 7. Influence de la temp. sur les courbes $i_m = f(t_{red})$: (1) 20° ; (2) 40° ; (3) 50° ; (4) 70°C. Conditions opératoires : électrolyte : KSCN 2 M ; (Fe^{2+}) : 9×10^{-6} M ; préélectrolyse : -1.5 V ; pH : 7.2 ; vitesse de balayage : 20 mV s^{-1} ; surface d'électrode : 0.86 mm^2.

désoxygénée des quantités croissantes d'Al(III) (Fig. 5). Celui-ci, au pH 7, s'hydrolyse rapidement en hydroxyde lequel possède des propriétés d'adsorption assez analogues à $Fe(OH)_3$. On voit sur cette Figure que l'addition d'Al(III) accroit considérablement le pic de dissolution. Des concentrations trop élevés d'Al(III) provoquent un étalement du pic ce qui est naturel, la couche d'hydroxyde adsorbée gênant le processus d'oxydation électrochimique lorsqu'elle est trop épaisse.

II.2. *Influence de la température*

L'effet de la température sur le pic du fer (Fig. 6, courbe 1) est très différent de celui que l'on obtient avec un élément type facilement amalgamable tel que le Zn (Fig. 6, courbe 2). La Fig. 6, courbe 1, obtenue en prenant pour t_{red} une valeur comprise dans le secteur X de la Fig. 7, courbe 1, reflète trois phénomènes : la forte augmentation de i_m en fonction de T dans les secteurs I et III prouve l'existence de réactions chimiques superposées à la réaction électrochimique, alors que la diminution de i_m en II prouve l'existence d'un phénomène d'adsorption.

Nous avons comparé l'allure de la Fig. 6, courbe 1 avec l'influence de la température sur les courbes $i_m = f(t_{red})$ (Fig. 7).

Nous avions représenté l'allure de la courbe $i_m = f(t_{red})$ à 25°C, en ref. 1 (Fig. 5) mais pour une concentration de Fe(II) faible, c'est à dire que cette étude s'était alors limitée au secteur X. On peut constater, en augmentant t_{red} ou la concentration de Fe(II) que cette courbe présente, l'allure générale dessinée en courbe 1 (Fig. 7).

Plusieurs expériences[3] nous ont permis de penser que dans le secteur X, le Fe^0 est protégé par $Fe(OH)_3$ présent comme impureté en solution, alors que dans le secteur Z la protection s'effectue par oxydation chimique du dépôt, en Fe^{2+}, puis en Fe^{3+}, lequel ne tarde pas à précipiter. La quantité de $Fe(OH)_3$ de la solution susceptible de s'adsorber sur l'électrode est limitée dans une mesure qui dépend des isothermes de Langmuir correspondants, ce qui permet d'expliquer la présence d'un

palier dans le secteur Y : la quantité d'hydroxyde présent sur l'électrode est alors maximum, et la protection du dépôt ne peut plus être améliorée par un simple processus d'adsorption.

La Fig. 7 a confirmé cette hypothèse en montrant que les deux réactions secondaires supposées (protection par adsorption simple et par oxydation chimique) évoluent indépendamment l'une de l'autre. Le comportement des parties X et Y de la courbe en fonction de l'augmentation de T s'explique en considérant que le film protecteur adsorbé commence à se désorber de manière importante à partir de 40°C environ, provoquant ainsi une diminution du pic. Pour des températures inférieures, l'augmentation de i_m en fonction de T est due à ce que la vitesse de réduction de Fe^{2+} est régie par une réaction chimique antécédente (I.1) toujours fortement influencée par la température.

Par contre, la Fig. 7 montre que le deuxième mécanisme de protection (secteur Z) se manifeste toujours plus considérablement lorsque T augmente, indiquant que ce phénomène consiste non pas en un processus d'adsorption simple, mais plus probablement en une réaction chimique. Lorsque T dépasse 60°C, ce processus finit par masquer les deux autres.

II.3. *Influence des agents complexants*

Les solutions que nous utilisons contiennent toujours une certaine quantité de Fe(III), cet élément étant présent comme impureté dans le KSCN 2 M à la concentration de 2×10^{-6} M. Nous avons cherché à montrer l'importance de la présence de $Fe(OH)_3$ en ajoutant à la solution des complexants du Fe(III) pour éviter la formation de ces hydroxydes.

La complexation du Fe(III) peut se calculer au moyen du facteur α défini par la relation :

$$\alpha = \frac{\text{concn. du Fe(III) sous toutes ses formes}}{\text{concn. du Fe(III) non complexé}}$$

$$\alpha = \frac{(Fe^{3+})_{tot}}{(Fe^{3+})} \tag{4}$$

Ce facteur intervient dans le produit de solubilité de l'hydroxyde ferrique selon l'équation :

$$PS = 10^{-36} = \frac{(Fe^{3+})_{tot}}{\alpha} \times (OH^-)^3 \tag{5}$$

Dans nos conditions (pH = 7 ; $(Fe^{3+})_{tot} = 2 \times 10^{-6}$ M) la précipitation de $Fe(OH)_3$ n'a pas lieu si α est supérieur ou égal à $10^{9.3}$. Or, dans notre milieu, α peut être calculé par la relation :

$$\alpha = 1 + \beta_1^{OH}(OH^-) + \beta_2^{OH}(OH^-)^2 + \beta_1^{SCN}(SCN^-) + \beta_2^{SCN}(SCN^-)^2 + \beta_3^{SCN}(SCN^-)^3 + \beta_4^{SCN}(SCN^-)^4 + \beta_5^{SCN}(SCN^-)^5 \tag{6}$$

et vaut, pour $(SCN^-) = 2$ M et pH = 7 :

$$\alpha = 10^{8.6}$$

Cette valeur est très proche de $10^{9.3}$ et nous avons pensé que l'apparition d'un

pic en milieu KSCN 2 *M* pouvait être dûe à ce que le Fe(III) se trouve dans des conditions limites pour sa précipitation comme hydroxyde. En effet, Stumm[5] a montré récemment que la précipitation d'hydroxydes tels que $Fe(OH)_3$ ou $Al(OH)_3$ s'effectue par l'intermédiaire de complexes hydroxylés polynucléaires du type $Fe_n(OH)_m^{(3n-m)}$, de poids moléculaire quelques fois très élevé. Or, d'une part ces complexes ont une tendance toute particulière à être adsorbés, en raison de leur faible hydratation et des nombreux groupes OH qu'ils possèdent, et d'autre part ces composés de transition de la précipitation des hydroxydes se trouvent à un état relativement stables lorsque les conditions sont telles que l'hydroxyde se trouve à la limite de sa précipitation.

La Fig. 8 montre qu'en effet, l'augmentation du facteur α par adjonction d'acétylacétone au milieu provoque une diminution du pic d'oxydation du fer lorsque α est supérieur ou égal à $10^{9.5}$. De même, des expériences effectuées en milieu F^-, lequel est moins complexant que KSCN, montrent que la diminution de α en dessous de 10^8 provoque une forte diminution du pic de dissolution. Ces résultats expliquent l'absence de pic de dissolution dans les électrolytes que nous avions essayé au cours de nos essais préliminaires : seul le KSCN 2 *M* offrait les conditions de complexation nécessaire.

Notons cependant que les complexes polyhydroxylés, polynucléaires du Fe(III) sont des molécules en chaines qui peuvent prendre en solution des structures variant entre la forme allongée et la forme "en boule", selon la nature et la concentration de l'électrolyte et ceci par simple modification des champs électriques qui agissent

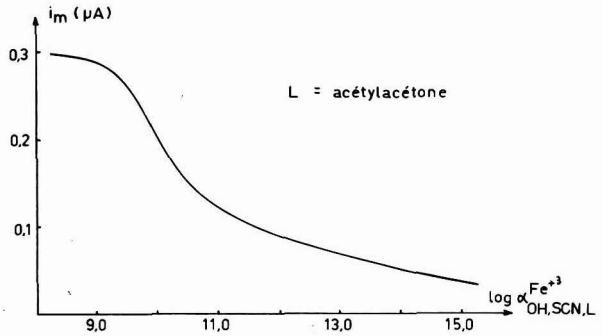

Fig. 8. Influence du degré de complexation du Fe(III) sur le pic de dissolution du Fe^0. Conditions opératoires : électrolyte : KSCN 2 *M* ; (Fe^{2+}) : 4×10^{-6} *M* ; préélectrolyse : 2 min à -1.5 V ; vitesse de balayage : 20 mV s^{-1} ; *T* : 20°C ; surface d'électrode : 0.86 mm^2.

sur les charges portées par ces complexes. Or il est certain que cette structure stéréochimique doit également avoir une importance sur la protection effectuée par ces complexes. Il est donc très probable que l'effet complexant de l'électrolyte n'est pas le seul facteur déterminant dans ce phénomène de protection.

CONCLUSION

Ce travail nous a permis de montrer que la mise au point d'un dosage du fer par polarographie inverse doit tenir compte principalement :

– du potentiel de préélectrolyse, celui-ci devant être suffisamment négatif pour réduire le Fe(II), mais pas trop pour éviter la pénétration du Fe^0 dans le mercure;
– de l'oxydation possible du dépôt sur l'électrode: tout oxydant du Fe^0 présent en solution est susceptible de gêner le dosage.
– de la protection du Fe^0 métallique par adjonction d'un composé susceptible de s'adsorber sur l'électrode de manière reproductible. Toutefois, ce composé ne doit pas former un film trop compact, pour ne pas gêner la dissolution électrochimique. Quelques expériences dans ce domaine nous ont montré que la thiourée pouvait être susceptible de former un film protecteur valable.

Ces quelques inconvénients peuvent cependant être surmontés et sont contrebalancés par la grande sensibilité de cette méthode, puisqu'elle permet de détecter des concentrations de Fe(II) de l'ordre de 10^{-7} M, ainsi que par la grande sélectivité que lui procure l'étroitesse du pic de dissolution. Enfin, les caractéristiques de cette méthode offrent la possibilité de doser le Fe(II) et le Fe(III) séparément ce qui n'est pas possible dans la plupart des méthodes spectrophotomètriques actuelles.

REMERCIEMENTS

Nous exprimons nos vifs remerciements au Fond National Suisse de la Recherche Scientifique, qui a mis à notre disposition l'appareillage et les subsides nécessaires à la réalisation de ces recherches.

RÉSUMÉ

Dans ce travail, nous avons étudié les réactions secondaires qui peuvent influencer l'allure du pic de dissolution du fer en polarographie inverse. Elles sont de deux natures:
– les polarogrammes classiques, les courbes du courant instantanné sur une goutte tombante, l'influence de l'oxygène dissous sur le pic de dissolution du fer obtenu par balayage anodique, ainsi que d'autres études montrent que le fer déposé peut être très facilement réoxydé par les oxydants chimiques de la solution;
– l'influence de la température ainsi que celle des hydroxydes de Fe(III) ou Al(III) présents en solution sur le pic de dissolution montre que le dépôt de fer peut être protégé contre une oxydation chimique, par adsorption de composés non électroactifs, en particulier des complexes du type $Fe_n(OH)_m^{(3n-m)}$. Ce film adsorbé ne doit pas être trop compact pour ne pas gêner le processus de dissolution électrochimique.

SUMMARY

In this work we have studied secondary reactions that can influence the shape of the dissolution peak of iron obtained by anodic stripping polarography. We observed two kinds of reactions:
– classical polarograms, $i=f(t)$ curves on the DME, the influence of dissolved oxygen on the dissolution peak of iron obtained by anodic stripping, and other studies, show that deposited iron can be very easily oxidized by chemical oxidants in the solution.
– the effect of temperature on the dissolution peak, as well as of the presence of Fe(III)

or Al(III) hydroxides in solution, shows that the iron deposit can be protected against chemical oxidation by adsorption of non-electroactive compounds, particularly of complexes such as $Fe_n(OH)_m^{(3n-m)}$. This adsorbed film should not be too compact in order to avoid the inhibition of the electrochemical dissolution process.

BIBLIOGRAPHIE

1 J. BUFFLE, D. MONNIER ET W. HAERDI, *Chimia (Aarau)*, 21 (1967) 578.
2 W. HAERDI, J. BUFFLE ET D. MONNIER, *J. Electroanal. Chem.*, 23 (1969) 81.
3 J. BUFFLE, Thèse de doctorat, Genève, 1968.
4 V. E. IVANOV ET Z. A. IOFA, *Dokl. Akad. Nauk SSSR*, 137 (1961) 1149.
5 W. STUMM ET C. R. O'MELIA, *J. Am. Water Works Assoc.*, 60 (1968) 515.

ELECTROANALYTICAL CHEMISTRY AND INTERFACIAL ELECTROCHEMISTRY
Elsevier Sequoia S.A., Lausanne – Printed in The Netherlands

STUDIES OF THE POLAROGRAPHIC AND COULOMETRIC BEHAVIOUR OF AROMATIC NITRO-COMPOUNDS

I. NITROBENZENE IN ETHANOL

S. K. VIJAYALAKSHAMMA AND R. S. SUBRAHMANYA
Department of Inorganic and Physical Chemistry, Indian Institute of Science, Bangalore-12 (India)

(Received November 15th, 1968; in revised form, April 1st, 1969)

INTRODUCTION

A good deal of work has been done on the d.c. polarographic behaviour of nitrobenzene[1-6] using one concentration of an organic solvent (mostly below 10%) with a view to increasing the solubility of the nitro-compound. The reduction of nitrobenzene is known to be pH-dependent and the reduction mechanism has been studied by a number of workers[7-10]. Alkaline reduction of nitrobenzene on a large scale gives products such as azobenzene, azoxybenzene and hydrazobenzene all of which have two nucleii in the molecule[7,8] but little work has been done on the polarographic reduction in alkaline solutions. Information regarding the nature of the products formed during the polarographic reduction of nitrobenzene can be obtained from the limiting current values, provided the value of the diffusion coefficient is known. In the present work, an attempt has been made to obtain diffusion coefficients using a McBain–Dawson cell. The number of electrons involved in the reduction has been independently determined by coulometry. Since the reduction is irreversible, the number of electrons involved in the rate-determining step has been obtained using the theory of irreversible waves. The formulation of the rate-determining step is facilitated by a.c. polarographic methods. In the present paper, the techniques of d.c., a.c. and Fournier polarography, coulometry, and diffusion coefficient measurement under polarographic conditions have been used to study the reduction of nitrobenzene.

EXPERIMENTAL

Both a manual set-up and a pen-recording polarograph (Radiometer Polariter PO4) were used in the present work. The details of measurement have already been described[12]. The capillaries used in polarography had m values of 1.175 and 1.243 mg s^{-1} and drop times of 4 s and 4.1 s in 1 N potassium chloride solutions. The temperature of the investigations was $30 \pm 0.1°C$. The supporting electrolyte used was lithium chloride, the concentration of which was adjusted to give an ionic strength of 0.5 M.

Diffusion coefficient measurements were made using the McBain–Dawson cell as already described[13].

TABLE 1

EFFECT OF ETHANOL CONCENTRATION ON THE POLAROGRAPHIC BEHAVIOUR OF NITROBENZENE AT DIFFERENT pH-VALUES

Total ionic strength, 0.5 M; 1:1 electrolyte; capillary characteristics: $m = 1.175$ mg s^{-1}, $t = 4.0$ s; supporting electrolyte, LiCl.

Buffer	*pH of aq. soln.*	*Ethanol concn./%* (*v/v*)	*Wave I*		$-(E_{\frac{3}{4}} - E_{\frac{1}{4}})$/ *mV*	*Wave II*		$-(E_{\frac{3}{4}} - E_{\frac{1}{4}})$/ *mV*
			$i_d/\mu A$	$-E_{\frac{1}{2}}/V$		$i_d/\mu A$	$-E_{\frac{1}{2}}/V$	
HCl, 0.5 M		10–70	8.04– 6.60	0.150– 0.205	50–60	2.40 1.90	0.665– 0.695	—
HCl, 0.1 M	1	0–40–90	8.01– 5.54– 8.17	0.185– 0.240– 0.305	60–55–75	2.33– 2.04– 2.90	0.680– 0.740– 0.755	
HCl, 0.01 M	2	0–40–80	7.15– 5.83– 6.13	0.255– 0.310– 0.385	80–65–65	2.29– 2.33– 2.63	0.800– 0.775– 0.810	
Citrate buffer	2.75	10–50	6.87– 5.33	0.292– 0.396	65–80	2.61– 2.25	0.798– 0.859	90–60
Citrate buffer	3.9	10–50	6.63– 5.56	0.355– 0.470	70–77	1.66– 1.05	0.905– 0.952	70–62
Citrate buffer	4.15	10–50–70	6.51– 4.74– 5.68	0.390– 0.475– 0.550	60–80	0.95– 0.47– 0	0.970– 1.0 (?)	60
Citrate buffer	4.56	10–50	6.51– 5.80	0.380– 0.510	59–61	0.59– 0	0.948–	—
Citrate buffer	5.3	10–50	6.40– 5.68	0.425– 0.536	52–60	—	—	—
Acetate buffer	4.7	0–40–90	6.58– 5.54– 8.17	0.380– 0.490– 0.655	60–65–80	—	—	—
Ammonia buffer	9.0	0–40–90	6.84– 5.54– 6.71	0.630– 0.700– 0.760	75–60–55	—	—	—
Acetate soln.	7.4	0–40–90	6.86– 5.54– 7.00	0.635– 0.750 0.885	90–100–85	—	—	—
Borate buffer	7.18	10–50	6.63– 5.80	0.570– 0.694	80–64	—	—	—
Borate buffer	8.11	10–50	6.63– 5.92	0.615– 0.722	74–52	—	—	—
Borate buffer	9.5	10–50	6.20– 5.51	0.646– 0.767	52–65	—	—	—
Borate buffer	10.0	10–50	5.39– 5.39	0.657– 0.775	48–64	—	—	—
NaOH, 0.01 M		0–40–90	6.86– 5.54– 7.00	0.695– 0.785– 0.885	70–85–90	—	—	—
NaOH, 0.1 M		0–40–80	7.14– 5.40– 5.68	0.705– 0.800– 0.870	80–85–90	—	—	—
NaOH, 0.5 M		10–50–70	6.63– 5.30– 5.80	0.720– 0.794– 0.801	53–84–61	—	—	—

The a.c. polarographic outfit is essentially the same as that described by Breyer and Gutmann[14]. A Philips oscilloscope (G.M. 3156/01) was used to measure the a.c. drop across a 100-Ω resistance introduced into the circuit. In Fournier polarographic measurements, the current was calculated from the iR drop across 10,000 Ω, shorted by a high capacity condenser (4000 μF electrolytic condenser). The potential of the DME with respect to the SCE was measured independently using a Tinsley potentiometer.

Controlled potential electrolysis at a large mercury pool cathode was carried out using either the automatic potentiostat (Shandon) or the manual circuit of Lingane[15]. The platinum disc anode was kept in saturated KCl solution and connected to the cathode compartment with an agar bridge. The quantity of electricity passed was determined by a hydrogen–oxygen coulometer[16] or a silver coulometer.

Both nitrobenzene and ethanol were purified by standard methods. All chemicals used were of reagent-grade.

RESULTS

1. *Effect of ethanol on the half-wave potential, $E_{\frac{3}{4}} - E_{\frac{1}{4}}$, and the diffusion current constant at various pH values*

Polarograms obtained in 0.1 M hydrochloric acid solutions at different ethanol concentrations are given in Fig. 1. The first wave is well defined while the second is extended; however, the wave shape improves at higher concentrations of ethanol. In pure aqueous solutions, the second wave extends over a wide range of potentials, and its presence can easily be overlooked. In 99% ethanol, however, the second wave appears to be split up (indicated by an arrow). Polarograms obtained in 0.5 and 0.01 M hydrochloric acid are similar to those given in Fig. 1. When the pH is increased, the second wave decreases in height and completely disappears at pH 4.7. The results of the analysis of all the waves are given in Table 1. These results indicate that the value of $E_{\frac{3}{4}} - E_{\frac{1}{4}}$ is >60 mV in all cases, indicating the irreversibility of the reduction process. The half-wave potentials of both waves increase with ethanol concentration in a given buffer solution. At a given ethanol concentration, the half-wave potentials increase with pH until pH ≈ 9, and thereafter remain constant. In general, the limiting current of the first wave in any given buffer decreases with ethanol concentration, reaches a minimum value, and again increases. The plot of $E_{\frac{1}{2}}$ *vs.* pH is a straight line except for acetate solutions of pH 7.4 in which the half-wave potential is more negative.

2. *Effect of concentration of nitrobenzene on the diffusion current constant*

The diffusion current constant was found to be a constant with a mean deviation of about ± 0.10 for both the first and second waves in all base solutions.

3. *A.c. and Fournier polarographic measurements*

The results obtained with a.c. polarographic measurements at various pH values in 10, 30, 50, and 70% ethanol solutions are presented in Table 2. These results indicate that the a.c. wave height is practically zero below pH 4.7. At this pH, a small peak appears. This height increases to nearly double the height when the pH is increased to 9. In strong alkaline solutions (pH >11) this height is further doubled. The summit potential is more positive than the d.c. half-wave potential in solutions

TABLE 2

A.C. POLAROGRAPHIC CHARACTERISTICS IN VARIOUS BASE SOLUTIONS

Nitrobenzene concentration, 0.98 mM; a.c. frequency, 50 Hz, a.c. measured across 100 Ω; a.c. amplitude, 30 mV; m, 1.243 mg s^{-1}; t, 4.1 s in 1 M KCl.

pH (*buffer*)	*EtOH concn./% v/v*	$-E_{\frac{1}{2}}/V$	$-E_s/V$	$-(E_{\frac{3}{4}}-E_{\frac{1}{4}})/V$	*A.c. height/μA*
1	10	0.195	—	0.060	—
(HCl)	30	0.210	—	0.060	—
	50	0.255	—	0.060	—
	70	0.290	—	0.070	—
2	10	0.255	—	0.070	—
(HCl)	30	0.280	—	0.060	—
	50	0.330	—	0.060	—
	70	0.375	—	0.070	—
4.7	10	0.395	0.450	0.060	3.0
(acetate)	30	0.460	0.480–0.540	0.060	3.0
	50	0.535	0.560–0.620	0.065	3.0
	70	0.600	0.640	0.060	4.0
7.4	10	0.680	0.690	0.075	13.0
(acetate)	30	0.750	0.740	0.085	16.0
	50	0.795	0.770	0.090	13.0
	70	0.830	0.795	0.090	16.0
9.0	10	0.640	0.670	0.060	7.0
(ammonia)	30	0.680	0.700	0.060	6.0
	50	0.720	0.720	0.060	8.0
	70	0.750	0.760–0.790	0.055	7.0
11.3	10	0.715	0.705	0.065	20.0
(0.01 M NaOH)	30	0.765	0.735	0.070	18.0
	50	0.800	0.770	0.070	15.0
	70	0.845	0.805	0.080	16.5
(13)	10	0.735	0.705	0.080	19.0
(0.1 M NaOH)	30	0.780	0.745	0.080	17.0
	50	0.810	0.770	0.085	17.0
	70	0.837	0.805	0.080	16.0

containing 0.1 M NaOH, 0.01 M NaOH and 0.1 M sodium acetate. In ammonia and acetate buffer, the summit potentials are more negative. It is interesting that in the former set of solutions, the d.c. waves are extended while in the latter set of solutions the d.c. waves are steeper.

The effect of the concentration of nitrobenzene on the a.c. peak height is given in Table 3. The a.c. height continues to increase with concentration even at 9.29 mM nitrobenzene in a medium of pH 4.7 but tends to flatten out even at a concentration of about 4 mM in alkaline solution.

The Fournier polarogram is slightly shifted with respect to the d.c. polarogram towards more positive potentials. The a.c. voltage superposed is 30 mV and the size

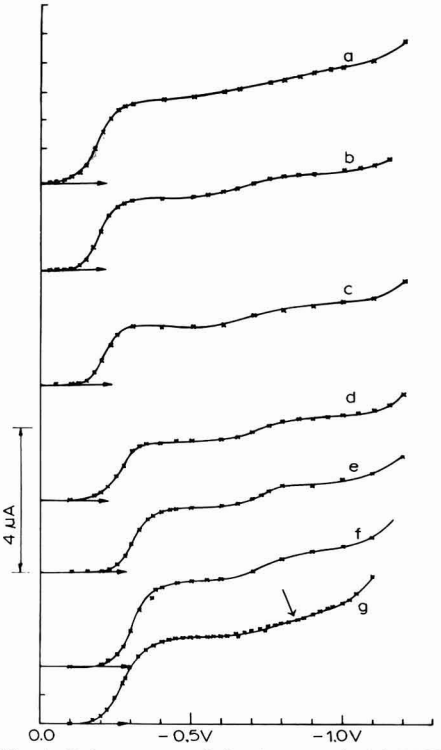

Fig. 1. Polarograms of nitrobenzene in 0.1 *M* HCl at different concns. of ethanol: (a) 0, (b) 10, (c) 30, (d) 50, (e) 70, (f) 90, (g) 99%.

TABLE 3

EFFECT OF CONCENTRATION OF NITROBENZENE ON THE A.C. WAVE CHARACTERISTICS IN 50% EtOH

pH	*$PhNO_2$ concn./mM*	*E_s/V*	*Wave height/μA*
2	0.98	No clear wave	—
0.01 *M* HCl	4.95	No clear wave	—
4.7	0.98	−0.590	3
Acetate buffer	1.24	−0.590	4
	2.48	−0.580	20
	6.19	−0.590	26
	9.29	−0.600	34
9	0.98	−0.740	8
Ammonia buffer	2.48	−0.760	23
	3.71	−0.760	32
	4.95	−0.760	32
0.01 *M* NaOH	0.12	−0.770	3
	0.98	−0.770	15
	1.24	−0.770	17
	2.48	−0.780	31
	3.71	−0.770	42
	4.95	−0.780	46

of the Fournier shift is quite small, but this clearly indicates the irreversibility of the process.

4. *Coulometric reduction of nitrobenzene*

Coulometric analysis of nitrobenzene was carried out at various pH values in the presence of different concentrations of ethanol. Polarograms were taken at intermediate stages in the reduction. Some typical polarograms in 50% ethanol are presented in Figs. 2, 3, 4 and 5. The number of electrons taking part in the reduction under different conditions are presented in Table 4.

It can be seen that the values in sodium acetate and sodium hydroxide solutions are non-integral and time-dependent. In these cases, the reduction current does not get reduced to zero at the end of the reduction, indicating the non-applicability of the coulometric procedure. Similar cases have been noticed by Elving[17] in the reduction of purines.

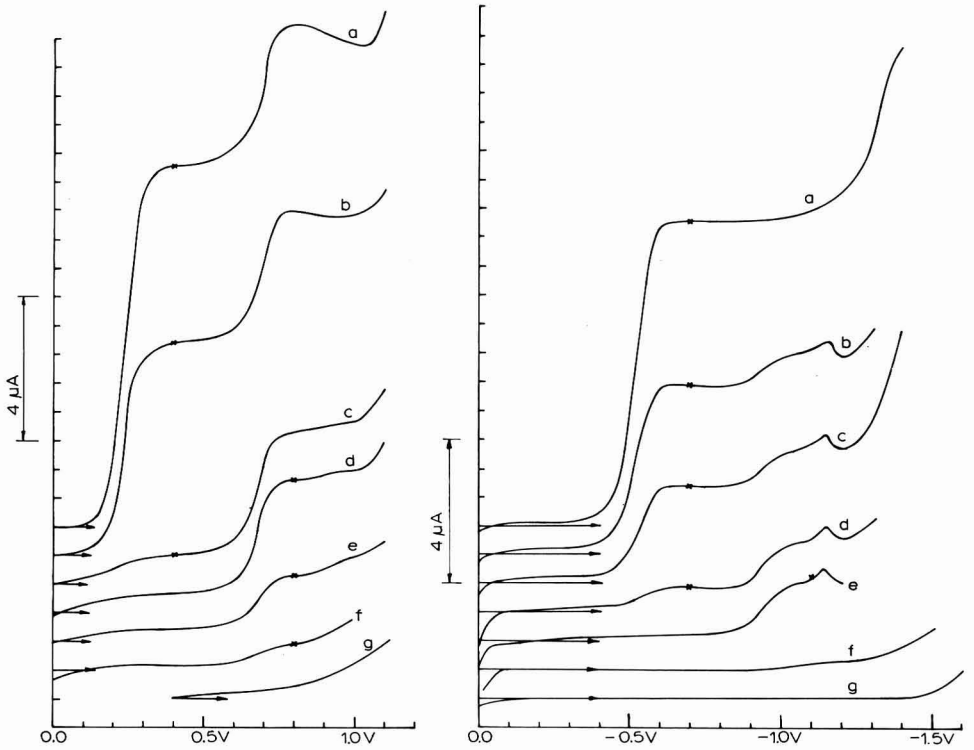

Fig. 2. Polarograms of nitrobenzene in 0.1 *M* HCl containing 50% ethanol at different stages in reduction. The arrow indicates the zero current for the corresponding polarogram. (a) polarogram of unreduced nitrobenzene soln., (b, c, d) polarograms of nitrobenzene after reduction to different extents at −0.4 V, (e, f, g) polarograms of nitrobenzene after further reduction at −0.8 V to different extents.

Fig. 3. Polarogram of nitrobenzene in acetate buffer (pH 4.7) containing 50% ethanol at different stages in reduction. The arrow indicates the zero current for the corresponding polarogram. (a) polarogram of unreduced nitrobenzene soln., (b, c, d, e) polarograms of nitrobenzene solns. after reduction to different extents at −0.7 V, (f) polarogram after further reduction at −1.1 V, (g) polarogram of the base soln.

TABLE 4

n-VALUE OBTAINED IN THE COULOMETRIC STUDY OF ETHANOLIC NITROBENZENE SOLUTIONS

EtOH concn./% v/v	*Buffer used*	*Pot. of redn. I/V*	n_1	*Pot. of redn. II/V*	n_2
10	0.1 *M* HCl	−0.4	4.10	−0.9	1.80
30	0.1 *M* HCl	−0.4	4.15	−0.9	2.18
50	0.1 *M* HCl	−0.4	4.03	−0.9	2.28
70	0.1 *M* HCl	−0.4	4.05	−0.9	2.70
10	0.01 *M* HCl	−0.4	4.14	−0.9	1.78
30	0.01 *M* HCl	−0.4	3.91	−0.9	2.18
50	0.01 *M* HCl	−0.4	3.91	−0.9	2.12
70	0.01 *M* HCl	−0.4	4.18	−0.9	2.33
10	0.1 *M* NaAc+0.1 *M* HAc	−0.5	3.80	−1.0	1.93
10	0.1 *M* NaAc+0.1 *M* HAc	−1.0	6.07	—	—
30	0.1 *M* NaAc+0.1 *M* HAc	−0.6	3.89	−1.15	1.62
50	0.1 *M* NaAc+0.1 *M* HAc	−0.7	3.95	−1.1	2.05
70	0.1 *M* NaAc+0.1 *M* HAc	−0.7	3.96	−1.3	2.54
10	0.1 *M* NaAc	−0.7	3.95	—	—
30	0.1 *M* NaAc	−0.8	4.05	—	—
50	0.1 *M* NaAc	−1.0	5.2*	—	—
50	0.1 *M* NaAc	−0.8	>6.0*	—	—
70	0.1 *M* NaAc	−0.8	>5.5*	—	—
10	0.1 *M* AmCl+0.1 *M* AmOH	−0.8	4.09	—	—
30	0.1 *M* AmCl+0.1 *M* AmOH	−0.8	4.07	—	—
50	0.1 *M* AmCl+0.1 *M* AmOH	−0.8	4.10	—	—
50	0.1 *M* AmCl+0.1 *M* AmOH	−1.5	>7*	—	—
70	0.1 *M* AmCl+0.1 *M* AmOH	−0.8	4.15	—	—
10	0.01 *M* NaOH	−0.8	>4.3*	—	—
30	0.01 *M* NaOH	−0.8	>4.8*	—	—
50	0.01 *M* NaOH	−0.8	>6.2*	—	—
70	0.01 *M* NaOH	−0.9	>7.0*	—	—
10	0.1 *M* NaOH	−0.9	>6.0*	—	—
30	0.1 *M* NaOH	−0.9	>5.7*	—	—
50	0.1 *M* NaOH	−0.9	>4.5*	—	—
70	0.1 *M* NaOH	−0.9	>5.8*	—	—

* n value is time-dependent

5. *Diffusion coefficient measurement*

The variation of the diffusion coefficient with ethanol concentrations and pH are presented in Table 5. It is seen that, in general, the diffusion coefficient attains a minimum around 50% ethanol solutions in a given buffer. At a given ethanol concentration, the diffusion coefficient shows little variation with pH in acid solutions, but rises considerably towards the neutral region and again decreases in highly alkaline solutions. The maximum value at all ethanol concentrations is in the pH range 7–9.

DISCUSSION

1. *Ratio of the height of the first to the second polarographic waves and the coulometric reduction of nitrobenzene*

The results presented in Table 1 indicate the presence of a second wave up to

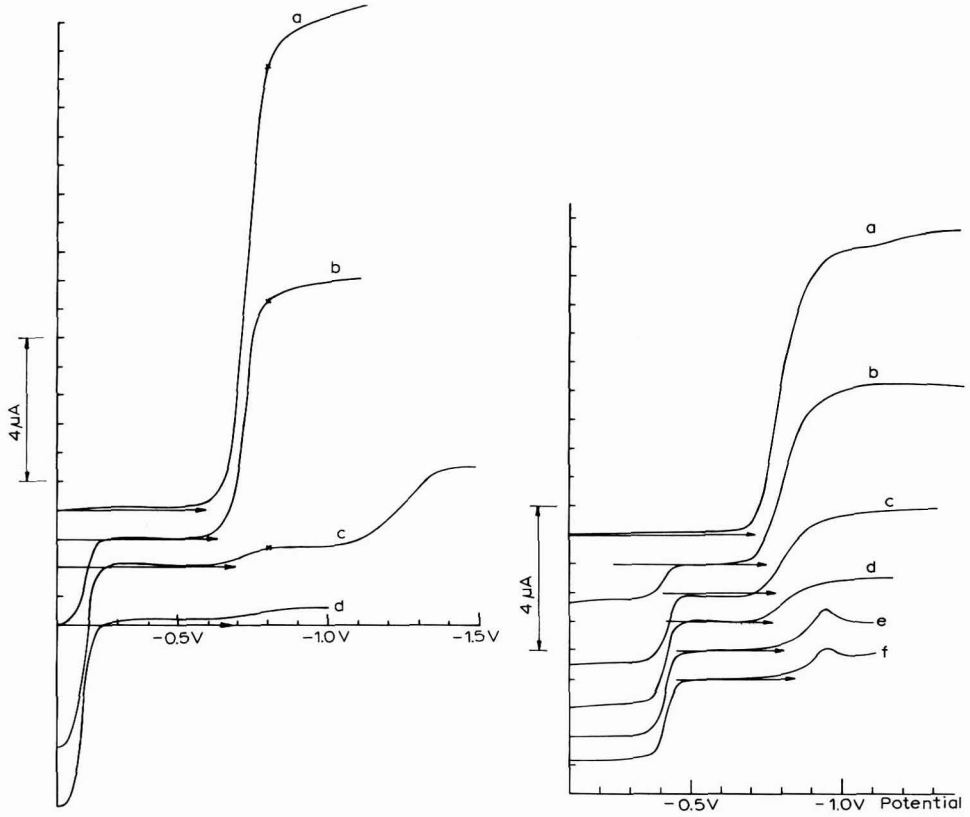

Fig. 4. Polarograms of nitrobenzene in ammonia buffer of pH 9.0 containing 50% ethanol at different stages in reduction. The arrow indicates the zero current for the corresponding polarogram. (a) Polarogram of unreduced nitrobenzene soln., (b, c, d) polarograms of nitrobenzene soln. after reduction to different extents at −0.8 V.

Fig. 5. Polarograms of nitrobenzene in 0.01 *M* NaOH soln. containing 50% ethanol at different stages in reduction. The arrow indicates the zero current of the corresponding polarogram. (a) Polarogram of of the unreduced nitrobenzene soln., (b, c, d, e, f) polarograms of nitrobenzene solution after reduction to different extents at −0.9 V.

pH 4.6 at all concentrations of ethanol, although the ratio of the height of the second wave to that of the first continually decreases with pH, being always less than 0.5. Coulometric reduction at −1.1 V gives, however, a value of 2 for the second wave even at pH 4.7, where the second wave height is negligibly small. When a solution of nitrobenzene in acetate buffer (pH, 4.7) is reduced at the early part of the diffusion current region of the first wave (−0.5 to −0.7 V), a new wave appears at more negative potentials, corresponding probably to the second wave observed at lower pH. This solution on further reduction at the diffusion region of the new wave, gives a value of 2 for *n* (Fig. 3 and Table 4).

Pearson[1] has pointed out that although β-phenylhydroxylamine is not easily reducible, its hydrochloride is more easily reduced, giving rise to the second wave. Taking the p*K* value of β-phenylhydroxylammonium ion as 3.2 (aqueous value)[18]

TABLE 5

DIFFUSION COEFFICIENT (10^6 $D/cm^2 s^{-1}$) IN DIFFERENT MEDIA

Buffer (pH)	*EtOH concn.*			
	10%	30%	50%	70%
0.1 *M* HCl (1)	8.7	6.6	5.6	5.5
0.01 *M* HCl (2)	9.3	7.0	5.4	5.4
Acetate (4.7)	8.9	6.0	5.4	5.9
Acetate (7.4)	12.4	8.9	6.8	8.8
Ammonia (9.0)	12.3	9.3	8.9	10.0
0.01 *M* NaOH (11.3)	10.6	8.4	7.8	9.2
0.1 *M* NaOH (13)	7.8	6.7	5.8	7.4

one expects a full height of the second wave in 0.1 *M* HCl solutions, since the ratio of the equilibrium concentration of β-phenylhydroxylammonium ion to the amine is 160. Although this does not hold good for solutions of pH 1, it is still valid in a qualitative way above pH 2. The smaller height of the second wave in 0.1 *M* acid solutions cannot be attributed to the partial conversion of β-phenylhydroxylamine[22] to *p*-aminophenol, since this transformation requires at least 2 *M* acid.

It appears therefore that the half-wave potential of the primary product of reduction lies beyond the final current rise. However, it gets converted to a more easily reducible form in acidic solutions, the rate of conversion depending upon pH. In coulometric reduction, the duration of reduction is quite high and the easily reducible form is regenerated rapidly and we get a value of 2 for *n*. In polarographic reduction however, the duration of reduction is confined to the lifetime of the drop, and different heights for the second wave are obtained at various pH values.

2. *Dependence of reduction on pH and ethanol concentration*

The half-wave potential of the first wave of nitrobenzene (Fig. 6) becomes more negative with increase in ethanol indicating a higher energy of reduction. At a given concentration of ethanol, the half-wave potential of the first wave increases rapidly with pH until about pH 9 and then remains practically constant (Fig. 7). This shows that in acid solutions hydrogen ions take an active role in the rate-determining process of the reduction.

3. *Values of n from the Ilkovic equation and coulometric measurement*

In the case of the first wave, the coulometric and Ilkovic values of *n* are in the neighbourhood of 4 in solutions of pH 1, 2 and 4.7. In ammonia buffer and 0.01 *M* alkali, however, the *n* values from the Ilkovic equation are far lower (*ca.* 3) than those from coulometry. It is not possible to consider the *n* values obtained in coulometric measurements in sodium hydroxide solutions as valid, since highly abnormal values for *n* are obtained (>4) (Table 4). Low values for *n* of the order of 3 cannot be identified with any known reduction product.

It appears from these results that the diffusion coefficients from the McBain–Dawson cell are not applicable to the micro-diffusion process occurring under polarographic conditions. In the present work, the value of *D* to be used in the Ilkovic equation is calculated from the coulometric value of *n* (4) in acid solutions since

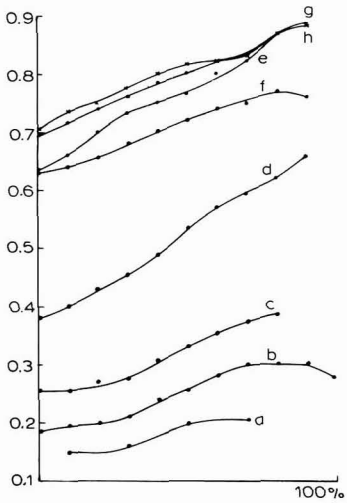

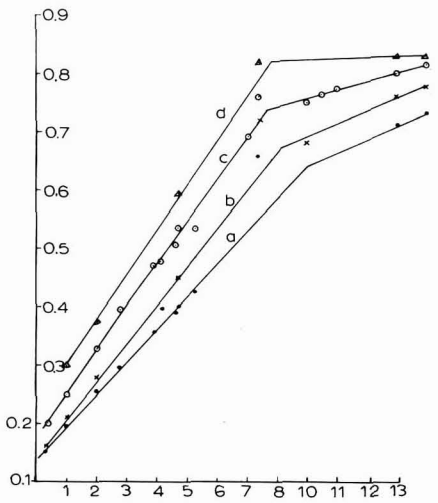

Fig. 6. Variation of $E_{\frac{1}{4}}$ with concn. of ethanol in different buffer solns. (a) 0.1 *M* HCl, (b) 0.01 *M* HCl, (c) citrate buffer (pH 2.95), (d) acetate buffer (pH 4.7), (e) sodium acetate soln. (0.1 *M*), (f) ammonia buffer (pH 9.0), (g) 0.01 *M* NaOH and (h) 0.1 *M* NaOH.

Fig. 7. Variation of $E_{\frac{1}{4}}$ with pH at a given ethanol concn.: (a) 10, (b) 30, (c) 50, (d) 70% EtOH.

coulometry gives a constant value for n at all concentrations of ethanol. The variation (4–12%) of the diffusion coefficient with pH at constant ethanol concentration does not follow any particular trend. The mean values of the diffusion coefficient between pH 1 and 9 have been used for calculating n values in sodium hydroxide solutions, and these values are given in Table 6.

4. *Nature of the electrode process corresponding to the first and second polarographic waves*

The first wave in the polarogram obtained in solutions of pH 1, 2, 4.7 and 9 is quite symmetrical, but the second wave in the acid solutions extends over a wide range of voltages (Fig. 1). In pure aqueous solutions the wave spreads out over a

TABLE 6
VALUES OF n BY DIFFERENT METHODS

EtOH concn./%	*Buffer*	I	$D^{\frac{1}{4}} \times 10^3$ *(exptl.)*	$I/D^{\frac{1}{4}}$ *(exptl.)*	*n by polarog. exptl. $D^{\frac{1}{4}}$ values*	*n coul.*	*n using average value of D*
10	0.01 *M* NaOH	6.71	3.249	2070	3.41	>4.3	4.00
30	0.01 *M* NaOH	5.83	2.901	2011	3.31	>4.7	4.03
50	0.01 *M* NaOH	5.83	2.797	2135	3.52	>6.2	4.10
70	0.01 *M* NaOH	6.27	3.040	2048	3.38	>7	4.00
10	0.1 *M* NaOH	6.71	2.793	2403	3.96	>6	4.00
30	0.1 *M* NaOH	6.13	2.586	2370	3.90	>5.7	4.23
50	0.1 *M* NaOH	5.4	2.404	2246	3.70	>4.5	3.79
70	0.1 *M* NaOH	5.97	2.711	2203	3.63	>5.8	3.81

range of 0.4 V. On the other hand, in 99% ethanol, this wave splits into two. These results can be explained on the basis of the theory developed by Delahay[19].

When a fully irreversible polarographic step is due to one rate-determining step in the electron addition process, followed by a fast step, the characteristics of the polarographic wave are determined by the slow step. When there are two rate-determining steps, the shape of the wave depends on the relative values of the rate constants of the first and the second steps. The wave flattens out as the rate of the second step decreases; when the ratio k_1/k_2 is larger than 100, a split in the wave is observed. When k_1/k_2 is very large (∞), only the portion of the wave corresponding to the first step is noticed. In these cases, the lower half of the wave is governed by the kinetics of the first step. When k_1/k_2 is less than 1, the wave has the same shape as in the case of a process governed by the kinetics of the first rate-determining step. The effect of the second step is not noticeable at all in the shape of the wave, but contributes to the current.

The single symmetrical second wave noticed in solutions containing 50–60% EtOH can be taken as due to a single rate-determining step. The flattening out of this wave, both with increase and decrease of EtOH, indicates a change in the mechanism of the electrode process. This effect is very clearly visible in 99% EtOH where the second wave splits into two waves. In these solutions, the rate constant of the first step is at least 100 times larger than that of the second step.

In sodium acetate and sodium hydroxide solutions, even the first wave is not symmetrical. In these cases, the wave is characterised by the elongated bend before the diffusion current plateau. These cannot be attributed to two species of nitrobenzene in sluggish equilibrium but are due to two consecutive rate-determining electrochemical steps.

The methods developed by Delahay[20] and Koutecký[21] *et al.* have been used to determine the number of electrons in the potential-determining step, the rate constant of this step, and the potential-dependence of α of the electrode process corresponding to the first wave. Delahay's solution of the differential equation for the diffusion of the depolariser to the stationary electrode, adopted to the growing electrode by multiplication by a factor $\sqrt{\frac{7}{3}}$, gives

$$\frac{i}{1256nm^{\frac{2}{3}}t^{\frac{2}{3}}D_o^{\frac{1}{2}}*C} = \frac{k_f}{D_o^{\frac{1}{2}}} \times \frac{1}{\tau^{\frac{2}{3}}} \int_0^{\tau} t^{\frac{2}{3}} \exp \frac{k_f^2 t}{D_o} \operatorname{erfc} \frac{k_f t^{\frac{1}{2}}}{D_o^{\frac{1}{2}}} \, dt = \frac{k_f}{D_o^{\frac{1}{2}}} \times \bar{\beta} \qquad (1)$$

For different probable values of $k_f/D_o^{\frac{1}{2}}$ and t, the value of $\bar{\beta}$ was computed using graphical evaluation of the integral in eqn. (1). $(k_f/D_o^{\frac{1}{2}})\bar{\beta}$ was calculated and plotted *vs.* $k_f/D_o^{\frac{1}{2}}$. The experimental value of the left-hand side of eqn. (1) was calculated for different points on the polarogram, and the values of $k_f/D_o^{\frac{1}{2}}$, corresponding to these values of $(k_f/D_o^{\frac{1}{2}})\bar{\beta}$, were read out from the graphs. From the values of $k_f/D_o^{\frac{1}{2}}$, the value of k_f was evaluated using the diffusion coefficient calculated from the Ilkovic equation.

Koutecký *et al.*[21] have given a general treatment of the problem of a slow electrode process for a growing electrode. For the case of spherical diffusion to a growing electrode, the following relationship holds, when the reduction process is fully irreversible.

$$i_{irr} = i_d\{\bar{F}(\chi_1) - \xi\bar{H}(\chi_1)\}$$

where $\xi = 50.4\ D^{\frac{1}{2}}m^{-\frac{1}{3}}t^{\frac{1}{6}}$

TABLE 7

RATE CONSTANTS AND TRANSFER COEFFICIENTS

pH	*EtOH*/% *v/v*	$(E_{\frac{3}{4}} - E_{\frac{1}{4}})/V$	*A.c. height*/μA	αn_a		α		$-\log k^0_{fh}$	
				Delahay	*Koutecký*	*Delahay*	*Koutecký*	*Delahay*	*Koutecký*
1	10	0.060	—	0.72	1.18	0.36	0.59	2.575	1.98
	30	0.060	—	0.83	1.07	0.42	0.54	2.810	2.22
	50	0.060	—	0.72	0.89	0.36	0.44	3.450	3.15
	70	0.070	—	0.83	0,86	0.42	0.43	4.030	3.902
2	10	0.070	—	1.14	Non-linear	0.57	Non-linear	3.280	Non-linear
	30	0.060	—	0.74	1.02	0.37	0.51	3.845	3.48
	50	0.060	—	0.82	0.82	0.41	0.41	4.420	4.17
	70	0.070	—	0.66	1.17	0.33	0.59	4.560	4.55
4.7	10	0.060	3.0	0.71	0.82	0.36	0.41	5.035	8.17
	30	0.060	3.0	0.66	0.81	0.33	0.40	5.568	8.99
	50	0.065	3.0	0.62	0.76	0.31	0.38	6.250	9.67
	70	0.060	4.0	0.78	0.88	0.39	0.44	7.617	11.49
9.0	10	0.060	7.0	0.60	0.78	0.30	0.39	7.126	10.98
	30	0.060	6.0	0.66	0.98	0.33	0.49	7.974	13.71
	50	0.060	8.0	0.84	0.88	0.42	0.44	9.833	13.26
	70	0.055	7.0	0.59	0.90	0.30	0.45	8.168	13.80

$$\chi_1 = \left(\frac{12t_1}{7D}\right)^{\frac{1}{2}} k_f$$

The values of the functions $\bar{F}(\chi_1)$ and $\bar{H}(\chi_1)$ have been tabulated for various values of χ_1. Theoretical plots of $\bar{F}(\chi_1) - \xi\bar{H}(\chi_1)$ *vs.* χ_1 have been made on the basis of tables given by Koutecký and coworkers. The values of χ_1 corresponding to the values of i/i_d at various potentials along the polarographic wave are read out from the theoretical plots. From the values of χ_1, k_f is calculated from the relationship given above.

The plots of log k_f *vs.* E were drawn for the polarograms at various pH-values and different concentrations of ethanol. (Figs. 8 and 9). In general, the qualitative nature of the plots obtained by both methods is practically the same. The plots are practically linear except Koutecký's plots for 10% ethanol solutions in hydrochloric acid and ammoniacal solutions. In a few cases there is a little curving off when $i > 0.8\, i_d$. It has been concluded, therefore, that there is only one rate-determining step in the electrode reaction. The value of αn_a for the polarograms obtained under various conditions are included in Table 7. The values of $E_{\frac{3}{4}} - E_{\frac{1}{4}}$ for these polarograms are in the neighbourhood of 0.060 V. Since no a.c. wave height is obtained in acid solutions and those obtained in solutions of acetate and ammonia buffer are not

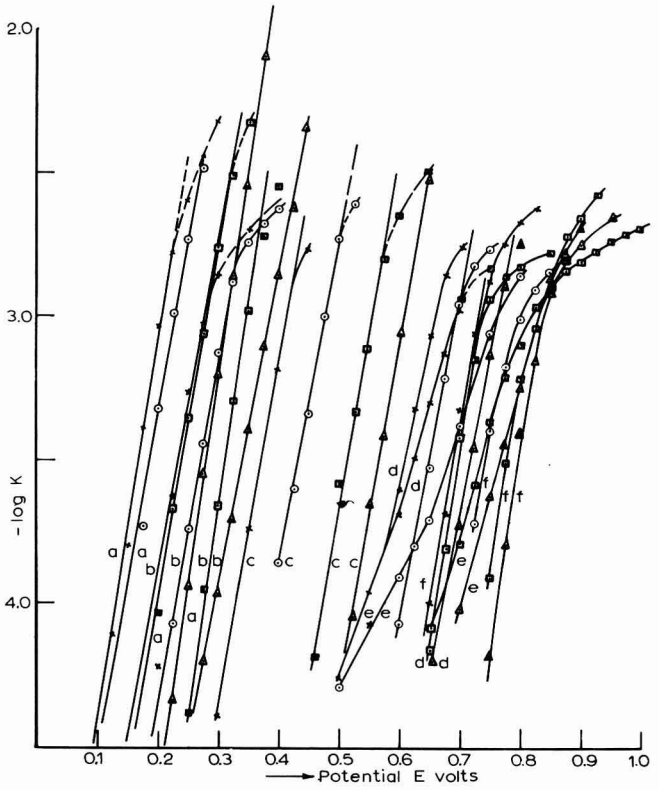

Fig. 8. $-\log k$ (or pK) *vs.* E plots (Delahay method) of nitrobenzene in aq. ethanol solns. of different pH. (a) 0.1 *M* HCl, (b) 0.01 *M* HCl, (c) pH 4.7, (d) pH 9, (e) 0.1 *M* NaAc, (f) 0.1 *M* NaOH. (×) 10; (⊙) 30; (■) 50; (▲) 70% ethanol.

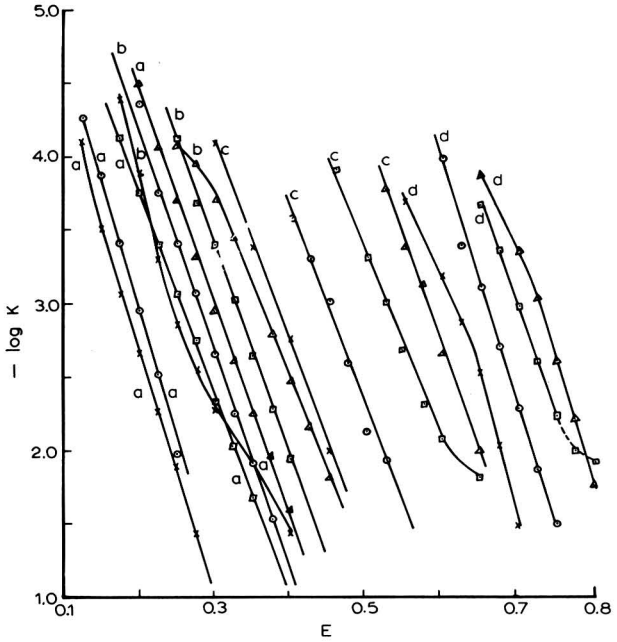

Fig. 9. – Log k *vs.* E plots (Koutecký method) of nitrobenzene in aq. ethanol solns. of different pH. (a) 0.1 *M* HCl, (b) 0.01 *M* HCl, (c) acetate buffer pH 4.7, (d) ammonia buffer pH 9. (×) 10, (⊙) 30, (■) 50, (▲) 70% ethanol.

as high as could be expected in reversible processes, it can be concluded that no step in the electrode process is reversible. Since the possibility of a one-electron rate-determining step is excluded by the value of $E_{\frac{3}{4}} - E_{\frac{1}{4}}$ of 0.060 V, it is reasonable to conclude that the rate-determining step involves the addition of 2 electrons.

On this basis the value of α has been calculated and given in the same Table. The values of α calculated by the two methods do not agree exactly. Based on the relative values of α in any one set of calculations, it can be concluded that α depends upon the nature of the process. The slight curvature of the log k_f *vs.* E plots noticed in some cases is probably due to the potential-dependence of α[19].

In sodium acetate and sodium hydroxide solutions, the plots of log k_f *vs.* E are non-linear, indicating more than one rate-determining step.

The values of $-\log k^0_{fh}$ have also been included in the same Table. It has not been possible to give the value of k_{sh}, since the standard potential of the system, nitrobenzene–β-phenylhydroxylamine is not known.

Although nitrosobenzene–phenylhydroxylamine forms a reversible couple and nitrosobenzene appears to be an intermediate, no a.c. wave can be expected either in acid or in alkaline medium because the potential of nitrobenzene reduction is in the diffusion current region of nitrosobenzene. The appearance of an a.c. wave in ammonia solutions and its non-appearance in acid solutions can only be explained by assuming the following mechanism,

$PhNO_2H_2^{2+} + 2e \rightarrow PhNO_2H_2$ in acid medium

$PhNO_2 + 2e \rightarrow PhNO_2^{2-}$ in ammonia solution

since protonated nitrobenzene is expected to be present in acid solutions. The movement of the charged $PhNO_2^{2-}$ at the electrode surface may be responsible for the a.c. wave.

The a.c. wave also appears in sodium hydroxide solutions. Examination of the Delahay plots indicates the existence of more than one rate-determining step. It is quite likely that $PhNO_2^-$ is formed, the movement of which at the electrode surface gives rise to the a.c. wave.

On the basis of polarization curves taken in acid solutions, Fleischmann *et al.*[11] postulate that the reduction of nitrobenzene to phenylhydroxylamine occurs by way of an initial irreversible one-electron step. Kastening[8] electrolyzed nitrobenzene at a rapid rate (half-time of reduction < 1 min) and examined the product spectroscopically. He has shown that $C_6H_5NO_2^-$ is formed by the primary one-electron reduction of nitrobenzene. The formation of the same anion radical is shown by ESR methods by Koopmann and Gerischer[9] who studied the electrochemical reduction of nitrobenzene at a gold amalgam electrode in weakly alkaline solutions. The same anion radical has been reported in non-aqueous solutions by other workers[10]. The results obtained by these investigations lend support to the postulation made in this paper regarding the formation of the charged nitrobenzene species on the basis of the a.c. polarographic experiment. The formation of a yellow-coloured product attributed to the charged anion of nitrobenzene in alkaline solutions by Kastening[8] and Koopmann and Gerischer[9] has also been observed by the present authors in alkaline dioxane solutions. As indicated by Kastening, the lifetime of the anion radical appears to be greatest in alkaline solutions.

SUMMARY

A detailed polarographic (a.c. and d.c.) and coulometric investigation of nitrobenzene has been made at various pH values in the presence of different concentrations of ethanol. Below pH 4.7, two waves are apparent but above this pH, the second wave does not appear. Coulometric evidence indicates that the first and second waves correspond to the four- and two-electron processes, respectively. The coulometric method was not applicable in sodium hydroxide and sodium acetate solutions. When the diffusion coefficients (from the diaphragm cell) are used in the Ilkovic equation, no reliable conclusions can be reached for the number of electrons involved in the reduction process in alkaline solutions. The a.c. polarographic method gives evidence for the formation of species such as: $C_6H_5NO_2H_2^{2+}$, $C_6H_5NO_2^-$ and $C_6H_5NO_2^{2-}$. Analysis of d.c. polarographic data by Delahay's treatment of irreversible waves, indicates that the number of electrons involved in the rate-determining step is 2. In sodium hydroxide solutions, however, the first main wave is split indicating more than one rate-determining step.

The results presented in this paper indicate that the first wave in the reduction of nitrobenzene is a four-electron process at all pH values. The second wave, which appears below pH 4.7, corresponds to a two-electron process irrespective of wave heights. The difference in the a.c. polarographic behaviour in acid and alkaline solutions has given evidence for the formation of species like $C_6H_5NO_2H_2$, $C_6H_5NO_2^-$, and $C_6H_5NO_2^{2-}$.

ACKNOWLEDGEMENT

The authors wish to thank Professor M. R. A. Rao for helpful discussions.

REFERENCES

1 J. PEARSON, *Trans. Faraday Soc.*, 44 (1948) 683.
2 I. A. KORSHUNOV AND A. S. KIRILLOVA, *J. Gen. Chem., USSR, Eng. Transl.*, 18 (1948) 785.
3 J. E. PAGE, J. W. SMITH AND J. G. WALLER, *J. Phys. Colloid Chem.*, 53 (1949) 545.
4 M. FIELDS, C. VALLE, JR. AND M. KANE, *J. Am. Chem. Soc.*, 71 (1949) 421.
5 M. SUZUKI, *J. Electrochem. Soc. (Japan)*, 22 (1954) 112.
6 I. BERGMANN AND J. C. JAMES, *Trans. Faraday Soc.*, 48 (1952) 956.
7 PAUL KARRER, *Organic Chemistry*, Elsevier, Amsterdam, 1938, p. 412.
8 B. KASTENING, *Electrochim. Acta*, 9 (1964) 241.
9 R. KOOPMANN AND H. GERISCHER, *Ber. Bunsenges*, 70 (1966) 127.
10 D. H. GESKE AND A. H. MAKI, *J. Am. Chem. Soc.*, 82 (1960) 2671; A. H. MAKI AND D. H. GESKE, *ibid.*, 83 (1961) 1852; W. KEMULA AND R. SIODA, *Bull. Acad. Polon. Sci. Ser. Sci. Chim.*, 10 (1962) 507, 513; T. FUGINAGA, Y. DEGUCHI AND K. UMEMOTO, *Bull. Chem. Soc. Japan*, 37 (1964) 822.
11 M. FLEISCHMANN, I. N. PETROV AND W. F. K. WYNE-JONES, *Proc. First Australian Conference on Electrochemistry*, 1963, p. 500.
12 R. S. SUBRAHMANYA, *Proc. Indian Acad. Sci.*, 42A, (1955) 267.
13 C. S. RAMANATHAN AND R. S. SUBRAHMANYA, *Proc. Indian Acad. Sci.*, 47A, (1958) 379.
14 B. BREYER AND F. GUTMANN, *Trans. Faraday Soc.*, 42 (1946) 650.
15 J. J. LINGANE, *Ind. Eng. Chem. Anal. Ed.*, 17 (1945) 332.
16 J. J. LINGANE, *J. Am. Chem. Soc.*, 67 (1945) 1916.
17 D. L. SMITH AND P. J. ELVING, *J. Am. Chem. Soc.*, 84 (1962) 1412.
18 I. BERGMANN AND J. C. JAMES, *Trans. Faraday Soc.*, 50 (1954) 65.
19 T. BERZINS AND P. DELAHAY, *J. Am. Chem. Soc.*, 75 (1953) 5716.
20 P. DELAHAY, *J. Am. Chem. Soc.*, 75 (1953) 1430.
21 J. KOUTECKÝ, *Collection Czech. Chem. Commun.*, 18 (1953) 597; J. WEBER AND J. KOUTECKÝ, *ibid.*, 20 (1955) 980; J. KOUTECKÝ AND J. CIZEK, *ibid.*, 21 (1956) 836.
22 S. WAWZONEK, *Anal. Chem.*, 21 (1949) 63.

ELECTROANALYTICAL CHEMISTRY AND INTERFACIAL ELECTROCHEMISTRY
Elsevier Sequoia S.A., Lausanne – Printed in The Netherlands

THE ELECTRICAL CONDUCTIVITY OF URANYL ACETATE IN WATER AND WATER–DIOXANE MIXTURES

E. M. KHAIRY, AFAF EL-SAID MAHGOUB AND A. I. MOSAAD
Chemistry Department, Faculty of Science, Cairo University (U.A.R.)
(Received November 19th, 1968; in revised form, March 16th, 1969)

INTRODUCTION

The conductance of uranyl salts in aqueous, non-aqueous, and in mixed solvents has been investigated at several temperatures and various concentrations[1-9]. The conductance of uranyl fluoride in aqueous solutions was first studied by Dean[1] at 25°C at concentrations ≥ 0.125 *N*. Brown *et al.*[2] extended the study to lower concentrations within the temperature range 0–90°C. They indicated that uranyl fluoride behaved as a very weak 1:1 electrolyte, and obtained values for the dissociation constant of $4.63–4.85 \times 10^{-5}$ in the concentration range $1 \times 10^{-4}–1 \times 10^{-2}$ *N*, assuming the dissociation reaction to be:

$$UO_2F_2 \rightleftharpoons UO_2F^+ + F^- \quad (1)$$

Johnson *et al.*[3] assumed that F^- ions could not occur in significant concentration, but would preferentially undergo the reaction:

$$2\,UO_2F_2 + H_2O \rightleftharpoons UO_2OHF + H^+ + UO_2F_3^- \quad (2)$$

This accounts for the acidity of the solution as well as the extremely low conductance values observed.

Conductance measurements of uranyl chloride in the concentration range $5 \times 10^{-3}–2 \times 10^{-4}$ *N* at different temperatures were carried out by Goldenberg and Amis[4] in pure water, and in water–ethanol mixtures. Assuming that the principal ionization of uranyl chloride is similar to that proposed by Secoy, *et al.* for uranyl fluoride, an average value of 5.0×10^{-2} for the dissociation constant was obtained, indicating a weak electrolyte. The corresponding value for uranyl sulphate over the concentration range $5 \times 10^{-5}–5 \times 10^{-3}$ *M* was found[5] to be $\sim 5.9 \times 10^{-4}$.

The hydrolysis of the uranyl ion in solutions of its various salts has also been extensively investigated[9-14]. Singh and Ahmad[9] reported from pH-measurements that the hydrolysis of uranyl nitrate, sulphate and acetate at a mole dilution of 1280 was 17.54, 8.50, and 2.13%, respectively. Longsworth and MacInnes[10] suggested various hydrolytic equilibria with respect to uranyl chloride, nitrate, sulphate and acetate, in fair agreement with experimental results. The conclusions were based, within a moderate concentration range, on the single hydrolytic reaction:

$$2\,UO_2^{2+} + H_2O \rightleftharpoons U_2O_5^{2+} + 2\,H^+ \quad (3)$$

From a study of the variation of absorption of uranyl perchlorate with pH, Sutton[12,14] observed a strong increase in absorption throughout the spectrum at pH values $\geqq 2.5$. This was attributed to stepwise hydrolysis, involving the initial formation of the $U_2O_5^{2+}$ and $U_3O_8^{2+}$ polyuranyl complexes; this was also confirmed by cryoscopic measurements. At pH $\leqslant 2$ hydrolysis did not take place; between pH 2.5 and 3, $(U_2O_5^{2+})_{aq}$ predominated, whereas $(U_3O_8^{2+})_{aq}$ was presumably formed at pH $\geqq 3$. Sutton assumed that further hydrolysis of $U_3O_8^{2+}$ would lead ultimately to the formation of different hydroxy compounds, probably $[U_3O_8(OH)]^+$, $U_3O_8(OH)_2$, $[U_3O_8(OH)_3]^-$ or $[U_3O_8(OH)_4]^{2-}$. This scheme was further supported by Raman spectra measurements carried out by Sutton[12], as well as by isotopic ^{18}O exchange made by Crandall[13].

The present work is designed chiefly to obtain further information regarding the conductance of uranyl acetate in water and water–dioxane mixtures, and the influence of solvent composition and dielectric constant on the dissociation mechanism.

EXPERIMENTAL

The conductance of solutions of AnalaR anhydrous uranyl acetate (Riedel–de Haën A.-G. Seelze bei Hannover, West Germany) in water and in water–dioxane mixtures was determined over the concentration range ~ 0.05–5×10^{-5} *M* (*cf.* Table 1). The dioxane used in this investigation was purified and dried according to recommended methods[15].

The dielectric constant of each solvent was measured using a multi-dekameter type DK 06 (Wissenschaftlich Technische Werkstätten GmbH. Weilheim Oberbayern). The density and viscosity of the different solvents also have been determined at 25°C (*cf.* Table 1).

The pH values of the different solutions investigated were measured using a pH-meter (Lseibold type GLD, Wien) with an accuracy of ± 0.05 pH unit (*cf.* Tables 2 and 3).

The experimental procedure was essentially the same as described in a previous publication[16]. The conductance measurements were carried out in solutions prepared by the usual dilution method in a closed cell immersed in an oil thermostat adjusted at $25^\circ \pm 0.02^\circ$C. Measured volumes of conductivity water, specific conductance $\sim 2 \times 10^{-6}\ \Omega^{-1}\ cm^{-1}$, or of the appropriate water–dioxane mixture (specific conductance, *cf.* Table 1) were added to the stock solution of known concentration in an atmosphere of purified nitrogen. Before each addition the solvent conductance was determined, and in every case was subtracted from the measured conductance of the solution.

The solution resistance was measured using an a.c. conductivity bridge of high precision (Leeds and Northrup Co., Philadelphia, U.S.A.) with an accuracy of better than $\pm 0.02\%$. A frequency of 1000 cycles/s was used throughout the measurements. A sensitive oscillograph (Hartmann and Braun AG, Frankfurt/Main) was used as a null detector.

Spectrophotometric measurements of uranyl acetate in pure water, pure dioxane and water–dioxane mixtures were made in the visible range, at room temperature, using a Beckmann D.K. recording spectrophotometer.

TABLE 1

MOLAR CONDUCTANCE OF URANYL ACETATE IN WATER AND WATER–DIOXANE MIXTURES AT 25°C

$C \times 10^2$/ mol l^{-1}	$\varkappa \times 10^4$/ Ω^{-1} cm^{-1}	Λ/ Ω^{-1} cm^2 mol^{-1}	$C \times 10^2$/ mol l^{-1}	$\varkappa \times 10^4$/ Ω^{-1} cm^{-1}	Λ/ Ω^{-1} cm^2 mol^{-1}
$D=80.4$	$\eta=0.00895$	$\varkappa_s=2.01\times10^{-6}$	$D=30$	$\eta=0.01946$	$\varkappa_s=3.25\times10^{-6}$
5.00	8.410	16.82	5.00	1.405	2.81
2.50	5.036	20.14	2.50	0.5885	2.35
1.25	3.466	27.72	1.25	0.2953	2.36
0.625	2.262	36.18	0.625	0.1675	2.68
0.3125	1.438	46.02	0.3125	0.0990	3.17
0.1563	0.909	58.14	0.1563	0.0629	4.03
0.0780	0.521	66.73	0.0780	0.0378	4.84
0.0390	0.320	82.05	0.0390	0.0216	5.55
0.0195	0.183	93.74	0.0195	0.0129	6.61
0.00975	0.109	111.79			
$D=57.7$	$\eta=0.01420$	$\varkappa_s=3.4=10^{-6}$	$D=20$	$\eta=0.01935$	$\varkappa_s=0.68\times10^{-6}$
2.50	1.816	7.26	2.50	0.3773	1.509
1.25	0.914	7.31	1.25	0.1848	1.478
0.625	0.555	8.88	0.625	0.0919	1.470
0.3125	0.340	10.88	0.3125	0.0474	1.515
0.1563	0.2177	13.96	0.1563	0.0255	1.630
0.0780	0.1277	16.47	0.0780	0.0139	1.783
0.0390	0.0744	18.97	0.0390	0.0075	1.910
0.0195	0.0386	19.82	0.0195	0.00412	2.113
0.00975	0.0200	20.51	0.00975	0.00256	2.629
			0.00488	0.00169	3.458
			0.00244	0.00149	6.101

$C \times 10^2$	$*\varkappa \times 10^4$	$\times 10^4$	Λ
$D=10$	$\eta=0.01621$	$\varkappa_s=0.202\times10^{-6}$	
1.25	0.03041	0.02839	0.2271
0.625	0.01369	0.01157	0.1713
0.3125	0.00659	0.00457	0.1462
0.1563	0.00367	0.001645	0.1054
0.0780	0.00223	0.000206	0.0264
0.0390	0.00180		
0.0195	0.00160		
0.00975	0.00140		

* Specific conductance without solvent correction.

C = molar concn., Λ = molar conductance, $\varkappa$ = specific conductance, $\varkappa_s$ = specific conductance of the pure solvent, D = dielectric constant of the medium, and η = viscosity of the solvent.

Stability of uranyl acetate solutions

Aqueous solutions of uranyl acetate are invariably stable with time. In contrast a yellowish turbidity has been observed in water–dioxane solutions, particularly in the higher concentrations of dioxane and increasing in sunlight,indicating the formation of a hydrolysis product sparingly soluble in the organic solvent. Conductance measurements have therefore been made with freshly prepared solutions in the absence of sunlight.

TABLE 2

CORRECTED CONDUCTANCE OF URANYL ACETATE IN WATER AT 25°C AND VARIATION OF SOLUTION pH

$C \times 10^3$	*pH*	Λ *measured*	Λ' *(corrected for* H^+*)*
12.50	4.40	27.72	26.59
6.25	4.49	36.18	34.36
3.12	4.57	46.02	43.00
1.56	4.64	57.00	51.81
0.78	4.70	66.50	57.44
0.484	4.76	76.00	63.29
0.390	4.78	82.05	66.98
0.195	4.87	96.00	71.98
0.098	5.03	111.79	78.30

TABLE 3

pH OF URANYL ACETATE IN WATER AND WATER–DIOXANE MIXTURES* AT 25°C

Wt.% *dioxane*	0%		25%		58%		70%		82%	
C/mol l^{-1}	0.025	0.001	0.025	0.001	0.025	0.001	0.025	0.001	0.025	0.001
pH	4.30	4.75	4.65	4.95	5.05	6.00	5.12	6.40	5.44	5.78

* pH of water or water–dioxane mixture $\cong 6.7$.

RESULTS AND DISCUSSION

Solvent conductance

The conductivity of pure water used was found experimentally to be $\sim 2.0 \times 10^{-6}$ Ω^{-1} cm^{-1}. Pure dioxane has a very low electrical conductivity (5×10^{-15} $\Omega^{-1} cm^{-1}$ [17]) and therefore the gradual addition of dioxane to water would be expected to lead to a progressive decrease in conductance. However, it was found experimentally that the addition of dioxane to water (up to 25% dioxane, $D = 57.7$) led to a sharp increase of conductance. Between 25% and 58% dioxane a gradual decrease occurred. With further increase of dioxane concentration there was a rapid decrease of conductance. The former behaviour may be due to hydrogen bond formation between the lone pairs of electrons on the oxygen atoms of the dioxane and the hydrogen atoms of the undissociated water molecules, leading to increased conductance.

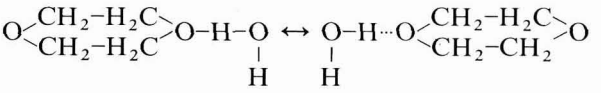

The subsequent decrease is normal and could be explained by the gradual replacement of water by dioxane having less conducting power.

Hydrolysis mechanism

pH-measurements (Table 3) of the uranyl acetate solutions in water and water–

dioxane mixtures show that the salt undergoes hydrolysis depending on its concentration and the solvent constitution. The pH drop (pH ~6.7 to pH 4.5) is considerable in water and in mixed solvents having high water content. This indicates that uranyl acetate hydrolyses yielding polyuranyl complexes, with liberation of H^+-ions and increase of acidity. This may proceed in the same way as described by Sutton[14] for uranyl perchlorate. The higher pH-value in solvents of low water content indicates that hydrolysis is less marked. It is also clear that the drop in pH-value due to hydrolysis is greater (in the same solvent medium) the higher the concentration of the salt solution.

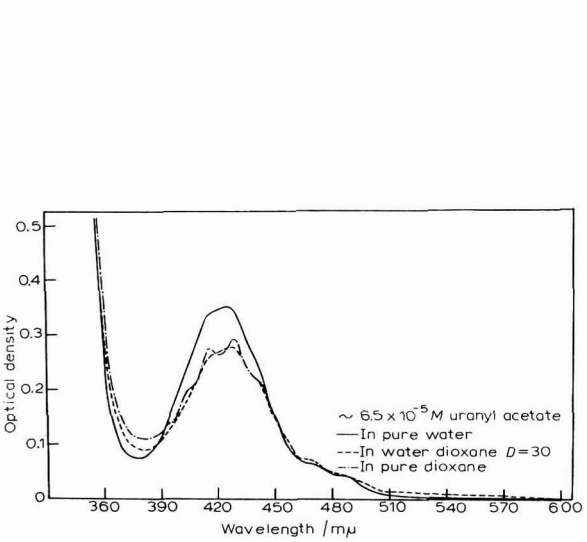

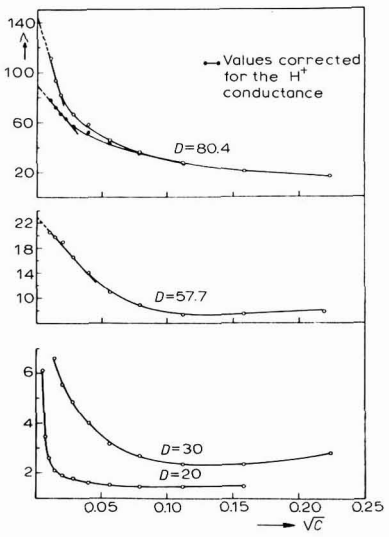

Fig. 1. Representative absorption curves of uranyl acetate in water and water–dioxane mixtures.

Fig. 2. Λ *vs.* $\sqrt{C}$ curves for uranyl acetate at 25°C.

In all solvents the pH is above 3, where the triuranyl complex $(U_3O_8^{2+})_{aq}$ is the more probable hydrolysis product[14] (this is further substantiated by spectrophotometric measurements). The absorption curves (Fig. 1) of uranyl acetate solutions obtained in different media at a concentration of $\sim 6.5 \times 10^{-3}$ M, show two well-defined peaks at wave lengths ~429 and 416 nm. The shape of the curves as well as the positions of the peaks are comparable with those corresponding to the $(U_3O_8^{2+})_{aq}$ species. The following simple dissociation and hydrolysis pattern may be assumed:

$$\begin{aligned} UO_2(AcO)_2 &\rightleftharpoons UO_2AcO^+ + AcO^- \\ &\rightleftharpoons UO_2^{2+} + AcO^- \\ 2\,UO_2^{2+} + H_2O &\rightleftharpoons U_2O_5^{2+} + 2\,H^+ \\ U_2O_5^{2+} + UO_2^{2+} + H_2O &\rightleftharpoons U_3O_8^{2+} + 2\,H^+ \\ AcO^- + H^+ &\rightleftharpoons AcOH \end{aligned} \qquad (4)$$

Estimation of Λ_0, K_1 and K_3 from conductance data

A plot of the molar conductance Λ *vs.* $\sqrt{C}$ is given in Fig. 2 for solvents of

different dielectric constant. These relations are straight lines at the concentration ranges $\sim 8\times10^{-4}$–1×10^{-4} M in water and $\sim 1.5\times10^{-3}$–1×10^{-4} M in the water–dioxane mixture of $D=57.7$. The limiting conductance Λ_0 in both solvents can be obtained, to a first approximation, by extrapolation of the experimental results to zero concentration. For other solvents of lower dielectric constant, $D=30$ and 20, the plot of Λ *vs.* $\sqrt{C}$ approaches the conductance axis asymptotically and only a rough estimate of Λ_0 by extrapolation is possible. Walden's rule ($\Lambda_0\eta_0\approx$constant) is used in some cases as an empirical approach.

Assuming that uranyl acetate behaves under the prevailing conditions as a weak electrolyte, the measured conductance values, Λ, can be analysed according to theoretical concepts (chiefly those of Fuoss and Kraus[18-21] or/and Shedlovsky[22]). If the views advocated by Secoy *et al.*[2] and Goldenberg and Amis[4] that both uranyl fluoride and chloride behave as 1 : 1 electrolytes are adopted, the principal ionization of uranyl acetate in aqueous and mixed solvents may be represented by:

$$UO_2(AcO)_2 \rightleftharpoons UO_2AcO^+ + AcO^- \tag{5}$$

The approximate extrapolated Λ_0-values are used to calculate the dissociation constant $K_1=[UO_2AcO^+][AcO^-]/[UO_2(AcO)_2]$, from Ostwald's relation:

$$K_1 = \frac{\alpha^2 C}{1-\alpha} \quad \text{with} \quad \alpha = \frac{\Lambda}{\Lambda_0} \tag{6}$$

The approximate K_1-values obtained by this method are almost constant over the concentration ranges shown in Table 4, at different dielectric constants of the solvents. This confirms the validity of the above assumption.

TABLE 4

APPROXIMATE K_1-VALUES ACCORDING TO EQN. (2) AND RANGES OF ITS STABILITY

D	$^*\Lambda_0$	K_1/mol l^{-1}	Concn. range
80.4	146	$\sim 0.5\times10^{-3}$	2.5×10^{-3}–3.2×10^{-2}
	†90	$\sim {}^\dagger 1.6\times10^{-3}$	
57.7	23	$\sim 1.4+10^{-3}$	4.0×10^{-4}–8.0×10^{-3}
30	8	$\sim 0.7\times10^{-3}$	1.7×10^{-4}–2.5×10^{-3}
20	10	$\sim 1.0\times10^{-5}$	2.5×10^{-5}–4.0×10^{-4}

* Exptl. limiting molar conductance.

† Values corrected for the H^+-ion conductance.

As a result of hydrolysis of the uranyl salt in water, UO_2^{2+} ions may eventually be replaced by other ionic species such as $U_2O_5^{2+}$ or/and $U_3O_8^{2+}$ with subsequent release of H^+, or protonated solvent molecules. This affects the conductance and requires correction[23]. This correction, $\Delta\Lambda$, is related to the corresponding correction in specific conductance, $\Delta\varkappa$, by the following:

$$1000\,\Delta\varkappa = C_{H^+}\cdot\lambda_{H^+},$$

from which $\Delta\Lambda = 1000\,\Delta\varkappa/C$ where $\lambda_{H^+}=350\ \Omega^{-1}\,cm^{-1}$ and values of C_{H^+} are determined from the pH values given in Table 2. If the $\Delta\Lambda$ values are subtracted from the measured Λ values the corrected Λ' values are obtained.

It is recognized that correction related to formation of complex ionic uranyl species is negligibly small compared with that due to variation of $[H^+]$ and it has therefore been found satisfactory, within the limits of accuracy of the measurements, to introduce the latter correction in the measured values in order to calculate both Λ_0 and K_1. No correction has been attempted for the mixed solvents because the necessary data for H^+-ion conductance in these media is lacking. The H^+-correction gave a marked decrease in the conductance of aqueous solutions, particularly at appreciable dilution (Table 2). The corresponding extrapolated Λ_0 values, as well as the uncorrected values in mixed solvents, need further refinements according to the methods of Kraus–Bray[24] and Fuoss–Kraus[18], represented respectively by the relations:

$$\frac{1}{\Lambda} = \frac{1}{\Lambda_0} + \frac{\Lambda C}{K_1 \Lambda_0^2} \tag{7}$$

$$\frac{F(x)}{\Lambda} = \frac{1}{\Lambda_0} + \frac{1}{K_1 \Lambda_0^2} \cdot \frac{\Lambda f^2 \pm C}{F(x)} \tag{8}$$

Both formulae have been applied to data obtained within the concentration ranges where Ostwald K_1 values remain practically constant. Λ_0 and K_1 are obtained from a plot of $1/\Lambda$ *vs.* ΛC using eqn. (7). Λ_0 may also be calculated according to eqn. (8) from the intercept $(1/\Lambda_0)$ of the plot $F(x)/\Lambda$ *vs.* $\Lambda f^2 \pm C/F(x)$, and K_1 from its slope $(1/K_1\Lambda_0^2)$; the values of Λ_0 thus obtained are used to repeat the calculation until a refined reproducible value of Λ_0 is obtained. The curves obtained in aqueous and mixed solvents following the above two methods are given in Figs. 3 and 4, respectively. Although the method of Kraus and Bray, based on the Ostwald dilution law, is incompatible with the present theory of interionic attraction, it yields in the present case results that agree with those obtained by the more rigorous method of Fuoss and Kraus. This coincidence verifies the proposed mechanisms, without the necessity of applying more rigorous calculations according to other systems (*e.g.* that due to Shedlovsky[22]). In water Λ_0 obtained by the two methods, after introducing a H^+-ion correction, is about 70; it approaches 100 for uncorrected conductance values. Subtracting the value of 40.9[25] for $\lambda_0(AcO^-)$ from the corrected $\Lambda_0 = 70$, gives $\lambda_0(UO_2^{2+}) = 29.1$, which is of the same order of magnitude as the values 32 and 30.9 obtained from

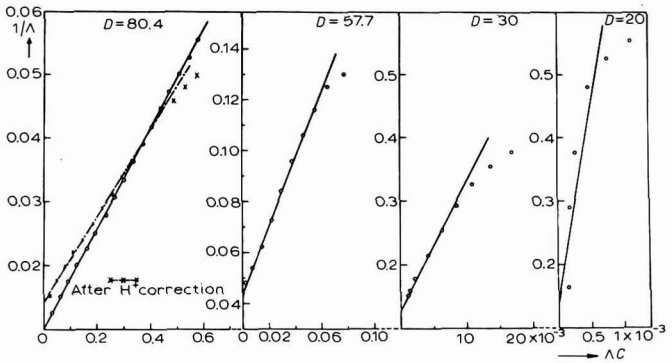

Fig. 3. $1/\Lambda$ *vs.* ΛC for uranyl acetate after the method of Kraus and Bray.

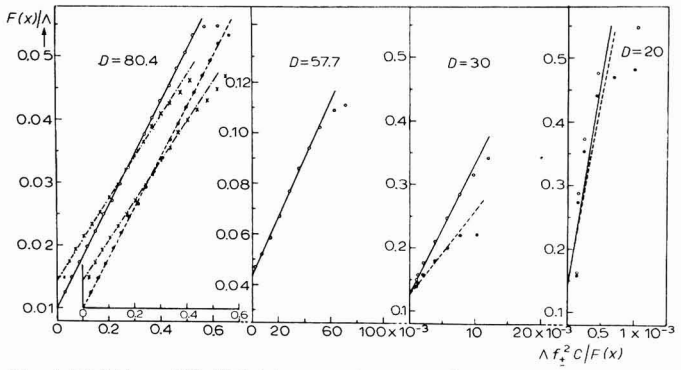

Fig. 4. $F(x)/\Lambda$ *vs.* $\Lambda f_{\pm}^2 C/F(x)$ for uranyl acetate after the method of Fuoss and Kraus. (○——○) First approximation, (●----●) second approximation, (×——×) after H^+ correction.

uranyl fluoride[1] and uranyl chloride[4] data corrected only for the conductance of H^+-ions.

The dissociation constant K_1 of uranyl acetate in water has similar values (as calculated by the methods of Kraus–Bray and Fuoss–Kraus) before and after introducing the H^+-ion corrections (Table 5). For other mixed solvents, Λ_0 is 23, 8, and 7 for the mixtures containing 25, 58 and 70 wt.% dioxane, respectively. The corresponding K_1-values are also of the same order of magnitude according to the above two methods.

Plots of log Λ *vs.* log C are shown in Fig. 5 for solvents of different dielectric constant. At $D=80.4$, 57.7 and 30, Λ first decreases gradually up to $\sim 0.4\times10^{-3}$ M, and then more rapidly, tending to a steady value with increasing concentration. At $D=20$, on the other hand, the initial decrease of Λ is more pronounced than at higher dielectric constants. The conductance then assumes a more or less constant value over a wide concentration range. This corresponds to the occurrence of a minimum which is clearly demonstrated at $D=30$. At higher dielectric constants the curves tend to exhibit such minima especially at higher concentration ranges.

K_1 may be calculated in another way in cases where minima can be traced in log Λ–log C curves. Thus in solvents of $D=30$ and 20, K_1 can be determined from

TABLE 5

K_1, K_3, a_1 AND a_3 FOR URANYL ACETATE IN WATER–DIOXANE MIXTURES

D	$*\Lambda_0$	$K_1/mol\ l^{-1}$				$K_3\times10^2/mol\ l^{-1}$		$a_1\times10^8/cm$	$a_3\times10^8/cm$
		Eqn. (7)	*Eqn.* (8)	*Eqn.* (9)	*Eqn.* (10)	*Eqn.* (9)	*Eqn.* (13)		
80.4	100	1.25×10^{-3}	1.25×10^{-3}					0.41	
	†70	†3.14×10^{-3}	†3.14×10^{-3}					†0.45	
57.7	23	1.4×10^{-3}	1.62×10^{-3}					0.64	
30	8	0.8×10^{-3}	1.13×10^{-3}	0.63×10^{-3}	0.54×10^{-3}	0.63	1.25	1.40	0.56
20	7	3.4×10^{-5}	3.57×10^{-5}	6.0×10^{-5}	4.6×10^{-5}	0.18	0.20	1.79	0.82

* Limiting molar conductance calcd. by the methods of Kraus–Bray and Fuoss–Kraus.
† Values corrected for the conductance of H^+-ions.

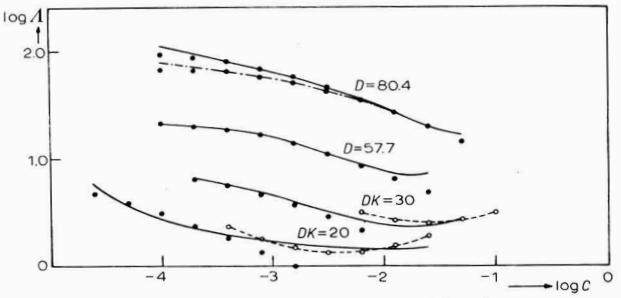

Fig. 5. Log Λ/log C curves for uranyl acetate at 25°C. (——) exptl. values, (–·–·) values corr. for conductance of H^+, (●) calcd. values according to eqn. (6), (○– – –○) calcd. according to eqn. (14).

the intercept of a plot of $\Lambda\sqrt{C}\,g(C)$ *vs.* $(1-\Lambda/\Lambda_0)C$, whereby straight lines can be traced through the region of the minima (Fig. 6) in accordance with the relation[20]:

$$\Lambda\sqrt{C}\,g(C) \approx \sqrt{K_1\,\Lambda_0} + \frac{\sqrt{K_1\,\Lambda_{0_3}}}{K_3}(1-\Lambda/\Lambda_0)C \tag{9}$$

where Λ_{0_3} corresponds to the triple ion ($=\frac{1}{2}\Lambda_0$) and Λ_0 values are deduced from eqns. (7) and (8). The dissociation constant K_1 (at $D=30$ and 20) can also be determined from the minima by substitution in eqn. (10).

$$K_1 = \frac{(C\Lambda^2)_{\min}}{4\Lambda_0^2} \tag{10}$$

The values of the dissociation constant K_1 determined by the above four relations are of the same order of magnitude (see Table 5).

The above data, as well as the shapes of the log Λ–log C curves, indicate that the dissociation of uranyl acetate in water and in mixed solvents of high dielectric

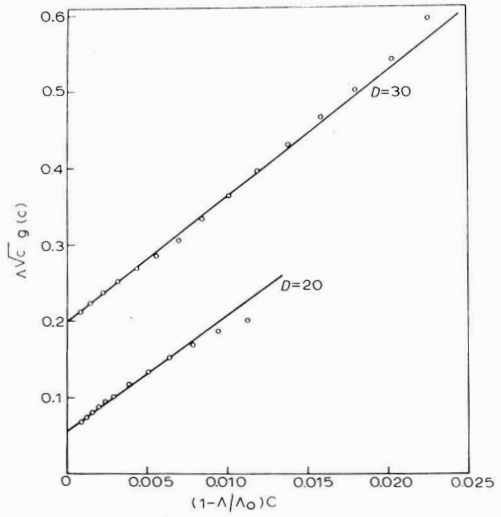

Fig. 6. Graphical representation of eqn. (9) for uranyl acetate in water–dioxane mixtures at $D=30$ and 20.

constant ($D=57.7$) is incomplete over the whole concentration range. The relatively small conductance values, together with the observed decrease with increase of concentration, may be correlated to the progressive formation of slightly dissociated ion-pairs as well as to the behaviour as a weak electrolyte. The occurrence of the minima is assumed to be associated with the formation of charged triple ions. The conductance of such ions increases, after the attainment of the minima, with further increase of concentration. The formation of the triple ion may be represented by the general scheme (11).

$$\left.\begin{aligned} UO_2(AcO)_2 + UO_2AcO^+ &\rightleftharpoons (UO_2)_2(AcO)_3^+ \\ UO_2(AcO)_2 + AcO^- &\rightleftharpoons UO_2(AcO)_3^- \end{aligned}\right] \tag{11}$$

Therefore, K_3 can be represented by:

$$K_3 = \frac{[UO_2(AcO)_2][UO_2AcO^+]}{[(UO_2)_2(AcO)_3^+]}$$

or

$$K_3 = \frac{[UO_2(AcO)_2][AcO^-]}{[UO_2(AcO)_3^-]} \tag{12}$$

The constancy of the conductance values measured at $D=20$ over a wide concentration range, suggests the possibility of another source for the triple ion, which may be represented by[23]

$$2\,UO_2(AcO)_2 \rightleftharpoons (UO_2)_2(AcO)_3^+ + AcO^- \tag{13}$$

$$K_3 = [UO_2(AcO)_2]^2/[(UO_2)_2(AcO)_3^+][AcO^-]\,.$$

The above mentioned factors influencing the conductance of uranyl acetate may also be correlated with the extent of hydrolysis of uranyl ion in the different media. The hydrolysis of uranyl acetate gives rise to $U_2O_5^{2+}$ or/and $U_3O_8^{2+}$ which, having less ionic mobility than the UO_2^{2+} ions, leads to a decrease in conductance. Hydroxy ionic species of the form, $U_3O_8OH^+$, $U_3O_8(OH)_3^-$ or $U_3O_8(OH)_4^{2-}$ may also be formed. At the same time H^+-ions will be produced which react with water molecules giving rise to hydronium ions, or more complex protonated water aggregates, causing an increase in conductance. The increase in conductance due to H_3O^+ ions, or protonated aggregates, is presumably greater in pure water than in mixed solvents, hence the sharp drop of conductance on adding dioxane to water. With further increase of dioxane concentration, $\sim 25\%$, the conductance gradually decreases. This may be explained on the basis of the gradual replacement of water by dioxane in the solvation shells of the uranyl and acetate ions, and the consequent partial repression of hydrolysis of the uranyl ions.

The abnormal behaviour observed in dilute solution, at $D=10$, *viz.* the decreased conductance and decreased pH may be attributed to the formation of slightly dissociated or soluble uranyl hydroxy species. These may include $(U_3O_8)OH^+$, $U_3O_8(OH)_3^-$, and $U_3O_8(OH)_4^{2-}$, together with the slightly soluble hydroxide $U_3O_8(OH)_2$. The formation of the latter was revealed by the appearance of turbidity in relatively dilute solutions.

The dissociation constant, K_3, for the triple-ion dissociation can be calculated

from either relation (9) or (13)[20].

$$K_3 = \frac{C_{\min}\Lambda_{0_3}}{\Lambda_0} \tag{13}$$

The K_3-values thus obtained (Table 5) are of the same order of magnitude for each dielectric constant, but become smaller at lower D.

Using the K_1 and K_3 values given in Table 5, one can derive calculated values for the conductance; these are found to agree fairly well with the experimental values (*cf.* Fig. 4). Within relatively low concentration ranges, beyond the range of formation of the triple ion, Λ values can be calculated according to eqn. (6) using only K_1. At higher concentrations, around the occurrence of the minima, K_1 and K_3 are both used to evaluate the respective conductance values, by substitution in eqn. (9), after rearrangement and simplification in the form

$$\Lambda = \frac{\Lambda_0\sqrt{K_1}}{\sqrt{C}} + \frac{\Lambda_{0_3}\sqrt{K_1}\sqrt{C}}{K_3} \tag{14}$$

Calculation of a_1 and a_3

From the dissociation constants, K_1 and K_3, the distance between the centres of charge of the contacting ions (ion-pair), a_1[26] and of the triple-ion a_3[21] can be calculated in the different solvents (Table 5). It is apparent that a_1 increases with increase of dioxane content of the medium. Normally, a_1 depends on the atomic properties of the constituent ions of the electrolyte, but since the ions are probably solvated, it may also depend on the atomic properties of the solvent. Thus the increase of a_1-values with increasing dioxane content can be attributed to the gradual replacement of water by the larger dioxane molecules in the solvation shells of the uranyl and acetate ions. Moreover, the association of the ions with decreasing dielectric constant may also contribute to increase of a_1. The values of a_3 also increase with increase of dioxane content of the medium.

SUMMARY

The conductance of $\sim 5\times10^{-2}$–5×10^{-5} M uranyl acetate solutions in water and water–dioxane mixtures has been measured at 25°C. The dissociation constants K_1 for the ion-pair, and K_3 for the triple-ion dissociation of uranyl acetate are evaluated in each solvent up to 70 wt.% dioxane, using Λ_0-values calculated after the methods of Fuoss–Kraus–Bray. Using these K_1- and K_3-values, the interionic charge distances for ion-pair, a_1, and the triple-ion, a_3, are estimated. These measurements indicate that uranyl acetate behaves in water and in water–dioxane mixtures as a weak electrolyte, as previously predicted for other uranyl salts. In the mixed solvent of 82 wt.% dioxane ($D = 10$) the conductance of solutions $< 7.8\times10^{-4}$ M uranyl acetate is less than that of the pure mixed solvent. This behaviour is tentatively ascribed to hydrolysis, with subsequent formation, under the prevailing conditions, of the slightly dissociated or insoluble uranyl hydroxy species.

Comparison of the conductance and spectrophotometric and pH-measurements with those obtained for other uranyl salts corroborates the view that the $U_3O_8^{2+}$ ionic species represents the main hydrolysis product.

REFERENCES

1 G. R. DEAN, *Metallurgical Project, No. CC 2092*, Sept., 1944.
2 R. D. BROWN, W. B. BUNGER, W. L. MARSHALL AND C. H. SECOY, *J. Am. Chem. Soc.*, 76 (1954) 1580.
3 J. S. JOHNSON, K. A. KRAUS AND T. F. YOUNG, *J. Am. Chem. Soc.*, 76 (1954) 1436.
4 N. GOLDENBERG AND E. S. AMIS, *Z. Physik. Chem. Frankfurt*, 22 (1959) 63.
5 R. D. BROWN, W. B. BUNGER, W. L. MARSHALL AND C. H. SECOY, *J. Am. Chem. Soc.*, 76 (1954) 1532.
6 C. DITTRICH, *Z. Physik. Chem.*, 29 (1899) 449.
7 H. C. JONES, *Carnegie Inst. Wash. Publ.*, 170 (1912).
8 A. P. WEST AND H. C. JONES, *J. Am. Chem. Soc.*, 44 (1913) 508.
9 B. SINGH AND G. AHMAD, *J. Chim. Phys.*, 34 (1937) 351.
10 L. G. LONGSWORTH AND D. A. MACINNES, *U.S. At. Energy Comm. Rep.*, MDDC 911 (1947).
11 E. RABINOWITCH AND R. LINN BELFORD, *Spectroscopy and Photochemistry of Uranyl Compounds*, Pergamon Press, New York, 1964, pp. 91–100.
12 J. SUTTON, *Nature*, 169 (1952) 235.
13 H. W. CRANDALL, *U.S. At. Energy Comm. Rep.*, MDDC 1294, (1947).
14 J. SUTTON, *Natl. Res. Council Can., At. Energy Project Rep.*, CRC 325 (1947).
15 A. I. VOGEL, *Practical Organic Chemistry*, Longmans Green and Co., New York, London, 1948, p. 175.
16 W. STROHMEIER, AFAF EL-SAID MAHGOUB AND F. GERNERT, *Z. Elektrochem.*, 65 (1961) 85.
17 A. WEISSBERGER AND E. PROSKAUER, *Organic Solvents and Methods of Purification*, Clarendon Press, Oxford, 1935, 139.
18 R. M. FUOSS AND C. A. KRAUS, *J. Am. Chem. Soc.*, 55 (1933) 476; R. M. FUOSS, *ibid.*, 57 (1935) 488.
19 R. M. FUOSS AND C. A. KRAUS, *J. Am. Chem. Soc.*, 55 (1933) 1019.
20 R. M. FUOSS AND C. A. KRAUS, *J. Am. Chem. Soc.*, 55 (1933) 2387; D. J. MEAD AND R. M. FUOSS, *ibid.*, 62 (1940) 1720.
21 R. M. FUOSS AND C. A. KRAUS, *J. Am. Chem. Soc.*, 57 (1935) 1.
22 T. SHEDLOVSKY, *J. Franklin Inst.*, 225 (1938) 739.
23 B. B. OWEN AND R. W. GURRY, *J. Am. Chem. Soc.*, 60 (1938) 3074.
24 C. A. KRAUS AND W. C. BRAY, *J. Am. Chem. Soc.*, 35 (1913) 1315.
25 I. M. KOLTHOFF AND P. J. ELVING, *Treatise on Analytical Chemistry*, Part I, Vol. 4, John Wiley and Sons, New York, London, 1963, p. 2578.
26 N. BJERRUM, *Kgl. Danske Vidensk. Selskab*, 7 No. 9 (1926), see also, H. S. HARNED AND B. B. OWEN, *The Physical Chemistry of Electrolytic Solutions*, Reinhold Publ. Corp., New York, 1950.

ELECTROANALYTICAL CHEMISTRY AND INTERFACIAL ELECTROCHEMISTRY
Elsevier Sequoia S.A., Lausanne – Printed in The Netherlands

PREPARATION AND PHYSICO-CHEMICAL PROPERTIES OF SOME ORGANO-URANYL COMPLEXES

AHMAD MOSTAFA, E. M. KHAIRY, AFAF EL-SAID MAHGOUB AND A. I. MOSAAD
Chemistry Department, Faculty of Science, Cairo University, Giza (U.A.R.)
(Received February 4th, 1969; in revised form, March 16th, 1969)

INTRODUCTION

The possibility of chelation in hydroxyfurochromones having a free hydroxyl group in a position *peri* to the pyrone carbonyl group, *e.g.* 5-norvisnagin[1] has recently been discussed. Colour tests with uranyl acetate for hydroxyfurochromones and related substances have been carried out[1]. The colour developed in a solution containing 5-norvisnagin and uranyl acetate is red. On dilution of the reaction mixture with water, a scarlet red precipitate, readily extractable with chloroform to give a deep-red solution, is obtained.

Hydroxy-9-xanthenone with the hydroxyl group in the 1-position, forms stable chelated compounds with metal salts[2].

8-hydroxyquinoline (oxine), with a donating nitrogen atom, is known to form chelated compounds with metallic ions of composition MR_2, MR_3 or MR_4 ($R = C_9H_6ON$), depending on the co-ordination number of the metal and other structural considerations. Uranyl ions form with oxine the complex $UO_2(C_9H_6ON)_2$[3]. Pavlorskaya and Reibel[4] from optical and potentiometric data showed that the dark red complex formed by adding 8-quinolinol in 2.5 *M* AcOH solution to UO_2^{2+} in the presence of pyridine has the composition UO_2^{2+} : oxine = 1 : 1. Wendlant[5] by thermogravimetric studies, reported the formation of a 2 : 1 complex which adds an additional molecule of reagent, $UO_2(C_9H_6NO)_2 \cdot C_9H_6NOH$, behaving thus as a solvated chelate. Duval[6] reported that this form is stable up to 157°C, whereas Wendlant claimed stability up to 230°C. Thermal decomposition results in the loss of the extra oxine molecules, yielding the chelate, $UO_2(C_9H_6NO)_2$.

The present communication is concerned with physico-chemical studies on some organo-uranyl complexes. The reagents are: 5-norvisnagin, 1-hydroxy-9-xanthenone, and 8-hydroxyquinoline, chosen to furnish different donating atoms, *i.e.* nitrogen atoms in oxine, and carbonyl oxygen in 5-norvisnagin and 1-hydroxy-9-xanthenone. Conductometric, spectrophotometric and microanalytical techniques were used.

EXPERIMENTAL

Materials

5-Norvisnagin was synthesized by demethylation of visnagin[7]; 1-hydroxy-9-xanthenone was prepared by the method of Pankajamani and Seshadri[8], and 8-

quinolinol was the commercial product (May and Baker Ltd., Dagenham, England). Since anhydrous uranyl acetate (AnalaR, Riedel-de Haën A.-G. Seelze bei Hannover, West Germany) hydrolyses, fresh solutions were always prepared just before use. Pure dioxane, and water–dioxane mixture (dielectric constant $D = 30$) were used as solvents.

The organo-uranyl complexes were prepared in the ratio 1 : 2 (uranyl : ligand) in the case of 5-norvisnagin and oxine, and 1 : 3 with 1-hydroxy-9-xanthenone. The complexes precipitate immediately on direct mixing of an aqueous uranyl acetate solution with a solution of the reagent in pure dioxane. They were filtered off, washed thoroughly with redistilled water and then with pure dioxane to ensure complete removal of excess reagents. The oxine complex was recrystallized from acetone or chloroform; two differently coloured crystals separated: one dark brown in colour and the other in the form of orange-red needles. The 5-norvisnagin complex was recrystallised only from acetone, when dark violet crystals were obtained. In the case of 1-hydroxy-9-xanthenone, neither acetone nor chloroform could be used for re-crystallization, as the complex decomposed giving the starting materials (detected from molecular weight and melting point measurements); with dioxane a very small yield of the scarlet red complex was obtained.

Techniques

In conductometric titrations, the organic reagent was dissolved in water–dioxane mixture ($D = 30$) at a concentration 10 times that of uranyl acetate solution in the same solvent. The reagent was added by means of a microburette to 10 ml of a solution of uranyl acetate under a pure nitrogen atmosphere. After each addition the solution resistance was measured at constant temperature (25° ±0.02°C), using an a.c. conductivity bridge of high precision (Leeds and Northrup Co. Philadelphia U.S.A.) (accuracy better than ±0.02%), with an audio frequency electron tube oscillator as a source of alternating current (1000 Hz). A sensitive oscilloscope (Hartmann and Braun AG Frankfurt/Main) served as a null detector.

Spectrophotometric measurements of uranyl complexes both in the original solution and in the dioxane solution of the recrystallized product were made in the visible and u.v. ranges. Experiments were carried out at room temperature using a Beckmann, D.K. recording spectrophotometer, with matched 1-cm fused silica cells. The composition of the uranyl complexes were determined using the continuous

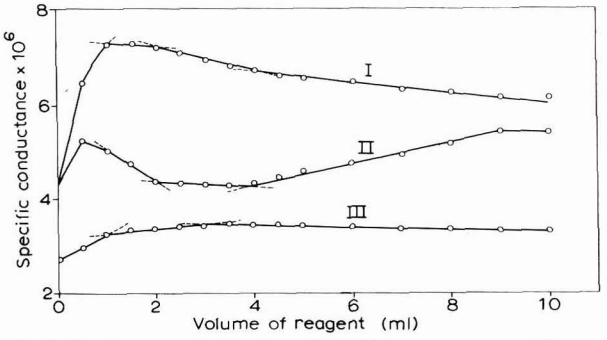

Fig. 1. Conductometric titration of UO_2^{2+} ions *vs.* reagent: (I), 5-norvisnagin; (II), 8-quinolinol; (III), 1-hydroxy-9-xanthenone.

variation method[9] with 5-norvisnagin and 8-quinolinol, and the molar ratio method[10] in the case of 1-hydroxy-9-xanthenone. In the former method, a series of solutions containing x ml of 6.25×19^{-3} M uranyl acetate in dioxane were mixed with $(10-x)$ ml of reagent dissolved in dioxane at the same concentration; the mixtures were investigated spectrophotometrically. In the molar ratio procedure 2 ml-aliquots of a 5×10^{-4} M uranyl acetate solution in pure dioxane were placed in 5 test tubes, and different volumes, 1, 2, 4, 6 and 8 ml of 1-hydroxy-9-xanthenone in dioxane at the same concentration were added; the total volume was then made up to 10 ml with dioxane. Blanks were carried out for the uranyl acetate and the xanthone solutions in pure dioxane. The difference between the optical density of the mixture and the sum of the optical densities of the pure reagent and uranyl acetate gave the optical density of the complex.

RESULTS AND DISCUSSION

Conductometric measurements

The specific conductance, calculated from resistance measurements, was corrected for solvent conductance and volume changes. The values thus obtained were fairly reproducible within $\pm 1\%$, and are plotted against the volume of the titrant (reagent) in Fig. 1. In all cases there is an initial increase in conductance, which is presumably due to liberation of hydrogen during complex formation. After the first break, the three complexing agents show different behaviour, regarding the types and composition of the complexes formed. In the case of 5-norvisnagin complexes (curve I) the curve passes through three breaks corresponding to the compositions 1 : 1, 1 : 2 and 1 : 4, uranyl : ligand, respectively. After the first break, the conductance decreases slightly with addition of reagent, possibly as a result of the progressive formation of the uncharged 1 : 2 complex. A more marked decrease in conductance after the second break is observed up to the third break, corresponding to the formation of the uranyl complex in the ratio 1 : 4. The latter is probably formed by the addition of two molecules of the reagent to the 1 : 2 complex, behaving thus as a solvated uncharged chelate $(UO_2R_2)(RH)_2$, with lower mobility. This explains the further decrease of conductance after the attainment of the last break, on the addition of excess reagent.

In the case of 1-hydroxy-9-xanthenone (curve III), the first break corresponding to the 1 : 1 complex is followed by a slight gradual increase in conductance up to the second break occurring at a molar ratio of 1 : 3 (uranyl : ligand). This slight increase in conductance may be tentatively attributed to the formation of the less stable 1 : 2 complex together with the 1 : 1 complex, with subsequent dissociation of the former and hence increased conductance. This may also be the set-up between the 1 : 2 and 1 : 3 complex depending on the equilibrium conditions prevailing. Finally, the 1 : 3 complex predominates, as revealed by the distinct break.

The conductance of the solution containing the 8-hydroxyquinoline complex (curve II), increases up to about 2 : 1 uranyl : ligand, then falls, passes through two breaks at the mole ratios 1 : 1 and 1 : 2, and then remains more or less constant up to 1 : 4, where a break occurs associated with a considerable increase of conductance on the addition of excess reagent. The constancy of the conductance between the 1 : 2 and 1 : 4 mole ratios may be taken as indicating the stability of the former complex,

with excess reagent molecules entering as solvating molecules in the 1 : 2 chelate, or remaining as such in solution. The increase of conductance after the apparent 1 : 4 ratio may probably be correlated with the acid dissociation of reagent molecules to give H^+ ions in solution. This may be initiated by the polarising effect of the negative oxygens in the 1 : 2 complex, with subsequent increase of the acidity of the hydrogen in the hydroxyl group of the reagent.

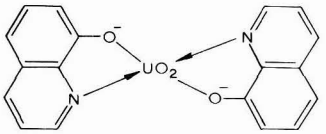

An intermediate stage may occur involving the formation of hydrogen bonds between the solvating molecules and the two oxygens in the chelate. Thus, the 1 : 4 complex may be tentatively represented by:

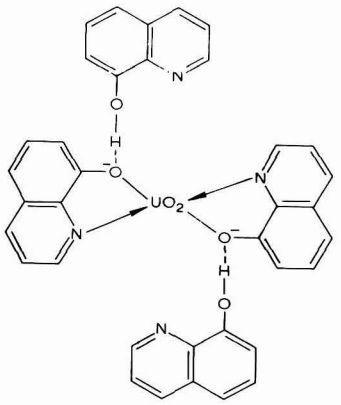

This will be resolved by further structural studies.

Spectrophotometric studies of complexes formed in solutions

The stability of UO_2^{2+} ions has been investigated in pure dioxane and in water–dioxane mixture ($D = 30$). The absorption spectra of uranyl acetate reveal the stability of UO_2^{2+} in both solvents up to a concentration of 6.25×10^{-3} M, in which range the optical density obeys Beer's law. There is no apparent difference in the spectra in the non-aqueous or mixed solvent, but since UO_2^{2+} is known to undergo hydrolysis, pure dioxane is preferable for spectrophotometric measurements of the uranyl complexes formed with different reagents.

The maximum absorption of uranyl acetate in pure dioxane occurs at 425 nm, and that of the pure 5-norvisnagin at 353 nm. Using the continuous variation method with 5-norvisnagin–uranyl mixtures, a maximum band appears at $\lambda = 413$ nm, which may be ascribed to the formation of a stable complex.

Pure oxine solution gives λ_{max} 315 nm. The corresponding uranyl complex shows a maximum band at $\lambda = 374$ nm, using the same experimental method. Figure

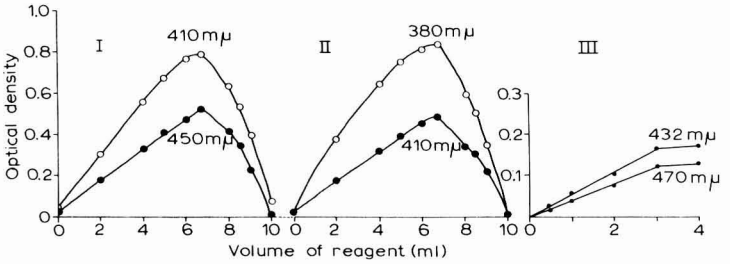

Fig. 2. Composition of uranyl complexes of: (I) 5-norvisnagin, (II) 8-quinolinol, (III) 1-hydroxy-9-xanthenone. (I) and (II) by the continuous variation method, (III) by the molar ratio method.

2 shows the optical density plotted against volume of reagent for 5-norvisnagin and 8-quinolinol complexes (curves I and II) at the absorption maxima and at other wave lengths on the corresponding absorption curves. These yielded maxima at the molar composition of 1 : 2 (uranyl : ligand) in both cases, thus revealing the distinct stability of the corresponding complexes.

Applying the continuous variation method, the absorption maximum of pure 1-hydroxy-9-xanthenone solution occurs at 355 nm. In the region of 400–500 nm no characteristic peak is detected for the complex of uranyl–1-hydroxy-9-xanthenone. However, it is obvious that the optical density of the UO_2^{2+} transition at 425 nm has increased owing to the formation of the complex. To identify the complexes formed, the molar ratio method is used to obtain the absorption curves at different reagent additions. The corresponding curves of optical density–volume of reagent are shown in Fig. 2, curve III, presenting the data observed at the wave lengths of maximum absorption and shoulder on the absorption curves. The curves show breaks at the molar ratio 1 : 3 (uranyl : ligand).

The stable forms of the above complexes as identified from spectrophotometric studies may be represented by:

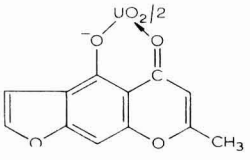

5-norvisnagin

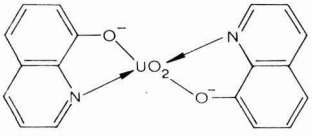

8-hydroxyquinoline

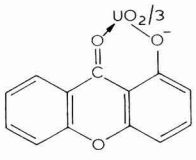

1-hydroxy-9-xanthenone

Absorption spectra of precipitated complexes

Further information regarding the composition and light absorption of uranyl complexes formed in solution may be gained by studying the properties of precipitated complex phases in the mole ratios indicated by conductometric and spectrophotometric results. The spectra of these complexes, together with those of the pure uranyl and pure organic reagents are scanned in the region 600–200 nm. The results obtained are outlined in the following discussion:

Uranyl–5-norvisnagin 1 : 2 *complex*. Spectra of dioxane solutions containing different concentrations of the complex precipitated from solution and recrystallized from acetone (Fig. 3) each show an absorption band at 413 nm with a longer wave length shoulder at 485 nm. The molar extinction coefficient (ε) of the complex at λ_{413} is 6600 l mol^{-1} cm^{-1}, whereas that of uranyl acetate at its λ_{max} (428 nm) is 52.0 l mol^{-1} cm^{-1}. Thus there is a slight blue shift in the complex maximum in addition to the great intensification of the band. This suggests that the transition, slight in the UO_2^{2+} ions, becomes much greater when the complex is formed. This may be due to differences in symmetry between the simple uranyl ion and the complex. It is inter-

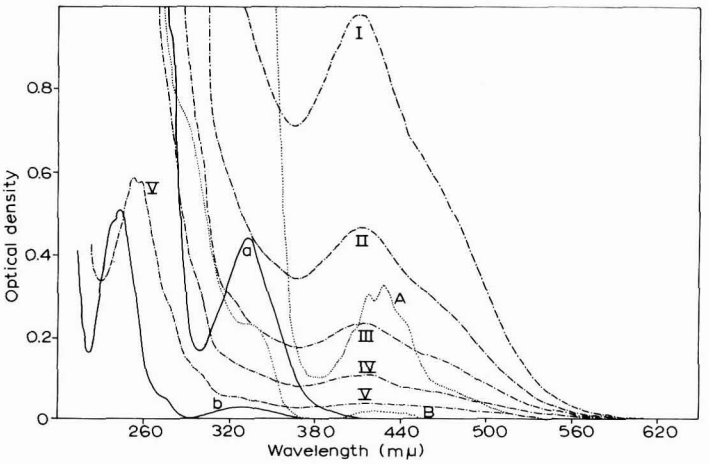

Fig. 3. Absorption spectra in pure dioxane of: (·····) uranyl acetate: A = 6.25×10^{-3}, B = 5×10^{-4} *M*; (——) 5-norvisnagin: a = 6.25×10^{-5}, b = 5×10^{-6} *M*; (–·–·–) uranyl–5-norvisnagin complex (1 : 2): I = 1.427×10^{-4}, II = 0.712×10^{-4}, III = 0.35×10^{-4}, IV = 0.165×10^{-4}, V = 0.58×10^{-5} *M*.

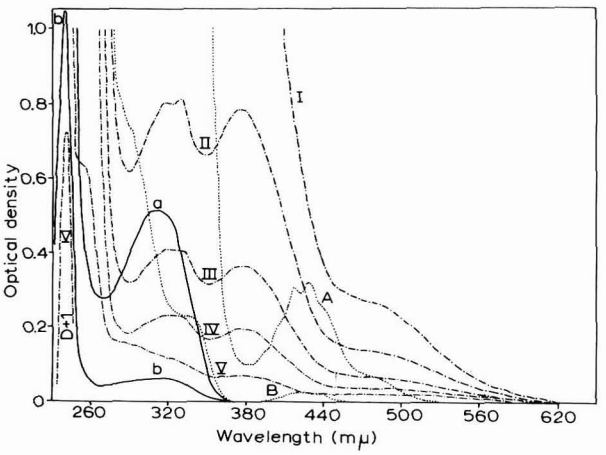

Fig. 4. Absorption spectra in pure dioxane of: (·····) uranyl acetate: A = 6.25×10^{-3}, B = 5×10^{-4} *M*; (——) 8-quinolinol: a = 1.56×10^{-5}, b = 1.56×10^{-6} *M*; (–·–·–) uranyl–8-quinolinol complex (1 : 2): I = 3×10^{-4}, II = 1.5×10^{-4}, III = 0.75×10^{-4}, IV = 0.42×10^{-4}, V = 1.87×10^{-5} *M*.

esting to note that 5-norvisnagin shows a transition at 334 nm with $\varepsilon \simeq 7000$ l mol^{-1} cm^{-1}, which does not appear as a separate band in the spectrum of the complex. Also, the reagent band occurring at 245 nm is red-shifted to 252 nm in the complex spectrum. This is expected since the energy levels in the complex will be lower than that of the reagent.

The peaks of maximum absorption characteristic of the complex are closely comparable to those obtained due to complex formation in solution at the same mole ratio.

Uranyl-8-hydroxyquinoline 1 : 2 complex. The spectrum of the complex crystallized from acetone (brown) is shown in Fig. 4. A characteristic peak of the complex at 375 nm ($\varepsilon \simeq 5000$ l mol^{-1} cm^{-1}), comparable to that obtained by the continuous variation method, on mixing uranyl acetate with the reagent, can clearly be identified. The reagent peak at 314 nm ($\varepsilon \simeq 3500$ l mol^{-1} cm^{-1}) is red-shifted and intensified in the complex (λ_{330}; $\varepsilon \simeq 5400$ l mol^{-1} cm^{-1}).

The spectrum of the complex crystallized from chloroform (red-orange) is scanned for comparison with that obtained from acetone; the band maxima do not differ in the two cases. However, the maxima at 375 and 330 nm of the former complex are greatly intensified compared with those of the latter ($\varepsilon \simeq 9500$ and 5000 l mol^{-1} cm^{-1}, respectively).

The stability of the uranyl–8-hydroxyquinoline complex of the 1 : 2 composition, as revealed by conductivity and spectrophotometric measurements, corroborates the results reported by Irving and Rosotti[11] for the stability constant of that complex species. These authors reported the values 11.25 and 9.64 for log K_1 and log K_2.

Uranyl–1-hydroxy-9-xanthenone 1 : 3 complex. The spectra at different concentrations are shown in Fig. 5. The complex transition at 434 nm ($\varepsilon \simeq 4200$ l mol^{-1} cm^{-1}) can be safely related to the uranyl transition at 428 nm ($\varepsilon \simeq 52.0$ l mol^{-1} cm^{-1}).

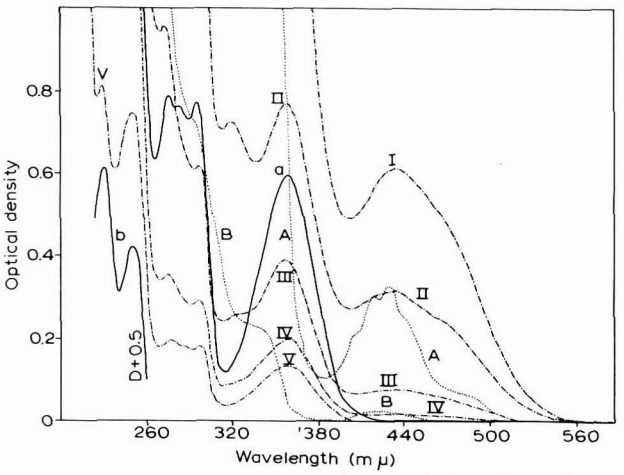

Fig. 5. Absorption spectra in pure dioxane of: (·····) uranyl acetate: A = 6.25×10^{-3}, B = 5×10^{-4} *M*; (——) 1-hydroxy-9-xanthenone: a = 1×10^{-4}, b = 0.5×10^{-5} *M*; (–·–·–) uranyl–hydroxy-xanthenone complex (1 : 3): I = 1.45×10^{-4}, II = 0.72×10^{-4}, III = 0.36×10^{-4}, IV = 0.18×10^{-4}, V = 0.1×10^{-4} *M*.

TABLE 1

ABSORPTION MAXIMA AND MOLAR EXTINCTION COEFFICIENTS

Compound	*Crystallising medium*	λ_{max}/nm	*log* (ε/*l mol*$^{-1}$ *cm*$^{-1}$)
Uranyl acetate	—	428	1.72
		416	1.68
		338	1.57
5-Norvisnagin	—	334	3.85
		245	5.02
Uranyl–5-norvisnagin complex	Acetone	413	3.82
		252	5.01
8-Quinolinol	—	314	3.55
		240	5.83
Uranyl–8-quinolinol complex	Acetone	375	3.70
		330	3.73
		316	3.73
		240	4.97
	Chloroform	375	3.98
		330	3.99
		316	3.98
		240	5.59
1-Hydroxy-9-xanthenone	—	356	3.77
		294	3.88
		274	3.89
		250	4.27
		230	4.35
Uranyl–1-hydroxy-9-xanthenone complex	Dioxane	434	3.62
		358	4.03
		318	3.70
		296	4.23
		274	4.29
		250	4.87
		230	4.91

TABLE 2

ANALYSIS OF THE INSOLUBLE URANYL COMPLEXES

Complex	*Colour of complex*	*Crystallising medium*	*Uranium*/%		*Carbon*/%		*Complex composition proposed (uranyl : ligand)*
			Theor.	*Found*	*Theor.*	*Found*	
Uranyl–5-norvisnagin	dark violet	Acetone	34	31.7	41.1	41.07	$UO_2(R)_2$
Uranyl–8-quinolinol	dark brown	Acetone	37.77	37.74	42.8	39.9	$(UO_2(R)_2)_2R$
	red orange	Chloroform	33.8	29	46	41	$UO_2(R)_2R$

As can be seen, the transition has become much more allowed for the complex than for the simple UO_2^{2+} ion. The pure reagent maximum ($\varepsilon_{356} \simeq 5900$ l mol^{-1} cm^{-1}) has been slightly red-shifted with respect to the complex ($\varepsilon_{358} \simeq 10700$ l mol^{-1} cm^{-1}). The spectrum shows clearly a unique band at 318 nm ($\varepsilon \simeq 9950$ l mol^{-1} cm^{-1}) which can be considered characteristic of the complex. The vibrational structure of the reagent band around 280 nm is relatively less distinct on complex formation. The common feature of the spectra is the intensification of the different transitions owing to complex formation, as was the case with the 5-norvisnagin–uranyl complex.

Absorption maxima and molar extinction coefficients (log ε) of the compounds studied are shown in Table 1.

The analysis for uranium and carbon for the precipitated complexes of 5-norvisnagin and 8-quinolinol are shown in Table 2. Because of the difficulty in obtaining good crystals of the uranyl–1-hydroxy-9-xanthenone complex, it could not be analysed.

The above data show similar compositions for the uranyl–5-norvisnagin and uranyl–8-hydroxyquinoline complexes. In the latter, solvation of the 1 : 2 complex takes place, presumably in an approach to the proposed composition. When chloroform is used for crystallization there is a considerable change of colour as well as intensity of absorption of the uranyl–8-quinolinol complex. This may be correlated to structural changes involving distortions of the crystal field, and there may also be changes in the extent of solvation.

ACKNOWLEDGEMENT

The authors wish to express their thanks to the Pregl-Lab of the University of Graz, Austria, for carrying out the chemical microanalysis for the complexes investigated.

SUMMARY

Conductometric and spectrophotometric studies on the complexes of uranyl ions with 5-norvisnagin, 1-hydroxy-9-xanthenone and 8-hydroxyquinoline have been carried out in pure dioxane and dioxane–water mixture, $D = 30$.

In every case, conductometric titration shows breaks corresponding to the formation of more than one type of complex. For both 5-norvisnagin and 8-quinolinol breaks correspond to the ratios uranyl : ligand of 1 : 1, 1 : 2 and 1 : 4; with 1-hydroxy-9-xanthenone, the compositions 1 : 1 and 1 : 3 are identified.

Spectrophotometric studies covering the visible and u.v. range indicate considerable stability of the 1 : 3 complex with 1-hydroxy-9-xanthenone (applying the molar ratio method). The continuous variation method establishes the existence of 1 : 2 uranyl complexes with both 5-norvisnagin and 8-quinolinol.

Complexes precipitated from the above media at the stable compositions indicated, are spectrophotometrically scanned in the region 600–200 nm. Characteristic peaks for these complexes are observed at the same wave lengths as shown in solution. Microanalysis for carbon and uranium in the complexes separated are in fairly good agreement with the compositions proposed, especially for 5-norvisnagin and 8-hydroxyquinoline where pure crystals of the complexes could be prepared.

REFERENCES

1 A. MUSTAFA, N. A. STRKOVSKY AND E. ZAKI, *J. Org. Chem.*, 25 (1960) 794.
2 P. PFEIFFER, E. BREITH, E. LÜBBE AND T. TSUMAKI, *Ann.*, 503 (1933) 84.
3 A. I. VOGEL, *A Text-book of Quantitative Inorganic Analysis*, Longmans, London, 1961, p. 128.
4 M. P. PAVLORSKAYA AND I. M. REIBEL, *Zh. Neorgan. Khim.*, 5 (1960) 393.
5 W. W. WENDLANT, *Anal. Chem.*, 28 (1956) 499.
6 C. DUVAL, *Inorganic Thermodynamic Analysis*, Elsevier, New York, 1953, pp. 502–511.
7 A. SCHÖNBERG AND N. BADRAN, *J. Am. Chem. Soc.*, 73 (1951) 2960.
8 K. S. PANKAJAMANI AND T. R. SESHADRI, *J. Sci. Ind. Res. India*, 13B (1954) 396.
9 W. C. VOSBURGH AND G. R. COOPER, *J. Am. Chem. Soc.*, 63 (1941) 437.
10 J. H. YOE AND A. L. JONES, *Ind. Eng. Chem., Anal. Ed.*, 16 (1944) 111.
11 H. IRVING AND H. S. ROSOTTI, *J. Chem. Soc.*, 3 (1954) 2910.

ELECTROANALYTICAL CHEMISTRY AND INTERFACIAL ELECTROCHEMISTRY
Elsevier Sequoia S.A., Lausanne – Printed in The Netherlands

STUDIES OF MEMBRANE PHENOMENA

I. EFFECT OF TEMPERATURE ON DIFFUSION OF ELECTROLYTES THROUGH A PARCHMENT-SUPPORTED SILVER IODIDE MEMBRANE

FASIH A. SIDDIQI AND SURENDRA PRATAP
Department of Chemistry, Aligarh Muslim University, Aligarh (India)
(Received February 6th, 1969)

INTRODUCTION

The findings of Teorell[1] that gastric mucosal membrane, in some formal aspects at least, behaved exactly like parchment membrane led us to investigate a very large number of parchment-supported membranes as models for biological membranes. In previous communications[2-5] the membrane potential (E) was related to the permeability (P) parameter by a Freundlich adsorption-type equation $E = aP^{1/n}$, and the constants a and n characterizing the membranes were evaluated. It soon was realized that the electrolytic resistance of the membrane R_m plays an important role in the diffusion process. This communication deals with the determinations of the membrane resistance R_m, the membrane concentration potential, E_m, and diffusion rate D_r, at various temperatures. The evaluation of the energy and enthalpy of activation of diffusion of biologically important electrolytes and their relationship with various thermodynamic quantities of aqueous ions is also considered. These investigations emphasize the importance of hydration and the energetics of the associated processes in membrane phenomena. The fixed charge theory of Teorell[6], and Meyer and Sievers[7] as well as the views of Sollner[8], Gregor[9], Schmid[10] and Eisenman[11] have been applied to elucidate the electrochemical nature of the membranes investigated.

EQUATION USED FOR DIFFUSION RATE MEASUREMENT

The equations used in these investigations to calculate diffusion rates were modifications of those which apply to the migration of ions under the influence of a potential gradient. The equation:

$$\frac{dQ_+}{dt} = \frac{1}{Z_+ R_m F}\left[\frac{Z_-}{Z_+ + Z_-}\frac{E_m}{E_{c+}} + \frac{Z_+}{Z_+ + Z_-}\right][E_{c+} - E_m] \qquad (1)$$

where

Q_+ = mmoles of cations
Z_+, Z_- = valency of cation and anion respectively
E_m = membrane concentration potential
E_{c+} = potential difference (mV) equivalent to a given difference in cation concentration

E_{c^-} = potential difference (mV) equivalent to a given difference in anion concentration
F = Faraday (96,500 C)
R_m = electrolytic resistance of membrane (Ω)
t = diffusion time (s),

which was deduced by Kittleberger[12], was employed for the determination of the diffusion rate. For uni-univalent electrolytes, $Z_+ = Z_-$, eqn. (1) then becomes

$$D_r = \frac{dQ}{dt} = \frac{dQ_+}{dt} = \frac{1}{FR_m}\left[\tfrac{1}{2}\frac{E_m}{E_{c^+}} + \tfrac{1}{2}\right][E_{c^+} - E_m] \quad (2)$$

where D_r is the diffusion rate and Q is mmoles of salt.

EXPERIMENTAL

Preparation of parchment-supported silver iodide membrane

The membrane was prepared by impregnating parchment paper with silver iodide. The paper was first soaked with distilled water and then tied carefully to a glass tube (cylinder). A 0.2 *M* solution of potassium iodide was put inside the paper container which was then suspended for 72 h in a 0.2 *M* $AgNO_3$ solution contained in a beaker. The parchment paper was then taken out and washed repeatedly with distilled water to remove the adsorbed electrolytes. The solutions of potassium iodide and silver nitrate were then interchanged. The paper was then immersed in them for another 72 h. This process was repeated a number of times until a very fine deposit of silver iodide was obtained on the paper. The membrane, yellow in colour, was observed under a microscope; there was a fine deposition over the whole surface.

Apparatus and procedure

The assembly used for the diffusion rate measurement is shown in Fig. 1. It consisted of two half-cells (125-ml capacity) having flanges to fit each other. The vertical female joints, T and T′, attached to each half-cell provided introduction for the electrolyte and the conductivity cell electrodes. The test membrane in the form of a disc slightly larger than the cell was installed between the flanges of the half-cells. One Ag/AgCl J-shaped electrode and one Ag/AgCl disc electrode passed through two narrow holes in each half-cell very close to the membrane as shown in Fig. 1. A narrow tube was slipped over the ends of the J-shaped and the disc electrodes and waxed firmly. Some mercury was also placed in each of the tubes to provide connection to the copper wire leads.

The conductivity cell electrodes dipping in the salt solutions in the two half-cells were used to determine the salt concentration of the test solutions. Various salt solutions (KCl, NaCl and LiCl) were prepared from B.D.H. AR-grade chemicals. Initially, they were usually 0.2 *M* and 0.002 *M* in the two half-cells. No appreciable change was observed within 5–6 h in 0.2 *M* electrolyte concentration and we have therefore assumed this concentration to be practically unchanged.

The potential difference between the Ag/AgCl J-shaped electrodes in test solutions on opposite sides of the membrane is the algebraic sum of concentration potential E_{c^-} and membrane potential E_m. E_{c^-} was obtained by calculation from the measured concentrations of the two test solutions and $(E_m + E_{c^-})$ was obtained

directly. The membrane concentration potential E_m was then obtained by subtraction. Under the conditions of the experiment, the dilute side was always positive and E_m was taken with its proper sign.

The electrolytic resistance of the membrane R_m was determined by applying an external e.m.f. to the Ag/AgCl disc electrodes in the solutions on opposite sides of the membrane and measuring the change in the potential difference of the Ag/AgCl J-shaped electrodes. To determine the current in the circuit, the IR drop across a known resistance R (1000 Ω) in series with the cell was also measured. This measuring current was kept as low as possible in order to minimise the transfer of ions during the 2 or 3 min required for each resistance measurement.

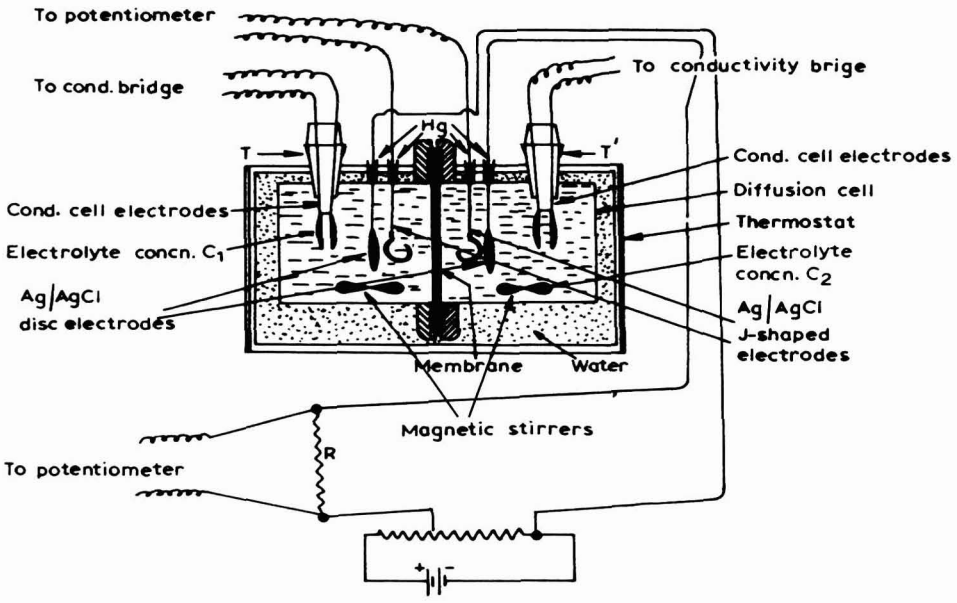

Fig. 1. Apparatus for diffusion rate measurement and electric circuit for measurement of the membrane resistance R_m.

The experimental procedure involved setting up a cell with a membrane and silver–silver chloride electrodes (both J-shaped as well as disc-shaped). Known volumes of the two test solutions (approx. 125 ml of each) were introduced and the conductivity cell electrodes fixed in place. The assembly had magnetic stirrers in each half-cell and was placed in a thermostat maintained at the required temperature. The measurements needed were the determination of (*a*) the salt concentration of the two test solutions, (*b*) the membrane concentration potential and (*c*) the membrane resistance in order to compute the diffusion rate.

Two sets of calibration curves were needed in this experiment, one to obtain the concentration from the measured conductivity and the other to obtain the concentration potential E_{c+}. In the first case, the curves were plots of conductance *vs.* concentration. The curves from which concentration potentials were obtained were plots of e.m.f. *vs.* log *fc* from the equation:

$$\text{e.m.f.} = \frac{2.303\ RT}{F} \log fc \qquad (3)$$

(for uni-univalent electrolytes)

For all electrolytes, E_{c+} was equal to the difference between the e.m.f. values of the dilute and concentrated test solutions.

With R_m in ohms and E_{c+} and E_m in millivolts, eqn. (2) gives the rate of diffusion of an electrolyte through the membrane in mmol s^{-1}.

The potential and conductance measurements were made by means of a Pye precision vernier potentiometer (No. 7568) and Cambridge conductivity bridge (No. L-350140), respectively.

RESULTS AND DISCUSSION

The equation for the diffusion rate for a uni-univalent electrolyte is given by eqn. (2) which clearly shows that D_r depends mainly upon two main factors, membrane resistance R_m and membrane potential E_m. The changes in the diffusion rate over a range of nearly 6 h for the chlorides of alkali metal ions are shown in Fig. 2. The variations in the membrane resistance and membrane potential over the same time range are shown in Figs. 3 and 4 respectively. As the diffusion rate depends markedly

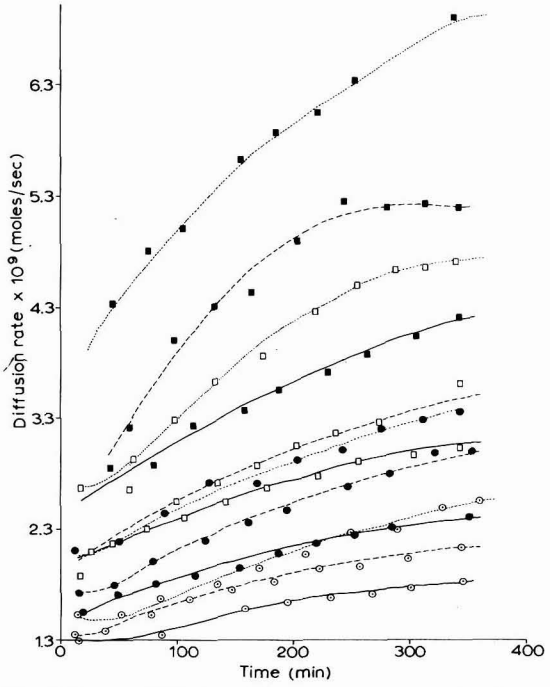

Fig. 2. Rates of diffusion (D_r) of various electrolytes through silver iodide membrane at different temps. LiCl (straight lines): (⊙) 10°, (●) 18°, (□) 25°, (■) 35°C. NaCl: the same with a dashed line. KCl: the same with a dotted line.

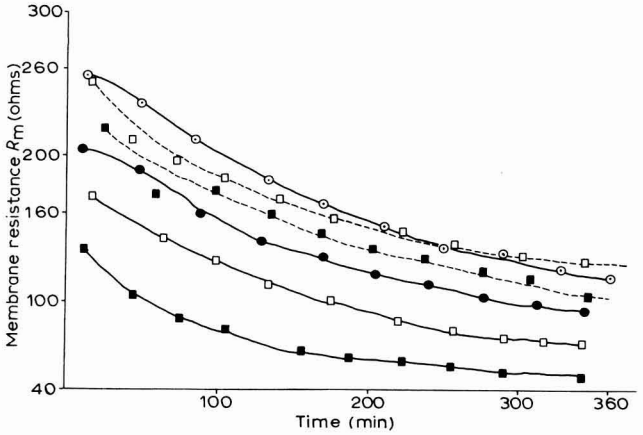

Fig. 3. Plots of membrane resistance *vs.* time for KCl at different temperatures, and for NaCl and LiCl at 25°C (dashed lines). KCl: (⊙), 10°; (●), 18°; (□), 25°; (■), 35°C. NaCl: (■); LiCl: (□).

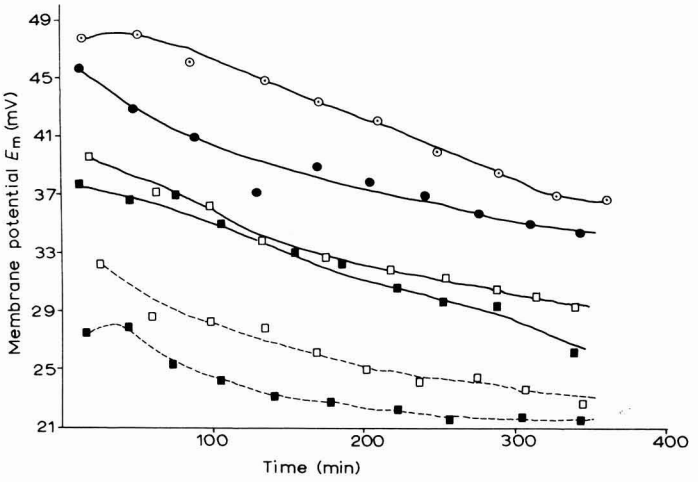

Fig. 4. Plots of membrane potential *vs.* time for KCl at different temperatures and for NaCl and LiCl at 25°C (dashed lines). Designations as in Fig. 3 for KCl. Dotted lines: NaCl: (□); LiCl: (■).

on temperature, it was thought worthwhile to study the effect of temperature on membrane resistance and membrane potential. The behaviour of membrane resistance and membrane potential for KCl at various temperatures is shown in Figs. 3 and 4 respectively. The effect of temperature on membrane resistance and membrane potential was found to be similar for NaCl and LiCl; representative curves for NaCl and LiCl at 25°C are also shown in the same Figures.

In order to obtain the energy of activation of diffusion of the three electrolytes (*viz.* KCl, NaCl and LiCl), plots of log D_r *vs.* $1/T$ (T is the absolute temperature) were drawn for the three electrolytes and from the slope, the energy of activation E_A, was evaluated. As is clear from Figs. 2, 3 and 4, the changes in D_r, R_m and E_m are appreciably lower after 300 min, so these values at 340 min were chosen for each

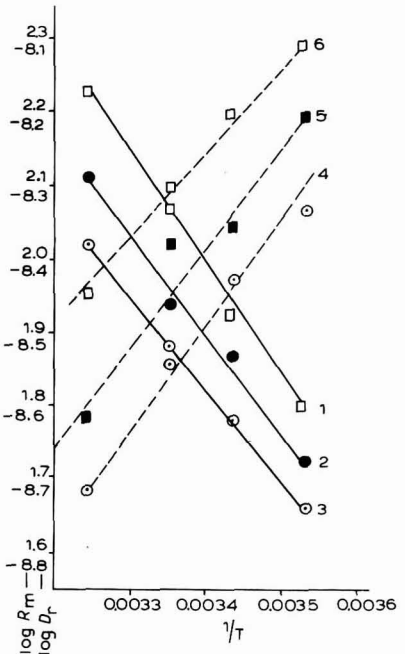

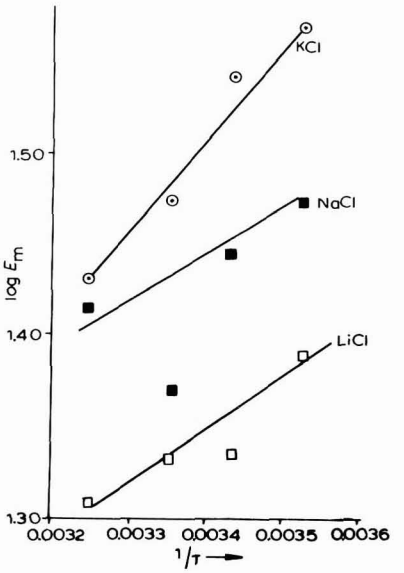

Fig. 5. Plots of log D_r (full line) and log R_m (dashed line) *vs.* $1/T$ (both at 340 min) for different electrolytes. (□) (1), KCl; (●) (2), NaCl; (⊙) (3), LiCl. (⊙) (4), KCl; (■) (5), NaCl; (□) (6), LiCl.

Fig. 6. Plots of log E_m *vs.* $1/T$ for different electrolytes.

TABLE 1

VALUES OF MEMBRANE RESISTANCE R_m, MEMBRANE POTENTIAL E_m, AND DIFFUSION RATE D_r (AT THE 340TH MINUTE) FOR VARIOUS ELECTROLYTES AT DIFFERENT TEMPERATURES USING PARCHMENT-SUPPORTED SILVER IODIDE MEMBRANE

($C_1/C_2 = 0.2\ M/0.002\ M$)

Electrolyte	*Temp./°C*	R_m/Ω	E_m/mV	$10^9\ D_r/\ mol\ s^{-1}$
KCl	10	118.0	37.0	2.50
	18	94.5	34.8	3.37
	25	72.0	29.7	4.70
	35	48.0	27.0	6.83
NaCl	10	158.5	29.7	2.12
	18	111.5	27.9	2.94
	25	106.0	23.5	3.45
	35	61.0	26.0	5.20
LiCl	10	198.5	24.5	1.82
	18	160.0	21.6	2.39
	25	126.0	21.4	3.07
	35	90.0	20.3	4.18

electrolyte to make a comparative study. In order to draw the plots of log D_r, log R_m and log E_m *vs.* $1/T$, the values of D_r, R_m and E_m chosen for each electrolyte at each temperature were those at the 340th minute. The plots of log D_r and log R_m *vs.* $1/T$ for different electrolytes are shown in Fig. 5; those of log E_m *vs.* $1/T$ are shown in Fig. 6. The values of D_r, R_m and E_m for different electrolytes at different temperatures (at the 340th minute) are summarized in Table 1.

The energies of activation of diffusion for the three electrolytes are in the order: KCl, 6974; NaCl, 6132; LiCl, 5675 cal mol^{-1}.

The enthalpies of activation $\Delta H^{\neq}$ (at 25°C) for the three electrolytes are as follows: KCl, 6382; NaCl, 5540; LiCl, 5083 cal mol^{-1}.

A critical evaluation of the experimental results on the diffusion rates has to take into consideration the following factors which are responsible for slowing down the diffusion through the membrane compared to the diffusion in free solution.

1. A part of the cross section of the membrane is occupied by the frame-work (cellular material and silver iodide precipitate).
2. Diffusion of the electrolyte takes place through a tortuous and hence longer path.
3. The frame-work impedes the diffusion of large hydrated ions.
4. Interaction of the fixed ionic groups of the frame-work retards the diffusion.

Moreover, pore geometry also plays a role in explaining the retardation in diffusion rate. In the system investigated, all homogenous membrane elements are taken to be charged, rigid capillary structures or gels which may be adequately described by the classical fixed charge theory of Teorell. The charged membrane is to be viewed as a set of parallel capillaries having a diameter large with respect to the thickness of the electrical double layer at the walls.

The interpretation of the results of the diffusion rate studies can be discussed in terms of ionic sizes, solvation, mobilities, adsorption properties and other thermodynamic properties. The theory put forward by Gregor[9] in relation to the ionic selectivity depends largely on the use of hydrated ionic volumes. As our discussion is largely dependent upon ionic hydration, it seems necessary to mention some concept of ionic hydration as applied to membrane phenomena. Levine and Bell[13] have considered the region of water surrounding an ion as a coordinated hydration shell, and call it an ion complex. Its formation and breaking would be accompanied by substantial free energy and entropy changes. Stern and Amis[14] considered that ions may possess solvation sheaths of water molecules "bound" to give distinct molecular species. Stokes and Robinson[15] have given the number of bound molecules (N_h) in their hydration shell by the interaction of ions and the surrounded water. This number N_h is not the same as the conventional number of water molecules in the first layer around the ion, it is rather a number introduced to allow for the average effect of all ion–solvent interaction. The following are the values of N_h and a_0 (mean distance of approach in Å units) for the three cations[18]

	N_h	a_0 (Å)
KCl	1.9	3.63
NaCl	3.5	3.97
LiCl	7.1	4.32

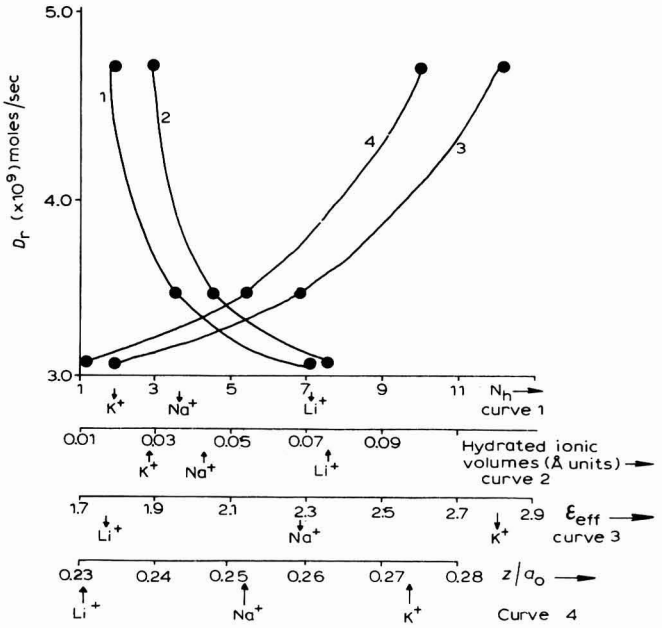

Fig. 7. Plots of: (1), N_h; (2), hydrated ionic volumes; (3), E_{eff}; (4), Z/a_0 *vs.* D_r, where the D_r values are those at 340 min and 25°C.

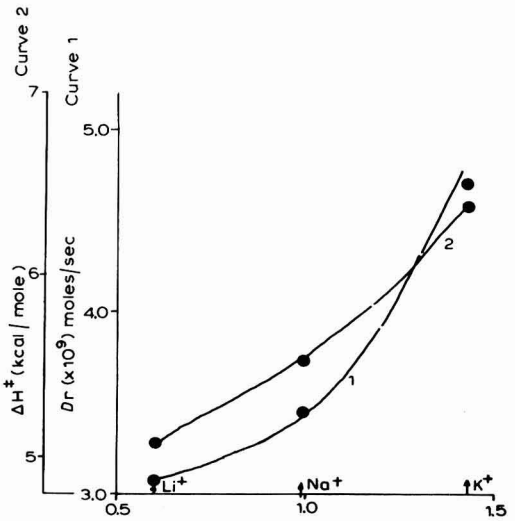

Fig. 8. Plots of: (1), D_r; (2) $\Delta H^{\neq}$ *vs.* heats of hydration. D_r-values are those at the 340th min and 25°C; $\Delta H^{\neq}$-values are those at 25°C.

According to Gregor's theory of ion selectivity[9], of two exchangeable cations the one with the smaller hydrated radius will be preferred by the exchanger. Depending on the size and electrical charge pattern of a pore, it may either admit or repel a solute particle. This is the basis of ion selectivity and applies equally to the material in a thin sheet (a membrane) or in bulk (an ion exchanger). It has been proposed by Mullins[16] that the hydration of the materials of the pores themselves may provide a favourable water environment for particular ions or molecules, so that they slip into the pore away from their previous water molecules. According to the Mullins argument this could result in selection of a particular size with discrimination against both smaller and larger hydrated ions. However it is more general to regard the state of hydration as being in a dynamic condition so that a fraction f of the number of a given kind of particles in the solution has a reduced hydration corresponding to excess energy ΔE/mole, according to the Boltzmann distribution $f = \exp(-\Delta E/RT)$. Thus, it can be said that those ions that have lost sufficient water of hydration to become smaller than the pore, can enter the material.

To obtain a quantitative relation between the ease of penetration and the ion size (hydrated) it will be necessary to know the electrostatic force that acts between the ions and the material of the membrane, since this force provides energy equal to ΔE to displace water of hydration. Eisenman[11] has pointed out that the order of the ease of penetration of univalent cations will depend upon the energy for the ion-fixed charge interaction. The values of the activation energies as determined for a silver iodide membrane for the three electrolytes are found to lie between 5.6 and 7.0 kcal mole^{-1}. It is quite probable that the pores of the membrane may have such a size that they allow some of the hydrated sheaths along with the ions to pass through. However in Fig. 7, plots of the hydration numbers and the hydrated ionic volumes *vs.* D_r show that Li^+ having the highest value has the lowest D_r value. The plots of D_r and enthalpy of activation $\Delta H^{\neq}$ *vs.* heats of hydration (Fig. 8) of the individual ions show that Li^+ having the lowest value of heat of hydration has the lowest values of D_r and $\Delta H^{\neq}$.

Noyes[17] while dealing with the thermodynamics of ion hydration as a measure of the effective dielectric properties of water, has regarded the thermodynamic changes during hydration as a measure of the effective dielectric properties of solvent and shows that $\varepsilon_{\text{effective}}$ is primarily a function of the size (crystallographic radii) of such a cation and is virtually independent of charge on it. As, during the diffusion process, adsorbability and polarizability play an important part which will certainly influence and thereby diminish the effective hydration (the higher adsorbability of Li^+, Na^+, K^+ are linked closely with their stepwise stronger polarizabilities and, hence, effective hydration is diminished to a larger extent[8]) it would be quite logical to relate the effective dielectric constant with D_r. The plots of ε_{eff} *vs.* D_r are shown in Fig. 7, the highest values of ε_{eff} of K^+ giving the largest value of D_r.

ACKNOWLEDGEMENT

The authors are grateful to Dr. S. M. F. Rahman, Head of the Chemistry Department, for providing facilities for carrying out these investigations.

SUMMARY

The diffusion of LiCl, NaCl and KCl through parchment-supported silver

iodide membrane has been studied at various temperatures. The diffusion rate is in the order: KCl > NaCl > LiCl. The membrane resistance R_m and the membrane potential E_m are found to decrease with increase in temperature. The membrane resistance is in the order: $R_m(LiCl) > R_m(NaCl) > R_m(KCl)$ whereas the membrane potential is in the order: $E_m(KCl) > E_m(NaCl) > E_m(LiCl)$. The results have been discussed in the light of TMS theory and the views of Sollner, Gregor and Eisenman. The diffusion rate and the enthalpy of activation of diffusion have been related to the number of hydration, heats of hydration and other ionic quantities.

REFERENCES

1 T. TEORELL, *Discussions Faraday Soc.*, 21 (1956) 9.
2 W. U. MALIK AND S. A. ALI, *Kolloid-Z*, 175 (1961) 139.
3 W. U. MALIK AND F. A. SIDDIQI, *Proc. Indian Acad. Sci.*, A 56 (1962) 206.
4 W. U. MALIK AND F. A. SIDDIQI, *J. Colloid Sci.*, 18 (1963) 161.
5 W. U. MALIK, H. ARIF AND F. A. SIDDIQI, *Bull. Chem. Soc. Japan*, 40 (1967) 1741.
6 T. TEORELL, *Proc. Soc. Exp. Biol. Med.*, 33 (1935) 282; *Z. Elektrochem.*, 55 (1951) 460; *Proc. Nat. Acad. Sci., U.S.*, 21 (1935) 152; *J. Gen. Physiol.*, 21 (1937) 107.
7 K. H. MEYER AND J. F. SIEVERS, *Helv. Chim. Acta*, 19 (1936) 649, 665, 987.
8 K. SOLLNER, *J. Phys. Chem.*, 49 (1945) 47, 171; *J. Electrochem. Soc.*, 97 (1950) 139 C; *Ann. N.Y. Acad. Sci.*, 57 (1953) 177.
9 H. P. GREGOR, *J. Am. Chem. Soc.*, 70 (1948) 1293; 73 (1950) 642.
10 G. SCHMID, *Z. Elektrochem.*, 54 (1950) 424, *ibid.*, 55 (1951) 229; *ibid.*, 56 (1952) 181; G. Schmid and H. Schwarz, *Z. Elektrochem.*, 55 (1951) 295; *ibid.*, 55 (1951) 684; *ibid.*, 56 (1952) 35.
11 G. EISENMAN, *Biophys. J., Suppl.*, 2 (1962) 259; G. EISENMAN, in A. KLEINZELLER AND A. KOTYK (Eds.), *Membrane Transport and Metabolism*, Academic Press, New York, 1961, pp. 163–179.
12 W. W. KITTLEBERGER, *J. Phys. Chem.*, 55 (1949) 392.
13 S. LEVINE AND G. M. BELL, *Discussions Faraday Soc.*, 42 (1966) 9.
14 K. H. STERN AND E. S. AMIS, *Chem. Rev.*, 59 (1959) 1.
15 R. H. STOKES AND R. A. ROBINSON, *J. Am. Chem. Soc.*, 70 (1948) 1870.
16 R. J. HARRIS (Ed.), *Transport and Accumulation in Biological Systems*, Butterworths Scientific Publ. (London), 1960 edition.
17 R. M. NOYES, *J. Am. Chem. Soc.*, 84 (1962) 513.
18 H. S. HARNED AND B. B. OWEN, *Physical Chemistry of Electrolyte Solutions*, Reinhard Publishing Corp., New York, N.Y., 3rd ed., 1955, p. 548.

ELECTROANALYTICAL CHEMISTRY AND INTERFACIAL ELECTROCHEMISTRY
Elsevier Sequoia S.A., Lausanne – Printed in The Netherlands

STUDIES OF MEMBRANE PHENOMENA

II. DETERMINATION OF MEMBRANE POTENTIALS AND EVALUATION OF THE MEMBRANE FIXED CHARGE DENSITY AND PERMSELECTIVITY OF PARCHMENT-SUPPORTED SILVER IODIDE MEMBRANE

FASIH A. SIDDIQI AND SURENDRA PRATAP
Department of Chemistry, Aligarh Muslim University, Aligarh (India)

(Received February 6th, 1969)

INTRODUCTION

For the characterisation of the selectivity of ionic membranes, the electrical potentials arising across the ionic membrane have been measured by constructing a cell of the type

$$\text{Ref.electrode} \mid \underset{1}{\text{Solution}} \mid \text{Membrane} \mid \underset{2}{\text{Solution}} \mid \text{Ref. electrode}$$

the reference electrodes being the saturated calomels connected to the solutions by means of a KCl–agar bridge. The cell potential in this method gives directly the membrane potential. The calculation of the membrane potential and the theoretical approaches for it have been classified into three main groups: (*a*) the idealised theory of Teorell, Meyer and Sievers (TMS) and its refinements[1]; (*b*) the pseudo-thermodynamic approach and the treatment based on thermodynamics of irreversible processes[2] and (*c*) the kinetic approach[3].

In part I of these investigations, the electrochemical behaviour of the membrane was treated on the basis of TMS theory. In this communication the evaluation of Donnan potentials, diffusion potentials, membrane fixed charge density and permselectivity has been carried out on the basis of the TMS model of an ionic membrane.

EXPERIMENTAL

Preparation of the silver iodide membrane

The membrane was prepared as described in Part I[19].

Measurement of the membrane potential

The potential developed by setting up the concentration cell of the type described by Michaelis[4]

$$\text{SCE} \mid \underset{a_1}{\text{Solution}} \mid \text{Membrane} \mid \underset{a_2}{\text{Solution}} \mid \text{SCE}$$

$$a_1 = 10a_2$$

was taken as a measure of the membrane potential. The measurements were carried out using a Pye precision vernier potentiometer (No. 7568).

RESULTS AND DISCUSSION

The results of the membrane potential measurements may be discussed in terms of the theories put forward by Michaelis[4], Meyer and Sievers[5] and also by Teorell[6]. Michaelis held the view that the selective permeability and potential of the collodion membranes were due to preferential adsorption modifying the differential diffusion rates. Willis[7] extended this theory to cupric ferrocyanide, and Malik and Siddiqi[8] applied it to a large number of parchment-supported metal ferro- and ferricyanide membranes thus confirming the earlier view of Sollner[9] that the behaviour of collodion membrane is due to the surface charges fixed on the membrane matrix.

For the evaluation of membrane fixed charge density ($\omega\bar{x}$) by the potentiometric method, Teorell[6] and Meyer[10] have given a method which has been developed and reviewed by Lakshminarayaniah[11]. Recently, Altug and Hair[12] have given an ingenious and indirect method, which has also been developed on the lines of Teorell's model, for the evaluation of $\omega\bar{x}$.

The essential feature of the original fixed charged theory of Teorell[6] was the assumption that the overall membrane potential was composed of three potential jumps: two Donnan potentials at each solution–membrane interface (denoted by π_1 and π_2), and one residing inside the membrane, the internal potential or driving potential being denoted by $\phi_2-\phi_1$. The overall total membrane potential E_{calc} is thus given by:

$$E_{calc} = (\pi_1+\pi_2)+(\phi_2-\phi_1) \tag{1}$$

π_1 and π_2 have been calculated according to the equation:

$$\pi_1 = \frac{-RT}{F}\ln r_1 \tag{2(a)}$$

and

$$\pi_2 = \frac{RT}{F}\ln r_2 \text{ (for uni-univalent electrolytes)} \tag{2(b)}$$

where r_1 and r_2, the Donnan distribution ratios, are determined with the help of the equation

$$r = \left\{1+\left(\frac{\omega\bar{x}}{2a}\right)^2\right\}^{\frac{1}{2}} - \left(\frac{\omega\bar{x}}{2a}\right) \tag{3}$$

where a is the external solution concentration. The diffusion potential $\phi_2-\phi_1$ for uni-univalent electrolyte is given by:

$$\phi_2-\phi_1 = \frac{u-v}{u+v}\frac{RT}{F}\ln\left(\frac{a_1(r_1u+v/r_1)}{a_2(r_2u+v/r_2)}\right) \tag{4}$$

u and v being the cation and anion mobilities in the membrane. However, in the present calculations, these are assumed to be the same as in solution. Owing to the practical difficulty of measuring ionic activity in the membrane phase, concentrations have

been used in place of activities, as suggested by Altug and Hair[12].

In order to determine the fixed charge density of a parchment-supported silver iodide membrane, various values (*e.g.* -0.4 *N*, -0.1 *N*, etc.) were given to $\omega\bar{x}$ and for each value the total membrane potential was calculated for different concentrations of KCl using the above equations. The curves of total membrane potential *vs.* concentration were plotted for various $\omega\bar{x}$-values. At the same time, a curve was plotted between the experimentally determined membrane potential values for KCl and the concentrations of KCl (the concentration range being the same in the two cases). The fixed charge density $\omega\bar{x}$ is then the same as that of the theoretical curve which overlaps the experimental curve.

The values of the Donnan potential $(\pi_1+\pi_2)$, the diffusion potential $(\phi_2-\phi_1)$, and the total membrane potential E_{calc} for various concentrations of KCl (for various values of $\omega\bar{x}$) are given in Table 1A. The values of the observed membrane potential E_{obs} across the silver iodide membrane for various concentrations of KCl are given in Table 1B, (Fig. 1).

TABLE 1A

CALCULATED VALUES OF DONNAN POTENTIAL $(\pi_1+\pi_2)$, DIFFUSION POTENTIAL $(\phi_2-\phi_1)$ AND TOTAL MEMBRANE POTENTIAL E_{calc} ACROSS THE SILVER IODIDE MEMBRANE IN KCl OF VARIOUS CONCENTRATIONS, ASCRIBING VARIOUS VALUES TO $\omega\bar{x}$ (THE MEMBRANE FIXED CHARGE DENSITY) (AT 20°C)

$\omega\bar{x}/N$	*Concns.* $a_1/a_2/M$	$(\pi_1+\pi_2)/mV$	$(\phi_2-\phi_1)/mV$	E_{calc}/mV
-0.4	1/0.1	31.4	-0.74	30.66
	0.1/0.01	56.58	-0.05	56.53
	0.05/0.005	57.73	-0.01	57.72
	0.01/0.001	58.2	0.00	58.2
	0.001/0.0001	58.2	0.00	58.2
-0.1	1/0.1	10.89	-1.07	9.82
	0.1/0.01	46.21	-0.38	45.83
	0.05/0.005	53.3	-0.17	53.13
	0.01/0.001	57.85	0.00	57.85
	0.001/0.0001	58.2	0.00	58.2
-0.06	1/0.1	6.72	-1.1	5.62
	0.1/0.01	38.5	-0.58	37.92
	0.05/0.005	48.51	-0.32	48.19
	0.01/0.001	55.9	-0.12	55.78
	0.001/0.0001	58.2	0.00	58.2
-0.02	1/0.1	2.27	-1.12	1.15
	0.1/0.01	19.7	-0.96	18.74
	0.05/0.005	31.2	-0.75	30.45
	0.01/0.001	53.2	-0.17	53.03
	0.001/0.0001	58.2	0.00	58.2
-0.01	1/0.1	1.12	-1.28	-0.16
	0.1/0.01	10.89	-1.07	9.82
	0.05/0.005	19.68	-0.95	18.73
	0.01/0.001	46.25	-0.38	45.87
	0.001/0.0001	57.85	0.00	57.85

TABLE 1B

OBSERVED VALUES OF MEMBRANE POTENTIAL E_{obs} ACROSS THE SILVER IODIDE MEMBRANE IN KCl AT VARIOUS CONCENTRATIONS (AT 20°C)

Concn. a_1/a_2	1 *M*/0.1 *M*	0.1 *M*/0.01 *M*	0.05 *M*/0.005 *M*	0.01 *M*/0.001 *M*	0.001 *M*/0.0001 *M*
Observed membrane potential E_{obs} (mV)	0.4	13.9	23.0	41.0	51.67

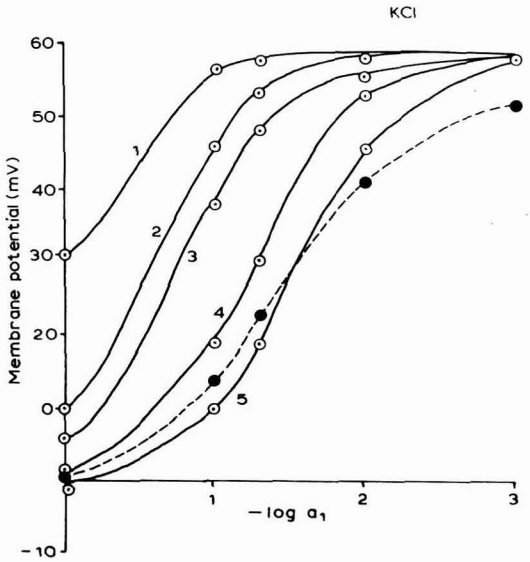

Fig. 1. Membrane potentials across silver iodide membrane in KCl of varying concns. (⊙) Calcd. values assuming $\omega\bar{x}$ equal to: (1) −0.4, (2) −0.1, (3) −0.06, (4) −0.02, (5) −0.01 *N*. (●) Observed values (with dashed line).

The fixed charge density of the silver iodide membrane was thus found to be −0.01 *N*. Assuming the same value for fixed charge density, the values of Donnan potentials, diffusion potentials and total membrane potentials were calculated for NaCl, LiCl and NH_4Cl at various concentrations. The calculated and observed values are given in Table 2 and shown in Figs. 2, 3 and 4.

A very good agreement between the observed and calculated values of membrane potential is observed in the case of KCl and NH_4Cl, thus showing that the behaviour of the silver iodide membrane is closely allied to Teorell's model. The agreement is only fair for NaCl but in the case of LiCl the deviation is quite marked. It should be noted that in our calculations we have assumed that the ionic mobilities in the membrane are the same as those in the free solution. The diffusion data in the literature show that the ion mobilities go through a considerable change in a charged phase, and hence apparent anionic mobilities (assuming cationic mobilities to be constant) were calculated as suggested by Willis[7].

The electrochemical nature of the membrane and its influence on the mobilities

TABLE 2

CALCULATED VALUES OF DONNAN POTENTIAL $(\pi_1+\pi_2)$, DIFFUSION POTENTIAL $(\phi_2-\phi_1)$ AND TOTAL MEMBRANE POTENTIAL E_{calc} (ASSUMING $\omega\bar{x}=-0.01$ N), AND THE OBSERVED VALUES OF MEMBRANE POTENTIAL E_{obs} ACROSS THE SILVER IODIDE MEMBRANE IN NaCl, LiCl AND NH_4Cl OF VARIOUS CONCENTRATIONS (AT 20°C)

Electrolyte	*Concns.* $a_1/a_2/M$	$(\pi_1+\pi_2)/mV$	$(\phi_2-\phi_1)/mV$	E_{calc}/mV	E_{obs}/mV
NaCl	1/0.1	1.12	−12.12	−11.0	−0.9
	0.1/0.01	10.89	−11.96	−1.07	8.20
	0.05/0.005	19.68	−10.99	8.69	20.11
	0.01/0.001	46.25	−4.8	41.45	40.75
	0.001/0.0001	57.85	−0.1	57.73	48.7
LiCl	1/0.1	1.12	−19.1	−17.98	0.5
	0.1/0.01	10.89	−19.22	−8.33	13.1
	0.05/0.005	19.68	−18.08	1.6	18.34
	0.01/0.001	46.25	−8.38	37.87	40.57
	0.001/0.0001	57.85	−0.22	57.63	47.75
NH_4Cl	1/0.1	1.12	−1.16	−0.04	−0.13
	0.1/0.01	10.89	−1.1	9.79	15.45
	0.05/0.005	19.68	−0.99	18.69	21.6
	0.01/0.001	46.25	−0.39	45.86	43.4
	0.001/0.0001	57.85	0.00	57.85	45.0

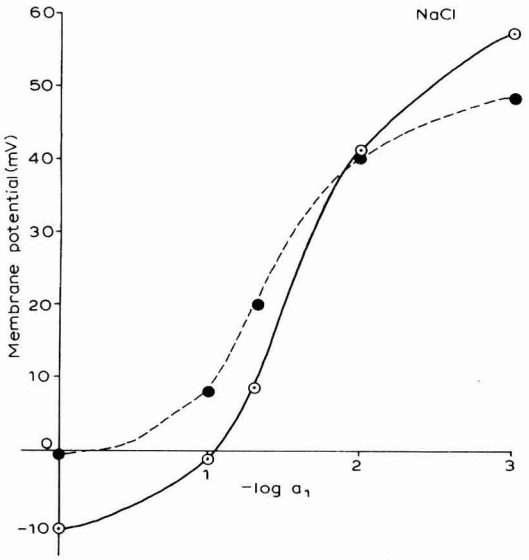

Fig. 2. Membrane potentials across silver iodide membrane in NaCl of varying concns. (⊙) Calcd. values assuming $\omega\bar{x}=-0.01$ N; (●) observed values.

of anions were also studied by calculating the mobility from the equation:

$$E_m = \frac{\frac{u}{z_+} - \frac{v}{z_-}}{u+v} \times \frac{RT}{nF} \ln \frac{f_1 c_1}{f_2 c_2} \qquad (E_m \text{ is the membrane potential}) \qquad (5)$$

where the various terms have their usual meanings. This procedure has been used by Willis[7] in the case of a cupric ferrocyanide membrane, and Malik and Siddiqi[8] in the case of a large number of metal ferrocyanide and ferricyanide membranes. The apparent anionic mobilities were calculated over the concentration range 1 – 0.0001

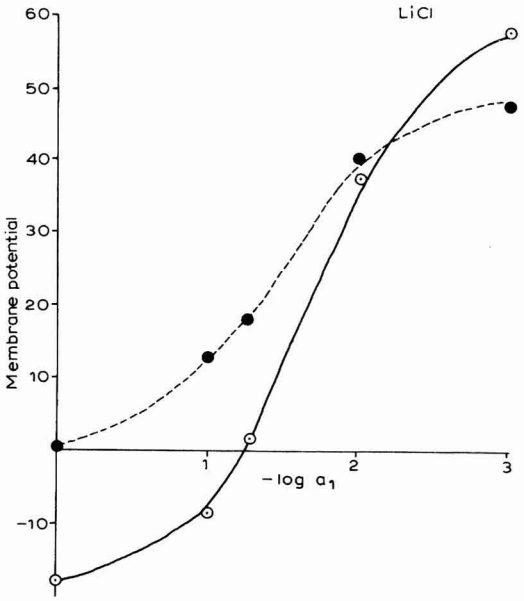

Fig. 3. Membrane potentials across silver iodide membrane in LiCl of varying concns. (⊙) Calcd. values assuming $\omega\bar{x} = -0.01$ N; (●) observed values.

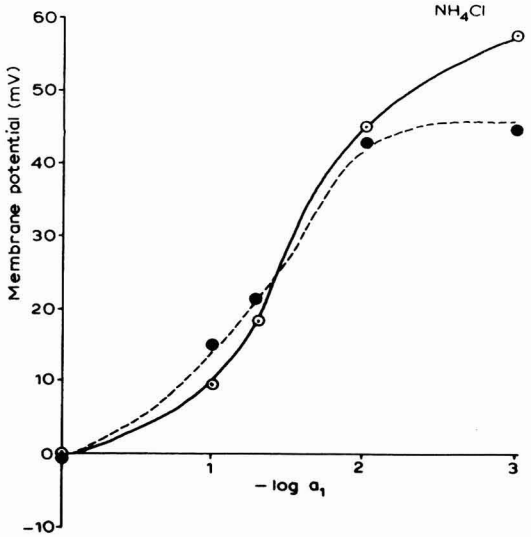

Fig. 4. Membrane potentials across silver iodide membrane in NH_4Cl of varying concns. (⊙) Calcd. values assuming $\omega\bar{x} = 0.01$ N; (●) observed values.

M, keeping $a_1/a_2 = 10$. The values of the mobility u for NH_4^+, K^+, Na^+, and Li^+ were taken to be those in free solution. The plots of $\log 1/a_1$ (where a_1 is the higher concentration) *vs.* apparent anion mobility for all the four electrolytes are shown in Fig. 6. The values of the transport numbers of cations t_+ were calculated from the equation:

$$t_+ = \frac{z_+ z_-}{z_+ + z_-}\left(\frac{E_m F}{RT \ln \frac{f_1 c_1}{f_2 c_2}}\right) + \frac{z_+}{z_+ + z_-} \tag{6}$$

for different electrolytes at various concentrations. The transport numbers of chloride

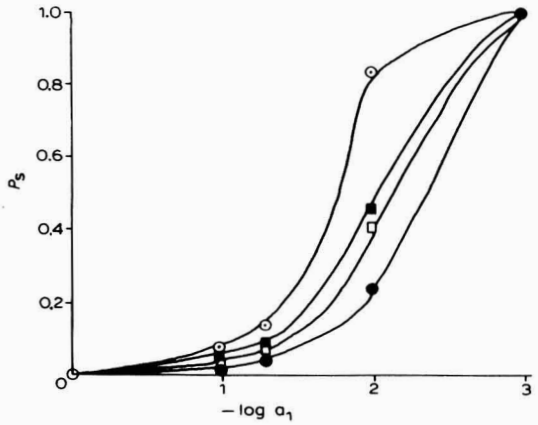

Fig. 5. Plots of P_s *vs.* $\log 1/a_1$ for various electrolytes. (⊙) NH_4Cl, (●) KCl, (□) NaCl, (■) LiCl.

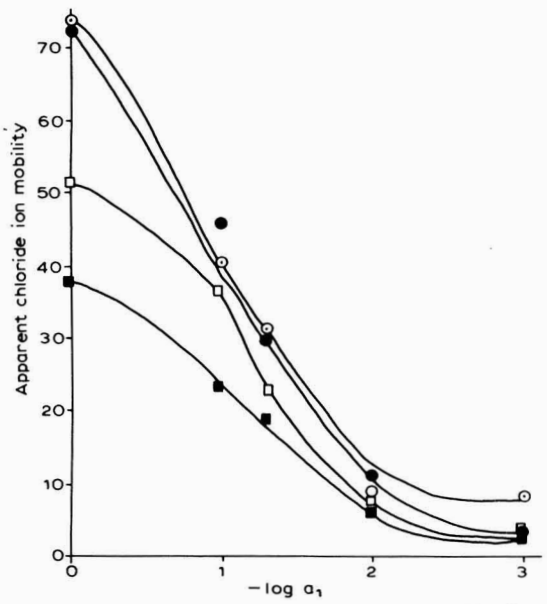

Fig. 6. Plots of apparent an ion mobility *vs.* $\log 1/a_1$ for various electrolytes. Designations as Fig. 5.

ion in an anionic membrane such as permionic ARX-44 were investigated by Clark *et al.*[13]. They plotted t_- against $\bar{n}$ where $\bar{n}$ is the geometric mean of the concentrations of two solutions across the membrane. A similar procedure was adopted in the case of the membrane under investigation and log $\bar{n}$ was plotted against t_+ for different cations; the plots are shown in Fig. 7. From the Figure it is quite clear that the values of the transport numbers of cations continue to decrease with increase in concentration. Jacobs[14] while using membranes of polymethacrylic acid in KOH solution over a wide concentration range found similar behaviour, *i.e.* t_+ decreased with increasing concentration of the electrolyte.

The permselectivity P_s[15] of the membrane is given by

$$P_s = \frac{\bar{t}_+ - t_+}{1 - t_+} \tag{7}$$

where $\bar{t}_+$ is the transport number in the membrane phase under highly idealized conditions of the TMS model 1 and is given by:

$$\bar{t}_+ = \frac{E_m}{2\,E_{max}} + 0.5 \tag{8}$$

According to Spiegler *et al.*[16], the permselective materials are defined as the media which transfer certain types of ion in preference to others. Tolliday *et al.*[17] have reported that cupric ferrocyanide membrane behaves similarly in some respects to the electronegative membrane of Sollner. The values of P_s calculated from the above equations are plotted *vs.* log $1/a_1$ (see Fig. 5). The permselectivity P_s increases abruptly in the region log $1/a_1 \rightarrow$ 1.5–2.5. The values of t_+, $\bar{t}_+$, P_s and apparent anion mobility for various concentrations of different electrolytes are summarized in Table 3.

The chief results of all these investigations show that the membrane potential can be determined with reasonable accuracy, and that in the case of a dilute solution it is somewhat closer to the maximum value (highest value of t_+ and therefore greatest

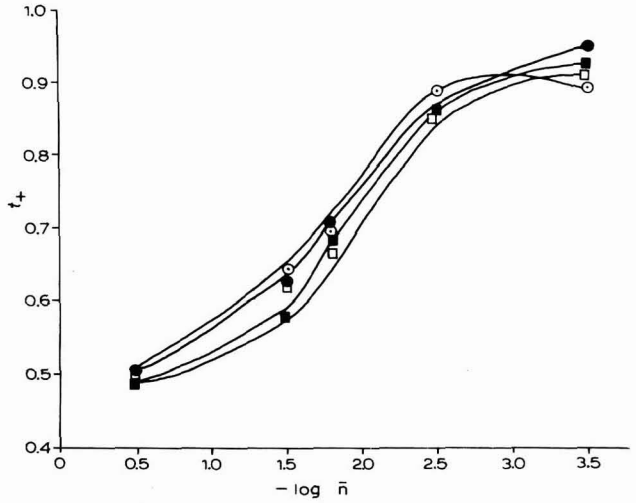

Fig. 7. Plots of t_+ *vs.* log $1/\bar{n}$ for various electrolytes. Designations as Fig. 5.

TABLE 3

VALUES OF t_+, $\bar{t}_+$, P_s AND APPARENT ANION MOBILITY FOR VARIOUS ELECTROLYTES AT DIFFERENT CONCENTRATIONS FOR SILVER IODIDE MEMBRANE (AT 20°C)

Electrolyte	*Concns.* $a_1/a_2/M$	t_+	$\bar{t}_+$	P_s	*Apparent anion mobility*/* $cm^2\,\Omega^{-1}\,equiv.^{-1}$
NH_4Cl	1/0.1	0.498	0.498	0.0	73.7
	0.1/0.01	0.643	0.671	0.0784	40.7
	0.05/0.005	0.698	0.74	0.139	31.6
	0.01/0.001	0.887	0.982	0.84	9.3
	0.001/0.0001	0.893	1	1	8.8
KCl	1/0.1	0.5038	0.504	0.0004	72.3
	0.1/0.01	0.628	0.634	0.0161	43.6
	0.05/0.005	0.709	0.722	0.0446	30.2
	0.01/0.001	0.863	0.896	0.241	11.7
	0.001/0.0001	0.9507	1	1	3.8
NaCl	1/0.1	0.491	0.491	0.00	51.6
	0.1/0.01	0.575	0.584	0.02	37.0
	0.05/0.005	0.682	0.706	0.074	23.3
	0.01/0.001	0.86	0.918	0.411	8.1
	0.001/0.0001	0.9248	1	1	4.1
LiCl	1/0.1	0.504	0.505	0.002	38.1
	0.1/0.01	0.620	0.637	0.0447	23.6
	0.05/0.005	0.667	0.692	0.075	19.4
	0.01/0.001	0.859	0.924	0.461	6.4
	0.001/0.0001	0.917	1	1	3.5

* Relative to free solution mobility of K^+ being taken as 73.5.

value of P_s). With more concentrated solutions this is not so, the membrane potential is progressively smaller than the maximum value. This is readily explained in terms of a decrease in membrane selectivity with increasing concentration of co-ions and diffusion of electrolyte through the membrane. All ion exchange membranes lose permselectivity with increase in concentrations of the solutions they separate. The parchment-supported silver iodide membrane shows high selectivity in the dilute range. In some ways this membrane is similar to an anion exchange membrane. This view is further confirmed by the observation of Heymann and Rabinov[18] that, like purified cellulose, parchment also contains exchangeable cations (and therefore acid groups) as part of its structure which may account for its negative charge. The exchangeable cations of this structure will be free to move in the pores and give an apparent increase in the cation mobility and therefore a decrease in the anion mobility (Fig. 6). Within the pores there will be a diffuse ionic atmosphere from the charged wall. The thickness of this atmosphere depends upon electrolyte concentration; in very dilute solutions of the electrolyte which are in contact with the membrane, the thickness becomes so great that only cations are present in the pores and the membrane is cation-permeable only (high value of P_s). As the concentration increases, the thickness of the ionic atmosphere decreases and anions will also be present; at high enough concentrations the ionic atmosphere will be negligible in comparision to the pore radius and the effect of the membrane vanishes.

Spiegler *et al.*[16] working with ion-exchange resin systems have explained the loss in permselectivity as due to increasing penetration of anions and cations into cation and anion exchange resins, respectively, and to the water transport. If the solutions are concentrated, the membrane acts as an inert material and the potential difference between the two solutions approaches the liquid junction potential value.

ACKNOWLEDGEMENT

The authors are grateful to Dr. S. M. F. Rahman, Head of the Chemistry Department, for providing facilities for carrying out these investigations.

SUMMARY

Membrane potentials across parchment-supported silver iodide membrane in NH_4Cl, KCl, NaCl and LiCl solutions of various concentrations have been determined to evaluate fixed charge density ($\omega\bar{x}$) and permselectivity of the membrane; $\omega\bar{x}$ of silver iodide membrane has been found to be -0.01 *N*. The effect of concentration on transport numbers, apparent anion mobility and permselectivity has been studied. The results have been discussed in the light of the TMS theory.

REFERENCES

1 K. H. MEYER AND J. F. SIEVERS, *Helv. Chim. Acta*, 19 (1936) 649, 665, 987. T. TEORELL, *Proc. Soc. Expt. Biol. Med.*, 33 (1935) 282; *Proc., Nat. Acad. Sci. U.S.*, 21 (1935) 152; *Z. Elektrochem.*, 55 (1951) 460; *Discussions Faraday Soc.*, 21 (1956) 22.
2 G. SCATCHARD, *J. Am. Chem. Soc.*, 75 (1953) 2883; *Discussions Faraday Soc.*, 21 (1956) 30; G. J. HILLS, P. W. M. JACOBS AND N. LAKSHMINARAYANIAH, *Proc. Roy. Soc., (London)*, A 262 (1961) 257; Y. KOBATAKE, *J. Chem. Phys.*, 28 (1958) 146; A. J. STAVERMAN, *Trans. Faraday Soc.*, 48 (1952) 176.
3 M. NAGASAWA AND I. KAGAWA, *Discussions Faraday Soc.*, 21 (1956) 52; M. NAGASAWA AND Y. KOBATAKE, *J. Phys. Chem.*, 56 (1952) 1017.
4 L. MICHAELIS, *Kolloid-Z*, 62 (1933) 1; MICHAELIS AND FUJITA, *Biochem. Z.*, 142 (1923) 398; *Z. Physik. Chem.*, 110 (1924) 266.
5 K. H. MEYER AND J. F. SIEVERS, *Helv. Chim. Acta*, 19 (1936) 649.
6 T. TEORELL, *Proc. Soc. Expt. Biol. Med.*, 33 (1935) 282; *Z. Elektrochem.*, 55 (1951) 460; *Proc. Natl. Acad Sci. U.S.*, 21 (1935) 152; *J. Gen. Physiol.*, 21 (1937) 107.
7 G. M. WILLIS, *Trans. Faraday Soc.*, 38 (1942) 172.
8 W. U. MALIK AND F. A. SIDDIQI, *Proc. Indian Acad. Sci.*, A 56 (1962) 206; *J. Colloid. Sci.*, 18 (1963) 161; *Bull. Chem. Soc. Japan*, 40 (1967) 8, 1741.
9 K. SOLLNER, *J. Phys. Chem.*, 49 (1945) 47; *J. Electrochem. Soc.*, 97 (1950) 139 C; *Ann. N.Y. Acad. Sci.*, 57 (1953) 177.
10 K. H. MEYER, *Trans. Faraday Soc.*, 33 (1937) 1073.
11 N. LAKSHMINARAYANIAH, *J. Appl. Polymer Sci.*, 10 (1966) 1687.
12 I. ALTUG AND M. L. HAIR, *J. Phys. Chem.*, 72 (1968) 599.
13 J. T. CLARK, J. A. MARINSKY, W. JUDA, N. W. ROSENBERG AND S. ALEXANDER, *J. Phys. Chem.*, 56 (1952) 100.
14 P. W. M. JACOBS, *Discussions Faraday Soc.*, 21 (1956) 198.
15 A. G. WINGER, G. W. BODAMEN AND R. KUNIN, *J. Electrochem. Soc.*, 100 (1953) 178.
16 K. S. SPIEGLER, R. L. YOEST AND M. R. J. WYLLIE, *Discussions Faraday Soc.*, 21 (1956) 174.
17 J. D. TOLLIDAY, E. F. WOODO AND E. J. HARTUNG, *Trans. Faraday Soc.*, 45 (1949) 148.
18 E. HEYMANN AND G. RABINOV, *J. Phys. Chem.*, 47 (1943) 655.
19 F. A. SIDDIQI AND S. PRATAP, *J. Electroanal. Chem.*, 23 (1969) 137.

ELECTROANALYTICAL CHEMISTRY AND INTERFACIAL ELECTROCHEMISTRY
Elsevier Sequoia S.A., Lausanne – Printed in The Netherlands

CHEMICAL AND ELECTROCHEMICAL REACTIONS OF NICKEL–NITROHYDROXYLAMINIC COMPLEXES IN UNBUFFERED MEDIUM*

A. CĂLUŞARU
Institute for Atomic Physics, Bucharest (Rumania)
(Received March 19th, 1969)

INTRODUCTION

A study of the reactions occurring between some metallic ions and sodium nitrohydroxylaminate, $Na_2N_2O_3$, demonstrates the complexing properties of this substance. In the case of nickel, conductometric determinations indicated the formation of two complexes: a monochelatic complex in the presence of excess nickel ions and a dichelatic in excess of nitrohydroxylaminate ions[1]. A polarographic study in ammoniacal buffer established the formation of the complex: $[Ni(N_2O_3)_2(NH_3)(H_2O)]^{2-}$. This complex is the result of a reaction between the nitrohydroxylaminate and nickel–ammino-complexes[2].

In this paper, the equilibrium reactions of nickel nitrohydroxylaminate complexes in unbuffered medium are investigated polarographically.

EXPERIMENTAL

The preparation and the purification of sodium nitrohydroxylaminate has been described previously[3]. A polarograph LP 60 was used. The polarographic cell has the cathodic compartment above the anodic compartment (a calomel electrode). The electric contact between the compartments was made through an orifice of 3 mm. This cell, constructed following Dr. Smoler's design[4], has the following advantages: (1) small electric resistance; (2) elimination of the solution mixture; (3) easy manipulation.

The capillary constants are: $m = 2.32$ mg s^{-1} and $t_1 = 3.67$ s in 0.1 M KCl solution, open circuit and $h = 85$ cm.

RESULTS

1. *Effect of sodium nitrohydroxylaminate concentration*

The addition of sodium nitrohydroxylaminate to a nickel-containing solution produces two effects (Fig. 1): (a) the division of the nickel wave; (b) the diminishing of this wave.

The division of the nickel wave in the presence of sodium nitrohydroxylaminate

* Paper presented to the Eleventh International Conference on Coordination Chemistry, Haïfa (Israel), September, 1968.

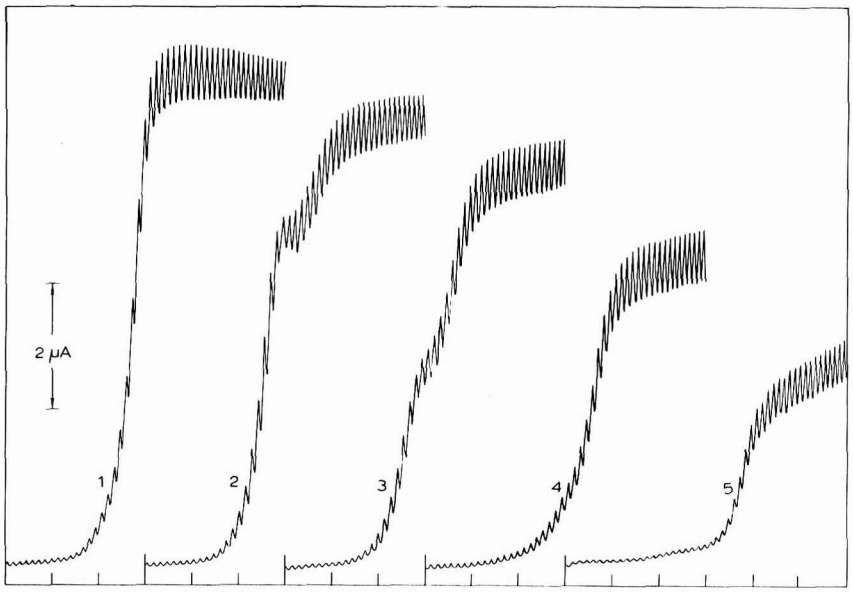

Fig. 1. Effect of $Na_2N_2O_3$ concn. on the polarographic wave of nickel. Ni^{2+}, 1×10^{-3} *M*; KCl, 2×10^{-2} *M*; gelatine, 0.02% (only for curves 1–3); $Na_2N_2O_3$: (1) 0; (2) 0.5; (3) 1; (4) 2; (5) 4.5 *M*. Starting potential, −0.4 V; anode SCE; 200 mV/absc.

TABLE 1

EFFECT OF SODIUM NITROHYDROXYLAMINATE CONCENTRATION ON THE RATIO OF POLAROGRAPHIC WAVES

No.	$Na_2N_2O_3/M$	Ni^{2+}	I_1/mm	I_2/mm
1	0	1×10^{-3}	217	0
2	0.5×10^{-3}	1×10^{-3}	148	50
3	1×10^{-3}	1×10^{-3}	90	90
4	2×10^{-3}	1×10^{-3}	0	138
5	4.5×10^{-3}	1×10^{-3}	0	81

indicates the formation of a nickel–nitrohydroxylaminic complex. The wave of the nitrohydroxylaminic complex is at more negative potentials than those of the hydrated nickel ion wave. Table 1 shows the ratio of the wave heights as a function of sodium nitrohydroxylaminate concentration. It is clear that in the case of low concentrations of sodium nitrohydroxylaminate the nickelnitrohydroxylaminic complex contains two ligand ions.

2. *Effect of the ionic strength*

The charge of nitrohydroxylaminic complexes is different from the charge of the simple nickel ion, owing to the two negative charges of the nitrohydroxylaminic ion. The possible nitrohydroxylaminic complexes of nickel are as follows: $[Ni(N_2O_3)(H_2O)_4]^0$, $[Ni(N_2O_3)_2(H_2O)_2]^{2-}$ and $[Ni(N_2O_3)_3]^{4-}$. The simple nickel ion has two positive charges and the half-wave potential of the corresponding wave

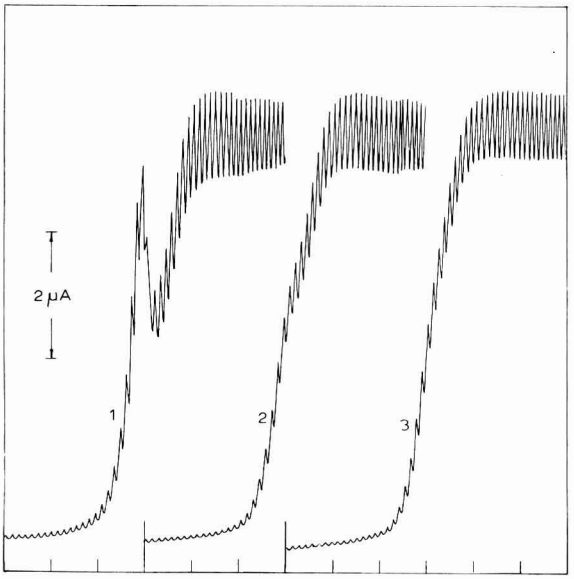

Fig. 2. Effect of the ionic force on the waves of nickel and the nitrohydroxylaminic complex. Ni^{2+}, 1×10^{-3} M; $Na_2N_2O_3$, 1×10^{-3} M; KCl: (1) 0.01; (2) 0.05; (3) 0.1 M. Starting potential, -0.4 V; anode SCE; 200 mV/absc.

will, therefore, be displaced in the region of more negative potentials by increasing the ionic strength. In the case of the all other complexes the displacement of the waves will be produced in the region of more positive potentials. By increasing the value of the ionic strength in solution from 0 to 0.1 (Fig. 2), the potentials in Table 2 were obtained. From this Table the displacement of the potentials is in the direction expected for increase of ionic strength. Identical results were obtained by using sodium perchlorate instead of potassium chloride.

TABLE 2

EFFECT OF THE IONIC STRENGTH ON THE NICKEL HALF-WAVE POTENTIALS IN THE PRESENCE OF SODIUM NITROHYDROXYLAMINATE (10^{-3} M)

Nickel concentration, 1×10^{-3} M, SCE anode

No.	*KCl/M*	*First wave* $E_{\frac{1}{2}}/V$	*Second wave* $E_{\frac{1}{2}}/V$
1	0	−0.890	−1.140
2	0.01	−0.900	−1.130
3	0.02	−0.940	−1.135
4	0.03	−0.940	−1.125
5	0.04	−0.945	−1.125
6	0.05	−0.960	−1.120
7	0.07	−0.950	−1.110
8	0.10	−0.975	−1.120

3. *Effect of temperature*

Temperature has a marked effect on the polarographic wave in the system nickel–sodium nitrohydroxylaminate. Curve 2 on Fig. 3 shows that at 25°C, in a large excess of nitrohydroxylaminate, only one wave with a small height is formed and this wave is displaced towards more negative potentials; this can be seen more easily in Fig. 1. At a temperature of 56°C (curve 4, Fig. 3) the wave height is considerably increased, being comparable with the height of the nickel wave. At the same time a new wave appears at distinctly more positive potentials. This wave is located in the region of the nickel wave (curve 3, Fig. 3). Curve 5 on Fig. 3 shows that nitrohydroxylaminic ion in the absence of nickel does not form any wave in the potential region where the two waves appear in the presence of nickel ions.

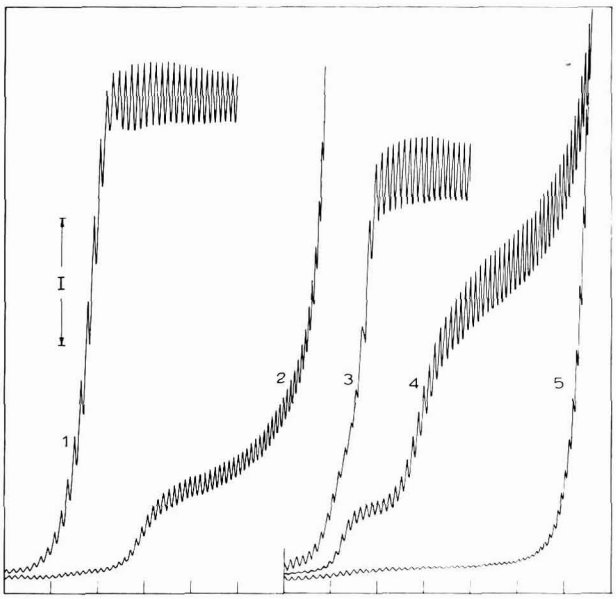

Fig. 3. Effect of temp. on the Ni^{2+} (10^{-3} *M*) wave in the presence of $Na_2N_2O_3$ (8.8×10^{-3} *M*); KCl, 2×10^{-2} *M*. (1) Ni^{2+} wave without $Na_2N_2O_3$ at 25°C; (2) same wave with $Na_2N_2O_3$ at 25°C; (3) Ni^{2+} wave without $Na_2N_2O_3$ at 56°C; (4) same wave with $Na_2N_2O_3$; (5) the polarogram in the solution: $Na_2N_2O_3$, 8.8×10^{-3} *M*; KCl, 2×10^{-2} *M*; temp. 56°C. Starting potential, −0.6 V. I = 2 μA for curves 1 and 2; I = 4 μA for curves 3, 4 and 5. Anode SCE; 200 mV/absc.

4. *Effect of the height of the mercury head*

The character of the waves appearing in the system, nickel–sodium nitrohydroxylaminate, may be established by plotting the wave height as a function of the square root of the height of the mercury head. In the case of the first wave, corresponding to curve 4 on Fig. 3, a straight line (see Fig. 4) was obtained. Concomitant with the diffusion component, the existence of a strong kinetic effect is to be observed, because the extrapolation of the straight line intercepts the ordinate axis at 50 mm above the origin.

In order to establish the character of the second wave (curve 4, Fig. 3) it is of advantage to use lower temperatures when the first wave does not appear. It can be

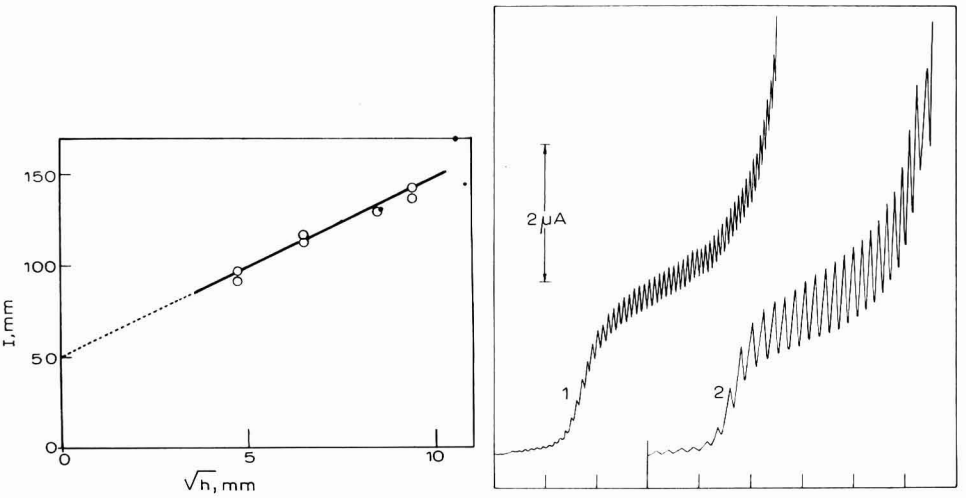

Fig. 4. Variation of the first wave height (curve 4, Fig. 3) as a function of the square root of the mercury head height. Temp. 56°C.

Fig. 5. Effect of the height of mercury head on the Ni^{2+} (10^{-3} *M*) wave in excess $Na_2N_2O_3$ (4.5×10^{-3} *M*). (1) $h = 85$; (2) $h = 43$ cm; starting potential, -0.8 V; anode SCE; 200 mV/absc.

seen from Fig. 5 that the height of the mercury head pratically does not affect the height in excess of sodium nitrohydroxylaminate. This independence of the height of the mercury head shows the kinetic character of this wave.

DISCUSSION

From Fig. 1 and Table 1 it follows that for low sodium nitrohydroxylaminate concentrations (0–1×10^{-3} *M*) at a nickel ion concentration of 1×10^{-3} *M*, the ratio of wave heights shows the formation of a complex with two ligand ions. In the region of the first wave the nickel ions present in solution and the nickel ions resulting from the complex dissociation are discharged. The electrode reaction is therefore as follows:

$$[Ni(N_2O_3)_2(H_2O)_2]^{2-} + 4\,H_2O \underset{\sigma_1\rho_1}{\overset{\rho_1}{\rightleftharpoons}} [Ni(H_2O)_6]^{2+} + 2\,N_2O_3^{2-} \qquad (1)$$

$$+ 2e \downarrow \varepsilon_1^{1/2}$$

$$\text{Ni(Hg)}$$

$\varepsilon_1^{1/2}$ is the half-wave potential. ρ_1 is the rate of the dissociation reaction and $\sigma_1\rho_1$ the rate of formation of the nitrohydroxylaminic complex, according to the notation used currently[2]. σ_1 is given by the ratio:

$$\sigma_1 = \frac{\{[Ni(N_2O_3)_2(H_2O)_2]^{2-}\}}{\{[Ni(H_2O)_6{}^{2+}\}} \qquad (2)$$

Reaction (1) shows that the electrode reaction is preceded by a dissociation reaction of the complex containing two nitrohydroxylaminic ligands to the hydrated nickel ions.

At room temperature the kinetic effect represented by reaction (1) is small, because the ratio of the wave heights corresponding to the simple and complex ion at $0\text{–}2 \times 10^{-3}$ M $N_2O_3^{2-}$ concentrations is identical with the theoretical value in the case of a complex with two ligands. Therefore, the equilibrium of reaction (1) is practically displaced to the left-hand side.

The diminishing of the total wave heights, corresponding to the discharge of the simple and complex nickel ions (Fig. 1) shows the formation of a non-reducible complex, containing more than two ligand groups $N_2O_3^{2-}$. It is possible that the 4 negative charges of a complex with 3 ligands may suffer a strong electrostatic repulsion from the negatively polarised electrode and thus cannot be reduced on the cathode. The effect of an inhibition phenomenon, owing to nitrohydroxylaminate adsorption, is not probable, because the negative part of the electrocapillary curve is not modified by the presence of large sodium nitrohydroxylaminate concentrations, in neither simple nor nickel complex form.

If we consider the formation of the simple nickel complexes it follows that with a very large nitrohydroxylaminate excess, the only possibility is the formation of the complex with three ligands. In the case of a high ratio of sodium nitrohydroxylaminate to nickel concentration, the chemical and electrode reactions are as follows:

$$[Ni(N_2O_3)_3]^{4-} \underset{\sigma_2\rho_2}{\overset{\rho_2}{\rightleftharpoons}} [Ni(N_2O_3)_2(H_2O)_2]^{2-} \underset{\sigma_1\rho_1}{\overset{\rho_1}{\rightleftharpoons}} [Ni(H_2O)_6]^{2+} \qquad (3)$$

$$+2e\,\underset{Ni(Hg)}{\Big\|}\varepsilon_2^{1/2} \qquad +2e\,\underset{Ni(Hg)}{\Big\|}\varepsilon_1^{1/2}$$

In this reaction $\varepsilon_1^{1/2}$ represents the half-wave potential of the corresponding wave and the double arrow indicates an electron transfer reaction.

The equilibria represented by reaction (3) are clearly showed by polarogram 4 on Fig. 3. At a temperature of 56°C, ρ_1 reaches a great enough value and therefore the wave of hydrated nickel ions appears very clearly. The kinetic character of this wave is shown in Fig. 4. The rate constant ρ_2 must be greater than ρ_1, because the corresponding wave is large enough even at the room temperature and the kinetic component of this wave is predominant (Fig. 5).

SUMMARY

The addition of sodium nitrohydroxylaminate in a unbuffered nickel solution produces two effects: (1) the division of the nickel wave; (2) the diminishing of this wave. These two effects show the formation of nickel–nitrohydroxylaminic complexes. The double nickel wave formed at relatively small sodium nitrohydroxylaminate concentrations contains in the first part the discharge of the simple hydrated nickel ion, and in the second part the discharge of a nickel complex with two nitrohydroxylaminic ligands. The diminishing of the wave is produced by the formation of a non-reducible nickel complex, containing three nitrohydroxylaminic ligands. The waves corresponding to the two-ligand complex and to the hydrated nickel ion (at 56°C) in a large excess of sodium nitrohydroxylaminate have, however, an important kinetic character. These experimental results indicate the following chemical and electrochemical reactions:

$$[Ni(N_2O_3)_3]^{4-} \rightleftharpoons [Ni(N_2O_3)_2(H_2O)_2]^{2-} \rightleftharpoons [Ni(H_2O)_6]^{2+}$$
$$+2e \downarrow\!\!\downarrow \qquad +2e \downarrow\!\!\downarrow$$
$$Ni(Hg) \qquad Ni(Hg)$$

REFERENCES

1 J. Vepřek-Šiška, V. Pliška and F. Šmirous, *Collection Czech. Chem. Commun.*, 24 (1959) 3548.
2 A. Căluşaru and J. Kůta, *Collection Czech. Chem. Commun.*, 32 (1967) 1331.
3 A. Căluşaru and J. Kůta, *Collection Czech. Chem. Commun.*, 31 (1966) 814.
4 I. Smoler, *Collection Czech. Chem. Commun.*, 33 (1968) 1036.
5 J. Koryta, *Collection Czech. Chem. Commun.*, 23 (1958) 1048; 24 (1959) 2903; 24 (1959) 3057.
6 J. Heyrovský and J. Kůta, *Principles of Polarography*, Publishing House of the Czechoslovak Academy of Sciences, Prague 1965, p. 369.

Elsevier Sequoia S.A., Lausanne – Printed in The Netherlands

SHORT COMMUNICATIONS

Polarography of Fe(III)-hematoporphyrin(IX)

The polarographic reduction of Fe(III)-protoporphyrin(IX) has been the subject of several studies[1-3] which have shown that Fe(III)-protoporphyrin exists primarily as a dimer in the pH range 7–12.5. The reduction product, Fe(II)-protoporphyrin, also exists as a dimer from pH 9–12.5 but a monomeric product is formed at other pH values[3]. In addition the product polymerizes with time as shown by the fact that no anodic current is measured with a DME when a solution of the Fe(II)-protoporphyrin is produced by controlled potential electrolysis. The tendency to form dimers and polymers is eliminated if the solutions under investigation are made with a mixture of water and ethanol[1].

In order to gain more information about the structure of metalloporphyrin dimers, a series of experiments was performed using Fe(III)-hematoporphyrin(IX) rather than Fe(III)-protoporphyrin(IX). The only difference between hematoporphyrin and protoporphyrin is that the former has $-CHOHCH_3$ in the 2- and 4-positions of the porphyrin ring while the latter has $-CH=CH_2$ groups[4]. Both porphyrins have two $-CH_2CH_2COOH$ groups which might act to form a linkage between one Fe-porphyrin unit and the iron center of another[5], thus producing dimers. On the other hand, water[6] may be the bridging group between two iron centers. However, it has been shown by X-ray crystallographic analysis that the dimer of N-hydroxyethylenediaminetriacetate complex of Fe(III) is held together by an oxo-bridge[7] which might also be expected in porphyrin dimers.

Experimental

Fe(III)-hematoporphyrin(IX) was synthesized from ferric acetate and hematoporphyrin(IX) dihydrochloride (Nutritional Biochemical Corporation). Two grams of ferric acetate were dissolved in 45 ml of glacial acetic acid and air was removed by bubbling nitrogen through the solution. A slight excess of hydrazine was added to reduce the iron to the +2 oxidation state. Forty-five ml of a deaerated solution containing one gram of hematoporphyrin dihydrochloride in glacial acetic acid was mixed with the ferrous acetate solution while still passing nitrogen. The solution was allowed to stand overnight and 300 ml of air-saturated distilled water was added. The Fe(III)-hematoporphyrin precipitate was separated from the solution by centrifugation, washed three times with water and vacuum dried over P_2O_5.

Polarograms were recorded on a Sargent Model XVI polarograph or a Beckman Electroscan 30 using standard techniques.

Results and discussion

Polarograms were recorded for the reduction of Fe(III)-hematoporphyrin(IX) to Fe(II)-hematoporphyrin(IX) in aqueous buffers (pH values between 8.4 and 9.2). The ionic strength was varied between 0.18 and 1.0 with sodium nitrate and the concentration of Fe(III)-hematoporphyrin between 0.37 and 0.90 m*M*.

The average value for $E_{\frac{3}{4}} - E_{\frac{1}{4}}$ was 54 mV in good agreement with the theoretical value of 56 mV for a reversible one-electron reduction of a monomeric reactant to a monomeric product. Plots of log $[i/(i_d - i)]$ *vs.* E were straight and had a slope of 60 mV. The ratio of diffusion current to concentration was constant and the value of the $E_{\frac{1}{2}}$ was independent of concentration at constant pH ($E_{\frac{1}{2}} = -0.496$ V *vs.* SCE at pH 8.7). The $E_{\frac{1}{2}}$ did vary with pH, $\Delta E_{\frac{1}{2}}/\Delta$pH being equal to -60 mV indicating that one hydroxide ion was produced for each electron transferred. The value of the diffusion current varied directly as the square root of the height of the mercury column indicating a diffusion-controlled process.

This evidence indicates conclusively that the electrode reaction is a reversible one-electron reduction without kinetic complications and that dimers are not involved. The electrode reaction may thus be formulated:

$$\begin{bmatrix} H_2O \\ | \\ Fe(III) - P \\ | \\ OH \end{bmatrix} + H_2O + e^- \rightleftharpoons \begin{bmatrix} H_2O \\ | \\ Fe(II) - P \\ | \\ H_2O \end{bmatrix} + OH^-$$

where $-$P symbolizes the hematoporphyrin ring.

These results are in direct contrast to those found for Fe(III)-protoporphyrin (IX)[3]. In this case it has been shown that Fe(III)-protoporphyrin exists as a dimer in the pH range 7–12.5, and that this material is reduced to a dimer below pH 9 and to a monomer above pH 9. Moreover, it was determined that the reduction product, Fe(II)-protoporphyrin, polymerized with time over the pH range studied as shown by the fact that no anodic current could be recorded for a solution of the reduction produced by controlled potential electrolysis. When this experiment was tried here for Fe(II)-hematoporphyrin, an anodic polarographic wave was found that was equal in diffusion current and $E_{\frac{1}{2}}$ to the cathodic wave recorded before controlled potential electrolysis. Thus, Fe(II)-hematoporphyrin does not polymerize as does its protoporphyrin analogue.

At first glance it might seem surprising that the substitution of $-CHOHCH_3$ groups for $-CH{=}CH_2$ on the porphyrin ring would cause such a large difference in the tendency of iron prophyrins to form dimers or polymers. However, the vinyl group is known to have strong electron-withdrawing power[4], and thus enhances the tendency of the metal ion in the protoporphyrin ring to coordinate with various ligands. Apparently, the added coordinating power enables dimers or even polymers to form in aqueous solution. Unpublished work in this laboratory on the complexes of nitrogenous ligands with Fe(II) proto- and hematoporphyrins also confirms the fact that Fe(II)-protoporphyrin always forms the stronger complexes with a particular ligand[8].

It should also be mentioned that the mechanism of the monomerization of Fe(III)/Fe(II)-protoporphyrins by ethanol[1] appears to be due to the fact that ethanol can act as a ligand, replacing water coordinated with the central iron ion[9]. If ethanol can replace water (but not hydroxide)[1,9] and can prevent dimerization it may be that the coordinated water is a necessary component of the bridge between two iron porphyrins when a dimer is formed. On the other hand, it may be that the increased complexing ability found with protoporphyrins is of precisely the right strength to

allow formation of discrete dimers (with a carboxylate bridge) and yet to prefer coordination with ethanol when the latter is available.

Acknowledgement

This investigation was supported in part by National Science Foundation Grant GP-8565.

Department of Chemistry,
Louisiana State University in New Orleans,
New Orleans, Louisiana 70122 (U.S.A.)

J. G. MONTALVO JR.
D. G. DAVIS

1 D. G. DAVIS AND R. F. MARTIN, *J. Am. Chem. Soc.*, 86 (1966) 1365.
2 T. M. BEDNARSKI AND J. JORDAN, *J. Am. Chem. Soc.*, 86 (1964) 5690.
3 T. M. BEDNARSKI AND J. JORDAN, *J. Am. Chem. Soc.*, 89 (1967) 1552.
4 J. E. FALK, *Porphyrins and Metalloporphyrins*, Elsevier, New York, 1964.
5 R. LEMBERG AND J. W. LEGGE, *Hematin Compounds and Bile Pigments*, Interscience, New York, 1949.
6 R. I. WALTER, *J. Biol. Chem.*, 196 (1951) 151.
7 S. J. LIPPARD, H. SCHUGAR AND C. WALLING, *Inorg. Chem.*, 10 (1967) 1825.
8 D. G. DAVIS AND J. G. MONTALVO, unpublished experiments.
9 H. R. GYGAX AND J. JORDAN, *Disc. Faraday Soc.*

Received October 25th, 1968

J. Electroanal. Chem., 23 (1969) 164–166

Theoretical calculation of polarographic solution resistance
Comment on the paper by Britz and Bauer

In their calculation of the solution resistance R_s between the DME and counter electrode in a polarographic cell, Britz and Bauer[1] have incorrectly calculated the area of the truncated spherical shell of radius r surrounding the mercury drop of radius a. Referring to Fig. 1 in their paper, eqn. (4) should read

$$A = \int_{\cos^{-1}(a/r)}^{\pi} 2\pi r^2 \sin\theta \, d\theta \tag{1}$$

Integration yields

$$A = 2\pi r(a+r) \tag{2}$$

The same result can be obtained from a standard mensuration formula[2]. On substituting for A, their eqn. (5) becomes

$$R_s = \frac{\rho}{2\pi} \int_a^d \frac{dr}{r(r+a)} \tag{3}$$

Integration by partial fractions gives the result:

$$R_s = \frac{\rho}{2\pi a} \ln \frac{2d}{d+a} \tag{4}$$

In the limit, as d tends to infinity,

$$R_s^{\infty} = \frac{\rho}{2\pi a} \ln 2 \qquad (5)$$

The experimental values of a and d used in the calculations of Table 1[1] were 0.5 mm and 20 mm respectively. Recalculation of R_s using eqns. (4) and (5) result in the values presented in columns three and four of the following Table:

COMPARISON OF THEORETICAL CALCULATIONS WITH EXPERIMENTAL VALUES OF R_s

Electrolyte /M KCl	R_s/Ω			
	Exptl.	*Eqn.* (8)[1]	*Eqn.* (4)	*Eqn.* (5)
1.00	20.5	18.3	17.8	18.5
0.10	155	158	155	161
0.01	1380	1440	1407	1460

The values for R_s calculated from eqns. (4) and (5) are in surprisingly good agreement with the experimental results of Britz and Bauer. The assumption of radial current flow, however, cannot be valid close to the face of the capillary. The correct solution to the problem must be obtained from a solution of Laplace's equation with appropriate boundary conditions.

Department of Chemistry, University of Toronto, Toronto, Ontario (Canada) D. F. TAYLOR

Department of Chemistry, Carleton University, Ottawa, Ontario (Canada) R. G. BARRADAS

Taylor and Barradas are correct in their statements. The effect of the corrected calculation is small in magnitude, but indicates that our model of a truncated sphere with radial current flow is rather better than we had thought. It is also correct that a physically true treatment will involve solution of the Laplace equation; we are developing a computer program capable of this, though for a somewhat different purpose. The main point of our original article stands, that the model is considerably better than others in use, and the equations of Taylor and Barradas enhance the value of the model by showing that application involves only a very simple calculation.

Department of Chemistry, University of Kentucky, Lexington, Kentucky 40506 (U.S.A.) H. H. BAUER
D. BRITZ

1 D. BRITZ AND H. H. BAUER, *J. Electroanal. Chem.*, 18 (1968) 1.
2 *Handbook of Chemistry and Physics*, Chemical Rubber Publishing Company, 48th ed., 1967, p. A258.

Received September 10th, 1968

Elsevier Sequoia S.A., Lausanne – Printed in The Netherlands

Interfacial tension measurements between mercury and dilute aqueous electrolytes

Introduction

There has been some interest[1-3] in the comparison of electrocapillary data obtained from capillary electrometer and electrode capacitance measurements for the mercury–aqueous electrolyte interface. Some of the discrepancies between these two types of measurement have been shown[3,4] to be caused by variations of the contact angle between Hg and glass on changes of potential.

The present communication describes the application of a maximum "bubble" pressure method for electrocapillary measurements of fluoride solutions, where changes of contact angle are known to occur. In principle, this method should be independent of the contact angle[5] and it has been applied before[6] to the study of Na_2SO_4 solutions.

Experimental

The apparatus used is shown in Fig. 1. Nitrogen gas was admitted to reservoir I through taps F and G. The rate of increase of pressure was controlled by means of the greaseless screw tap G and by the regulation of the inlet pressure. The ballast A was included to even out any sudden pressure changes in the system and also to permit the gradual increase in pressure in I. The gas flow was stopped when Hg drops started to form at the capillary tip, by closing tap F. The maximum pressure the mercury

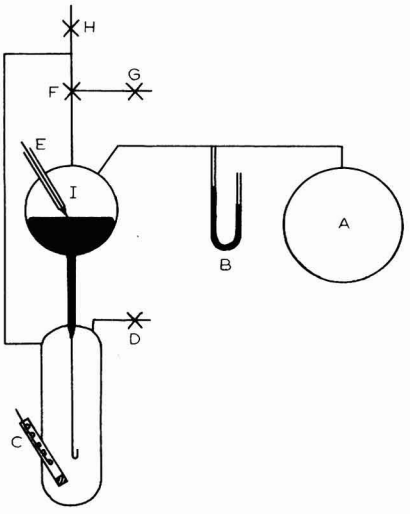

Fig. 1. Diagram of apparatus. (A) Ballast; (B) Hg manometer; (C) Ag/AgCl ref. electrode; (D, F and G) N_2-inlet taps; (H) N_2-outlet tap; (E) Pt contact to Hg; (I) Hg reservoir.

"bubble" could stand was read from manometer B by means of a cathetometer reading to 0.01 mm. The mercury head over the capillary was added to this reading. The height of this head did not change appreciably during the course of an experiment. The flow of mercury through the capillary was stopped by applying pressure to the cell by closing tap H and letting N_2 gas pass from the pressure line to the cell. This was found necessary since the flow of mercury through the capillary did not stop when the pressure was lowered to a value smaller than the maximum "bubble" pressure. This effect was probably caused by the mechanical momentum associated with the moving liquid metal inside the capillary.

The solutions were degassed with White Spot quality N_2 and the potentials were applied through a Ag/AgCl/0.1 *N* KCl reference electrode with a Tinsley potentiometer type 3387 B for the 0.1 *N* solutions. For the 0.01 *N* solutions, the potential was applied through a Hg pool electrode and measured with respect to the Ag/ACl electrode. A galvanometer was put in series to detect any polarization current flowing through the cell while the pressure was being increased. The moment Hg drops started to form could be determined, at potentials sufficiently far from the ECM, by the sudden flow of current through the galvanometer. At potentials near to the ECM, the appearance of drops was observed visually.

Two different types of capillaries were used. A simple drawn-out capillary dipped vertically in the solution worked satisfactorily with a 0.1 *N* KCl solution, but gave results lower in the anodic branch than those obtained from the integration of capacitance data for a more dilute KCl solution[7] and for KF solutions, and also showed a not very reproducible behaviour in this potential region. These two effects were probably due to both a finite contact angle on anodic potentials and the sticking of the Hg to the capillary walls. These difficulties were overcome by using an inverted (U-shaped), uniform bore, siliconized capillary. Under these conditions, the method is identical with a maximum bubble pressure experiment. Another advantage of an inverted capillary of uniform bore was that the rate of movement of the Hg inside the capillary could be easily regulated by the rate of increase of pressure. The correction for deviations of the meniscus shape from an hemisphere was negligible for the radius employed (0.0014 cm)[5].

KCl was purified by two crystallizations of the AnalaR product from tridistilled water. B.D.H. KF was recrystallized four times in polyethylene beakers. The salt was acidified with AnalaR HF and fired in a Pt dish to destroy any traces of surface-active materials before use. The water employed in the preparation of the solutions was distilled three times, twice from alkaline permanganate solutions, and in the case of the fluoride solutions, it was boiled before use, to eliminate the possibility of carbonate formation.

Results and Discussion

The 0.1 *N* KCl solution was measured with a drawn-out capillary dipped vertically in the solution, and no difference with the capacitance data was observed (Fig. 2). This experimental arrangement gave results, however, which were dependent on the contact angle of the Hg, as can be seen in the dilute solutions studied (Figs. 2 and 4). The discrepancies previously reported[2] for 0.01 *M* KCl solutions, disappeared when a method of measurement independent of the contact angle, such as the one described, was employed.

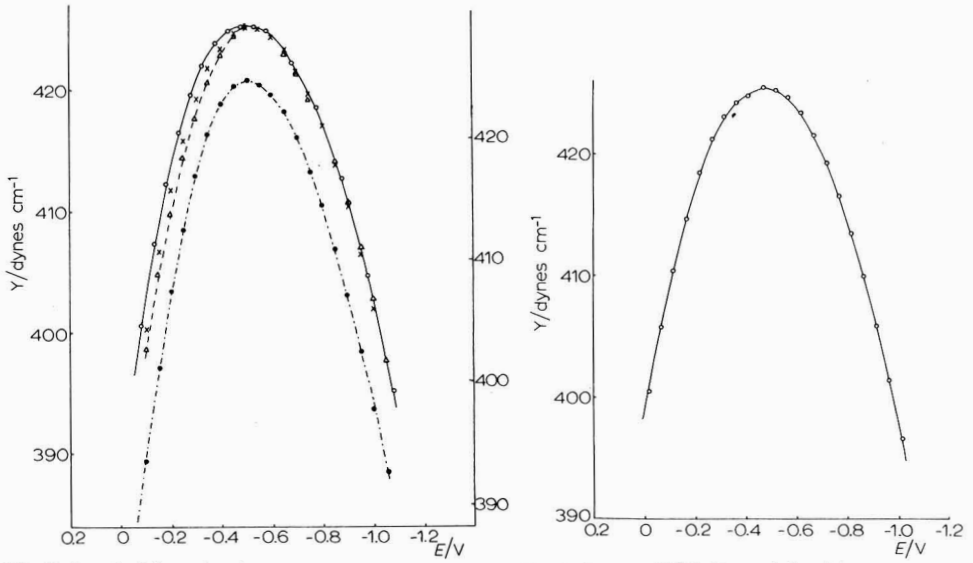

Fig. 2. Interfacial tension between Hg and 0.1, 0.01 *N* KCl solutions at 25°C. Potentials with respect to a 1 *N* calomel electrode. (–·–·–) 0.1 *N* KCl, Grahame integrated capacitance (ref. 8), (●) 0.1 *N* KCl, present method; (————) 0.01 *N* KCl, integrated capacitance (ref. 7), (○) 0.01 *N* KCl, present method, inverted siliconized capillary; (×) *idem*, but vertically dipped, drawn-out non-siliconized capillary; (△) 0.01 *N* KCl, electrometer results (ref. 2).

Fig. 3. Interfacial tension between Hg and 0.1 *N* KF at 25°C. (———) Integrated capacitance data (ref. 7), (○) present method, inverted capillary.

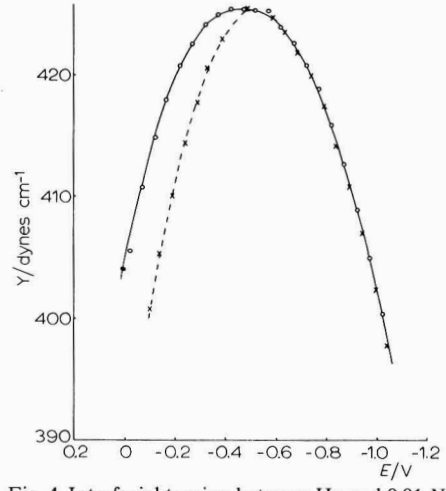

Fig. 4. Interfacial tension between Hg and 0.01 *N* KF at 25°C. (———) Integrated capacitance data (ref. 7), (○) present method, inverted capillary, (×) present method, vertical capillary.

The influence of a finite contact angle between Hg and glass in electrocapillary measurements can be clearly seen in the KF solutions (Figs. 3 and 4), where, as ob-

served by Lawrence *et al.*[3], the variation of the wetting properties of glass on anodic polarizations gave rise to electrocapillary data at variance with integrated capacitance results. As in the case of the 0.01 *N* KCl solution, the discrepancies disappeared when a maximum "bubble" pressure method was employed.

Chemistry Department, The University, Southampton S09 5NH, (England) D. J. SCHIFFRIN

1 R. PAYNE, *J. Electroanal. Chem.*, 15 (1967) 95.
1 J. O'M. BOCKRIS, K. MULLER, H. WROBLOWA AND Z. KOVAC, *J. Electroanal. Chem.*, 15 (1967) 101.
3 J. LAWRENCE, R. PARSONS AND R. PAYNE, *J. Electroanal. Chem.*, 16 (1968) 193.
4 R. PARSONS, *Rev. Pure Appl. Chem.*, 18 (1968) 91.
5 A. W. ADAMSON, *Physical Chemistry of Surfaces*, Interscience Publishers, London, New York, 1960.
6 J. JACKSON, *Trans. Faraday Soc.*, 36 (1940) 1248.
7 D. J. SCHIFFRIN, unpublished results.
8 M. A. V. DEVANATHAN AND P. PERIES, *Trans. Faraday Soc.*, 50 (1954) 1236.

Received April 22nd, 1969

Elsevier Sequoia S.A., Lausanne – Printed in The Netherlands

NEWS ITEM

THE URINARY MERCURY CONTENT OF ELECTROANALYTICAL CHEMISTS

The urinary level of mercury is used as a general index of exposure to mercury. While the level of mercury is not always correlated with the severity or appearance of clinical symptoms, at least 0.15 mg l^{-1} of mercury is excreted once clinical symptoms have been observed[1]. Different values have been given for normal urinary levels of mercury, such as 1 μg/day[2] and 5–90 μg/day[3]. However, the maximum normal excretion is generally considered to be 0.03 mg l^{-1}.

Electroanalytical and other chemists are constantly exposed to mercury. Because of the danger of this exposure, the author has made a practice of monitoring the urinary mercury levels of workers in his laboratory. The method of Nobel and Nobel[1] is employed. The laboratory is well ventilated and no significant levels of mercury have been observed. In specific, the level in a 29-year old worker (male) who has worked for 6 years and a 27-year old worker (male) who has worked for 3 years in the laboratory is less than 0.012 mg l^{-1}. It appears that with well ventilated laboratories, the urinary mercury level is no higher than in non-exposed individuals and that there is little danger of mercury intoxication under ordinary conditions. However, this sampling of a single laboratory is admittedly small and it is suggested that other workers present further evidence. Conditions of the laboratory which might be correlated with elevated or dangerous levels of mercury should be reported when excesses of 0.03 mg l^{-1} of mercury are found.

Department of Chemistry,
University of Kentucky,
Lexington, Kentucky 40506 (U.S.A.)

GARY D. CHRISTIAN

1 S. NOBEL AND D. NOBEL, *Clin. Chem.*, 4 (1958) 150.
2 G. W. MONIER-WILLIAMS, *Trace Elements in Food*, Chapman and Hall, London, 1949, p. 453.
3 M. BUCKNELL, D. H. HUNTER, R. MILTON AND K. M. A. PERRY, *Brit. J. Ind. Med.*, 3 (1946) 55.

Received February 15th, 1968; in revised form June 28th, 1968.

ELECTROANALYTICAL CHEMISTRY AND INTERFACIAL ELECTROCHEMISTRY App. 1
Elsevier Sequoia S.A., Lausanne - Printed in The Netherlands

PRELIMINARY NOTE

MECHANISTIC STUDIES OF THE DECOMPOSITION OF DIHALONITROBENZENE ANION RADICALS

The electrochemical behavior of monohalonitrobenzenes has been shown recently to depend upon the halogen substituent[1–5], steric interaction[5], electrolyte[1,2,4], solvent[1], and the applied potential[4]. In this communication we report the results of our investigation of the electrochemical reduction of dihalonitrobenzenes in dimethylformamide (DMF) and acetonitrile (AN) and the effect of applied potential on anion radical formation. A polarographic examination of 2,6-dihalonitrobenzenes has been reported recently[2], but the results were presented without interpretation.

The cyclic voltammetric examination of 2,6-dichloronitrobenzene in DMF–0.1 *F* tetraethylammonium perchlorate (TEAP) shows a single reduction peak near −1.13 V on the first cathodic sweep. After reversal of the potential scan at −1.5 V, the anodic sweep shows a smaller reoxidation peak near −1.07 V. No additional redox systems are seen on subsequent cycles. Chronoamperometric $it^{1/2}/C$ values measured at −1.5 V were observed to increase smoothly from a value corresponding to $n = 1$ for $t < 50$ ms to a value approaching $n = 2$ for $t > 4$ s. Reduction of 2,6-dichloronitrobenzene at −1.5 V in the cavity of an esr spectrometer gave a spectrum identical to that of *o*-chloronitrobenzene anion radical.

These results strongly suggest the chemical and electrochemical processes described in equations (1)–(4). Since the peak reduction potential of *o*-chloronitrobenzenes is only

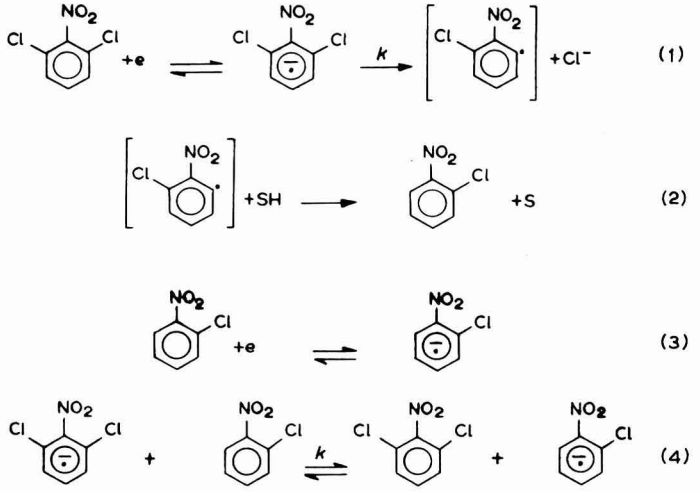

forty millivolts less anodic than that of 2,6-dichloronitrobenzene, separate cathodic waves

for the two reduction processes are not discernible. Analysis of the chronoamperometric data for the rate constant for loss of chloride ion from the anion radical of 2,6-dichloronitrobenzene gave a value of 0.12 s^{-1} in both DMF and AN.

It has been previously shown that the twisting of the nitro group from the benzene plane is reflected in the reduction potentials of the *o*-substituted nitrobenzenes. Using a previously obtained value of the reaction constant (ρ = 0.36 V) for the reduction of a series of nitrobenzenes in DMF[5], a Hammett substituent constant of 0.20 for an *ortho*- or *para*-substituted chlorine[6], and $E_{p/2}$ = −1.06 V for nitrobenzene[5], a value of $E_{p/2}$ = −0.92 V is predicted for the reduction of 2,6-dichloronitrobenzene. The difference of −180 mV between the observed value (−1.10 V) and the predicted value reflects the steric interaction between the nitro group and the two *ortho* substituents. This value is identical to the value measured previously for the steric interaction in 2,6-dimethylnitrobenzene[5], and is anticipated since the van der Waals radii for chlorine and methyl substituents are similar[7]. The presence of the second methyl group in the anion radical in 2,6-dimethylnitrobenzene was observed to cause the angle of twist to increase from approximately 30° to 65° and to cause a marked decrease in the hyperfine splitting constants in the *ortho* and *para* positions[8]. As we have seen here, relief of steric strain in the anion radical of 2,6-dichloronitrobenzene is possible by elimination of chloride ion. The steric interaction in the anion radical of *o*-chloronitrobenzene is considerably less (60 mV *vs.* 180 mV) and further halide loss is not observed.

Although the loss of chloride ion from the anion radical of 2,3-dichloronitrobenzene was not observed by either cyclic voltammetry or chronoamperometry ($t < 1$ sec), the dehalogenation was found to be complete by thin-layer chronoamperometry with current integration (n_{exp} = 1.97 at $t \cong 60$ sec). Loss of chloride ion from the 2-position and formation of *m*-chloronitrobenzene anion radical was confirmed by esr spectroscopy. Buttressing of the *ortho*-substituted chlorine by the second chlorine atom is reflected in the peak reduction potentials. Using $\sigma_{m,Cl}$ = 0.37[6] and other data given above, we find the steric interaction in 2,3-dichloronitrobenzene to be −110 mV, a value which is 50 mV greater than in *o*-chloronitrobenzene and *o*-nitrotoluene[5].

Reduction of 2,4-dichloronitrobenzene to its stable anion radical is indicated by both cyclic voltammetry and chronoamperometry. Steric interaction, as measured by the difference between the predicted and observed peaks, is 60 mV, the same as that observed for *o*-chloronitrobenzene[5]. Thin-layer coulometry indicates slow dehalogenation of the 2,4-dichloronitrobenzene anion radical (n_{exp} = 1.51). Formation of *p*-chloronitrobenzene anion radical was confirmed by esr spectroscopy. No loss of chloride ion is observed from *o*-chloronitrobenzene anion radical under the same conditions (n_{exp} = 1.01).

Although loss of chloride ion from the anion radical of *o*-chloronitrobenzene is not observed by either cyclic voltammetry or chronoamperometry in the potential range of 0 to −1.5 V, a cathodic sweep to more negative potentials shows two additional peaks at −1.94 and −2.16 V. The first of the two processes is attributed to the further reduction of *o*-chloronitrobenzene anion radical while the second is due to the reduction of nitrobenzene anion radical. Since nitrobenzene and *o*-chloronitrobenzene are reduced to their anion radicals at exactly the same potential[5], we illustrate these additional processes with *p*-bromonitrobenzene.

On the cathodic sweep (Fig. 1a), three reduction peaks are readily seen near −1.00, −1.94 and −2.16 V. As with *o*-chloronitrobenzene, the first process is the one-

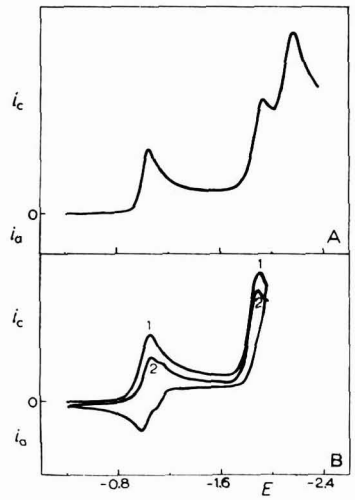

Fig.1. Voltammogram of *p*-bromonitrobenzene in 0.1 *F* TEAP–DMF. (A) Showing the three cathodic processes. (B) Scan reversed before the third cathodic process.

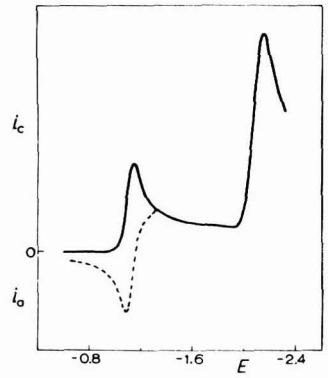

Fig.2. Voltammogram of nitrobenzene in 0.1 *F* TEAP–DMF: (——) single cathodic sweep showing the two cathodic processes and (- - - -) showing reversal of scan at −1.3 V after the first cathodic process.

electron reduction of *p*-bromonitrobenzene to its stable anion radical, the second is due to the reduction of *p*-bromonitrobenzene anion radical, while the third represents the reduction of nitrobenzene anion radical. That nitrobenzene anion radical is the product of the second cathodic process is readily seen by comparison of Figs. 1 and 2. If the direction of the potential scan is reversed just prior to the third cathodic process (Fig. 1b), a new redox couple appears at a potential slightly cathodic of the *p*-bromonitrobenzene system. This can only be seen if the second cathodic process is first made to occur Further comparison of Fig. 1 with Fig. 2 (authentic nitrobenzene) leaves no doubt as to the identity of either the new redox couple or the third cathodic process in Fig. 1a. Loss of bromide ion and formation of nitrobenzene anion radical at −2.0 V was confirmed by esr spectroscopy.

A comparison of the cyclic voltammetric results for the anion radicals of *p*-chloro- and *p*-bromonitrobenzene supports the interpretation for the second and third cathodic processes. *p*-Chloronitrobenzene anion radical is known not to lose chloride ion upon further reduction[4], and, hence, cannot give nitrobenzene anion radical as an electroactive product. Accordingly, *p*-chloronitrobenzene anion radical is observed to give only a single reduction wave at −1.90 V in DMF.

The observation that chloride ion is not lost from the anion radical of *p*-chloronitrobenzene at the potential of the second cathodic process suggests a dual pathway of dianion decomposition. The pathway for dianion decomposition should depend not only

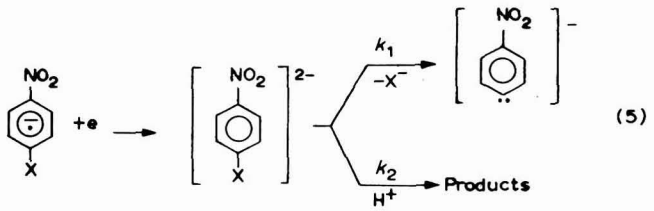

(5)

upon the ease of halide ion loss, but also upon the availability of protons. We observe that addition of water in concentrations up to 0.1 *F* decreases but does not entirely prevent elimination of bromide ion from the dianion of *p*-bromonitrobenzene. Addition of an equimolar quantity of phenol to *o*-chloronitrobenzene has been observed previously to impede dehalogenation, while a quantity three times greater was sufficient to completely suppress nitrobenzene anion radical formation[4].

The results presented above would suggest that reduction of 2,6-dibromonitrobenzene at −1.5 V should also give nitrobenzene anion radical. Although a weak esr

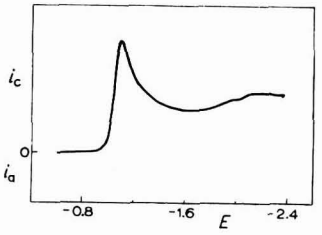

Fig.3. Single cathodic sweep of 2,6-dibromonitrobenzene in 0.1 *F* TEAP–DMF.

spectrum of nitrobenzene anion radical is observed, cyclic voltammetry (Fig. 3) of 2,6-dibromonitrobenzene shows that stepwise loss of bromide ion to give nitrobenzene anion radical cannot be the main reduction pathway. Controlled-potential electrolysis of a 2,6-dibromonitrobenzene solution to the point where $n = 2.0$ confirms the cyclic voltammetric observation. While 98% of the starting material was electrolyzed, only 8% *o*-bromonitrobenzene and 24% nitrobenzene were found by flame-ionization gas chromatography. No other species was detected in the gas chromatographic analysis, including

1,3-dibromobenzene. The latter would be the anticipated product if decomposition of the 2,6-dibromonitrobenzene anion radical were to occur by nitrite elimination. Oxidizable materials, such as the anion radical of nitrobenzene, were not found electrochemically. Reduction at an optically transparent electrode gave absorption throughout the visible region, indicating the formation of higher molecular weight species by a pathway not yet identified. Moderate fouling of the electrode surface was noted in all studies involving 2,6-dibromonitrobenzene.

Experimental

2,6-Dibromonitrobenzene was prepared by the oxidation of 2,6-dibromoaniline with 90% H_2O_2 and trifluoroacetic anhydride[9], m.p. 82–83° from ethanol. 2,6-Dichloronitrobenzene was prepared similarly by oxidation of 2,6-dichloroaniline, m.p. 70–71° from ethanol. The other aromatic nitrocompounds were commercially available and purified as required. The supporting electrolyte, tetraethylammonium perchlorate (TEAP), was prepared by the method of Kolthoff and Coetzee[10]. Dimethylformamide (DMF) and acetonitrile (AN) were prepared by previously described procedures and stored over Linde Type 4A molecular sieves[1]. All electrochemical experiments were performed at 22.5 ± 0.5° in a glovebag under a nitrogen atmosphere. The solutions were deaerated with prepurified nitrogen for a least 20 min prior to the electrochemical measurements. All potentials are with respect to the saturated calomel electrode. All instrumentation has been described previously[1].

Department of Chemistry,
Kansas State University,
Manhattan, Kansas 66502 (U.S.A.)

JAMES G. LAWLESS
M. DALE HAWLEY

1 J.G. Lawless and M.D. Hawley, *J. Electroanal. Chem.*, 21 (1969) 365.
2 T. Kitagawa and R. Nakashima, *Rev. Polarography (Japan)*, 13 (1966) 115.
3 T. Kitagawa, T.P. Layloff and R.N. Adams, *Anal. Chem.*, 35 (1963) 1086.
4 T. Fujinaga, Y. Deguchi and K. Umemoto, *Bull. Chem. Soc. Japan*, 37 (1964) 822.
5 J.G. Lawless and M.D. Hawley, submitted for publication.
6 P. Zuman, *Substituent Effects in Organic Chemistry*, Plenum Press, New York, N.Y., 1967, Chapter 3.
7 M. Charton, *J. Amer. Chem. Soc.*, 91 (1969) 615.
8 D.H. Geske, J.L. Ragle, M.A. Bambanek and A.L. Balch, *J. Amer. Chem. Soc.*, 86 (1964) 987.
9 W.D. Emmons, *J. Amer. Chem. Soc.*, 76 (1954) 3470.
10 I.M. Kolthoff and J.F. Coetzee, *J. Amer. Chem. Soc.*, 79 (1957) 870.

Received June 9th, 1969

App. 6 ELECTROANALYTICAL CHEMISTRY AND INTERFACIAL ELECTROCHEMISTRY
Elsevier Sequoia S.A., Lausanne – Printed in The Netherlands

PRELIMINARY NOTE

ELECTROCATALYTIC OXIDATION OF AMINES ON PLATINUM ELECTRODES. PART I. OXIDATION VIA COPPER COMPLEXES

The oxidation of Cu^{2+} ions to Cu^{3+} is facilitated by complexation by various ligands (*e.g.* IO_4^-, TeO_4^{2-}, glycine, biuretate)[1-3]. It has been suggested that the redox potential of such complexes may be lower than that of the hydrated ions[2,3]: *e.g.* the redox potential of the couple $(Cu(II)C_2H_3N_3O_2)^{2-}/(Cu(III)C_2H_3N_3O_2)^-$ is between 0.85–1.07 V[3], which means one volt lower than E° for the Cu(II)/Cu(III) couple in the aquo complex[4]. Furthermore, it has been shown that the amino complexes of Cu(III) are unstable in aqueous solutions[3,5-9], the Cu(III) oxidizing its ligands. Thus it seemed reasonable to expect that Cu(II) complexes might be oxidized electrolytically, resulting in specific catalytic oxidation of amines at the site of ligation to the copper.

We have, therefore, decided to study the voltammetric oxidation of amino complexes of copper on platinum electrodes. Relatively large catalytic waves have been observed in the presence of several ligands in the 0.7–1.0 V range.

Experimental

All experiments were carried out in an H-cell, with a saturated calomel electrode in one compartment. The stationary Pt electrode was supplied by Metrohm (No. EA 222). The electrode was cleaned before every experiment by dipping into a 2 *N* H_2SO_4 solution and rinsing with triply distilled water. The $CuEn_2$ solutions were not purged with nitrogen. Two types of polarographs were used for these experiments: Metrohm Polarecord E261R and Sargent Model XVI. A Metrohm Model E353B pH-meter was used for pH measurements.

All materials were of A.R. grade and were used without further treatment. Ethylenediamine (En) was introduced as ethylenediamine sulfate (Fluka purum grade). Tetra-L-alanine was supplied by Mils-Yeda. Triply distilled water was used throughout. All solutions were 0.1 *M* $NaClO_4$.

Results and discussion

Current potential curves of complexes of copper with ethylenediamine, ammonia, tetra-L-alanine (TLA) and EDTA were recorded and compared with the corresponding curves taken in identical solutions except for the copper.

Solutions of the copper ethylenediamine complex contained 10^{-3} *M* $CuSO_4$, 1.9×10^{-3} *M* En, in the pH range 8–12. As the stability constants for the formation of $CuEn_2^{2+}$ are $pK_1 = 10.7$ and $pK_2 = 9.2$ [10], and the dissociation constants of EnH_2^{2+} are

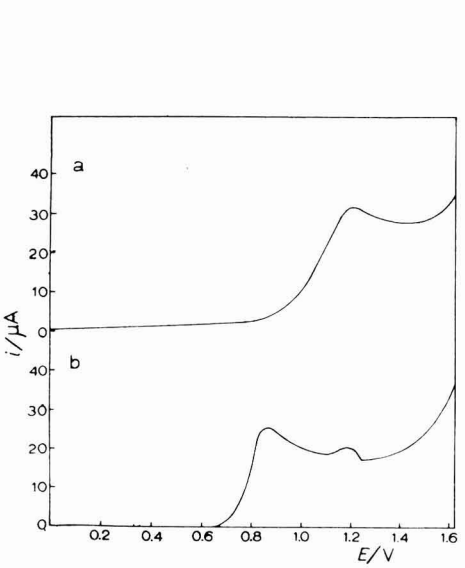

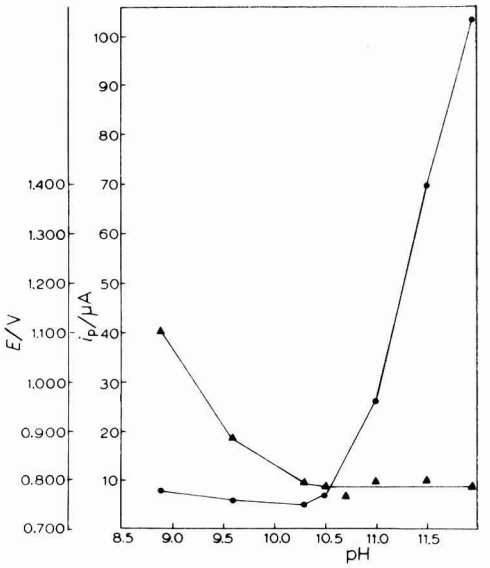

Fig.1. Current–potential curves: (a) lower curve, solution of 1 x 10^{-3} *M* $CuSO_4$, 1.9 x 10^{-3} *M* $EnSO_4$, 0.1 *M* $NaClO_4$ at pH = 11.0; (b) upper curve, solution of 1.9 x 10^{-3} *M* $EnSO_4$, 0.1 *M* $NaClO_4$ at pH = 11.0.

Fig.2. pH effects on the first wave: (●) Peak current of the first wave; (▲) half peak potential of the first wave. All solutions contained 1 x 10^{-3} *M* $CuSO_4$, 1.9 x 10^{-3} *M* $EnSO_4$ and 0.1 *M* $NaClO_4$.

pK_1 = 10.1, pK_2 = 7.0 [10], the solutions contained 9 x 10^{-4} *M* $CuEn_2^{2+}$ and 1 x 10^{-4} *M* $CuEn^{2+}$ and no free En.

A typical current–potential curve of $CuEn_2^{2+}$ is shown in Fig.1a. Fig.1b is the corresponding curve of En solution in the supporting electrolyte. The curves were taken at pH 11.0. It is evident that the presence of Cu^{2+} ions causes a shift in the potential of the wave. The dependence of the half-peak potential and of the peak current of the first wave on pH is given in Fig.2. However, when the solutions were buffered with 0.05 *M* sodium tetraborate to pH 9.2, no peaks on waves were obtained, but the decomposition potentials (derived from the point of intersection of the extrapolated line passing through the rising portion of the wave and that passing through the residual current portion) of solutions of $CuEn_2^{2+}$ were shifted to lower potentials by > 0.1 V relative to the decomposition potentials of the blank solutions. In the absence of buffer, similar results were obtained only above pH 12.

The experiments with $Cu(NH_3)_4^{2+}$ showed a shift in the decomposition potential which, in solutions containing 0.2 *M* NH_3, 0.1 *M* $NaClO_4$ at pH 11.1 and $CuSO_4$ in the concentrations: 0, 1 x 10^{-5} *M*, 1 x 10^{-4} *M* and 1 x 10^{-3} *M*, were determined as > 1.0 V, 0.97 V, 0.89 V and 0.83 V respectively. A small shift of the peak potential of about 0.06 V was observed also when Cu(II) was added in an equimolar concentration to solutions of TLA in a phosphate buffer at pH 7.9. No effect was observed when $CuSO_4$ was added to basic solutions of EDTA.

The formation of the first wave of $CuEn_2^{2+}$ and the shifts in potential observed with $Cu(NH_3)_4^{2+}$ and Cu(II)TLA must be due to the oxidation of Cu(II) to Cu(III). The

potential at which this oxidation occurs (0.7–1.0 V) is about one volt lower than the estimated oxidation potential of hydrated Cu(II)[4], in accordance with the estimated effect of amino ligands on the oxidation potential of Cu(II) ions[2]. Cu(III) amino complexes are known to be unstable in solution, oxidizing their ligands[3,5–9]. It is therefore plausible to assume that in the case of $CuEn_2^{3+}$ the ethylenediamine is oxidized also if the copper complex ion is adsorbed on the electrode surface.

Alternatively it may be argued that copper ions facilitate the direct oxidation of ethylenediamine. However, it is known that oxidation by radicals of amino compounds is hindered when the amino group is in its acid form[11,12], perhaps because of the loss of resonance stabilization of the radical formed by α-hydrogen abstraction[12]. Similar effects are expected upon ligation to metal cations.

The oxidation of ethylenediamine, like the oxidation of many organic compounds, is likely to proceed by a mechanism which decreases the pH of the solution. Such a process acidifies the double layer, resulting in two effects which might decrease the oxidation rate: (*a*) it decreases the concentration of OH^- ions which participate, in one way or another, in the reaction; (*b*) the pH of the double layer may reach a value below 6, where the complex $CuEn_2^{2+}$ is decomposed. The effect of pH on the peak current of the first wave is attributed to this acidification of the reaction layer. The effect of the buffer proves that when a sufficiently high concentration of a Brönsted base is provided, the same current can be obtained at a much lower pH, and that therefore one of the above mechanisms or both are operative.

Similar electrocatalytic oxidations are expected also by other cations, which have high unstable oxidation states. A detailed study of the copper and nickel ethylenediamine oxidations is in progress.

Acknowledgement

The authors are thankful to Dr. I. Hodara for helpful discussions.

Department of Inorganic and Analytical Chemistry, ILANA FRIED
The Hebrew University of Jerusalem, Israel
The Nuclear Research Centre, Negev, Israel DAN MEYERSTEIN

1 L. Malaprade, *Compt. Rend.*, 204 (1937) 979; L. Malatesta, *Gazz. Chim. Ital.*, 71 (1941) 467, 580; M. Lister, *Can. J. Chem.*, 31 (1953) 638; L. Jenovski, *Z. Anorg. Allg. Chem.*, 307 (1961) 208.
2 A. Levitzki and M. Anbar, *Chem. Commun.*, (1968) 403.
3 D. Meyerstein and W.A. Mulac, *Israel J. Chem.*, 6 (1968) 53.
4 W.M. Latimer, *The Oxidation States of the Elements and their Potentials in Aqueous Solutions*, Prentice–Hall, 2nd Edn., 1953, p.188.
5 M. Anbar, R.A. Muncz and P. Rona, *J. Phys. Chem.*, 67 (1963) 2708.
6 M. Anbar, *Mechanism of Inorganic Reactions,* Advances in Chemistry Series, 49 (1965) 126.
7 A. Levitzki, M. Anbar and A. Berger, *Biochemistry*, 6 (1967) 3757.
8 A. Levitzki and M. Anbar, *J. Am. Chem. Soc.*, 89 (1967) 4185.
9 D. Meyerstein, unpublished results.
10 G.H. McIntyre, Jr., B.P. Block and W.C. Fernelius, *J. Am. Chem. Soc.*, 81 (1959) 529.
11 M. Anbar and P. Neta, *Intern. J. Appl. Radiation Isotopes*, 18 (1967) 493.
12 M. Anbar, D. Meyerstein and P. Neta, *J. Chem. Soc.*, B (1966) 742.

Received May 30th, 1969

ELECTROANALYTICAL CHEMISTRY AND INTERFACIAL ELECTROCHEMISTRY App. 9
Elsevier Sequoia S.A., Lausanne – Printed in The Netherlands

PRELIMINARY NOTE

A HANGING MERCURY DROP ELECTRODE REFILLABLE FROM AN EXTERNAL RESERVOIR

Hanging mercury drop electrodes (HMDE) have found increasing applications in electrochemistry, both in the study of electrode reaction mechanisms and in electroanalytical chemistry. Many papers[1–10] can be found dealing with the design and handling of such electrodes. Recently[11] has been described the use of a HMDE in a drop volume method for the determination of the equilibrium interfacial tension. Further investigations, aiming at the utilisation of such a method for the automatic tracing of equilibrium electrocapillary curves, have shown the need of refilling the electrode without displacing the capillary from the solution. As a matter of fact this problem is rather generally met with, when using HMDE.

This communication describes a HMDE, which can be refilled easily and repeatedly from an external reservoir. Very recently, while our work was in progress, Kowalski[12] has published an ingenious solution to the same problem. We think however that this note deserves some attention, because of the very simple refilling procedure proposed.

The electrode assembly is schematically illustrated in Fig.1. It is formed by a micrometer screw (S) the rotation of which causes the penetration of a stainless steel piston (P) into a mercury chamber (M). The chamber communicates through the two way tap (T) with the capillary (C) or (C′) according to the position (a) or (a′) of the tap. One of the capillaries is used as electrode, the other one is connected to a mercury reservoir and is used for refilling the chamber.

Air-tight passage of the piston is ensured by the viton o-rings (O), deformed by fastening the screw (F) as proposed by Vogel[7]. The capillaries are fixed to the plexiglas block (B) in the same way, through the screws (R) and (R′) and the o-rings (Q) and (Q′). Fig.2 shows in particular a perspective view of the tap. The air-tight rotation of the tap is assured by a viton disc (D) pressed by a plexiglas screw (L) through a teflon washer (W). Communication of the mercury chamber with the capillary takes place through the groove (G), the steel cylinder (Y) assuring the arrest of the tap in the proper position.

The initial filling of the electrode is performed, as usual, connecting one of the capillaries to a vacuum pump with the piston in the lowest position. Mercury is then made to penetrate through the capillary so that the chamber is completely filled. Filling of the second capillary is made in the same way. The electrode is so ready for use. When the piston has come to the highest position, refilling of the chamber is performed simply by turning the tap from (a) to (a′) and sucking in mercury from a beaker. Suction is achieved as usual, shifting the piston down, by rotation of the micrometer screw.

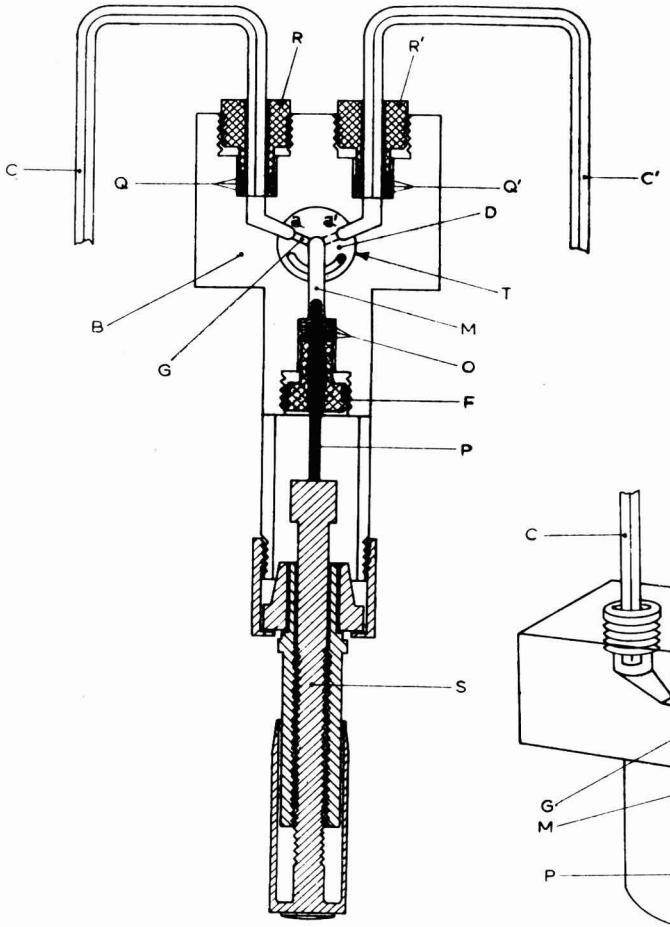

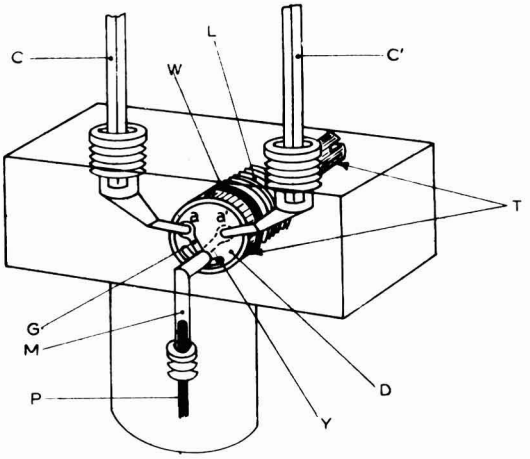

Fig. 1. A hanging mercury drop electrode refillable from an external reservoir.

Fig. 2. A hanging mercury drop electrode refillable from an external reservoir.

Acknowledgement

Assistance of Mr. M. Scarabottolo in the mechanical realisation of the electrode is gratefully acknowledged. This note is part of a program supported by Consiglio Nazionale delle Ricerche.

Institute of Chemistry "G. Ciamician",
University of Bologna (Italy) S. ROFFIA
Institute of Physical Chemistry,
University, Padova (Italy) E. VIANELLO

1 H. Gerischer, *Z. Physik. Chem.*, 202 (1953) 302.
2 W. Kemula and Z. Kublik, *Anal. Chim. Acta*, 18 (1953) 104.
3 J.E.B. Randles and W. White, *Z. Elektrochem.*, 59 (1955) 669.
4 V. Cermak, *Collection Czech. Chem. Commun.*, 24 (1959) 831.
5 Z. Kowalski, *Roczniki Chem.*, 35 (1961) 365.
6 F.V. Sturm and M. Ressel, *Z. Anal. Chem.*, 186 (1962) 63.
7 J.J. Vogel, *J. Electroanal. Chem.*, 8 (1964) 82.
8 J.M. Saveant and E. Vianello, *Electrochim. Acta*, 10 (1965) 905.
9 J. Riha, *The Hanging Mercury Drop in Polarography*, in P. Zuman and I.M. Kolthoff (Eds.), *Progress in Polarography*, Interscience Publishers Inc., New York, N.Y., 1962.
10 W. Kemula and Z. Kublik, *Application of Hanging Mercury Drop Electrodes in Analytical Chemistry*, in C.N. Reilley (Ed.), *Advances in Analytical Chemistry and Instrumentation, Vol. 2*, Interscience Publishers Inc., New York, N.Y., 1963.
11 S. Roffia and E. Vianello, *J. Electroanal. Chem.*, 15 (1967) 405; 17 (1968) 13.
12 Z. Kowalski, *J. Electroanal. Chem.*, 21 (1969) P9.

Received July 14th, 1969.

Vol. 23 No. 1 JOURNAL OF ELECTROANALYTICAL CHEMISTRY AND INTERFACIAL ELECTROCHEMISTRY OCTOBER 1969

CONTENTS

Anodic stripping pulse voltammetry
G. D. CHRISTIAN (Lexington, Ky, U.S.A.) 1

On the impedance of galvanic cells. XXVI. Application of the complex plane method in the case of mixed currents
B. G. DEKKER, M. SLUYTERS-REHBACH AND J. H. SLUYTERS (Utrecht, The Netherlands) 9

On the impedance of galvanic cells. XXVII. The temperature-dependence of the kinetic parameters of the hydrogen electrode reaction on mercury in concentrated HI
B. G. DEKKER, M. SLUYTERS-REHBACH AND J. H. SLUYTERS (Utrecht, The Netherlands) 17

The resistance and intrinsic time constant of glass electrodes
A. WIKBY AND G. JOHANSSON (Umeå, Sweden) 23

Adsorption of lead(II) chloride by chronoamperometric measurements
M. CASELLI AND P. PAPOFF (Bari, Italy) 41

Polarographischer Nachweis der Carbonyl–Schwefel-Wechselwirkung in Thiacyclanonen
R. HERZSCHUH UND R. BORSDORF (Leipzig, D.D.R.) 55

Effects of the electrical double layer and thiourea adsorption on polarographic catalytic currents of the nickel(II)–thiourea complex
Ya. I. TUR'YAN AND O. E. RUVINSKII (Yaroslavl, U.S.S.R.) 61

Effect of the electrical double layer and pyridine adsorption on the catalytic polarographic current of nickel(II)–pyridine complexes
YA. I. TUR'YAN AND O. N. MALYAVINSKAYA (Yaroslavl, U.S.S.R.) 69

Contribution à l'étude du dosage de submicrotraces de fer par polarographie inverse sur goutte de mercure pendante. I. Etat du fer sur l'électrode et mécanisme d'oxydation électrochimique
W. HAERDI, J. BUFFLE ET D. MONNIER (Genève, Switzerland) 81

Contribution à l'étude du dosage de submicrotraces de fer par polarographie inverse sur goutte de mercure pendante. II. Etude des réactions secondaires
J. BUFFLE, W. HAERDI ET D. MONNIER (Genève, Switzerland) 89

Studies of the polarographic and coulometric behaviour of aromatic nitrocompounds. I. Nitrobenzene in ethanol
S. K. VIJAYALAKSHAMMA AND R. S. SUBRAHMANYA (Bangalore, India) 99

The electrical conductivity of uranyl acetate in water and water–dioxane mixtures
E. M. KHAIRY, A. El-S. MAHGOUB AND A. I. MOSAAD (Cairo, U.A.R.) 115

Preparation and physico-chemical properties of some organo-uranyl complexes
A. MOSTAFA AND E. M. KHAIRY (Giza, U.A.R.) 127

Studies of membrane phenomena. I. Effect of temperature on diffusion of electrolytes through a parchment-supported silver iodide membrane
F. A. SIDDIQI AND S. PRATAP (Aligarh, India) 137

Studies of membrane phenomena. II. Determination of membrane potentials and evaluation of the membrane fixed charge density and permselectivity of parchment-supported silver iodide membrane
F. A. SIDDIQI AND S. PRATAP (Aligarh, India) 147

Continued on page 4 of cover

Continued from inside page of cover

Chemical and electrochemical reactions of nickel–nitrohydroxylaminic complexes in unbuffered medium
A. CĂLUȘARU (Bucharest, Rumania) 157

Short Communications
Polarography of Fe(III)-hematoporphyrin(IX)
J. G. MONTALVO JR. AND D. G. DAVIS (New Orleans, La, U.S.A.) 164

Theoretical calculation of polarographic solution resistance. Comment on the paper by Britz and Bauer
D. F. TAYLOR AND R. G. BARRADAS (Ottawa, Ont., Canada) 166

Interfacial tension measurements between mercury and dilute aqueous electrolytes
D. J. SCHIFFRIN (Southampton, Great Britain) 168

The urinary mercury content of electroanalytical chemists
G. D. CHRISTIAN (Lexington, Ky, U.S.A.) 172

Preliminary Notes
Mechanistic studies of the decomposition of dihalonitrobenzene anion radicals
J. G. LAWLESS AND M. D. HAWLEY (Manhattan, Kan., U.S.A.) . . . . . App. 1

Electrocatalytic oxidation of amines on platinum electrodes. Part I. Oxidation via copper complexes
I. FRIED AND D. MEYERSTEIN (Jerusalem and Negev, Israel) . . . . . App. 6

A hanging mercury drop electrode refillable from an external reservoir
S. ROFFFIA AND E. VIANELLO (Bologna and Padova, Italy) . . . . . App. 9